Far from equilibrium
Dynamics of entanglement and fluctuations

Hoogeveen, Marianne Lotje

Awarding institution:
King's College London

King's College, University of London

Doctoral Thesis

Far from equilibrium: dynamics of entanglement and fluctuations

Author:
Marianne Hoogeveen

Supervisor:
Dr. Benjamin Doyon

A thesis submitted in fulfilment of the requirements for the degree of Doctor of Philosophy

in the

Theoretical Physics Group
Department of Mathematics

December 2016

"Pooh?"

"Yes, Piglet."

"I've been thinking. . . "

"That is a very good habit to get into, Piglet."

- A.A. Milne, *Winnie-the-Pooh*

KING'S COLLEGE, UNIVERSITY OF LONDON

Abstract

Faculty of Natural & Mathematical Sciences
Department of Mathematics

Doctor of Philosophy

Far from equilibrium: dynamics of entanglement and fluctuations

by Marianne HOOGEVEEN

We consider the state of a one-dimensional critical quantum system after a "thermal cut-and-glue quench", which is a local quench in which two independently thermalized halves are connected to form a homogeneous infinite system and left to evolve unitarily until they reach a non-equilibrium steady state (NESS). This quench was studied in [1], and exact CFT results for the current and its fluctuations in the NESS were found. We add to these results by studying the growth of entanglement after the quench. Furthermore, we generalise to the case in which the system is not critical, but described by an integrable relativistic quantum field theory (IQFT) with diagonal scattering, and find exact expressions for the energy current and scaled cumulant generating function (CGF) in the NESS. Another generalisation we consider is the thermal cut-and-glue quench for N independently thermalised critical one-dimensional systems. These are made to form a quantum junction consisting of N one-dimensional critical systems that are connected at one point in a star graph configuration, with a particular, simple connection condition at the vertex. We find in this situation the exact energy current and scaled CGF in the NESS.

This thesis is based on the publications [2–4], which are incorporated in their published form in Chapters 3 and 4.

Acknowledgements

My fondest regards go out to my supervisor Benjamin Doyon, who is the best supervisor I could have wished for: inspiring and pragmatic. It has been eye-opening to watch your brain at work. Choosing you for a supervisor was one of the best decisions I ever made.

It has been a pleasure as well to be part of the "CFT clan", with Olalla, Gerard and Andreas, as well as Davide, Isao, Nick, Paul, Yixiong and Victor.

Furthermore, I would like to thank Matt for a warm welcome in the maths office and for his extraordinary artwork. Akram has greatly improved my knowledge of obscure English words, and he smuggles peanuts like no other.

Finally, I would like to thank Jorn for always being his playful self and making every day that much brighter. You are one of a kind, and I look forward to the rest of our life together. I am extremely lucky.

Contents

Chapter 1

Introduction

Condensed matter physics is the study of the behaviour of many quantum particles usually in strong interaction with each other. Starting from a one-particle description, one might think that describing these many-particle systems is extremely difficult. However, when describing certain systems that contain a very large number of particles, something interesting happens. In thermodynamic equilibrium, statistical mechanics drastically simplify the effective description of the state, which is reduced to finding a small number of thermodynamic quantities, such as the temperature, volume, pressure or entropy. Another powerful result is the fluctuation-dissipation theorem, stating that both for classical and quantum systems, the response to small perturbations from equilibrium depends only on equilibrium properties [5–9]. Much of the progress that has been made in describing quantum many-body systems has been for equilibrium systems. However, in nature, systems are not always close to equilibrium, and we often want to understand the dynamics underlying physical processes such as relaxation toward equilibrium or phase transitions.

Important experimental breakthroughs in the field of ultracold atomic gases (see [10] and references therein[1]) allow for a great degree of manipulation of the interactions of a system, and for a very sudden change of these interactions. Crucially, the dynamics of these gases is very slow compared to most condensed matter systems, which makes studying the dynamics feasible in an experimental setting.

[1] In particular, in [11] a gas in a one-dimensional optical lattice, a harmonic trap due to a combination of laser beams, was brought out of equilibrium by suddenly exciting slow-moving particles using two laser pulses. This resulted in two fast-moving opposite clouds of particles each behaving more or less like a pendulum due to the harmonic trap.

1.1 Quantum Phase Transitions

The description of matter usually changes when you consider the physics happening at different length scales. One example is the fact that on small scales, electromagnetism and the strong and weak forces govern the behaviour of matter, whereas at large scales, gravity becomes important. In general, small-scale interactions between particles can lead to very different emergent phenomena. A phase transition happens when a small change in the interactions of constituent particles has a dramatic effect on the emergent behaviour of the collective. This can be a discontinuous (or 'first order') phase transition, which happens when two distinct phases are present at the same time (an example is the melting of ice), and is characterised by a discontinuity of the first derivative of the free energy. Most phase transitions one encounters in nature are of this kind. Another kind of phase transition happens when instead of two phases competing at the transition point, the two phases at either side of the transition are continuously morphed into a third, 'critical' phase, which is characterised by large-scale correlation. An example of a continuous phase transition is the disappearance of spontaneous magnetisation as a ferromagnetic material is heated up to its paramagnetic phase. This type of phase transition is called a continuous (sometimes 'second order') phase transition, and has a continuous first-order derivative of the free energy. We will consider only phase transitions of the second, continuous, type.

Typically, a phase transition is between an ordered phase and a disordered phase. When approaching a critical point from the disordered phase, small regions where the material is ordered will begin to form, whose size increases as the system is tuned towards the critical point. In the example of the ferromagnetic transition these are small regions where the spins tend to be aligned. The typical size of these regions defines a distance scale, which diverges at the critical point. The result is that at the critical point, the difference between short- and long-distance behaviour disappears and one can effectively describe the critical phase by a scale invariant theory. Apart from this large length scale, systems also have short length scales, such as the lattice spacing. However, the description of a system near a critical point turns out to be highly insensitive to the precise form of interactions at this small scale. In the limit where the ordered regions become large compared to the lattice spacing, one can neglect the size of the lattice spacing and describe the system in terms of a continuum field theory. The fact that

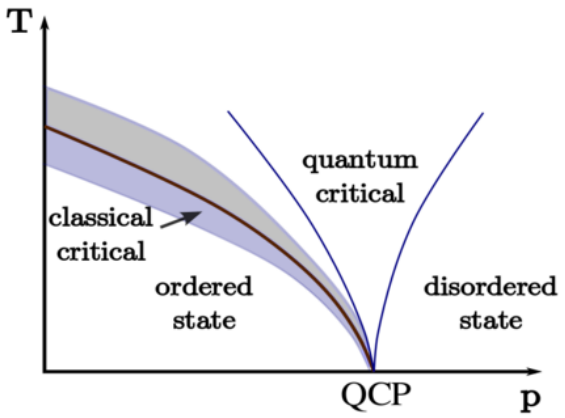

FIGURE 1.1: A Quantum Critical Point (QCP) is a point in a phase diagram where a continuous Quantum Phase Transition (QPT) takes place, which is a phase transition at zero temperature, due to a non-thermal control variable. This can be the result of the temperature at which a classical critical point occurs being depressed to zero.The Quantum Critical Regime is the part of the phase diagram in which (1) the temperature is high enough to overcome the energy gap caused by tuning slightly away from the QCP, and (2) the temperature is low enough for lattice effects not to be important for the description of the physics.

this continuum description of a critical point is insensitive to the microscopic details explains why some magnetic phase transitions may be described by the same theory as nonmagnetic phase transitions.

In this thesis we will be interested in the description of systems that are at or near a quantum critical point (QCP), which is a continuous quantum phase transition. By definition, a quantum phase transition is a transition which occurs at zero temperature, as a result of varying some non-thermal control parameter, such as applied magnetic field or pressure. Since classically the entropy at zero temperature has to vanish, a quantum phase transition can not be caused by the competition between energy and entropy, like its finite-temperature counterpart. Rather, it is a result of competition between different terms in the Hamiltonian describing the system. A common type of phase diagrams with a QCP has a line of finite-temperature critical points where the transition temperature is depressed to zero by varying a coupling constant (see figure 1.1). Around this finite-temperature critical line, the system can be described by a classical field theory, even though the transition temperature may be very low. This is due to the fact that close to a critical point, the length scale above which the behaviour changes qualitatively is very large. Around any nonzero temperature critical point, therefore, one has $kT > \omega$ where ω is some typical energy scale above which the behaviour of the system changes (for example an energy gap). This reasoning clearly breaks down for a quantum phase

transition, where the temperature is strictly zero. The behaviour at a QCP is expected to be characterized by competition between low-lying states [12]. This quantum critical behaviour is different from typical low energy behaviour, which can be understood in terms of quasi-particles on a ground state. This competition effect tends to break down away from the QCP on the zero temperature line, as an energy gap forms and the system chooses a ground state. However, if the temperature is increased such that this gap may be overcome the interplay between the different energy levels again becomes the dominant behaviour. The finite temperature region[2] of the phase diagram in which this quantum critical behaviour is important is called the quantum critical regime (QCR).

The case of one-dimensional quantum systems is a special one, because there are many cases that have an exact solution. This means that one can solve strongly interacting systems, which are inaccessible using perturbative methods. In particular, in the critical regime, the continuous description is scale invariant, and we can use the framework of two-dimensional conformal field theory (CFT). Slightly away from the critical point, where the temperature is not high enough to overcome the energy gap, but energy gap is still small, we may use massive quantum field theory (QFT). In this thesis we will consider the general situation where the field theory is integrable, namely it can be solved exactly using a technique called the Thermodynamic Bethe Ansatz (TBA).

A more thorough treatment of CFT and TBA will be the subject of Chapter 2.

1.2 Physical observables

As we want to better understand the dynamics of many-body quantum systems, we need physical objects whose behaviour we can study. Two widely studied objects in quantum dynamics are local observables and entanglement. The former are experimentally accessible, in the form of response functions, where the experimenter perturbs the system and measures a local response. Entanglement, although not measurable, contains useful information about the state of the system, since knowledge of the density matrix is in principle enough to compute all possible correlation functions. Studying suitable measures of the growth of entanglement in a nonequilibrium setting might therefore teach us more about the state of the system than expectation values of local observables could.

[2]Note that this region is also bound from above because at higher temperatures lattice effects will become important.

1.2.1 Energy current and fluctuations

When a Hermitian operator commutes with the Hamiltonian, the corresponding object is said to be conserved. For example, the fact that the Hamiltonian commutes with itself leads to the conservation of the total energy in a system. This statement does not immediately rule out the possibility that energy could disappear from one place and immediately reappear on the other side of the world. A stronger statement is that energy is locally conserved: Energy can neither be created nor destroyed, nor can it "teleport" from one place to another - it can only move by a continuous flow. A continuity equation defining a conserved current is the mathematical way to express this kind of statement. A typical system has three conservation laws; particle number, total energy, and total momentum. We shall focus on the energy current.

An empirical rule of heat transfer in solids is Fourier's law, which states that the rate of heat transfer is proportional to the gradient of the temperature,

$$J = -\kappa \nabla T, \tag{1.1}$$

where κ is a property of the material called the thermal conductivity. Close to equilibrium, the relation between the gradient and the current is approximately linear. The constant of proportionality is called the transport coefficient, which is what experiments often measure. One may define an energy density $u(x,t)$ which satisfies a continuity equation, $\partial_t u + \nabla \cdot J = 0$. Together with the notion of specific heat, defined via $\partial u/\partial T = c$, we can use this to obtain the heat diffusion equation (if c is constant):

$$\partial_t T = \nabla \cdot \left(\frac{\kappa}{c} \nabla T \right). \tag{1.2}$$

It is clear that Fourier's law implies diffusive transfer of energy. Dissipative currents such as the energy current in (1.1) increase entropy and bring the system back to thermal equilibrium. A microscopic picture is that the heat carriers (molecules, electrons, lattice vibrations, etc.) have random collisions and hence move diffusively. Fourier's law (1.1) relies on the establishment of a local thermal equilibrium through diffusion, and proving that this happens for systems with reversible dynamics (where the entire system is described by some Hamiltonian) is challenging [13]. In fact, for low-dimensional systems

(1D and 2D) it has been proved to break down [13–15], as there are anomalous non-local contributions to heat conduction, causing the basic assumption of local thermal equilibrium to break down. A conserved current leads to a nonzero Drude weight[3] [16, 17]. Specifically, close to equilibrium and assuming there is local Gibbs thermalization, a conserved current leads to ballistic transport of small perturbations. Under certain conditions, it has been proved that a conserved current leads to non-equilibrium ballistic transport [18].

Besides the energy current, we are also interested in its fluctuations, to generalize the powerful framework of thermodynamics to situations that are not close to equilibrium. When a system is far from equilibrium, the relaxation to equilibrium may take a very long time, or it may even be impossible. For systems that are not in equilibrium (and cannot be described by linear response), the fluctuation-dissipation relations do not hold. In order to extend the powerful framework of thermodynamics to situations when a system is not in (or near) thermodynamic equilibrium, equations generalizing the fluctuation-dissipation relation to out-of-equilibrium situations must be found. For classical systems that are driven out of equilibrium, so-called 'Fluctuation Theorems' (FT) have been found, describing how a system's irreversibility develops in time from a completely time-reversible system at short observation times, to a thermodynamically irreversible one at infinitely long times[4]. These are relations between the probability $P(\bar{\Omega}_t = A)$ of a random variable taking some value A, and the probability $P(\bar{\Omega}_t = -A)$ of this random variable taking the opposite value $-A$. This variable can be either the irreversible work performed on the system, or the entropy that is produced during a nonequilibrium

[3] The Drude weight is the weight of the singular part of the conductivity at $\omega = 0$ and depends on temperature. Generally, the existence of a Drude weight is connected to the presence of a conservation law, such as momentum conservation, which protects the current from decaying.

[4] The fluctuation theorem was derived to solve one of the fundamental paradoxes of statistical mechanics, Lochsmidts paradox. In 1876, Lochsmidt pointed out a fundamental problem associated with nonequilibrium thermodynamics: the macroscopic behaviour of a system is irreversible, as embodied in the second law, but the microscopic motion of all of the individual components is fully time reversible. Therefore for any system change, the opposite system change must also be possible. Even at that time, a resolution to the paradox was recognised by some. As noted by Maxwell: "The truth of the second law is a statistical, not a mathematical, truth, for it depends on the fact that the bodies we deal with consist of millions of molecules Hence the second law of thermodynamics is continually being violated, and that to a considerable extent, in any sufficiently small group of molecules belonging to a real body", and Boltzmann: "as soon as one looks at bodies of such small dimension that they contain only a very few molecules, the validity of this theorem [the Second Law] must cease". This means that the second law of thermodynamics is the limiting result of a statistical effect where the probability of observing the behaviour predicted from thermodynamics becomes more and more likely as the system size grows. However, for sufficiently small systems observed for short periods, we would expect to observe both types of behaviour. The fluctuation theorem quantifies this result.

process. There are various Fluctuation Theorems, but they are all of the form

$$\frac{P(\bar{\Omega}_t = A)}{P(\bar{\Omega}_t = -A)} \sim e^A, \tag{1.3}$$

where $\bar{\Omega}_t$ is the dissipation function, which quantifies the thermodynamic reversibility of a trajectory[5]. The dissipation function is like entropy production in that it can be used to indicate whether a system's behaviour is in accordance to the Second "Law" of thermodynamics (which is deemed to be the case if there is positive entropy production or dissipation). Negative dissipation is against the "Law", and is seen by the FT as being very unlikely. Close to equilibrium in large systems, where entropy production can be defined, the average dissipation is equal to the entropy production. However, unlike entropy production, the dissipation function is well-defined arbitrarily far from equilibrium and for systems of arbitrary size. Furthermore, it obeys a number of exact theorems: the FT, the Second "Law" inequality and various relaxation theorems. Dissipation is also the fundamental quantity required for all linear and nonlinear response theory both for driven and relaxing systems. Often, however, FTs are formulated for quantities such as irreversible work or entropy, depending on the particular setup. Particularly for quantum systems it is not always easy to find a suitable quantity (see [20]).

There are different FTs depending on whether the system in consideration is isolated or connected to a reservoir with which it can exchange energy and/or particles. The first FT was found by Evans and Searles [19, 21]. Classical FTs for work performed on an isolated system have been found for instance in [22, 23], and FTs for entropy production in thermostatted systems (these are systems that exchange only energy with a reservoir) with deterministic dynamics in e.g. [24, 25]. FTs for entropy production or transfer of heat or matter in systems with stochastic dynamics (these systems exchange energy and sometimes particles with a reservoir) were found e.g. in [26–30].

There are two different statements of the FT. If the time averages appearing in (1.3), $\bar{\Omega}_t$, are calculated from $t = 0$ and the ensemble averages used to compute the probability distribution $P(\bar{\Omega}_t)$ are taken over the initial ensemble, (1.3) is exact for all averaging durations t, and the theorem is called the transient FT (TFT). On the other hand if the

[5] It compares the probability of observing and arbitrary system trajectory with the probability of observing the time reverse of that trajectory (its conjugate anti-trajectory) in the same ensemble of trajectories [19]

time and ensemble averaging are carried out in a nonequilibrium steady state (NESS) [6] , after the relaxation of the initial transients, (1.3) is termed the steady state FT (SSFT), and furthermore it is only true asymptotically, as $t \to \infty$:

$$\lim_{t\to\infty} \frac{1}{t} \ln \frac{P(\bar{\Omega}_t = A)}{P(\bar{\Omega}_t = -A)} = A. \tag{1.4}$$

Extending these results to quantum systems poses some problems: first, defining the path that the state of the system takes is difficult, since one has to deal with the quantum probabilities. Secondly, whereas in classical systems one can assume that observing the state of the system doesn't affect the system itself, this is not the case for quantum systems; one has to come up with a measurement protocol that tells you what the state of the system is[7], for example taking an indirect measurement [31] or taking projective measurements at two different moments in time to measure the change in a quantity of interest (energy, charge, particles, etc.) [32]. In this thesis, we will consider fluctuations in the output of a two-point projective measurement of energy. This allows us to avoid the detailed modeling of detectors and their dynamics. The projective measurement can be viewed as an effective modeling of the effect of the system-detector interaction on the system or as resulting in a fundamental way from the quantum measurement postulate. Any other approaches for deriving FTs can be recovered in some limits of the two-point measurement approach [20], so this provides a unified framework from which the different types of FTs previously derived for quantum systems can be obtained.

We will study the energy current and its fluctuations in a non-equilibrium steady state, which will be described in more detail in section 1.4, in a situation in which Fourier's law does not hold due to the current being ballistic (i.e. not dissipative, as in (1.1)). The results are presented in Chapter 4.

1.2.2 Entanglement

Recent technological advances have made it possible to create entangled states in a controlled way. These are states that exhibit a new type of quantum correlation, which

[6] A nonequilibrium steady state (NESS) is a state where there is a current flowing (of electric charge or heat, for instance), but the current does not change in time. A precise definition of a steady state is that like in equilibrium, all intensive quantities (such as the current) are constant, while some extensive properties (like difference of total energy or charge) may change in time, but the second derivative is zero.

[7] hence, the notion of a FT in terms of probabilities of paths is not clear.

has no classical equivalent. This opens up the possibility of creating devices which rely on the manipulation of entangled states, and is one of the driving forces behind the fast growing field of quantum information. For a comprehensive review, see the book [33]. In the field of physics the study of entanglement is leading to profound new insights in both high and low energy physics. For instance, entanglement has been linked to quantum corrections to the entropy of a black hole, and led to the idea of black holes emitting so-called Hawking radiation. In condensed matter physics, the behaviour of certain measures of entanglement signal a Quantum Phase Transition[8], see the review [35].

1.2.2.1 Short history of entanglement

The idea of entanglement was born in the classic work by Eisntein, Podolski and Rosen [36], in which the question was posed whether quantum mechanics as a description of reality was complete. The argument that this could not be the case was made on the basis of what is now known as the EPR paradox: the existence of states in which measurements of two particles can be correlated even if the two particles are so far apart that they are not causally connected. These states are superpositions of two-particle states, and have the necessary feature that it is not possible to choose a basis in which the two-particle state becomes a product state of the single particle states. The term *entanglement* was coined by Schrödinger [37], referring to the fact that such EPR states cannot be factorised. The simplest examples of these entangled states are Bell states (nowadays often also referred to as EPR states), which consist of superpositions of two spin-1/2 states, for instance,

$$|\Psi_{\text{Bell}}\rangle = \frac{1}{\sqrt{2}} \left(|\uparrow\rangle_A \otimes |\uparrow\rangle_B - |\downarrow\rangle_A \otimes |\downarrow\rangle_B \right). \tag{1.5}$$

If the above two-particle state is created, and both particles are allowed to move away from each other, one can measure them at the same time and see whether the results are correlated. Looking at the state (1.5) one notices that both particle A and particle B have equal probability of having 'spin up' or 'spin down', when measured. However, if one of the particles is measured and found to be in the spin up state, say, then the other particle suddenly has a probability of 1 to be in the up state as well! Somehow it

[8] In particular, the divergence of correlations as a system is tuned to criticality, as discussed in Chapter 2, is always accompanied by the divergence of a suitably defined entanglement length [34].

appears that the result of the measurement of one particle is instantaneously known in the lab where the spin of the other particle is measured, even though the particles may be very far apart.

It was argued in [36] that this correlation should either be the result of instantaneous interactions ("spooky action at a distance"), which the authors dismissed on the basis of it violating the principle of relativity, or of some information 'hidden' in the separate states causing the results of all combined measurements to be known. The latter explanation was proposed as the solution, and models that contained this extra information came to be known as 'local hidden variable' (LHV) models. It wasn't until [38] that a method was devised to test whether a LHV model might explain these correlations, by comparing the different ways a pure entangled state such as the Bell state (1.5) and a state in a LHV model would transform under change of basis. This was done by considering the Bell state (1.5) and measuring the spins of the two particles in 3 directions, at equal angles of 120°. It was shown that if the possible outcomes for all directions were already known, as would be the case in a LHV model, then the two spins should have an opposite value at least 5 times out of 9 (or about 56%). It turned out that the spins had opposite value 50% of the time, which could be explained by normal rules of quantum mechanics. These tests, called Bell inequalities, provided a tool for experimental verification, and Bell's inequalities were soon shown to fail in the vast majority of experimental realisations (see for instance [39]), demonstrating that quantum entanglement is physical reality. Recently, a team in Delft have demonstrated the violation of Bell's inequality [40] in the strongest refutation to date of Einstein's hypothesis of local realism. It was shown that for pure states, Bell's inequalities are sufficient to characterise entanglement [41, 42]. However, further study of non-separable mixed states led to the discovery of entangled states that do admit the LHV model, and hence do not violate Bell's inequalities [43].

1.2.2.2 What is entanglement, and how do we measure it?

We have seen an example of an entangled state (1.5), and we know that a separable state, that is, a state that can be written as $|\Psi\rangle^{\text{sep}}_{A\cup B} = |\psi\rangle_A \otimes |\phi\rangle_B$ if it is a pure state, and as $\rho^{\text{sep}}_{A\cup B} = \sum_i p_i \, \rho^i_A \otimes \rho^i_B$ if it is a mixed state, contains no entanglement. In order to quantify entanglement, we need to find a suitable measure $E(\rho)$ of how far the state

ρ (pure or mixed) is from being separable. This turns out to be easier for pure states than for mixed states.

Two systems, let us call them A and B (we may talk of these systems as being Alice's and Bob's labs, respectively), are entangled if there exist *quantum correlations* between them: these are correlations that cannot be described as classical correlations. Classical correlations can be created between two quantum systems using local (quantum) operations and classical communication, together usually denoted 'LOCC' (Fig. 1.2). Any correlation that cannot be produced in this way (and is not the result of a classical

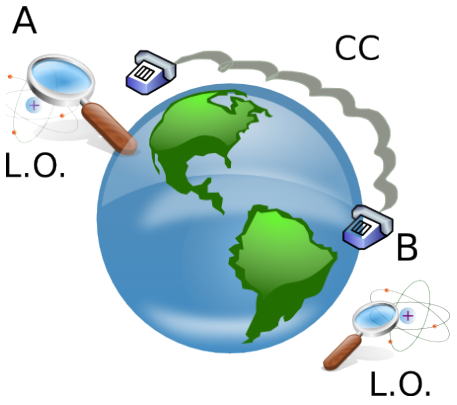

FIGURE 1.2: Local Operations ('LO') and Classical Communication ('CC').

nonlocal interaction [44]) is then a quantum correlation.

We will use this definition of entanglement, as correlations that cannot be created by LOCC alone, as well as the initial definition introduced by [36, 37], namely the correlations that are present between parts of a system that is in a quantum state that is not separable, to define a 'good measure' of entanglement to be a mapping from density matrices into positive real numbers which satisfies the following two conditions:

1. $E(\rho) = 0$ if the state ρ is separable
2. E does not increase under LOCC

A measure $E(\rho)$ which has these two properties is called an *entanglement monotone*[9].

We are now in a position to consider which measures of entanglement are suitable for our purpose of learning more about entanglement in many-body quantum systems. For

[9] Sometimes another requirement is added, namely that an entanglement measure is *convex*, which means that one requires $E(\sum_i p_i \rho_i) \leq \sum_i p_i E(\rho_i)$.

reasons that will become clear, we will consider first the case in which the total system is in a pure state, and later the case in which the total system is in a mixed state.

1.2.2.3 Pure states: Entanglement entropy

Let us now make the above ideas more precise. Consider a pure state $|\Psi\rangle_{A\cup B}$, which is defined on a Hilbert space $\mathcal{H}_A \otimes \mathcal{H}_B$. Now let us see what happens if we want to perform a measurement in system A only. We can represent this as the expectation value of an operator $\mathcal{O}_A$ which only acts on the Hilbert space of system A (or if we think of A and B as two spatially distinct regions, we might say $\mathcal{O}_A$ is only supported in A). We might write the expectation value in the following way

$$\langle \mathcal{O}_A \rangle = \mathrm{Tr}_{\mathcal{H}_A \otimes \mathcal{H}_B}(\rho_{A\cup B}\, \mathcal{O}_A) = \mathrm{Tr}_{\mathcal{H}_A}(\mathrm{Tr}_{\mathcal{H}_B}(\rho_{A\cup B})\mathcal{O}_A), \tag{1.6}$$

where we use the fact that the summation over states in system B can be performed separately, since the operator only acts on the Hilbert space of system A. Any effect of system B on the measurement performed by $\mathcal{O}_A$ on system A is now contained in the *reduced density matrix*

$$\rho_A = \mathrm{Tr}_{\mathcal{H}_B}(\rho_{A\cup B}). \tag{1.7}$$

If the system is separable, i.e. it can be written as $|\Psi\rangle^{\mathrm{sep}}_{A\cup B} = |\psi\rangle_A \otimes |\phi\rangle_B$, then the density matrix can be written as $\rho^{\mathrm{sep}} = |\psi\rangle_{AA}\langle\psi| \otimes |\phi\rangle_{BB}\langle\phi|$, and the reduced density matrix for system A becomes

$$\rho_A = \mathrm{Tr}_{\mathcal{H}_B}(\rho^{\mathrm{sep}}_{A\cup B}) = |\psi\rangle_{AA}\langle\psi|, \tag{1.8}$$

which is again a pure state.

If, however, the system is not separable, as is the case in the above Bell state (1.5), then the reduced density matrix becomes,

$$\rho_A = \mathrm{Tr}_{\mathcal{H}_B}(\rho^{\mathrm{Bell}}_{A\cup B}) = \frac{1}{2}\left(|\uparrow\rangle_{AA}\langle\uparrow| + |\downarrow\rangle_{AA}\langle\downarrow|\right). \tag{1.9}$$

This reduced density matrix cannot be written in the form $\rho = |\psi\rangle\langle\psi|$, and we say that system A is in a mixed state. We see that for a total system in a pure state, we can determine whether it is separable or not by considering the reduced density looking at

the reduced density matrix: for any separable state the reduced density matrix will be also that of a pure state, but for an entangled state, the reduced density matrix will be that of a mixed state. The entanglement is encoded in the spectrum of the reduced density matrix. However, we would like to find a single measure of the "amount" of entanglement between two systems, without having to compute all the eigenvalues of the reduced density matrix.

The above suggests we measure the entanglement between A and B by measuring the 'mixedness' of the reduced density matrix by computing its von Neumann entropy. In this context, it is usually referred to as *Entanglement Entropy* (EE):

$$S_A = -\operatorname{Tr}_{\mathcal{H}_A}(\rho_A \ln \rho_A). \tag{1.10}$$

Similarly, one may define

$$S_B = -\operatorname{Tr}_{\mathcal{H}_B}(\rho_B \ln \rho_B). \tag{1.11}$$

For pure states, we have $S_A = S_B$, since the eigenvalues of ρ_A and ρ_B are the same, and the EE depends only on the eigenvalues. The EE has several nice properties: additivity, convexity[10], and basis independence. For pure states, it turns out that any entanglement monotone that is additive on pure states and "sufficiently continuous"[11] must equal S_A on all pure states [45–47]. This uniqueness originates from the fact that the pure state entanglement can asymptotically be manipulated in a reversible manner [48] under LOCC. However, for mixed states the situation is less clear: the EE contains a contribution due to classical entropy, as well as entanglement[12].

1.2.2.4 Mixed states: Negativity

Finding a suitable entanglement measure in mixed states is less straightforward than in pure states. Firstly, as mentioned above, the EE acquires a classical contribution. Secondly, to identify entangled states, Bell inequalities are no longer a good indication, due to the existence of mixed entangled states that nevertheless allow for a LHV description (so-called "Werner states") [43]. These Werner states have the additional property that it is sometimes possible to *distill*[13] from many copies of a Werner state a new state

[10] which amounts to stating that the loss of classical information does not increase entanglement
[11] by which we mean, asymptotically continuous
[12] In fact, there is no unique measure of entanglement in mixed states, at least under LOCC
[13] see [48] for details on distillation

that does violate some Bell inequality [49]. Several measures for entanglement in mixed states have been proposed. One is *distillable entanglement*, which is a measure of how much entanglement can be extracted from a state using only LOCC. Another measure is the *entanglement of formation*, which is the entanglement required to create some state. Whilst for pure states these measures are both equal to the entanglement entropy, as they should, they are difficult to compute. For that reason, we will instead consider another measure based on the spectral data of the partial transpose of the reduced density matrix. A necessary condition for separability of a given density matrix is the positivity of the partial transpose of the density matrix [50], usually called the PPT criterion, or Peres criterion. Again considering a bipartite system, the criterion dwells on the fact that the partial transpose $((\rho^{\text{sep}}_{A\cup B})^{T_B} = \sum_i p_i \rho^i_A \otimes (\rho^i_B)^T$ of a separable density matrix ($\rho^{\text{sep}}_{A\cup B} = \sum_i p_i \rho^i_A \otimes \rho^i_B$) found by transposing one of the constituent density matrices is a valid density matrix. This readily follows from the fact that the transposed matrix $(\rho_B)^T$ is a valid density matrix, which leads to the positivity of the eigenvalues of $\rho^{T_B}_{A\cup B}$. Having a positive partial transpose is therefore a necessary criterion for separability. However, it is only sufficient for composite systems having dimensions 2×2 and 2×3 (two-qubit/qubit-trit systems), not for systems with a higher dimensional Hilbert space [51][14]. A quantitative measure of entanglement based on the PPT-criterion is the *negativity*, defined as

$$\mathcal{N} \equiv \frac{||\rho^{T_B}||_1 - 1}{2}, \tag{1.12}$$

where $||\rho^{T_B}||_1$ is the trace norm of the auxiliary matrix ρ^{T_B}, which is just the sum of the absolute values of its eigenvalues λ_i. In order to understand the meaning of the term "negativity", note that the trace of a matrix is invariant under partial transposition,

$$\text{Tr}(\rho^{T_B}) = \sum_i \lambda_i^{(+)} + \sum_j \lambda_j^{(-)} = \text{Tr}(\rho), \tag{1.13}$$

so the negativity is given by

$$\mathcal{N}(\rho) = \frac{1}{2}\left(\sum_i |\lambda_i^{(+)}| + \sum_j |\lambda_j^{(-)}| - 1\right) = \sum_j |\lambda_j^{(-)}|, \tag{1.14}$$

hence the name.

[14] although density matrices with positive partial transpose (PPT) have zero distillable entanglement - they may only have what is called *bound entanglement*.

The negativity is an entanglement monotone, but it is not additive. Therefore, a different measure is often used instead, namely the *logarithmic negativity*:

$$\mathcal{E}(\rho) = \ln ||\rho^{T_B}||_1, \tag{1.15}$$

which is trivially related to the negativity via the relation $\mathcal{N} = (e^{\mathcal{E}} - 1)/2$.

Both the negativity and the logarithmic negativity have the property that they are entanglement monotones [52, 53], although they do not reduce to the entanglement entropy for pure states[15]. Nevertheless, a significant advantage to considering negativity as a measure of entanglement is that it is based on properties of the density matrix, and therefore computable for larger systems.

1.3 Quantum quenches

A *quantum quench* is defined as an instantaneous change in the parameters that determine the dynamics of an isolated[16] quantum system. By instantaneous, we mean that the change is done in a time interval much shorter than any characteristic time scale of the model. This means that if initially the system was in the ground state, there is no time for the system to relax to the new ground state. Typically, one expects the state after the quench to evolve in time. To make this more precise, let us say that at $t = 0$, the system is in the ground state $|\psi_0\rangle$ of a Hamiltonian H_0. Then at $t > 0$ we instantaneously change some parameter of the Hamiltonian, thus obtaining a different Hamiltonian H such that $[H_0, H] \neq 0$. The state after the quantum quench is then simply $|\psi(t)\rangle = e^{iHt}|\psi_0\rangle$.

These quenches fall into two categories: a *global quench* is a change in parameters of the Hamiltonian that is translationally invariant, whereas under a *local quench* the change happens only in one or more localized regions. Examples of a global quench are the change of a mass parameter or homogeneous external magnetic field, and an example of a local quench is a sudden change of boundary conditions, for example as might be the result of adding links to connect two chains together. An important difference is that

[15] For pure states the logarithmic negativity is related [52] to the Rényi entropy of B for $n = 1/2$: $\mathcal{E} = S_B^{1/2} = 2 \ln \operatorname{Tr} \rho_B^{1/2}$.

[16] i.e. unitary time evolution

the energy added to the system after a local quench is often negligible, whereas after a global quench it may be quite large.

One of the first examples of a global quantum quench that was studied is the XY-Ising chain in a transverse field [54–57]. Using the mapping to free fermions, the time evolution of the transverse magnetization after an instantaneous change of the external transverse field was computed exactly. Much progress was made by Calabrese and Cardy, who studied quantum quenches where the post-quench Hamiltonian describes a conformal field theory (CFT). In their arguments they use a path integral approach and the well-known mapping of the quantum problem to a classical one in $d+1$ dimensions. The initial state $|\psi_0\rangle$, which is the ground state of the Hamiltonian H_0 with a mass gap m_0, plays the role of a boundary condition. In case of the $1+1$ dimensional problem, powerful techniques of boundary conformal field theory can be applied to study the time evolution of the entanglement entropy [58] as well as correlation functions [59, 60]. For the relaxation of a primary field operator Φ from the initial state $|\psi_0\rangle$, they found

$$\langle \Phi(t) \rangle \propto e^{-x\pi t/2\tau_0}, \tag{1.16}$$

$$\langle \Phi(\ell,t)\Phi(0,t)\rangle - \langle \Phi(0,t)\rangle^2 \propto \begin{cases} 0 & \text{for } t < \ell/2, \\ e^{-x\pi\ell/2\tau_0} - e^{-x\pi t/\tau_0} & \text{for } t > \ell/2, \end{cases} \tag{1.17}$$

where τ_0 is a non-universal constant and x is the scaling dimension of $\Phi(\ell)$. What is interesting to note is that both before and after the quench the system is in a pure state. Before the quench, it is described by CFT at temperature $T=0$, so there is no energy scale in the system, and correlation functions decay algebraically. After the quench, although the system is still in a pure state, correlation functions decay exponentially[17]. Their findings allowed a simple interpretation in terms of classical quasi-particles. The initial state $|\psi_0\rangle$ has an (extensively) high energy relative to the ground state of the Hamiltonian H, which governs the subsequent time evolution, and therefore acts as a source of quasi-particle excitations. Those quasi-particles originating from closely separated points (roughly within the correlation length ξ_0 of the ground state of H_0) are quantum entangled and particles emitted from points far away from each other are incoherent. If the quasi-particle dispersion relation is $E=\omega_k$, the classical group

[17] One way to think about this might be that although the system before and after the quench remains isolated, and therefore in a pure state, the quench involves pumping a potentially large amount of energy into the system, which in real life might be thought of as connecting it to a large reservoir.

velocity is $v_k = \partial_k \omega_k$. We assume that there is a maximum speed $v_m = \max_k |v_k|$. A quasi-particle of momentum k produced at ℓ is therefore at $\ell + v_k t$ at time t, assuming scattering effects can be ignored. These free quasi-particles have two distinct effects. Firstly, incoherent quasi-particles arriving at a given point ℓ from well-separated sources cause relaxation of (most) local observables. Secondly, entangled quasi-particles arriving at the same time t at points with separation $|\ell| \gg \xi_0$ induce quantum correlations between local observables. In the case where they travel at a unique speed v (as is the case for a CFT), therefore, there is a sharp "horizon" or light-cone effect: the connected correlations do not change from their initial values until time $t \sim |\ell|/2v$. After this time, they rapidly saturate to time-independent values. For large separations (but still much smaller than $2vt$), these decay exponentially.

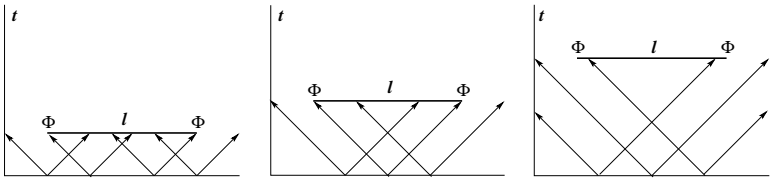

FIGURE 1.3: There is a *horizon effect*: correlations only begin to change after points come into mutual causal contact. Local observables with separation ℓ become correlated when left- and right-moving particles originating from the same spatial region $\sim m_0^{-1}$ can first reach them. In the first picture $2vt \ll \ell$, and the two fields $\Phi(0)$ and $\Phi(\ell)$ are still uncorrelated: $\langle \Phi(\ell)\Phi(0)\rangle \sim \langle \Phi \rangle^2$. In the middle figure they are just starting to be correlated, and in the last picture the correlation looks thermal: $\langle \Phi(\ell)\Phi(0)\rangle \sim e^{-2\pi \Delta_\Phi \ell / v\beta}$.

In this thesis, we will consider an example of a local quench, which will be described in the next section.

1.4 "Thermal cut-and-glue quench": connecting infinite thermal reservoirs

The transport properties of condensed matter systems are often measured by driving currents externally and measuring the resulting voltages or temperature differences. In cold atomic gas clouds, on the other hand, transport is more often measured by setting up transient out-of-equilibrium initial conditions and measuring the subsequent relaxation towards equilibrium. One such setup in which one can study the dynamics of a system that relaxes not to equilibrium, but to a nonequilibrium steady state (NESS), can be made by connecting the system to at least two thermal baths (or: reservoirs). This is

similar to when one connects a quantum system to a large bath to bring it in thermal equilibrium, but now one connects it to different baths, at different temperatures. The influence of the baths is to provide a way for the system to dissipate energy to, and at the same time energy can flow from the bath to the system.

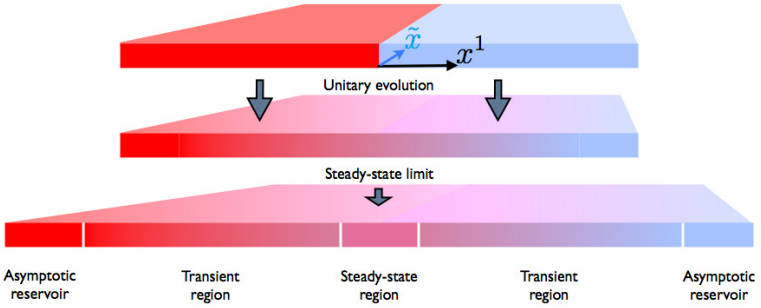

FIGURE 1.4: We consider two semi-infinite critical systems, initially thermalized at different temperatures. At time $t = 0$, the systems are connected along the directions in $\tilde{x}$, so that energy can flow between them in the x^1 direction. After time t, there is a sharply defined region of size $R \propto t$ in which there is a steady state description. We want to consider the behaviour of the entanglement between the left- and right baths as time evolves, and the energy current and its fluctuations in the steady state. (figure taken with permission from [61])

An simple example of such a setup is the so-called "cut-and-glue" quench, which is a local quench in which two systems are initially thermalised at different temperatures, and suddenly connected to allow energy to flow between them (see Figure 1.4). More precisely, the initial, disconnected, Hamiltonian is given by $H_0 = H^l + H^r$, where $H^{l/r}$ are the Hamiltonians of the left- and the right system, respectively. After the quench, the system is allowed to evolve unitarily with a Hamiltonian given by $H = H_0 + \Delta H$, where ΔH represents the connection between the left and the right system. Note that in general we do not need to know the detailed form of this term, but we do know that it does not commute with H_0, and that its contribution to the total energy is vanishingly small.

Since the total system including the baths can be considered isolated, the time evolution of the total system is unitary. The density matrix can then be related to the equilibrium density matrix by evolving unitarily with the full Hamiltonian:

$$\rho(t) = e^{-iHt}\rho(0)e^{iHt}, \tag{1.18}$$

where the equilibrium density matrix $\rho(0)$ corresponds to the system before it was connected to the baths, and the time evolution after connection is with the full Hamiltonian

of the system connected to the baths.

Constructing a steady state in this way, as a part of a larger system, has the advantage that one may consider models that are exactly solvable. Examples are free models of fermions or bosons. More generally, one can look at models that have interactions, but are integrable. In the case of a one-dimensional system, these may be solvable using Bethe Ansatz techniques if they are integrable, or when they are critical they can be described exactly using a Virasoro algebra.

1.4.1 Existence of the steady state

One may expect a steady state to occur after sufficient time in some finite region around the connection point. More precisely, for a local observable, the system will appear to be in a steady state if we take the limit of infinite system size, followed by the limit $t \to \infty$, keeping the support ℓ of the observable constant.

$$\langle \mathcal{O} \rangle_{\text{stat}} := \lim_{L \gg vt \to \infty} \langle \mathcal{O} \rangle (L; t), \qquad v, \ell \text{ constant.} \tag{1.19}$$

In this limit, the thermal reservoirs are infinitely far away, and excitations cannot reach the endpoints and be reflected, thus creating correlations. For a discussion of this limit, see [62–64].

The first study of the steady state limit (1.19) was done for the classical harmonic chain [65]. For quantum models, the XY model was treated in [66, 67], and for certain conditions in [68].

If the combined system can be described by a conformal field theory, it has been proved that after a suitable limit the system converges toward a steady state [1, 69].

Generically, one expects local thermalization to occur, and the heat current will satisfy Fourier's law (1.1). In the steady state limit (1.19) it is clear that since no part is kept at a fixed temperature, and the baths are effectively infinitely far apart, the gradient term in (1.1) goes to zero, and a purely diffusive current therefore also goes to zero. Nevertheless, a finite current may be supported if it has a ballistic component.

We expect there to be ballistic transport if there are certain conserved quantities to support the current, which is expected to be the case for the energy current in any integrable system [70–72]. In this many-body quantum system, we have ballistic transport if there is a nonzero current. In that case the density matrix in the region described by a steady state is the exponent of a sum of conserved charges. Another situation in which the energy current is conserved is close to a critical point, as the lattice effects are washed out by the long-range correlations, and the system becomes effectively translation invariant[18].

1.4.2 Research question

The aim of this thesis is to better understand the state of a one-dimensional quantum system after the thermal cut-and-glue quench. We will build upon previous work [1, 73], where the idea of a nonequilibrium steady state density matrix for energy transfer between two critical quantum wires was developed in the context of CFT. The authors proved that these systems converge towards steady states, and gave a general description of such non-equilibrium steady states in terms of quantum field theory data. They also computed the large deviation function of charge and energy transfer through the contact.

[18] In real life, we should get diffusive transport after a long time (which one cannot reach in simulations), due to the system being away from criticality because of the finite (though small) temperature.

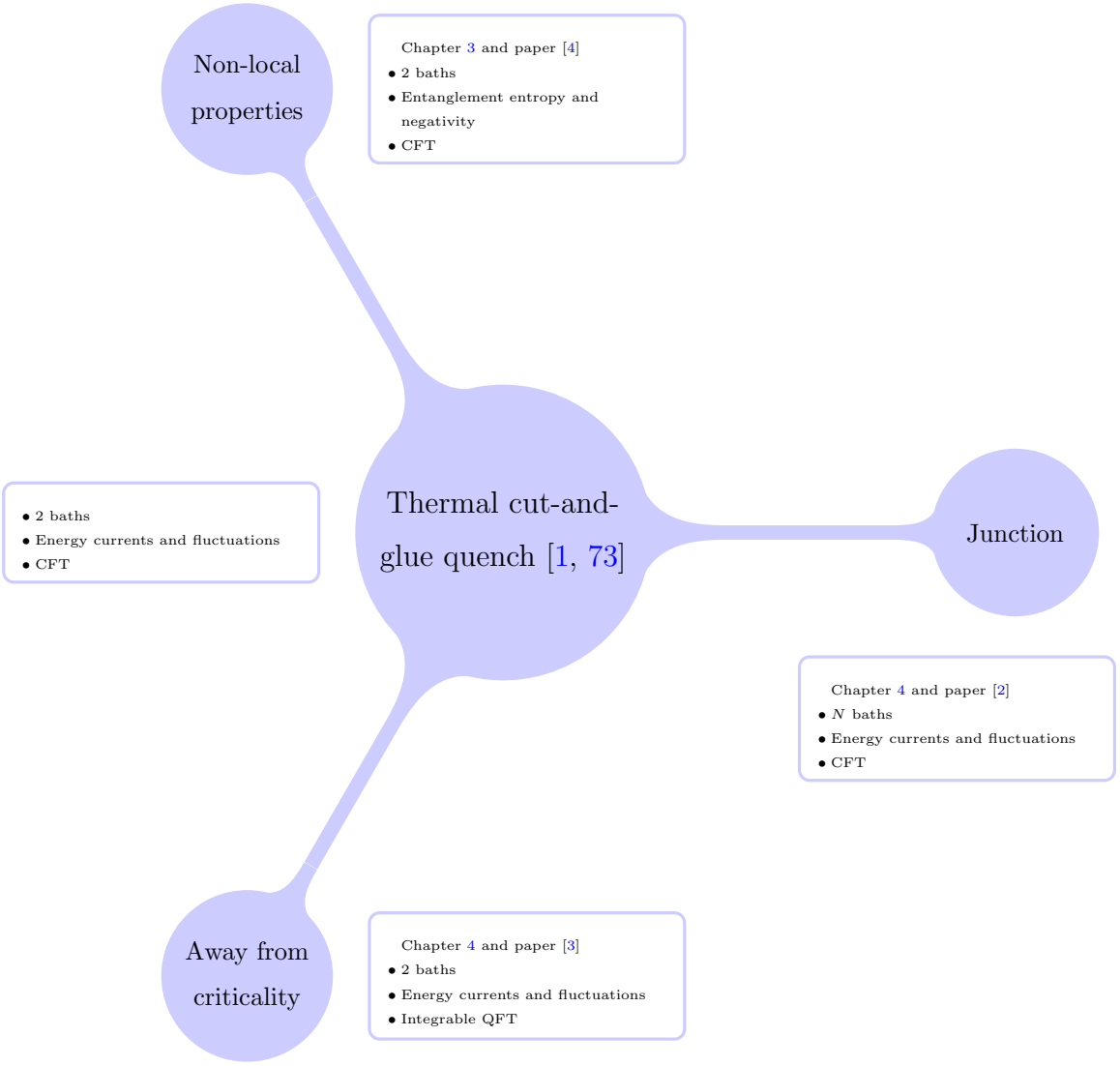

The results in [1, 73] are specific to the operators (energy and charge) that are considered, and describe the steady state. As discussed in section 1.2, one can learn more about the nonequilibrium state of the system after connecting the baths by studying properties of the density matrix, such as the entanglement entropy or the logarithmic negativity. Of these two, the latter is a good measure for entanglement in our setup, and we find general results for the case of two critical systems that have factorised pairing, which we will discuss in Chapter 3.

Furthermore, one may wonder how general the results in [1, 73] are when one considers a similar setup but for N systems connected in a specific way at one point (see Chapter 4 and [2] for details). One of the interesting questions to ask is if in this situation again universal fluctuation relations hold.

Another generalization one can make is to consider the same setup as in [1, 73], but for states that are not conformally invariant. In reality, tuning a system exactly to criticality is very difficult, and one expects a small gap to be present in the description. Therefore, the next generalization is the calculation of the steady-state energy current for general massive integrable QFT[19] (see Chapter 4 and [3]).

1.5 Outline of this thesis

Chapter 2 is an introduction to the description of the two types of one-dimensional quantum systems we will consider: the first are in the quantum critical regime, so that they can be described by a continuous gapless model, or a CFT. The second are perturbations away from criticality, so that the description is that of a continuous system with a gap. We will consider only the case in which the description is still integrable, and a description can be found using thermodynamic Bethe ansatz (TBA).

The next two chapters are devoted to the research papers on which this thesis is based:

In Chapter 3 we review the entanglement entropy and negativity in extended systems, both at zero temperature and finite temperature. This chapter concludes with the paper [4], written together with Benjamin Doyon, which appeared in the journal Nuclear Physics B.

Chapter 4 contains an introduction to thermodynamics away from equilibrium, and a more detailed description of the local quantum quench which we consider, and the steady state which occurs at late times. This chapter contains the paper [2], written together with Benjamin Doyon and Denis Bernard, which appeared in the Journal of Statistical Physics, as well as the paper [3], which is a collaboration with Olalla Castro-Alvaredo, Yixiong Chen and Benjamin Doyon, and which appeared in the Journal of Statistical Physics.

Finally, Chapter 5 contains a discussion of the results of the papers [2–4], as well as ideas for future directions this research could take.

[19] for which the form of the density matrix in the steady state was predicted in [74]

Chapter 2

One-dimensional (near-)critical quantum systems

In this chapter we will give a description of the physics of many-body quantum systems that are close to a so-called quantum critical point (QCP), which is the point in the phase diagram at which a continuous phase transition occurs due to a non-thermal control variable. Close to such a continuous quantum phase transition, a many-body system can be effectively described by a quantum field theory (QFT), with a mass that goes to zero as the system is tuned to criticality. The scale invariant field theory at the critical point often has additional symmetries, so that the QCP can be described by a Conformal Field Theory (CFT). We will consider general properties of CFTs. In the special case of two dimensions, we will find that a CFT has an infinite number of conserved charges, allowing us to find exact expressions for some correlation functions. We will then describe the situation in which the system is tuned away slightly from this quantum critical point, in such a way that the system can be described by a massive QFT, considering only the special case in which there still are infinitely many conserved quantities and the resulting system is an Integrable Quantum Field Theory (IQFT). We will review how the thermodynamics of this system can be described using the thermodynamic Bethe ansatz (TBA).

2.1 Many-body quantum systems

The microscopic constituents of matter are fairly well understood. At least at the level of protons, neutrons and electrons we have a good way of describing how these interact. There are several length scales that are important in finding a description of the system. One is a microscopic scale a at which interactions typically take place (for example the lattice spacing). Another may be the total size of the system. When many of these individual particles interact with each other, interesting things happen: the particles can form various types of ordered phases, or be in a phase that is completely disordered. Often the behaviour of the whole does not simply reflect the interactions at the microscopic level, and one can see very similar macroscopic behaviour in very different materials, or conversely, the tiniest change of temperature, pressure or magnetic field can have a profound effect on the macroscopic behaviour of the material. This is due to the fact that as many particles interact with each other, collective behaviour can emerge that is very different from the microscopic behaviour of the individual particles. The length scale ξ at which the behaviour changes is called the *correlation length*. For example, if you take a piece of material and break it up into smaller and smaller pieces, the macroscopic properties of the pieces do not change until you reach a size of around the correlation length.

The correlation length depends on the coupling constants of the theory describing the system, and it can therefore be varied by changing the parameters (temperature, pressure, external magnetic field, etc.). A special phase of the system is the *critical* phase, in which the correlation length is infinite, and fluctuations exist on all length scales. These are the critical points in the phase diagram at which a continuous phase transition occurs, and these turn out to have many special properties that make them both interesting and amenable to calculation. When a system is close enough to a critical point, the correlation length becomes much larger than the microscopic length scale: $\xi \gg a$, and one assumes that the lattice degrees of freedom at nearby lattice sites co-vary. This allows for an effective description in terms of a continuous function. This effective field theory description is very powerful, as it describes states in terms of excitations rather than the constituent particles, which means it is a good description of the important physics. Such a description turns out to be convenient for spotting symmetries that are very important in understanding phase transitions. Furthermore, as this description

does not include the microscopic details, its results may be applicable to a wider range of systems that share similar large-scale behaviour.

2.1.1 Scaling limit

The basic constituents that we will be looking at when describing quantum systems are quantum expectation values, as these could in theory be measured. These can be local observables $\langle \mathcal{O}(x) \rangle$, such as the local magnetisation at a site on the lattice, but one can also look at how these observables co-vary. This is measured in a *correlation function* $\langle \mathcal{O}(x)\mathcal{O}(y) \rangle$, which quantifies how microscopic variables co-vary across space and time. These correlation functions are a measure of order in a system.

Considering a one-dimensional lattice model, these observables $\mathcal{O}(x)$ will take values on the sites of the chain, so x then takes discrete values $i\,a$ with $i = 1, 2 \ldots$, and with a the lattice spacing. In the following, we will be interested in situations in which the fluctuations on the scale of the lattice spacing can be ignored. As discussed above, this is the case when a system is close enough to a critical point, and it can then be described more conveniently by taking the *scaling limit*, which is the limit where the lattice spacing a is sent to zero whilst keeping the correlation length (and the domain) fixed. Whether the scaling limit can be taken depends on the existence of the limit

$$\lim_{a \to 0} a^{-\sum_i^n \Delta_i} \langle \mathcal{O}_1(x_1) \cdots \mathcal{O}_n(x_n) \rangle = \langle \phi_1(x_1) \ldots \phi_n(x_n) \rangle, \tag{2.1}$$

where the powers $\{\Delta_i\}$ needed to regulate the expression are called the *scaling dimensions* of the fields $\{\phi_i\}$. Note that on the left-hand side of (2.1), we must understand the $\{x_i\}$ to mean "the nearest lattice sites to the points $\{x_i\}$". In the limit $a \to 0$, they take continuous values. The scaling limit is only valid for non-coincident $\{x_i\}$, and the correlation functions in (2.1) are singular when two fields coincide. However, it seems natural to assume that in the limit that two fields coincide, the properties of this composite field become those of a local field. Then, assuming that at each point we have a complete basis $\{\phi_i\}$, we can expand this composite field in the same local basis using the *operator product expansion* (OPE):

$$\langle \ldots \phi_i(x_i)\phi_j(x_j) \ldots \rangle = \sum_k C_{ijk}(x_i - x_j) \langle \ldots \phi_k(x_j) \ldots \rangle. \tag{2.2}$$

When $|x_i - x_j|$ is smaller than the separation between x_i and all other arguments in the correlation function, the coefficients C_{ijk} are independent of whatever else is inside the correlator. For the sake of brevity, one therefore often writes

$$\phi_i(x_i)\phi_j(x_j) = \sum_k C_{ijk}(x_i - x_j)\phi_k(x_j), \tag{2.3}$$

where it is understood that this equality is only valid inside a correlator, and in the limit $x_i \to x_j$. Since the correlation functions in the scaling limit do not depend on the lattice spacing a, one might as well have started with a different lattice spacing which is a fraction of the original: a/b. At the same time, this new model would be the same as having the original lattice spacing a, but multiplying all length scales in the system by b. Thus, we conclude that correlation functions in the scaling limit transform under scale transformations as

$$\langle \phi_1(bx_1) \dots \phi_n(bx_n)\rangle = b^{-\sum_{i=1}^n \Delta_i} \langle \phi_1(x_1) \dots \phi_n(x_n)\rangle. \tag{2.4}$$

The above scale transformation is often denoted as a transformation of the scaling field,

$$\phi(bx) = b^{-\Delta}\phi(x). \tag{2.5}$$

2.1.2 Effective description (Renormalisation group)

In the scaling limit, correlation function away from a critical point behave in the limit $|x - y| \to \infty$ as

$$\langle \phi(x)\phi(y)\rangle \sim e^{-|x-y|/\xi}, \tag{2.6}$$

where a is the lattice spacing and ξ the correlation length, indicating that observables tend to be uncorrelated on length scales larger than the correlation length. In a continuous description of the system in terms of the scaling fields $\phi(x)$, ξ will typically be proportional to the inverse of the mass of the lightest field.

Exactly at the critical point, the correlation length diverges (i.e., the mass scale goes to zero and the spectrum becomes gapless), and correlation functions behave like powers of the distance:

$$\langle \phi(x)\phi(y)\rangle \sim |x - y|^{-\Delta}, \qquad \xi = \infty, \tag{2.7}$$

where Δ is the scaling dimension of the field ϕ.

The behaviour of the correlation functions away from a critical point (2.6) and exactly at a critical point (2.7) tell us how fluctuations behave at different length scales: away from the critical point one can divide fluctuations into short-range fluctuations (on distance scales much shorter than the correlation length) and long-range fluctuations (on distance scales much longer than the correlation length), whereas at the critical point this division cannot be made and the system becomes scale invariant.

One can make these ideas exact by applying the ideas of the *renormalisation group* (RG) to phase transitions. An RG transformation is like 'zooming out' and looking at the same system from a larger distance, which makes sense, since a phase transition is a change in the macroscopic properties of a system. When describing the system near such a transition, one is not interested in its microscopic details, but rather the effective behaviour of many particles which becomes important at large length scales. The renormalisation group is a method of coarse-graining the description of the system, such that the large-length scale behaviour can be obtained.

Starting from a microscopic Hamiltonian describing a system with a short-distance (lattice) cutoff a, a renormalisation group (RG) transformation can be made by increasing the short-distance cutoff a by a certain factor and integrating out the degrees of freedom below this distance scale (coarse-graining). In order to compare the coarse-grained theory to the original model, one then rescales the distances and fields. After the RG transformation, the cutoff is the same as before the coarse-graining. If the integration has produced new couplings, these must be added to the original Hamiltonian, and the RG transformation is iterated, until no new terms appear. A single RG transformation is also called an *RG step*. One then compares the Hamiltonian before and after the transformation. The coupling constants in the Hamiltonian typically change after coarse-graining and rescaling. If after an RG step the coupling strength of a term increases, this term is called *relevant*, since at longer distances it will become more important. Conversely, if a coupling constant becomes smaller when looking at larger distance scales, it corresponds to an *irrelevant* term[1]. A coupling constant which does not change after an RG step is called *marginal*.[2]

[1] Irrelevant operators are operators that blow up in the UV, and are non-renormalisable. Adding irrelevant operators means that a different UV theory should be started from.

[2] Usually the RG equations can not be solved for the exact Hamiltonian and are solved perturbatively. One generally expects relevant terms to remain relevant, and irrelevant terms to remain irrelevant.

By taking the limit in which the rescaling is infinitesimal, one can obtain a set of differential equations called RG equations[3] for the coupling constants, which involve so-called *beta-functions*:

$$\frac{d\{g\}}{dl} = \beta(\{g\}) \tag{2.8}$$

where $\{g\}$ is the collection of coupling constants depending on l, and $l = \ln b$, where b is the length scale of the coarse-graining in the RG step.

In general, after an RG transformation, the system will have a smaller correlation length. Exceptions are when the correlation length before the RG step is either zero of infinity. These are called RG fixed points, and they correspond to points in the space of couplings where the system is scale invariant and the beta-function vanishes[4]. If all perturbations around this fixed point are (ir)relevant, then the fixed point is a repulsive (attractive) fixed point. In general, a fixed point will have both relevant and irrelevant directions. Such a fixed point is called a separatrix, and it is these types of fixed points that describe the critical points of a phase transition (see Figure 2.1)[5].

A typical RG flow describing a real-life system starts at a point in the space of couplings which is not a fixed point. We will call this the 'physical point', and the system is described by a theory which has as bare parameters these 'physical' values of the coupling constants and as a short-distance cutoff the spacing between the important degrees of freedom (e.g. spins, etc.). This is typically the lattice spacing. When a system is not tuned to a fixed point, an RG transformation will cause the theory to flow to a different theory with smaller correlation length giving the behaviour of the system at slightly longer distances. Following the flow all the way down to zero correlation length, one ends up in a scale invariant theory describing the ultra-long distance behaviour:

Exceptions to the latter rule are termed "dangerously irrelevant". Operators that are marginal to first order and become relevant at higher order are termed "marginally relevant".

[3] Note that this is a *local* equation in energy scale.

[4] A theory may be scale invariant for all couplings, in which case it has a beta function which is identically zero, or it may have some points in the space of all couplings for which beta function has a zero. In the latter case perturbing the system will break the scale invariance and depending on the dimension of the perturbing operator, lead away from the fixed point (relevant) or back to the fixed point (irrelevant). This way, one can define stable and unstable fixed points as being fixed points where all small perturbations lead to an RG flow which brings the system away from the fixed point (unstable), or back towards the fixed point (stable). Typically, there will be both relevant and irrelevant perturbations in the space of all couplings

[5] The reason why the critical phase is so difficult to reach can be seen from the RG flow diagram of the critical surface and the fact that a parameter that tunes the system through a phase transition must correspond to a relevant operator.

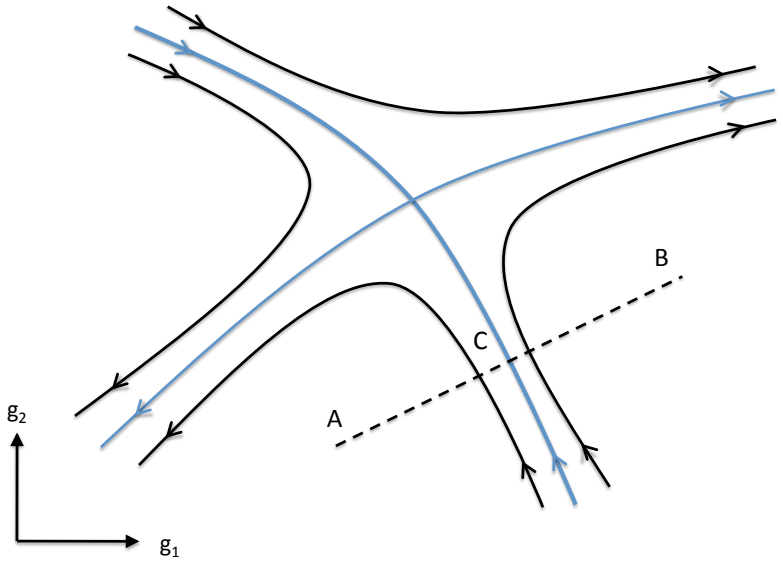

FIGURE 2.1: Renormalisation group flows near a fixed point with both a relevant and an irrelevant direction. A phase transition occurs when one tunes the system through the critical surface along a relevant direction which affects the value of ξ. The dotted line corresponds to the physical values of the coupling constants. The short-distance cutoff on the dotted line is typically the lattice spacing. Unless the system is at a fixed point, RG flows lead away from the physical line, towards a fixed point which gives the long-distance scale description (sometimes called IR fixed point). At points A and B, which do not lie on the critical surface, the correlation length is finite and RG flows will lead away from the critical surface, towards another fixed point which has $\xi = 0$ (not included in the figure). At point C, where the system is tuned through the critical surface, the correlation length is infinite, and the system flows towards the critical point.

an *IR fixed point*[6]. The flow towards the IR fixed point must be due to a relevant (or marginally relevant) field. This fact, and the fact that most fields are actually (marginally) irrelevant, means that only a handful of fields determine the IR fixed point. It is then possible for different systems to be described by the same IR fixed point. This is called *universality*.

[6]In some cases, one can also extend the flow back to the limit where the lattice cutoff goes to zero, by taking the system to be a low-energy description of a more general renormalisable quantum field theory. The passing to the general theory describing the high-energy limit is called *UV completion*. This general theory will have a *UV fixed point* which governs the ultra-short distance behaviour, from which the RG flow leads towards the physical point, and from there via the original RG flow to the IR fixed point.

2.1.3 Aside: the quantum-classical mapping

If one considers a d-dimensional quantum system in equilibrium that is close to a critical point, one can describe its universal properties using a $D = d + 1$-dimensional classical field theory, where the extra dimension has a finite length corresponding to the inverse temperature of the quantum system. This is called the *quantum-classical mapping*. The heuristic explanation is as follows: consider a quantum system close to a critical point, so that we can consider the scaling limit and use the quantum field theory language to describe its universal properties. If the system has some finite inverse temperature $\beta = 1/k_B T$, then the partition function looks like

$$\mathcal{Z} \sim \mathrm{Tr} e^{-\beta H_{\mathrm{QFT}}}, \tag{2.9}$$

which in the language of path integrals looks like an evolution of an imaginary length $i\beta$ along the time direction. The trace causes this imaginary time direction to be periodic with length β. We therefore talk about temperature of the quantum system being equivalent to an imaginary time scale. More formally stated, a quantum model defined on a d-dimensional space R^d maps onto a classical model on $R^d \times S^1$, where the circle S^1 has circumference β. In particular, the classical model in infinite $d + 1$-dimensional spacetime maps onto a d-dimensional quantum model at zero temperature.

2.2 Conformal Field Theory in 2 dimensions

When a system is exactly at a critical point, it can be described effectively by a theory that is scale invariant, i.e. it is invariant under global dilatation of the length scale: $x \mapsto \lambda x$. If one further assumes that the system has local interactions and can be described in the scaling limit by a translationally invariant and rotationally invariant theory, then according to Polyakov [75] it is invariant under the more general *local* scale

transformations (or conformal transformations)[7]:

$$x \mapsto \lambda(x)x. \tag{2.10}$$

The conformal transformations are the transformations that locally leave angles invariant. It can therefore be described as a rescaling that is slowly varying in space.

In order to find the generators, we consider infinitesimal conformal transformations:

$$x^\mu \to x^\mu + \epsilon^\mu, \tag{2.11}$$

where in order for the transformation to be a conformal transformation, we must have that the metric $g_{\mu\nu}$ transforms in such a way that

$$ds^2 = g_{\mu\nu}dx^\mu dx^\nu \to \rho(x)\, ds^2, \tag{2.12}$$

where the Einstein summation convention is used. This means that

$$\partial_\mu \epsilon_\nu + \partial_\nu \epsilon_\mu \propto g_{\mu\nu}. \tag{2.13}$$

Comparing the trace of both sides, we find that an infinitesimal conformal transformation (2.11) must satisfy

$$\partial_\mu \epsilon_\nu + \partial_\nu \epsilon_\mu = \frac{2}{D}\, \partial \cdot \epsilon\, g_{\mu\nu}. \tag{2.14}$$

Note that in the following, we will always consider either flat Euclidean space, $g_{\mu\nu} = \mathrm{diag}(1, 1 \cdots, 1)$ or flat Minkowski space-time $g_{\mu\nu} = \mathrm{diag}(-1, 1, \cdots, 1)$. As a shorthand, we will denote two-dimensional Euclidean space with $D = 2$, and one-dimensional Minkowski space-time with $D = 1 + 1$.

In two-dimensional Euclidean space ($D = 2$), the condition (2.14) gives the Cauchy-Riemann equations,

$$\partial_1 \epsilon_2 = -\partial_2 \epsilon_1, \qquad \partial_1 \epsilon_1 = \partial_2 \epsilon_2, \tag{2.15}$$

[7] This is due to the fact that for a local theory one can define a stress-energy tensor, and using invariance of the action under translation, rotation and dilatation, one can deduce that the stress tensor must be conserved, symmetric and traceless. One can use these properties to show that the action is then invariant under the conformal transformations, which satisfy (2.10). One often assumes more generally that a physical system that is scale invariant is also invariant under the conformal group, as long as it is local. This is due to the fact that counterexamples are in fact rare (an example can be found though in [76]).

and we can use complex coordinates $z, \bar{z} = x_0 \pm i x_1$, $\epsilon, \bar{\epsilon} = \epsilon_0 \pm i\epsilon_1$, to see that in $D = 2$, an infinitesimal conformal transformation is a transformation (2.11) where $\epsilon = \epsilon(z)$ is a holomorphic function of z, and $\bar{\epsilon} = \bar{\epsilon}(\bar{z})$ anti-holomorphic. These can be represented as an infinite Laurent series

$$\epsilon(z) = \sum_{n=-\infty}^{\infty} \epsilon_n z^{n+1}, \tag{2.16}$$

and we find that the generators of these local transformations are

$$l_n = -z^{n+1}\partial_z, \quad \bar{l}_n = -\bar{z}^{n+1}\partial_{\bar{z}}, \qquad n = 0, \pm 1, \pm 2, \ldots, \tag{2.17}$$

which have the following commutation relations

$$[l_m, l_n] = (m-n)l_{m+n}, \qquad [\bar{l}_m, \bar{l}_n] = (m-n)\bar{l}_{m+n}, \qquad [l_m, \bar{l}_n] = 0, \tag{2.18}$$

also known as the Witt algebra. We see that in $D = 2$ CFT there is a decoupling in the holomorphic and anti-holomorphic degrees of freedom. In the following, therefore, we will generally consider only the holomorphic degrees of freedom, and assume that a similar relation holds for the anti-holomorphic degrees of freedom.

Note that the generators l_n and $\bar{l}_n$ are not all well-defined globally. By considering a conformal transformation $v(z) = \sum_n a_n l_n = -\sum_n a_n z^{n+1}\partial_z$, and writing it in terms of the coordinate $w = 1/z$, it can be seen that the only choice leading to a well-defined transformation everywhere is one which has all a_ns set to 0 except for a_{-1}, a_0 and a_1. The exact same holds for the anti-holomorphic generators. In fact, the generators $l_0, l_{\pm 1} \cup \{\bar{l}_0, \bar{l}_{\pm 1}\}$ form a finite subalgebra of globally defined infinitesimal conformal transformations, with l_{-1} and $\bar{l}_{-1}$ the generators of translations, $l_0 + \bar{l}_0$ the generator of dilatations, $i(l_0 - \bar{l}_0)$ the generator of rotations and l_1 and $\bar{l}_1$ the generators of special conformal transformations.

2.2.1 Primary fields

A generalization of the notion of vectors or tensors for the conformal group are called *primary fields*. These are fields that transform under a generic conformal mapping as[8]

$$\Phi_n(z,\bar{z}) \mapsto \left(\frac{\partial z'}{\partial z}\right)^{h_n} \left(\frac{\partial \bar{z}'}{\partial \bar{z}}\right)^{\bar{h}_n} \Phi_n(z',\bar{z}'), \tag{2.19}$$

where $\left(\frac{\partial z'}{\partial z}\right)$ is the Jacobian of the mapping, and $(h_n, \bar{h}_n)$ are called the conformal dimensions of the field[9]. Considering only the holomorphic part, correlation functions of primary fields therefore satisfy the relation

$$\langle \Phi_1(z_1)\dots\Phi_n(z_N)\rangle = \left(\frac{\partial z'}{\partial z}\right)^{h_1}_{z=z_1} \dots \left(\frac{\partial z'}{\partial z}\right)^{h_N}_{z=z_N} \langle \Phi_1(z_1')\cdots\Phi_N(z_n')\rangle. \tag{2.20}$$

For the two-point function, the conformal group in two dimensions completely restricts its dependence on z_1 and z_2: firstly, due to translation and rotation invariance (which has Jacobian of unity), the two-point function can only depend on $z_{12} := |z_1 - z_2|$, and secondly, due to the behaviour of primary fields under scale transformations, the function has to be of the form

$$\langle \Phi_1(z_1,\bar{z}_1)\Phi_2(z_2,\bar{z}_2)\rangle = \frac{c_{12}}{z_{12}^{h_1+h_2}} \tag{2.21}$$

with c_{12} a normalisation constant. We can determine this further by imposing covariance under the special conformal transformations, which impose $h_1 = h_2$ for $z_{12} \neq 0$.

Similarly, we find that the three-point function takes the form

$$\langle \Phi_1(z_1,\bar{z}_1)\Phi_2(z_2,\bar{z}_2)\Phi_3(z_3,\bar{z}_3)\rangle = \frac{c_{123}}{z_{12}^{h_1+h_2-h_3} z_{23}^{h_2+h_3-h_1} z_{13}^{h_1+h_3-h_2}}. \tag{2.22}$$

The coefficients c_{12} and c_{123} are related to the coefficients in the OPE (2.3), and in particular, the conformal gauge, which sets the leading term in the OPE of a field with itself to 1, means that the coefficient c_{12} in (2.21) is 1 for $\Phi_1 = \Phi_2$.

[8] If the transformation holds only for global conformal transformations, it is called a *quasi-primary field*.

[9] The combination $d_n = h_n + \bar{h}_n$ is called the *anomalous scaling dimension*, and $s = h_n - \bar{h}_n$ the *spin* of the field $\Phi_n(z,\bar{z})$.

For $n \geq 4$ the correlation functions cannot be determined completely, since it is now possible to create conformally invariant cross ratios, e.g.

$$\frac{z_{12}z_{34}}{z_{13}z_{24}}, \tag{2.23}$$

and the correlation functions can only be defined up to an arbitrary function of all the cross ratios, of which there are $N(N-3)/2$ for an N-point function. For instance, a 4-point function depends on two cross ratios, and has the general form:

$$\langle \Phi_1(z_1,\bar{z}_1)\Phi_2(z_2,\bar{z}_2)\Phi_3(z_3,\bar{z}_3)\Phi_4(z_4,\bar{z}_4)\rangle = \mathcal{F}(x,\bar{x}) \prod_{i<j} z_{ij}^{-(h_i+h_j)+h/3} \prod_{i<j} \bar{z}_{ij}^{-(\bar{h}_i+\bar{h}_j)+\bar{h}/3}, \tag{2.24}$$

where $h = \sum_{k=1}^{n} h_k$ (similar for $\bar{h}$) and we note that the different conformally invariant cross ratios for 4 points are not independent, as they satisfy the relations

$$x = \frac{z_{12}z_{34}}{z_{13}z_{24}}, \qquad 1-x = \frac{z_{14}z_{23}}{z_{13}z_{24}}, \qquad \frac{x}{1-x} = \frac{z_{12}z_{34}}{z_{14}z_{23}}. \tag{2.25}$$

2.2.2 Energy momentum tensor

We may want to explore the conserved quantities associated to the global symmetries that conformal field theories exhibit. The energy momentum tensor $T_{\mu\nu}$ is the matrix of conserved currents associated to translation invariance:

$$\partial^{\mu} T_{\mu\nu} = 0. \tag{2.26}$$

Invariance under rotations further implies that it is symmetric. In a CFT, there is also scale invariance, which implies that

$$T^{\mu}_{\mu} = 0. \tag{2.27}$$

In complex coordinates, we have $T_{z\bar{z}} = T_{\bar{z}z} = 0$, and for T_{zz} and $T_{\bar{z}\bar{z}}$ the above conditions can be rewritten as

$$\partial_{\bar{z}} T_{zz} = 0, \qquad \partial_z T_{\bar{z}\bar{z}} = 0, \tag{2.28}$$

so that we find that the energy momentum tensor has holomorphic and anti-holomorphic components:

$$T(z) \equiv T_{zz}, \qquad \bar{T}(\bar{z}) \equiv T_{\bar{z}\bar{z}}, \tag{2.29}$$

which tells us that at criticality, $T = T(z)$ is an analytic operator, and $\bar{T} = \bar{T}(\bar{z})$ is an anti-analytic operator, at least at the classical level (and in the case of short-range interactions).

For a quantum CFT in 2 dimensions, it is assumed that inside correlation functions these analytic properties continue to hold (except at positions where other fields are inserted).

We might wonder whether the energy momentum tensor is a primary field. The answer is that it is not: it transforms under a conformal transformation $z \mapsto f(z)$ as

$$T(z) \mapsto (\partial f)^2 T\left(f(z)\right) + \frac{c}{12} S(f, z), \tag{2.30}$$

with the Schwarzian derivative

$$S(f, z) = \frac{\partial_z f \partial_z^3 f - \frac{3}{2}(\partial_z^2 f)^2}{(\partial_z f)^2}, \tag{2.31}$$

and the *central charge* c, which is part of the basic data of a CFT (along with the scaling dimensions $(h_j, \bar{h}_j)$ and the OPE coefficients C_{ijk}). The constant c is called the central charge because as we will see later this term results in a so-called *central extension* of the conformal algebra (2.45). Its value depends on the model in question, and the value $\bar{c}$ of the central charge for the anti-holomorphic algebra is the same as c for theories that are Lorentz invariant and have conserved two point function of the stress tensor. The central charge is additive: if we take two field theories and add their actions without adding a coupling term between them, then their energy momentum tensors add together, as do their central charges[10]. Furthermore, for a two-dimensional field theory that is unitary, invariant under rotations, and for which conservation of the stress-energy tensor holds, there exists a function of the coupling constants $C(\{\lambda_i\}) \geq 0$

[10]For this reason, it is often said that the central charge can be interpreted as a measure of degrees of freedom.

that decreases along the RG flows, and is stationary only at the fixed points. Its value at the fixed points coincides with the central charge c of the corresponding CFTs[11].

2.2.3 Holomorphic factorisation

It is well known that, although holomorphic factorisation in CFT is true at the level of Virasoro representations – that is, the factors are local fields – it does not hold, generically, at the level of the operator algebra. That is, the OPE between fields $\varphi_i(x)$ and $\varphi_j(y)$ is generically not the product of the OPEs between their individual holomorphic, $\varphi_i^+(x)\varphi_j^+(y)$, and anti-holomorphic, $\varphi_i^-(x)\varphi_j^-(y)$, components. For instance, one may have the diagonal structure (here for spinless fields)

$$\varphi_i(x)\varphi_j(y) = \sum_k C_{ij}^k \bar{C}_{ij}^k (x-y)^{d_k-d_i-d_j}\varphi_k(y) \tag{2.32}$$

instead of the factorized structure

$$\varphi_i(x)\varphi_j(y) = \sum_{k,k'} C_{ij}^k \bar{C}_{ij}^{k'} (x-y)^{\Delta_k^+ + \Delta_{k'}^- - d_i - d_j}\varphi_k^+(y)\varphi_{k'}^-(y). \tag{2.33}$$

One may say that although holomorphic and anti-holomorphic components are local, they generically have semi-local properties with respect to the operator algebra.

It is known that the particular structure of the OPEs constitute additional data of the CFT model under consideration, which, along with the central charge, the set of modules involved and the chiral OPE coefficients, fully characterize the CFT model. This additional data may be referred to as the pairing data of the model. Because of the separation between the chiral and anti-chiral components of the stress-tensor (and of other symmetry currents), highest-weight modules always appear, in any OPE, in a factorized fashion, hence the only pairing data necessary is that identifying the pairing between modules.

The pairing of holomorphic and anti-holomorphic components is a manifestation, at the CFT level, of the fact that, at the quantum-chain level, time-evolved fields are not in general locally supported on end-points of the light-cone, but rather are supported on the full interval lying inside the light-cone. Formally, we may represent this pairing as a

[11] It was first proved by Zamolodchikov in [77], and later a proof in integral form was given by Cardy in [78].

connection between holomorphic and anti-holomorphic components, and this connection constrains the OPEs involving the separate components.

Models in which the pairing is trivially factorized are those that are completely built out of symmetry currents: those where all representations involved are the representations associated to the symmetry algebra itself. Free-boson (harmonic chains) and free-fermion models display this property. By construction, in a model with trivially factorized pairing, the OPEs of twist fields in the replica model also trivially factorizes.

2.2.4 Quantisation

In the operator formalism, time plays a special role. If we want to consider states in a quantum field theory, therefore, we must first think about the space they live in and their evolution. Usually, one defines a quantum field theory on space-time, with coordinates (t, x) (where x denotes all the spatial coordinates, and t the time direction. For a $D = 1 + 1$ theory, x contains only one coordinate). States are defined at a point in time (also called 'time slice'), and evolve in time under unitary time evolution with the Hamiltonian: $|\psi(t)\rangle = \exp(-itH)|\psi(0)\rangle$. In the quantum theory, states can be expressed in terms of local operators acting on a Hilbert space. If the spectrum of H is discrete, one can think of the creation and annihilation operators as ladder operators. In a conformal quantum field theory, however, this approach has a problem: the lack of an energy scale means the energy spectrum of the states is continuous, and disentangling the eigenstates from one another is difficult. If the system can be mapped to a CFT on Euclidean space (i.e. from $D = 1 + 1$ to $D = 2$), there is a way around this. Since the system is scale invariant, we can simply consider states on radial slices instead of time slices (see Figure 2.2), so that the dilatation operator $\hat{D}$ (here we added a hat to distinguish from the space-time dimenion D) plays the role of the Hamiltonian, and states evolve as $|\psi(r)\rangle = \exp(-ir\hat{D})|\psi(0)\rangle$. The spectrum of $\hat{D}$ is discrete, due to the fact that if 'time' runs radially outward (along the line of a scale transformation) then 'space' is perpendicular to that, and therefore our new spatial direction is compact. Note that $L_0 + \bar{L}_0$ generates dilatations (so this will play the role of the Hamiltonian), and $i(L_0 - \bar{L}_0)$ generates rotations (so this will play the role of the momentum operator).

FIGURE 2.2: In the usual quantisation, in terms of eigenstates of the Hamiltonian operator, we have time and space as seen in the left picture. For a scale invariant system, however, the Hamiltonian does not have a discrete spectrum, and instead the dilatation operator is used to construct a discrete spectrum. Since this is also a symmetry operator of a scale invariant system, this is possible, and results in a description in which time runs radially outward, and the spatial direction is the circle. In this description, an operator inserted at the origin corresponds with an 'in'-state.

In our new coordinates, the distance from the origin plays the role of time, and correlation functions are considered to be radially ordered:

$$\langle \phi(z_1,\bar{z}_1)\phi(z_2,\bar{z}_2)\rangle \equiv \langle 0|\mathcal{R}\left(\phi(z_1,\bar{z}_1)\phi(z_2,\bar{z}_2)\right)|0\rangle, \tag{2.34}$$

where radial ordering is implemented by the operator $\mathcal{R}$:

$$\mathcal{R}\left(A(z)B(w)\right) = \begin{cases} A(z)B(w) & |z|>|w| \\ B(w)A(z) & |z|<|w|. \end{cases} \tag{2.35}$$

We can use the conformal symmetry to derive conformal Ward identities for the radially quantised theory. In $D=2$ CFT these simplify significantly, as we will see. Recall that we have a conserved current $j_\mu \equiv T_{\mu\nu}\epsilon^\nu$, with the associated conserved charge

$$Q = \int d\theta j^r(\theta) = \frac{1}{2\pi i}\oint dz\, T(z)\epsilon(z) + c.c.. \tag{2.36}$$

Then the transformation of a field $\phi(w,\bar{w})$ under a conformal transformation is given by

$$\delta_{\epsilon,\bar{\epsilon}}\phi(w,\bar{w}) = [Q,\phi(w,\bar{w})] = \frac{1}{2\pi i}\oint [dz\, T(z)\epsilon(z),\phi(w,\bar{w})] + \left[d\bar{z}\,\bar{T}(\bar{z})\bar{\epsilon}(\bar{z}),\phi(w,\bar{w})\right], \tag{2.37}$$

where the commutator is an equal-radius commutator. This means that there is an ambiguity, as one has to choose whether w and $\bar{w}$ are inside or outside the contour $\mathcal{C}$. This is resolved using the earlier realisation that in analogy to time-ordered operators in a correlator, we define operators to be radially ordered when we compute their correlation function (see (2.35)). Assuming operators to be radially ordered, we have for a

holomorphic field $A(z)$ that

$$\oint dz\,[A(z),B(w)] = \oint_{|z|>|w|} dz\,A(z)B(w) - \oint_{|z|<|w|} dz\,B(w)A(z) = \oint_{\mathcal{C}(w)} dz\,\mathcal{R}\left(A(z)B(w)\right), \tag{2.38}$$

where $\mathcal{C}(w)$ is the contour enclosing the point w (see Figure 2.3). The transformation

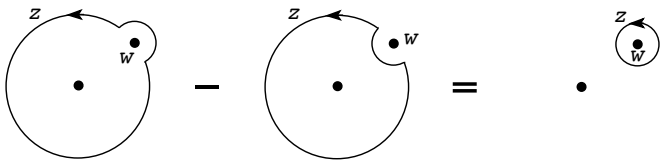

FIGURE 2.3: Path integral representation of an equal-radius commutator.

of our field ϕ is then given by the residue:

$$\delta_{\epsilon,\bar{\epsilon}}\phi(w,\bar{w}) = \frac{1}{2\pi i}\oint_{\mathcal{C}(w)} \left(dz\,\epsilon(z)\mathcal{R}\left(T(z)\phi(w,\bar{w})\right) + d\bar{z}\,\bar{\epsilon}(\bar{z})\mathcal{R}\left(\bar{T}(\bar{z})\phi(w,\bar{w})\right)\right). \tag{2.39}$$

This is where the simplification occurs. Since our conserved current is a sum of a purely holomorphic and a purely anti-holomorphic part, Cauchy's theorem can be used. For example, for a primary field we know how it should transform under an infinitesimal conformal transformation, so we can work out the singularities that should be there in the OPE between T and the field.

The upshot of this is that if we know the OPE between an operator and the energy momentum tensors $T(z)$ and $\bar{T}(\bar{z})$, then we immediately know how the operator transforms under conformal symmetry. Or conversely, if we know how an operator transforms then we know at least some part of its OPE with $T(z)$ and $\bar{T}(\bar{z})$. For example, the transformation law (2.19) for a primary field $\Phi(w,\bar{w})$ leads to the OPEs

$$T(z)\Phi(w,\bar{w}) = \frac{h}{(z-w)^2}\Phi(w,\bar{w}) + \frac{1}{z-w}\partial_w\Phi(w,\bar{w}) + \dots \tag{2.40}$$

$$\bar{T}(\bar{z})\Phi(w,\bar{w}) = \frac{\bar{h}}{(\bar{z}-\bar{w})^2}\Phi(w,\bar{w}) + \frac{1}{\bar{z}-\bar{w}}\partial_{\bar{w}}\Phi(w,\bar{w}) + \dots \tag{2.41}$$

By performing two conformal transformations in succession, one can determine the OPE of the energy momentum tensor with itself, which takes the general form

$$T(z)T(w) = \frac{c/2}{(z-w)^4} + \frac{2}{(z-w)^2}T(w) + \frac{1}{z-w}\partial T(w), \tag{2.42}$$

and similar for anti-holomorphic terms.

2.2.5 The Virasoro algebra

After quantisation, the algebra of local conformal transformations acquires an extra term due to the fact that the two-point function of the stress tensor no longer vanishes in general. A way to see this is by defining the generators of the conformal symmetry as the modes of the Laurent expansion of the stress tensor:

$$T(z) = \sum_{n\in\mathbb{Z}} z^{-n-2} L_n, \qquad \bar{T}(\bar{z}) = \sum_{n\in\mathbb{Z}} \bar{z}^{-n-2} \bar{L}_n, \tag{2.43}$$

which can be formally inverted by

$$L_n = \frac{1}{2\pi i} \oint dz\, z^{n+1} T(z), \qquad \bar{L}_n = \frac{1}{2\pi i} \oint d\bar{z}\, \bar{z}^{n+1} \bar{T}(\bar{z}). \tag{2.44}$$

Using the OPE of T with itself (2.42), and the same for $\bar{T}$, it can be shown using the methods outlined in the previous section that

$$[L_m, L_n] = (m-n)L_{m+n} + \frac{c}{12} m(m^2-1)\delta_{m+n,0}, \tag{2.45}$$

$$[\bar{L}_m, \bar{L}_n] = (m-n)\bar{L}_{m+n} + \frac{c}{12} m(m^2-1)\delta_{m+n,0}, \tag{2.46}$$

$$[L_m, \bar{L}_n] = 0. \tag{2.47}$$

2.2.6 Representations of the Virasoro algebra

The role of the Hamiltonian is played by the dilatation operator $L_0 + \bar{L}_0$. However, since the left- and right-moving parts of the energy-momentum tensor decouple, we can consider L_0 as the Hamiltonian for the right-moving part of the theory, and $\bar{L}_0$ for the left-moving part. The equivalent of an in-state is an operator inserted at the origin:

$$|\phi_j\rangle \equiv \lim_{z,\bar{z}\to 0} \phi_j(z,\bar{z})|0\rangle. \tag{2.48}$$

From the OPE with the energy momentum tensor we can deduce that

$$L_0|\phi_j\rangle = h_j|\phi_j\rangle, \tag{2.49}$$

where h_j is its holomorphic conformal dimension. In case the field inserted at the origin is primary, we further see that

$$L_n|\Phi_j\rangle = 0, \qquad n \geq 1. \tag{2.50}$$

From the commutation relations (2.45), we can infer that the L_n's (and $\bar{L}_n$'s) act as raising- and lowering operators, since:

$$[L_0, L_n] = -nL_n, \tag{2.51}$$

so that $L_0\left(L_{-n}|\phi_j\rangle\right) = (h_j + n)\,|\phi_j\rangle$, meaning that acting with L_n on a state shifts the eigenvalue by $-n$, so for $n > 0$ it is a lowering operator, and for $n < 0$ a raising operator.

We will consider only unitary theories, which follows automatically if the Hamiltonian is Hermitian. If we demand Hermiticity, the Virasoro generators must satisfy the following conjugation relation:

$$L_n^\dagger = L_{-n}. \tag{2.52}$$

From (2.50) we see that the spectrum of states is bounded from below, as states that are created by acting with a primary operator on the vacuum are annihilated by all the lowering operators. These states are usually called *highest-weight state*, and they have the property that it is annihilated by all L_n with $n > 0$ (which is why it is sometimes called a *lowest-weight state* instead). By acting with the raising operators L_{-n} $(n > 0)$ on the highest-weight states, one builds representations of the Virasoro algebra, called *Verma modules*. Obviously this results in an infinite tower of states. All states obtained in this way are called descendants.

2.3 Integrability

Conformal Field Theory is an example of an integrable field theory[12]. In general, non-integrable QFT must be solved perturbatively, which can be done only for weakly coupled systems. However, for CFT and other integrable theories, one can in principle find "exact"[13] expressions for correlation functions, regardless of the interaction strength.

[12] For the integrable structure of CFT, see [79] and references therein.
[13] see for a discussion of the notion of integrability the paper by [80]

It is possible to find a relevant deformation of CFT that results in massive integrable QFT, since an infinite number of integrals of motion can survive when perturbing a CFT by particular relevant operators which lead to integrable field theories that are not scale invariant [81]. The presence of these infinite integrals of motion gives huge simplifications for the possible scattering events: it means the scattering has to preserve the number of particles and the set of their momenta [82]. Also, one can apply a higher spin symmetry and conclude that all scattering processes can be regarded as a series of two-body scattering processes [83].

2.3.1 Intuitive picture of integrability

In order to get an idea of when a system might be integrable, consider a $2 \to 2$ scattering process in a 1+1-dimensional system.

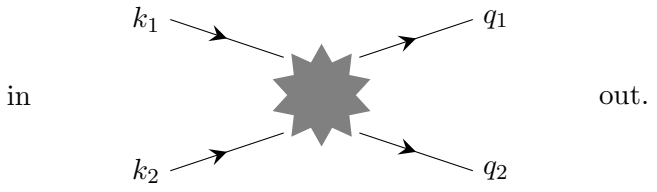

If we assume that energy and momentum are conserved, then we have the following two conserved quantities: $P = k_1 + k_2 = q_1 + q_2$ and $E = k_1^2 + k_2^2 = q_1^2 + q_2^2$. This has two solutions, $(k_1 = q_1, k_2 = q_2)$ and $(k_1 = q_2, k_2 = q_1)$. Now if we look at a process in which three particles scatter off each other,

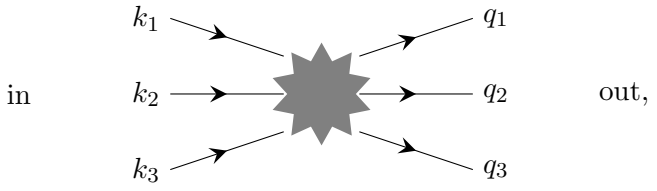

then the conservation of energy and momentum, giving the two equations $P = k_1 + k_2 + k_3 = q_1 + q_2 + q_3$ and $E = k_1^2 + k_2^2 + k_3^2 = q_1^2 + q_2^2 + q_3^2$, are insufficient to specify a solution. However, if there were a third conserved quantity, for instance $Q_3 = k_1^3 + k_2^3 + k_3^3 = q_1^3 + q_2^3 + q_3^3$, we would be able to solve for $\{q_1, q_2, q_3\}$ in terms of $\{k_1, k_2, k_3\}$. In this case, a solution has the property $\{k_1, k_2, k_3\} = \{q_1, q_2, q_3\}$.

In general, N of these 'suitable' conserved charges imply:

$$\{k_1, \ldots, k_N\}_{\text{in}} = \{q_1, \ldots, q_N\}_{\text{out}}. \tag{2.53}$$

The number of particles is conserved, as is the set of their momenta. Scattering is elastic. If we want to consider a system with an infinite number of degrees of freedom, such as a quantum field theory, then for this system to be integrable the number of these conserved quantities must be infinite as well.

2.3.2 Quantum Integrability

Let us make more precise what we mean when we say a quantum system is integrable. A definition for quantum integrability is those quantum systems which have an infinite set of conserved quantities ('charges') Q_j that are local, conserved and in involution, i.e. they satisfy the following properties:

- There is a set of quantities $\{Q_j\}$ that all commute with each other

$$[Q_j, Q_k] = 0 \qquad \forall j, k \tag{2.54}$$

  with one of the charges the Hamiltonian, so they are all conserved.

- The charges Q_j are local, i.e.

$$Q_j = \int f_j(x) dx \tag{2.55}$$

It was argued in [82] that the existence of such an infinite set of conserved charges is a necessary and sufficient condition for factorised scattering: Since these charges are local, one can consider asymptotic in/out states that are sufficiently separated so that the charges Q_n act on these asymptotic wave packets separately.

Let us construct these wave-packets as follows[14],

$$\Psi_i(x) = \int_{-\infty}^{\infty} dp\, e^{-a(p-p_i)^2} e^{ip(x-x_i)}. \tag{2.56}$$

[14] or we might replace $\exp(-a(p-p_i)^2)$ by another function of p, peaked around p_i

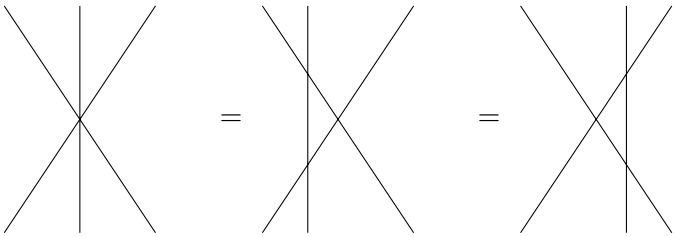

FIGURE 2.4: Yang-Baxter relation: By acting with a local conserved charge, a three-body scattering process can be seen to be equivalent to different series of two-body scattering processes.

Acting with the symmetry operator $\exp(ibQ_n)$ on each of the wave packets has the effect of shifting the peak of each wave packet:

$$x_i \to x_i - b\left[\frac{d}{dk}\omega_n(k)\right]_{k=k_i}, \tag{2.57}$$

where $\omega_n(k)$ is the eigenvalue of the symmetry operator. Considering an N-body scattering process, we can shift the centre of mass of all the particles (wave packets) by a different amount, and change the order in which they scatter off each other (see Fig. 2.4). Since $\exp(ibQ_n)$ commutes with the S-matrix, these many body scattering processes must be equivalent to a series of two-body scattering processes. For the case of three-body scattering, this gives the Yang-Baxter relation:

$$S(123) = S(23)S(13)S(12) = S(12)S(13)S(23), \tag{2.58}$$

where $S(ijk)$ denotes the scattering process between particles labeled i, j and k, respectively.

This gives the important result that the determination of the complete S-matrix for a 1+1-dimensional integrable theory reduces to the determination of the two-body S-matrix. The quantum inverse scattering theory, based on the Yang-Baxter relation, has placed the theory of exactly solvable models in a unified framework and has provided a powerful method for studying these models. The Yang-Baxter relation is a sufficient condition for solvability, and leads to a consistent and effective method to find new solvable models[15].

[15] in fact, an infinite number of solvable lattice models have been discovered using the quantum inverse scattering method in the last twenty years.

2.3.3 Integrable QFT

For a quantum field theory to be integrable, it must have no particle production (as scattering must be elastic). One might try to use Feynman diagrams to identify a Lagrangian that corresponds to an integrable quantum field theory (IQFT). As an example, consider a 1+1D QFT[16] with only one scalar field φ and Z_2 symmetry. We have the following Feynman rules:

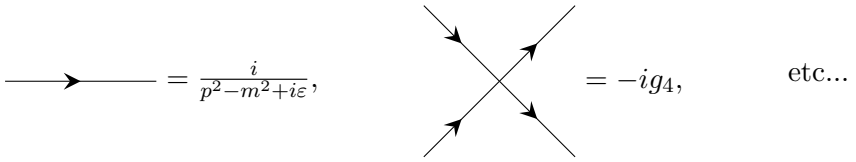

The Lagrangian for this theory is of the form

$$\mathcal{L} = \frac{1}{2}\left[(\partial_\mu\varphi)^2 - m^2\varphi^2\right] - \frac{g_4}{4!}\varphi^4 - \frac{g_6}{6!}\varphi^6 + \dots . \tag{2.59}$$

If we want to find out how the interaction strengths $\{g_i\}$ should be chosen in such a way that no particle production can take place (and we have elastic scattering, and therefore an integrable field theory), we analyze all possible production processes in turn, starting with the lowest: $(2 \to 4)$. The total amplitude for this production process is $\frac{i}{48m^2}(g_4^2 - g_6)$, so that if one chooses $g_6 = g_4^2$, this process is dynamically suppressed. Similarly, the analysis for the process $(2 \to 6)$ leads to the choice $g_6 = g_4^3$, etc. It turns out that the only Lagrangian theories with Z_2 symmetry that dynamically suppress all production processes are represented by the Lagrangian

$$\mathcal{L} = \frac{1}{2}\left[(\partial_\mu\varphi)^2 - m^2\varphi^2\right] \pm \frac{g^2}{4!}\varphi^4 - \frac{g^4}{6!}\varphi^6 \pm \frac{g^6}{8!}\varphi^8 + \dots . \tag{2.60}$$

When all signs are chosen positive, this corresponds to the so-called *sinh-Gordon model*, and when they are alternating, it is the *sine-Gordon model*.

The same analysis can be done with a more general Lagrangian which also has odd powers of the field. In that case, the Lagrangian takes the form

$$\mathcal{L} = \frac{1}{2}\left[(\partial_\mu\varphi)^2 - m^2\varphi^2\right] - \frac{g}{6}\varphi^3 + \frac{g^2}{8}\varphi^4 - \frac{g^3}{24}\varphi^5 + \dots . \tag{2.61}$$

[16] the only interesting IQFTs are 1+1 dimensional (otherwise they must have free or long-range interactions) [84].

Having a description in terms of an IQFT is not sufficient: in order to extract physical quantities of interest one needs a way of describing the thermodynamics. That is the subject of the next section.

2.4 Thermodynamic Bethe Ansatz

The thermodynamic Bethe ansatz (TBA) was developed more than twenty years ago by Yang and Yang [85], initially as a technique which allows to compute thermodynamic quantities for a system of bosons interacting dynamically via factorisable scattering. After Lieb and Liniger [86] took the thermodynamic limit of the periodic gas of interacting bosons, and wrote down the Bethe solution for the Bose gas with a delta function interaction at zero temperature, Yang and Yang wrote down an ansatz for the Gibbs partition function [85] (which was finally rigorously proved two decades later in [87]), and found a solution for the saddle point which led to the TBA equations. The incredible power of their result lies in the fact that for theories with local interactions the saddle point contribution dominates the partition function, so the problem now becomes finding the particle and hole densities that minimise the free energy. Later, Zamolodchikov and Zamolodchikov considered the thermodynamics of certain relativistic quantum field theories in [82], and A.B. Zamolodchikov generalised the arguments of Yang and Yang to the case of a system of particles which interact dynamically in a relativistic manner through a scattering matrix which belongs to an IQFT [88]. This latter approach, nowadays usually referred to as thermodynamic Bethe ansatz, has triggered numerous further investigations. The reason for this activity is at least twofold: on one hand the TBA serves as an interface between conformally invariant theories and massive integrable deformations of them and on the other hand it serves as a complementary approach to other methods and techniques. The TBA-approach allows to extract various types of information from a massive IQFT once its scattering matrix is known. Most easily one obtains the central charge of the Virasoro algebra of the underlying ultraviolet conformal field theory, the conformal dimension and the factor of proportionality of the perturbing operator, the vacuum expectation values of the energy-momentum tensor and other interesting physical and mathematical quantities. The TBA provides quantities which may be employed in other contexts, such as the computation of correlation functions. For instance, the constant of proportionality, the dimension of the perturbing field and

the vacuum expectation value of the trace of the energy-momentum tensor may be used in a perturbative approach around the OPE of a two-point function within a conformal field theory.

An important thing to note is that while off-shell particle creation complicates the procedure, one can always go far enough back in time to consider an "in" state in which all wave packets are sufficiently separated. More precisely, $|x_i - x_{i+1}| \gg \xi$, where ξ is again the correlation length (proportional to the inverse mass of the lightest particle). In that limit, the wave packets behave as if they were free, and one can represent the "in" state with the Bethe wave function. Similarly, after any interactions have taken place, we can write down an"out"-state which is sufficiently far in the future, so that all wave packets are again sufficiently separated:

$$\Psi(x_{i_1}, \ldots, x_{i_N}) = \prod_{k=1}^{N} e^{ip_{i_k} x_{i_k}}. \tag{2.62}$$

During the intermediate period in which wave packets can interact with each other, this simplification is of course not valid, but we can use what we know about the scattering matrix to relate in-states to out-states. This leads us to the quantisation conditions for bosons or fermions,

$$e^{ip_i L} \prod_{j \neq i}^{N} S_{ij}(\theta_i - \theta_j) = \pm 1, \qquad i = 1, \ldots, N, \tag{2.63}$$

where we have used the rapidity variables θ_i. The positive sign in (2.63) is the condition for bosons, and the negative sign the condition for fermions. This quantisation condition can be expressed in terms of the rapidities alone,

$$m_i L \sinh \theta_i + \sum_{j \neq i}^{N} -i \ln S_{ij}(\theta_i - \theta_j) = 2\pi n_i, \tag{2.64}$$

where $n_i \in \mathbb{Z}$ for bosons, and $n_i \in \mathbb{Z} + \frac{1}{2}$ for fermions. The numbers $\{n_i\}$ and the rapidities $\{\theta_i\}$ that solve the quantisation condition identify the Bethe states:

$$|n_1, \theta_1; \ldots; n_N, \theta_N\rangle. \tag{2.65}$$

The energy and momentum of these states are still given by

$$E = \sum_{i=1}^{N} m_i \cosh\theta_i, \qquad p = \sum_{i=1}^{N} m_i \sinh\theta_i, \tag{2.66}$$

but now the rapidities can only take up values that obey the condition (2.64). In general, this condition is very difficult to solve, as it involves a set of transcendental equations, but in the thermodynamic limit (sending both $L \to \infty$ and the number of particles $N_a \to \infty$, whilst keeping their ratio fixed), the spectrum of the rapidities that solve (2.64) becomes dense, and one can introduce continuous densities $\rho_a^{(r)}(\theta)$, which is defined as the number of particles with label a that have a rapidity between θ and $\theta + \Delta\theta$, divided by $L\Delta\theta$. In this limit, the energy per unit length of the system can be written as

$$E[\rho^{(r)}] = \sum_{a=1}^{n} \int_{-\infty}^{\infty} d\theta \; m_a \cosh\theta \rho_a^{(r)}. \tag{2.67}$$

When the system length L is much larger than the correlation length $\xi \sim m_1^{-1}$, the quantisation condition (2.64) becomes

$$\frac{m_a}{2\pi} \sinh\theta_i^{(a)} + \sum_{b=1}^{n} \left(\delta_{ab} * \rho_b^{(r)}\right)(\theta) = \frac{n_i^{(a)}}{L}, \tag{2.68}$$

with $\delta_{ij}(\theta) = -i \ln S_{ij}(\theta)$, and where $*$ is the convolution of the functions

$$(f * g)(\theta) = \int_{-\infty}^{\infty} \frac{d\theta'}{2\pi} f(\theta - \theta') g(\theta'). \tag{2.69}$$

To derive the thermodynamics of this integrable field theory, one must also find an expression for the entropy as a function of the particle (and hole) densities, and use this to minimise the free energy,

$$F[\rho, \rho^{(r)}] = E[\rho^{(r)}] - TS[\rho, \rho^{(r)}], \tag{2.70}$$

with respect to the two densities $\rho, \rho^{(r)}$. Here, F is the free energy, T is the temperature and S is the entropy. This can be done by using a Lagrange multiplier, and elegantly expressed by introducing the *pseudo-energies* $\epsilon_a(\theta)$, in terms of which the extremum

condition reduces to the integral equation

$$m_a R \cosh\theta = \epsilon_a(\theta) \pm \sum_{b=1}^{n} \int \frac{d\theta'}{2\pi} \varphi_{ab}(\theta - \theta') \log(1 \pm e^{-\epsilon_b(\theta')}), \tag{2.71}$$

where we have defined $\varphi_{ab}(\theta) := \frac{d}{d\theta}\delta_{ab}(\theta)$. This gives us the free energy at the extremum:

$$F = \mp \frac{1}{R} \sum_{a=1}^{n} \int_{-\infty}^{+\infty} \frac{d\theta}{2\pi} m_a \cosh\theta \ln\left(1 \pm e^{-\epsilon_a(\theta)}\right). \tag{2.72}$$

Technically the TBA-approach consists essentially of the following steps, first solving the TBA-equations with a given scattering matrix for the pseudo-energies, then using the solution to compute the free energy, and extract finally the quantities of interest from it (some interesting quantities can already be obtained from the knowledge of the pseudo-energies). Due to the fact that the TBA-equations are a system of coupled non-linear integral equations there exist no closed analytical solutions for them. Nonetheless, numerically this is in principle a well controllable problem (it becomes, however, quite complex for an increasing number of particle types) and the equations may be solved iteratively.

Chapter 3

Entanglement dynamics

In this chapter we will present the results of [4], after a short review on the replica method of calculating the Entanglement Entropy and the logarithmic negativity in QFT.

3.1 Entanglement in extended quantum systems

In the following, we will consider the methods for computing entanglement in the scaling limit. In this limit, measures such as the entanglement entropy (EE) and negativity, discussed in section 1.2.2, can be computed using path integral techniques. We will treat separately two cases: entanglement between parts of a system that is in a pure state and entanglement between parts of a system that is in a mixed state. If a system is in a pure state, the EE provides a computable and also intuitively clear way of representing entanglement. It possesses desirable qualities such as monotonicity, additivity, convexity and basis independence (see the discussion in section 1.2.2). However, for systems that are in a mixed state (which is the case for systems that are thermalised) the EE contains contributions due to classical entropy in a system. In order to find a way to quantify entanglement in a monotonic way for systems in a mixed states, one may instead consider negativity. Negativity does not reduce to the EE in the low-temperature limit[1], and its intuitive meaning is less clear than that of the EE. Nevertheless, it has the advantage, like the EE, of being computable for the type of systems we consider.

[1] rather, its zero-temperature behaviour is like a R´enyi entropy $S^{(1/2)}$

In this chapter, we will review the methods developed by [89–91] which computed the bi-partite entanglement entropy (defined in (1.10)) in the scaling limit using geometric quantities, using a method reminiscent of the replica trick in disordered (e.g. spin glass) systems (see for instance [92]). For mixed states, we will review the methods of [93, 94] to compute the logarithmic negativity, defined in (1.15).

3.1.1 Pure states: Entanglement Entropy

When dealing with a system with a finite number of degrees of freedom, as in the two-particle case discussed in Chapter 1, computing the eigenvalues λ_i of the reduced density matrix allows one to compute the entanglement entropy (1.10) as

$$S_A = -\sum_i \lambda_i \ln \lambda_i. \tag{3.1}$$

These eigenvalues are probabilities, and therefore $\lambda_i \in [0,1]$, and $\sum_i \lambda_i = 1$. It follows that the sum $\sum_i \lambda_i^n$ is absolutely convergent for any $n \geq 1$, and therefore it is analytic for all Re $n > 1$. This means one can take the derivative with respect to n for $n > 1$, and if the entropy is finite, then the first derivative converges to this value in the limit $n \to 1^+$:

$$S_A = -\lim_{n\to 1} \frac{\partial}{\partial n} \operatorname{Tr} \rho_A^n. \tag{3.2}$$

One way to calculate the entanglement entropy is to compute $\operatorname{Tr} \rho_A^n$ for a generic real n and use (3.2). In some cases $\operatorname{Tr} \rho_A^n$ may be easier to compute for n integer. In that case the calculation can be done using a type of replica trick: if one can compute $\operatorname{Tr} \rho_A^n$ for a positive integral n and one assumes that this can be analytically continued to a general complex value, one can use (3.2) to compute the entanglement entropy. The question remains whether this analytic continuation can be made, and yields a unique answer in the limit $n \to 1$. When the sum (3.1) is finite, the analytic continuation is unique [2], and yields an answer that equates to the result of the sum (3.1).

We are interested in computing suitable measures for entanglement (EE and negativity) in the scaling limit, which will give us the universal part of the behaviour near a quantum critical point (see Chapter 2). The EE diverges in the scaling limit [89–91], and whether the replica trick works in the scaling limit has not been proven in general.

[2] under the condition that the result does not increase exponentially as $\operatorname{Im}(n) \to \infty$

The reason why the replica trick is useful in the scaling limit is because computing the trace of the n-th power of the reduced density matrix in a QFT can be done using a path integral. If $\langle\phi|\rho|\phi'\rangle$ is one matrix element of the density matrix for a system at inverse temperature β, one can compute it by taking the path integral on the imaginary time interval $(0, \beta)$ over the Euclidean action and setting the field equal to $\phi(x)$ at $\tau = 0$ and $\phi'(x')$ at $\tau = \beta$. In order to ensure that $\operatorname{Tr}\rho = 1$, we have to normalize by a factor Z, which is the partition function.

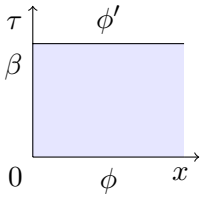

$$= Z\langle\phi|e^{-\beta H}|\phi'\rangle \tag{3.3}$$

$$= \int [d\phi(y,\tau)]\delta(\phi(y,0) - \phi'(x))\delta(\phi(y,\beta) - \phi(x))e^{-S_E}, \tag{3.4}$$

where S_E is the Euclidean action, and Z denotes the partition function: $Z = \operatorname{Tr} e^{-\beta H}$.

In the path integral, the partition function is computed by setting the value of the endpoints of the field equal to each other, and integrating over them. This is equivalent to considering the path integral over a cylinder.

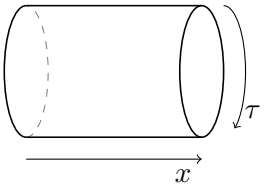

$$= Z = \operatorname{Tr} e^{-\beta H}. \tag{3.5}$$

For the reduced density matrix $\rho_A = \operatorname{Tr}_B \rho$, tracing only over the degrees of freedom in part B means that only at points in B the endpoints are sewn together.

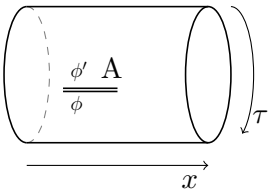

$$= Z\langle\phi|\rho_A|\phi'\rangle = Z\langle\phi|\operatorname{Tr}_B e^{-\beta H}|\phi'\rangle, \tag{3.6}$$

where ϕ and ϕ' now denote states in $\mathcal{H}_A$ only.

We can take a product of these reduced density matrices,

$$\sum_{\phi',\phi'',\cdots} \langle\phi|\rho_A|\phi'\rangle\langle\phi'|\rho_A|\phi''\rangle\cdots, \tag{3.7}$$

which amounts to sewing together one side of the cut on cylinder number 1 to the other side of the cut on the next cylinder, etc., as shown in the following figure.

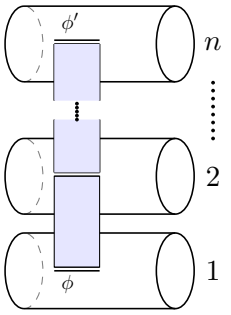

$$= Z^n\langle\phi|\rho_A^n|\phi'\rangle \tag{3.8}$$

Finally, tracing over the remaining degrees of freedom in A means connecting the last cylinder with the first cylinder. We are left with n cylinders that are cyclically connected via the degrees of freedom in A, let us call this Riemann surface $\mathcal{R}_n$. The zero-temperature case may be considered by taking the limit $\beta \to \infty$, which means that the geometry now becomes that of n sheets cyclically connected as described before. Therefore, $\mathcal{R}_n$ is generally referred to as an *n-sheeted Riemann surface*. If we call the partition function of the theory on this surface $Z_{\mathcal{R}_n}$, then we can compute the Rényi entropy using

$$\operatorname{Tr}\rho_A^n = \frac{Z_{\mathcal{R}_n}}{Z^n}. \tag{3.9}$$

Therefore, the computation of the entanglement entropy can be translated into the computation of partition functions on n-sheeted Riemann functions with $2N$ conical singularities, where N is the number of cuts. This can be effectively done by instead of having fields that can wind around the conical singularities and end up on a different sheet, making n copies of the fields, which each live on only one of the sheets, and defining operators that, when a field twists around them, send the field to the next sheet (or the previous one, depending on the direction). These operators are called *branch-point twist fields* [95, 96], and they arise out of the symmetry under permutation of the copies. The advantage to our n copy model is that now the fields are again local with respect to the n-copy Lagrangian (a property that was lost in the n-sheeted Riemann surface) [96].

The main property of the twist field of interest, associated with a cyclic permutation, is the exchange property

$$\varphi_i(y,t)\,\mathcal{T}(x,t) = \begin{cases} \mathcal{T}(x,t)\,\varphi_i(y,t) & (y<x) \\ \mathcal{T}(x,t)\,\varphi_{i+1}(y,t) & (x<y). \end{cases} \tag{3.10a}$$

Similarly, the "anti-twist" field, associated with the inverse cyclic permutation, satisfies

$$\varphi_i(y,t)\,\tilde{\mathcal{T}}(x,t) = \begin{cases} \tilde{\mathcal{T}}(x,t)\,\varphi_i(y,t) & (y<x) \\ \tilde{\mathcal{T}}(x,t)\,\varphi_{i-1}(y,t) & (x<y). \end{cases} \tag{3.10b}$$

The twist fields are local, primary fields, and their scaling dimension was found in [95, 97] to be

$$d_n = \frac{c}{12}(n-n^{-1}). \tag{3.11}$$

We will use the CFT normalization

$$\mathcal{T}(x)\tilde{\mathcal{T}}(y) \sim (x-y)^{-2d_n}. \tag{3.12}$$

In general, the trace of the product of reduced density matrices appearing in the expression for the Rényi entropy $S_A^{(n)}$ for a region A consisting of N cuts $A = [u_1, v_1] \cup \cdots \cup [u_N, v_N]$, is given, for an initial state represented by $\langle \cdots \rangle$, by the following $2N$-point function

$$\mathrm{Tr}\rho_A^n = c_n^N \delta^{2Nd_n} \langle \mathcal{T}(u_1)\tilde{\mathcal{T}}(v_1)\cdots\mathcal{T}(u_N)\tilde{\mathcal{T}}(v_N)\rangle_{\mathbb{C}}, \tag{3.13}$$

where $\sqrt{c_n}$ is a nonuniversal constant encoding the conical singularity at the positions of the twist fields (this depends on the number of sheets) [3], and δ is a short-distance regulator such as a lattice spacing. Note that the expression on the right-hand side of (3.13) is dimensionless, as the twist fields have dimension d_n.

3.1.2 Mixed states: (Logarithmic) Negativity

In the path integral, taking the transpose, which means exchanging the row and column indices of the reduced density matrix, corresponds to exchanging upper and lower edges

[3] Note the different way in which our constant c_n appears in the formulae compared to formulae in [91] and other papers of these authors: in our case, twist fields are finite CFT fields, hence the constant appears when a pair of twist fields is inserted, whereas in some other works it appears in the computation of the correlation function of twist fields.

of the cuts. This would mean we have to define new branch-point twist fields, depending on the number of sheets. If we consider the reduced density matrix ρ_A, where $A = A_1 \cup A_2 = [u_1, v_1] \cup [u_2, v_2]$, such that $\mathrm{Tr}(\rho_A)^n \propto \langle \mathcal{T}(u_1)\tilde{\mathcal{T}}(v_1)\mathcal{T}(u_2)\tilde{\mathcal{T}}(v_2)\rangle$, and take the partial transpose with respect to A_2, we have to compute the following correlation function:

$$\mathrm{Tr}(\rho_A^{T_2})^n \propto \langle \mathcal{T}(u_1)\tilde{\mathcal{T}}(v_1)\mathcal{T}^{n-1}(u_2)\tilde{\mathcal{T}}^{n-1}(v_2)\rangle, \tag{3.14}$$

where $\mathcal{T}^{n-1}$ has the property that it connects a field on sheet j with a field on sheet $j+n-1 (\mathrm{mod}\ n)$, and $\tilde{\mathcal{T}}^{n-1}$ connects a field on sheet j with a field on sheet $j-n+1 (\mathrm{mod}\ n)$. One may use the methods of [98, 99] to obtain the conformal dimensions of these fields. However, we may replace $\mathcal{T}^{n-1}(x) \to \tilde{\mathcal{T}}(x)$ and $\tilde{\mathcal{T}}^{n-1}(x) \to \mathcal{T}(x)$. Therefore, we do not have to introduce different twist fields at this stage, and we find the partial transposition simply has the effect of exchanging twist fields and anti-twist fields for the transposed region.

$$\mathrm{Tr}(\rho_A^{T_2})^n \propto \langle \mathcal{T}(u_1)\tilde{\mathcal{T}}(v_1)\tilde{\mathcal{T}}(u_2)\mathcal{T}(v_2)\rangle. \tag{3.15}$$

3.2 Review of existing EE and logarithmic negativity results

The entanglement entropy of a single interval of length ℓ in a one-dimensional system at $T = 0$ is given by [90, 91, 100]:

$$S_A = \frac{c}{3} \ln \frac{\ell}{\delta} + c_1', \tag{3.16}$$

with δ the lattice spacing, and where c_1' is simply the limit $n \to 1$ of the non-universal constant

$$c_n' := \frac{\ln c_n}{1-n}. \tag{3.17}$$

Despite their non-universal nature, the constants c_n' are known exactly for few integrable models [96, 101–104].

The logarithmic negativity at $T = 0$ for a single interval of length ℓ is given by [94]

$$\mathcal{E} = \frac{c}{2} \ln \frac{\ell}{\delta} + 2 \ln c_{1/2}. \tag{3.18}$$

The fact that for a single interval $\mathrm{Tr}\,\rho_A^n$ transforms under a general conformal transformation as a two-point function of primary operators means that it is simple to compute in other geometries. A simple generalization is to consider a finite-size system with periodic boundary conditions, or a system in a thermal mixed state. The result for the entropy at temperature $T = \beta^{-1}$ is [91, 105]:

$$S_A = \frac{c}{3} \ln \left(\frac{\beta}{\pi\delta} \sinh \frac{\pi\ell}{\beta} \right) + c_1'. \tag{3.19}$$

For low temperatures (or $\beta \gg \ell$), this result reduces to the zero-temperature result (3.16), as it should, whereas in the high-temperature limit ($\beta \ll \ell$), the result is linear in the interval length:

$$S_A = \frac{\pi c}{3\beta}\ell + c_1' \qquad (\beta \ll \ell). \tag{3.20}$$

At finite temperature, the computation of the negativity in [93, 94] has some subtleties, as discussed in [106], and the result for a single interval of length ℓ is

$$\mathcal{E} = \frac{c}{2} \ln \left(\frac{\beta}{\pi\delta} \sinh \frac{\pi\ell}{\beta} \right) - \frac{\pi c \ell}{2\beta} + f(e^{-2\pi\ell/\beta}) + 2 \ln c_{1/2}, \tag{3.21}$$

where $f(x) := \lim_{n_e \to 1} \mathcal{F}_n(x)$, i.e. the limit of $n \to 1$ starting from an even value of n, of the function $\mathcal{F}_n(x)$, which contains the remaining degrees of freedom in a four-point function, as discussed in Chapter 2. For high temperatures and at fixed interval length ℓ equation (3.21) is valid only as long as $\beta \gg \delta$ and so it never becomes negative, as it could seem at a first superficial look. Another fundamental feature is that the logarithmic negativity depends on the full operator content of the model through the function $f(x)$.

If we have a boundary,

$$S_A = \frac{c}{6} \ln \frac{2\ell}{\delta} + \tilde{c}_1', \tag{3.22}$$

where the constant $\tilde{c}_1'$ is given by the limit $n \to 1$ of $\tilde{c}_n' := \frac{\ln \tilde{c}_n}{1-n}$. The constants for the situation with a boundary and the situation without a boundary are related to the boundary entropy $\ln g$ [91, 107, 108] via

$$\tilde{c}_1' - \frac{c_1'}{2} = \ln g, \tag{3.23}$$

where $\ln g$ is the boundary entropy, first discussed by Affleck and Ludwig [109]. We recall that g is universal and depends only on the boundary CFT.

The entanglement between two semi-infinite halves, a sufficiently long time $t \gg \epsilon$ after a local"cut-and-glue" quench at $T = 0$, is given by[110]:

$$S_A(t \gg \epsilon) = \frac{c}{3} \ln \frac{t}{\delta} + k_0, \tag{3.24}$$

with $k_0 := \tilde{c}_1' + (c/6) \ln(\delta/\epsilon)$. The result (3.24) tells us that the leading long time behavior is only determined by the central charge of the theory in analogy with the ground state value for a slit.

For the logarithmic negativity between two adjacent intervals of length ℓ_1 and ℓ_2 at $T = 0$, [93, 94]:

$$\mathcal{E} = \frac{c}{4} \ln \frac{\ell_1 \ell_2}{\ell_1 + \ell_2} + \text{const.} \tag{3.25}$$

For the thermal cut-and-glue quench described in Chapter 1, the authors of [111] conjectured that the logarithmic negativity in the NESS reached after connecting reservoirs of different temperatures, $\mathcal{E}(\beta_l, \beta_r)$ is just the average of the thermal state logarithmic negativities, where the systems are thermalised at (inverse) temperatures β_l and β_r:

$$\mathcal{E}^{\text{NESS}}(\beta_l, \beta_r) = \frac{\mathcal{E}^{\text{eq}}(\beta_l) + \mathcal{E}^{\text{eq}}(\beta_r)}{2}. \tag{3.26}$$

The finite temperature logarithmic negativity for two intervals of equal length ℓ is given by

$$\mathcal{E}(\ell; \beta) = \frac{c}{4} \ln \left(\frac{\beta}{\pi \delta} \tanh \frac{\pi \ell}{\beta} \right) + \text{const.} \tag{3.27}$$

Numerical studies of the logarithmic negativity between two adjacent intervals of length ℓ at finite temperature in the harmonic chain [111] revealed the following behaviour as a function of time:

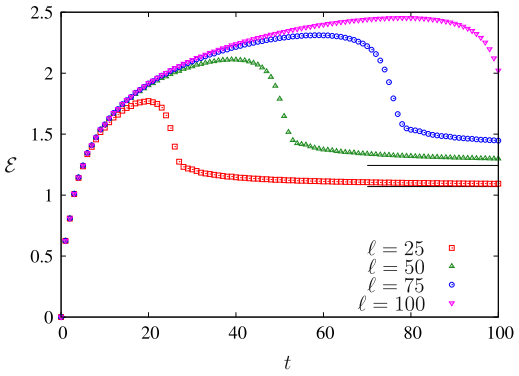

FIGURE 3.1: [111]

3.3 Overview of results

We have confirmed (3.26) for the NESS for general CFTs, and furthermore, found that for the special case of CFTs with trivial pairing data[4], a more general expression holds for all times t:

$$\mathcal{E}(t;\beta_l,\beta_r) = \frac{1}{2}\left(\mathcal{E}(t;\beta_l) + \mathcal{E}(t;\beta_r)\right), \tag{3.28}$$

where the expressions on the right-hand side are just the logarithmic negativities after connecting two baths of equal temperature.

For the transient regime, we found that in general, disentangling the left- and right thermal baths might not be possible, unless the CFT model has trivial pairing data. For the case of trivial pairing data, we found expressions that require knowledge of the specific CFT model in question. However, for very short times after the quench, and in the prethermal regime (which is reached as one takes the limit $\ell > t \to \infty$, so as not to reach the steady state), exact expressions could be found. The evolution of the logarithmic negativity just after the quench is independent of the temperature and the length ℓ of the intervals:

$$\mathcal{E}(t;\beta) = \frac{c}{2}\ln\frac{t}{\delta} + \ln C_{\mathcal{T}\mathcal{T}}^{\mathcal{T}^2} + \ln c_{1/2} + 3\ln g, \qquad (t \ll \text{ any other scale}). \tag{3.29}$$

[4]This refers to the pairing between holomorphic and antiholomorphic modules of the CFT. The OPE between fields $\varphi_i(x)$ and $\varphi_j(y)$ is generically not the product of the OPEs between their individual holomorphic, $\varphi_i^+(x)\varphi_j^+(y)$, and anti-holomorphic, $\varphi_i^-(x)\varphi_j^-(y)$, components. The particular structure of the OPEs constitute additional data of the CFT model under consideration, which may be referred to as the pairing data of the model. Models in which the pairing is trivially factorised are those that are completely built out of symmetry currents: those where all representations involved are the representations associated to the symmetry algebra itself. Free-boson (harmonic chains) and free-fermion models display this property.

It does have some non-universal contributions. The logarithmic negativity in the prethermal regime is given by

$$\mathcal{E}(t;\beta) = \frac{c}{2}\ln\frac{\beta}{2\pi\delta} + 3\ln C_{\mathcal{T}\mathcal{T}}^{\mathcal{T}^2} + \ln c_{1/2} + 3\ln g, \qquad (\ell > t \to \infty), \tag{3.30}$$

which tells us that if the intervals are large enough, and we wait long enough, the logarithmic negativity reaches a plateau, which is different from the thermal plateau that is reached in the steady state. Taking the difference of these two expressions, we obtain a universal function of t/β.

A possible explanation of why the negativity just after the quench does not depend on the temperatures of the reservoirs is that the initial buildup of entanglement is due to the fastest particles, which make up the sharp front between the reservoirs and the steady state. After a while, slower particles become important as well.

Personal contributions

The following section consists of the third paper [4] on which this thesis is based. In this paper I performed all the computations, with input and ideas from my supervisor.

Available online at www.sciencedirect.com

ScienceDirect

Nuclear Physics B 898 (2015) 78–112

NUCLEAR PHYSICS B

www.elsevier.com/locate/nuclphysb

Entanglement negativity and entropy in non-equilibrium conformal field theory

Marianne Hoogeveen *, Benjamin Doyon

Department of Mathematics, King's College London, London, United Kingdom

Received 25 May 2015; accepted 22 June 2015

Available online 23 June 2015

Editor: Hubert Saleur

Abstract

We study the dynamics of the entanglement in one-dimensional critical quantum systems after a local quench in which two independently thermalized semi-infinite halves are joined to form a homogeneous infinite system and left to evolve unitarily. We show that under certain conditions a nonequilibrium steady state (NESS) is reached instantaneously as soon as the entanglement interval is within the light cone emanating from the contact point. In this steady state, the exact expressions for the entanglement entropy and the logarithmic negativity are in agreement with the steady state density matrix being a boosted thermal state, as expected. We derive various general identities: relating the negativity after the quench with unequal left and right initial temperatures with that where the left and right temperatures are equal; and relating these with the negativity in equilibrium thermal states. In certain regimes the resulting expressions can be analytically evaluated. Immediately after the interval intersects the light cone, we find logarithmic growth. For a very long interval, we find that the negativity approaches a plateau after sufficiently long times, different from its NESS value. The NESS value is reached instantly as soon as the entire interval is contained in the light cone. This provides a theoretical framework explaining recently obtained numerical results.

* Corresponding author.
E-mail address: marianne.hoogeveen@gmail.com (M. Hoogeveen).

http://dx.doi.org/10.1016/j.nuclphysb.2015.06.021

1. Introduction

Finding ways to quantify the entanglement of quantum many body systems is an interesting problem with various applications, for instance as a tool for detecting quantum critical behavior, and topological phases [1,2]. A measure of the quantum entanglement for bipartite systems in a pure state is the Entanglement Entropy (EE),

$$S_A = -\operatorname{Tr} \rho_A \ln \rho_A, \tag{1}$$

which is calculated using the reduced density matrix $\rho_A = \operatorname{Tr}_B \rho$, where ρ is the density matrix of the whole system, and A and B are complementary parts of the system. Together with the Rényi entropies,

$$S_A^{(n)} = \frac{1}{1-n} \ln \operatorname{Tr} \rho_A^n, \qquad \lim_{n\to 1} S_A^{(n)} = S_A, \tag{2}$$

this encodes a lot of information about the entanglement [3–6]. A striking feature of the EE is the universal behavior it displays near a Quantum Phase Transition. This allows one to compute it using methods from Quantum Field Theory, or, exactly at criticality, Conformal Field Theory (CFT). In [7,8], a field theory method was introduced to compute the entanglement entropy using the replica trick, whereby $\operatorname{Tr} \rho_A^n$ is interpreted as a partition function on an n-sheeted Riemann surface.

When a system is in a mixed state, the EE is not a good measure of entanglement, as it contains a classical contribution from the entropy of the mixed state. A measure of entanglement that does not have this problem for mixed states is the *logarithmic negativity* [9], which was shown to be an entanglement monotone in [10]. The logarithmic negativity between two parts A_1 and A_2 (such that $A = A_1 \cup A_2$, and the total system is $A_1 \cup A_2 \cup B$) is given by

$$\mathcal{E}_{A_1,A_2} \equiv \ln ||\rho_A^{T_2}||_1 = \ln \operatorname{Tr} |\rho_A^{T_2}|, \tag{3}$$

where the trace norm $||\rho_A^{T_2}||_1$ is the sum of the absolute values of the eigenvalues λ_i of $\rho_A^{T_2}$, and $\rho_A^{T_2}$ is the partial transpose of ρ_A with respect to the tensor factor corresponding to A_2. Note that A_1 and A_2 need not be complementary parts of the system (which is the case only when $B = \emptyset$). In [11,12], a systematic way was developed to compute the logarithmic negativity using field theory methods.

Recently, the dynamics of entanglement out of equilibrium has seen a surge in interest, and this has been studied in a variety of cases. A system can be brought out of equilibrium by applying a quantum quench, which is a sudden change of a parameter in the Hamiltonian, such that the new Hamiltonian does not commute with the original one. This can be a global quench, such as a sudden change of a mass parameter, external magnetic field or interaction strength, or a local quench, such as a sudden change in interaction strength between two sites on a chain. Such situations offer insight into quantum physics out of equilibrium. A particular type of local quench is the so-called "cut and glue" quench, in which a system is cut into two pieces and glued together, possibly after the separate halves have been thermalized at different temperatures. This type of quench has been studied since a long time, especially from the viewpoint of constructing non-equilibrium steady states (NESS) (where the setup is referred to as the "partitioning approach") [13–15]. The thermodynamics of the NESS and its approach were studied in various quantum chains [16–20], and recently the energy current and fluctuations were studied in one-dimensional CFT [21–23] and in higher-dimensional CFT [24].

Numerical results for the EE after this type of quench, in which two infinite chains of free fermions in their respective ground states are connected at a point, were found in [25]. Analytical results for the more general case where the theories could be described by a CFT were found in [26] (with a correction in [27]). These results were generalized for systems of finite length [28], and re-obtained by developing the holographic dual of the local quench between two CFTs in their ground state [29]. In the same setup, the mutual information and EE after a local quench at zero temperature were calculated in [30], and in a nonequilibrium steady state in the presence of an energy current (in an infinite chain of free fermions) [31]. An analytical formula for the negativity after the quench was conjectured for the case in which the system reaches a nonequilibrium steady state with finite energy current [32], and numerical results were found for any time after the quench, confirming the relation for the NESS.

In this paper we consider the entanglement arising after the "cut and glue" quench in CFT with independently thermalized halves, where an energy current is generated and a nonequilibrium steady state is reached at late times. We confirm and generalize to a certain class of CFTs the results of [31,32]. We find that in certain CFTs, at any time, the negativity after the quench at different temperatures can be written in terms of negativities in systems where the temperatures are equal. We also find equations for various time regimes relating the negativity after the quench with equilibrium expressions, in which the effect of the time evolution is only present in a change of the intervals. For certain time regimes, we find analytical results for the finite time behavior before the NESS is reached.

We present new techniques using holomorphic (chiral) twist fields for computing measures of entanglement after a local quench, expanding previous results [8,33] (see also the various reviews in [27]). We consider both Rényi entropies and the logarithmic negativity, but we concentrate on the latter, as the former is not a good measure of entanglement when considering mixed states.

The organization of the paper is as follows. In Section 2, we describe the type of "cut and glue" quench we are interested in, and give an overview of important results in the literature, as well as the main results obtained in this paper. In Section 3, we review the properties of branch-point twist fields [34,35,33], and discuss *holomorphic twist fields*. We use these fields to find a relation between the EE after the quench in terms of equilibrium quantities. In Section 4 we finally describe the time evolution of the logarithmic negativity after a local quench using these holomorphic twist fields, and identify cases in which a universal result can be obtained. In particular, we find results for the nonequilibrium steady state (NESS), and the time evolution leading up to that. In Appendix A we confirm that the NESS, on (holomorphic) twist fields, can still be described [21,24] as a boosted thermal state. In Appendix B we find relations between structure constants that appear in OPEs of twist fields, in Appendix C we relate some of the nonuniversal constants in our results to the boundary entropy, and in Appendix D we relate the time evolution of the mutual information to quantities that can be computed in equilibrium.

Shortly after this paper appeared in preprint, another preprint [36] appeared, in which the negativity in the same setup was considered, but with both reservoirs at zero temperature. The results broadly agree with the low temperature limit of our results.

2. Local quench between independently thermalized systems

Consider two copies of a semi-infinite one-dimensional quantum system (say, a spin chain), separately prepared in generically different thermal states with inverse temperatures β_l and β_r. As the two copies are separately prepared, they are completely unentangled. At time $t = 0$, the two copies are connected at their boundary point, forming the left and right halves of a single

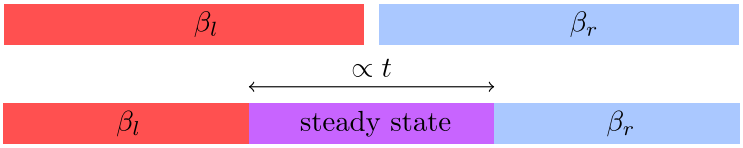

Fig. 1. We consider two semi-infinite critical systems, initially thermalized at different temperatures. At time $t = 0$, the systems are connected at a point so that energy can flow between them. After time t, there is a sharply defined region of size $R \propto t$ in which there is a steady state description. We want to consider the behavior of the entanglement between the left and right baths as time evolves.

infinite, homogeneous total system. The total system is then left to evolve unitarily. The process we are describing is a local quench: at time $t = 0$, the dynamics is suddenly changed from that of two disconnected semi-infinite systems to that of a single homogeneous total system, by adding a local connection (one or a few links in the spin chain). Because of the interaction thus created between the left and right subsystems, one expects the subsystems to become entangled as time goes on.

In the total system, energy can flow between the left and right subsystems, and because of the initial temperature imbalance an energy current develops. In certain situations, including those we will be considering here, after an infinitely long time a steady state emerges where energy flows constantly from one side to the other [16–23,37,38,24,39–41] (Fig. 1). This quench process is sometimes referred to as the "partitioning approach" for constructing non-equilibrium steady states (NESS) [13–15]. We are interested in the dynamics of the entanglement between the left and right subsystems in the presence of a developing energy current, and in the entanglement present in the steady state emerging at late times.

Let us denote by H^l and H^r the Hamiltonians of the left and right subsystems, respectively. The density matrix describing the initial state, with independently thermalized subsystems, is

$$\rho_0 = e^{-\beta_l H^l - \beta_r H^r}. \tag{4}$$

The expectation value taken in the initial state is denoted as

$$\langle \cdots \rangle_0 = \frac{\mathrm{Tr}(\rho_0 \cdots)}{\mathrm{Tr}(\rho_0)}. \tag{5}$$

Note that since $[H^l, H^r] = 0$, the expectation values factorize into the left and right systems: if $O_1(x)$ and $O_2(y)$ are local observables at positions $x < 0$ and $y > 0$, respectively, then

$$\langle O_1(x) O_2(y) \rangle_0 = \langle O_1(x) \rangle_l \langle O_2(y) \rangle_r \qquad (x < 0,\ y > 0), \tag{6}$$

where the expectation values $\langle \cdots \rangle_{l/r}$ are taken with respect to $e^{-\beta_l H^l}$ and $e^{-\beta_r H^r}$, respectively.

After the quench, a connection is added between the left and right subsystems, and the full Hamiltonian is

$$H = H^l + H^r + \delta H. \tag{7}$$

The term describing the connection δH does not commute with either H^l or H^r. Although it may have a vanishingly small effect on the value of the total energy, it affects the *dynamics* in an important way. The density matrix evolves with time according to the full Hamiltonian, $\rho_0(t) = e^{-iHt} \rho_0 e^{iHt}$, and for any time $t > 0$ it does not factorize into left and right subsystems anymore. Expectation values of observables in the state at time t after the quench can naturally be written in terms of expectation values with respect to ρ_0 of time-evolved observables,

(a) Before the quench: $t < 0$. (b) After the quench: $t > 0$.

Fig. 2. Before the time of connection, the systems (at low temperatures) are described by two copies of the same CFT, each on the half-line, with different temperatures. After the connection, the total system is described by a CFT on the line, but one cannot associate a temperature to the state.

$$\frac{\mathrm{Tr}(\rho_0(t)O)}{\mathrm{Tr}(\rho_0(t))} = \langle O(t)\rangle_0, \tag{8}$$

with $O(t) = e^{iHt}Oe^{-iHt}$ (see Fig. 3).

At all times $t > 0$, and in particular in the non-equilibrium steady state occurring at infinite times, the density matrix corresponds to non-trivial, generically non-thermal mixed states. Hence in order to study the dynamics of the entanglement after the quench and in the steady state in the presence of an energy current, we need to use a measure of entanglement that is appropriate for any mixed states. One such measure is the *logarithmic negativity* [9,10]. This provides real numbers characterizing the quantity of entanglement between any two subsystems in mixed states. That is, for any decomposition of the Hilbert space as $\mathcal{H} = \mathcal{H}_{A_1} \otimes \mathcal{H}_{A_2} \otimes \mathcal{H}_B$ (where $\mathcal{H}_B$ may be trivial) and for any density matrix ρ on $\mathcal{H}$, the logarithmic negativity $\mathcal{E}_{A_1,A_2}(\rho)$ gives a measure for the quantity of entanglement present in ρ between subsystems $\mathcal{H}_{A_1}$ and $\mathcal{H}_{A_2}$. The results of [11,12] provide, in field theory, the logarithmic negativity as a certain nontrivial limit on averages with respect to ρ of observables determined by A_1 and A_2. The observables involve the *branch-point twist fields*, which are local observables of the replicated (multi-copy) field theory model [34,35,33]. Hence we may use (8) in order to evaluate the entanglement negativity in field theory.

Below we will study the cases where $A_1 = [u_1, v_1]$ and $A_2 = [u_2, v_2]$ represent disjoint, contiguous sets of local degrees of freedom (sites in the quantum chain).

Let us now assume that the quantum system is *critical*, and that the dynamical exponent is unity (for instance a quantum chain at a critical point, such as the Heisenberg model). If we assume that the initial temperatures, β_l^{-1} and β_r^{-1}, of the left and right halves are small as compared to microscopic energy scales (for instance, the typical energy of a link in the quantum chain), we may describe the physics by using Conformal Field Theory (CFT). The quench process that we described above has been studied within CFT in [21,22], and as explained there, a current-carrying non-equilibrium steady state develops at late times. From standard CFT arguments, the fields that are in the same conformal family as the energy and momentum density separate into right and left movers. On each of the semi-infinite initial, separate, subsystems, right and left movers are related to each other via conformal boundary conditions at the endpoints, see Fig. 2. The effect of the local quench is to modify the dynamics in such a way that at times $t > 0$, right and left movers flow continuously through the total system, at the speed of light (the Lieb–Robinson velocity of the quantum chain). This has the effect of producing a light cone, outside which the initial independently thermalized states are observed, and inside which a non-equilibrium steady state occurs. The steady state is completely described by independently thermalizing right and left movers at inverse temperatures β_l and β_r, respectively, or equivalently by boosting a thermal state of rest-frame inverse temperature $\sqrt{\beta_l\beta_r}$ and boost velocity $(\beta_r - \beta_l)/(\beta_r + \beta_l)$; the latter picture of a boosted thermal state has a generalization to higher-dimensional CFT [24] (Fig. 1).

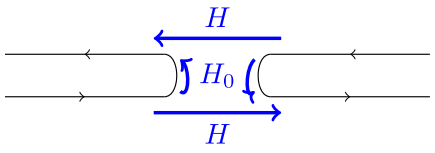

Fig. 3. Expectation values at time t after the quench are computed using time evolved observables on the disconnected state. The observables are evolved with the full Hamiltonian H, which includes the connection between the left and right systems.

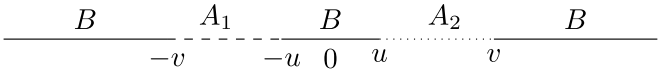

Fig. 4. The negativity between two parts $A_1 = [-v, -u]$ and $A_2 = [u, v]$ of finite length, and equal distance from the point of connection. The negativity is a measure for the entanglement between two (not necessarily complementary) regions A_1 and A_2 of a system $A_1 \cup A_2 \cup B$.

Below we will combine the CFT description of the quench problem and the emerging steady state with the twist-field expressions for logarithmic negativity in order to study the universal dynamics of entanglement in the presence of energy flows in critical systems.

Remark. The quantum-chain precursor to branch-point twist fields are cyclic replica permutation operators, studied in [42]. Generalizing the field-theory arguments of [11,12] and using these quantum-chain operators, one obtains the logarithmic negativity via averages of local observables in quantum chains. Hence, one may also use (8) in quantum chains in order to study the dynamics of the negativity, by replacing the observable O with products of cyclic replica permutation operators instead of branch-point twist fields.

2.1. Main results of this paper

We denote by $\mathcal{E}_{A_1,A_2}(t;\beta_l,\beta_r)$ the logarithmic negativity between degrees of freedom lying on subsets A_1 and A_2, a time t after the connection, with initial left and right inverse temperatures β_l and β_r respectively (see Fig. 2). In the following, we will denote the logarithmic negativity in equilibrium (i.e. in a system where no quench has taken place) at inverse temperature β by $\mathcal{E}^{\mathrm{eq}}_{A_1,A_2}(\beta)$. For technical reasons, calculations will mainly be restricted to CFT models with trivially factorized pairing between holomorphic and anti-holomorphic modules of the CFT (which we will refer to as *trivial pairing data*). However, certain results generalize to arbitrary pairing, as we will indicate. We find the following.

For CFT models with trivial pairing data, the logarithmic negativity between two intervals of equal length, $A_1 = [-v, -u]$ and $A_2 = [u, v]$ (Fig. 4) is given by the average of two expressions that each depend only on one of the temperatures,

$$\mathcal{E}_{[-v,-u],[u,v]}(t;\beta_l,\beta_r) = \frac{1}{2}\left(\mathcal{E}_{[-v,-u],[u,v]}(t;\beta_l) + \mathcal{E}_{[-v,-u],[u,v]}(t;\beta_r)\right), \tag{9}$$

where $\mathcal{E}_{[-v,-u],[u,v]}(t;\beta)$ is the negativity obtained from initially thermalizing both halves at the same temperature. We find different behavior for the latter function depending on the length $v-u$ of the intervals we are measuring, and the time t after connection.

Entanglement starts building after $t > u$. For intermediate times $u < t < v$, the following relation between the logarithmic negativity after the quench in terms of the equilibrium negativity between different intervals holds for CFT models with trivial pairing data:

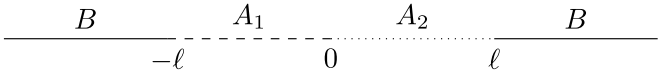

Fig. 5. Negativity between two parts A_1 and A_2 of finite length ℓ.

$$\mathcal{E}_{[-v,-u],[u,v]}(t;\beta) = \mathcal{E}^{\mathrm{eq}}_{[-v,-u]\cup[t,v],[u,t]}(\beta) + \ln C^{\mathcal{T}^2}_{\mathcal{T}\mathcal{T}} - \ln c_{1/2} + 3\ln g, \quad u < t < v. \tag{10}$$

Recall that the equilibrium negativities $\mathcal{E}^{\mathrm{eq}}_{\tilde{A}_1,\tilde{A}_2}$ are calculated in an infinite system where no quench has taken place; the effect of the quench is encoded in the now changed intervals $\tilde{A}_1 = [-v,-u]\cup[t,v]$ and $\tilde{A}_2 = [u,t]$. The constant $C^{\mathcal{T}^2}_{\mathcal{T}\mathcal{T}}$ is the limit $n \to 1$ from even n of a universal 3-point coupling characteristic of the CFT model, whereas $c_{1/2}$ is a non-universal constant that depends on the microscopic details of the quantum chain. Finally, we have a term which is a multiple of $\ln g$, the boundary entropy [43]. For late times, $t > v$, the observables measuring the negativity are in the NESS. The logarithmic negativity in the NESS does not depend on time, and the relation between the negativity after the quench and equilibrium expressions simplifies:

$$\mathcal{E}_{[-v,-u],[u,v]}(t;\beta) = \mathcal{E}^{\mathrm{eq}}_{[-v,-u],[u,v]}(\beta), \qquad t > v. \tag{11}$$

Note that in this regime the above relation (11) and the relation (9) are consistent with the state being a boosted thermal state with boost velocity $(\beta_r - \beta_l)/(\beta_r + \beta_l)$ and rest-frame inverse temperature $\sqrt{\beta_l\beta_r}$. This latter description is expected to hold for CFTs with nontrivial pairing data as well.

The equilibrium expressions for the negativity in the above relations generally depend on the CFT model in question, and therefore an explicit solution cannot be found from CFT methods. However, specializing to the case $A_1 = [-\ell, 0]$ and $A_2 = [0, \ell]$ (Fig. 5), we may find approximate solutions for certain limits of ℓ and t.

For instance, just after the quench, the logarithmic negativity calculated using (10), with $u = 0$ and $v = \ell$, becomes

$$\mathcal{E}_{[-\ell,0],[0,\ell]}(t;\beta) = \frac{c}{2}\ln\frac{t}{\delta} + \ln C^{\mathcal{T}^2}_{\mathcal{T}\mathcal{T}} + \ln c_{1/2} + 3\ln g, \qquad t \ll \text{ any other scale}, \tag{12}$$

where δ is a non-universal factor related to the lattice spacing of the underlying quantum chain and c is the central charge of the CFT model. Here all non-vanishing terms, in the small-t limit, have been accounted for. Note that the behavior just after the quench does not depend on the temperatures of the systems before the quench, or on the length ℓ of the intervals.

Another limit we can take is $\ell \gg t \to \infty$. In this limit, the equilibrium terms in (10), again specializing to $u = 0$ and $v = \ell$, can be found to be of the form

$$\lim_{s\to\infty} \mathcal{E}_{[-\infty,0],[0,\infty]}(s;\beta) = \frac{c}{2}\ln\frac{\beta}{2\pi\delta} + 3\ln C^{\mathcal{T}^2}_{\mathcal{T}\mathcal{T}} + \ln c_{1/2} + 3\ln g. \tag{13}$$

This indicates a plateau, which is different from the plateau reached in the NESS.

We expect the asymptotic result for small t (12) with (9) to hold for more general module pairing in the CFT, but in the "prethermal" regime, the result (13) may have corrections for CFTs with nontrivial pairing data. The difference between the logarithmic negativity just after the quench and in the limit $\ell > t \to \infty$ is a universal function of t/β:

$$\mathcal{E}_{[-\infty,0],[0,\infty]}(t;\beta) - \lim_{s\to\infty} \mathcal{E}_{[-\infty,0],[0,\infty]}(s;\beta) = \frac{c}{2}\ln\frac{2\pi t}{\beta} - 2\ln C^{\mathcal{T}^2}_{\mathcal{T}\mathcal{T}} \quad t \ll \text{ any other scale}. \tag{14}$$

One can interpret the second term as arising from the fact that the entanglement builds up around the two boundary points, which in this limit are far away from each other.

The logarithmic negativity in the NESS (i.e. for $t > \ell$) does not depend on time, and is given by

$$\mathcal{E}^{\mathrm{NESS}}_{[-\ell,0],[0,\ell]}(\beta) = \mathcal{E}_{[-\ell,0],[0,\ell]}(t > \ell;\beta) = \frac{c}{4}\ln\left(\frac{\beta}{2\pi\delta}\tanh\frac{\pi\ell}{\beta}\right) + \ln C^{\mathcal{T}^2}_{\mathcal{T}\mathcal{T}} + \ln c_{1/2}. \tag{15}$$

In this regime it is expected that this result does not depend on pairing data.

By taking the limits $\ell \to \infty$ and $t \to \infty$ of the logarithmic negativity in different order and subtracting the results, we can obtain the gap between the "prethermal" and the "thermal" plateaus:

$$\begin{aligned}\left(\lim_{t\to\infty}\lim_{\ell\to\infty} - \lim_{\ell\to\infty}\lim_{t\to\infty}\right)\mathcal{E}_{[-\ell,0],[0,\ell]}(t;\beta) &= \lim_{s\to\infty}\mathcal{E}_{[-\infty,0],[0,\infty]}(s;\beta) - \mathcal{E}^{\mathrm{NESS}}_{[-\infty,0],[0,\infty]}(\beta)\\ &= \frac{c}{4}\ln\frac{\beta}{2\pi\delta} + 2\ln C^{\mathcal{T}^2}_{\mathcal{T}\mathcal{T}} + 3\ln g.\end{aligned} \tag{16}$$

This is a universal function of the (inverse) temperature, and depends on the boundary entropy and the structure constant $C^{\mathcal{T}^2}_{\mathcal{T}\mathcal{T}}$.

2.2. Comparison to results in the literature

The CFT corresponding to the harmonic chain numerically studied in [32] has trivially factorized module pairing. Therefore, all above results should apply to this case. Using general CFT arguments and their numerical results, the authors of [32] conjectured an expression for the logarithmic negativity in the nonequilibrium steady state (NESS). Our result (15) at $c = 1$ confirms that this conjecture is correct. Further, other numerical results found in [32] for the regime before the system reaches the steady state suggest that the logarithmic negativity builds up quickly (logarithmically), and then saturates to a finite value, before hitting the NESS regime in which it saturates at a lower value. These general features are in agreement with the above results.

3. Branch-point twist fields and a real-time CFT approach to entanglement dynamics

As shown in [8,33] and [11,12], some measures of entanglement, such as the von Neumann and Rényi entropies, and the (logarithmic) negativity, can be expressed using the replica trick in terms of correlation functions of so-called *branch-point twist fields* [34,35,33], associated to the permutation symmetry of the copies. Branch-point twist fields exist in any replica, n-copy QFT model, and are associated with the symmetry under permutation of the copies. The main property of the twist field of interest, associated with a cyclic permutation, is the exchange property

$$\varphi_i(y,t)\,\mathcal{T}(x,t) = \begin{cases}\mathcal{T}(x,t)\,\varphi_i(y,t) & (y<x)\\ \mathcal{T}(x,t)\,\varphi_{i+1}(y,t) & (x<y).\end{cases} \tag{17a}$$

Similarly, the "anti-twist" field, associated with the inverse cyclic permutation, satisfies

$$\varphi_i(y,t)\,\tilde{\mathcal{T}}(x,t) = \begin{cases}\tilde{\mathcal{T}}(x,t)\,\varphi_i(y,t) & (y<x)\\ \tilde{\mathcal{T}}(x,t)\,\varphi_{i-1}(y,t) & (x<y).\end{cases} \tag{17b}$$

The twist fields are local, primary fields, and their scaling dimension was found in [34,35] to be

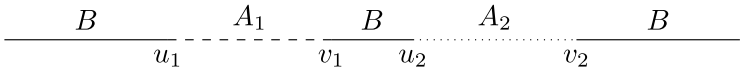

Fig. 6. A picture representing the negativity between part $A_1 = [u_1, v_1]$ (dashed line) and $A_2 = [u_2, v_2]$ (dotted line).

$$d_n = \frac{c}{12}(n - n^{-1}). \tag{18}$$

We will use the CFT normalization

$$\mathcal{T}(x)\tilde{\mathcal{T}}(y) \sim (x-y)^{-2d_n}. \tag{19}$$

In general, the trace of the product of reduced density matrices appearing in the expression for the Rényi entropy $S_A^{(n)}$ for a region A consisting of N cuts $A = [u_1, v_1] \cup \cdots \cup [u_N, v_N]$, is given, for an initial state represented by $\langle \cdots \rangle$, by the following $2N$-point function

$$\operatorname{Tr} \rho_A^n = c_n^N \delta^{2Nd_n} \langle \mathcal{T}(u_1)\tilde{\mathcal{T}}(v_1) \cdots \mathcal{T}(u_N)\tilde{\mathcal{T}}(v_N) \rangle, \tag{20}$$

where $\sqrt{c_n}$ is a nonuniversal constant encoding the conical singularity at the positions of the twist fields (this depends on the number of sheets),[1] and δ is a short-distance regulator such as a lattice spacing. Note that the expression on the right-hand side of (20) is dimensionless, as the twist fields have dimension d_n.

For the negativity, different configurations of twist fields are required. For instance, dividing a system into three subsystems A_1, A_2 and B, consider the negativity measuring of the entanglement between A_1 and A_2, disregarding the entanglement with the third subsystem B (Fig. 6).

In a state represented by $\langle \cdots \rangle$, the logarithmic negativity between the subsystems $A_1 = [u_1, v_1]$ and $A_2 = [u_2, v_2]$ (with $A = A_1 \cup A_2$ and T_2 denotes partial transposition with respect to A_2) is given by [11,12]

$$\begin{aligned} \mathcal{E}_{A_1,A_2} &= \lim_{\substack{n\to 1 \\ n \text{ even}}} \log \operatorname{Tr} |\rho_A^{T_2}|^n = \lim_{\substack{n\to 1 \\ n \text{ even}}} \log \operatorname{Tr} (\rho_A^{T_2})^n \\ &= \lim_{\substack{n\to 1 \\ n \text{ even}}} \log c_n^2 \delta^{4d_n} \langle \mathcal{T}(u_1)\tilde{\mathcal{T}}(v_1)\tilde{\mathcal{T}}(u_2)\mathcal{T}(v_2) \rangle, \end{aligned} \tag{21}$$

where we note that the last two equalities hold only when taking the limit $n \to 1$ analytically continuing from an even number of copies.

Note that in the expressions for the Rényi entropies (20) and the logarithmic negativity (21) we have not specified the state the system is in. In the following, we will consider the local quench as described in Section 2. Our density matrices will therefore have the following dependencies

$$\rho_A = \rho_A(t; \beta_l, \beta_r). \tag{22}$$

In some cases we will find relations between the negativity after the quench and negativities in equilibrium, where a system is thermalized at a certain inverse temperature β. We will denote the equilibrium expressions with

$$\rho_A^{\text{eq}} = \rho_A^{\text{eq}}(\beta). \tag{23}$$

[1] Note the different way in which our constant c_n appears in the formulae compared to formulae in [8] and other papers of these authors: in our case, twist fields are finite CFT fields, hence the constant appears when a pair of twist fields is inserted, whereas in some other works it appears in the computation of the correlation function of twist fields.

3.1. Chiral twist fields

In CFT, local fields decompose into local holomorphic (or chiral) and anti-holomorphic (or anti-chiral) components. Seen as generating Virasoro modules, local fields may be written as $\varphi(x) = \varphi^+(x)\varphi^-(x)$ (more precisely, there is a basis such that this holds). Under homogeneous time evolution, a local field $\varphi(x,t)$ evolves as $\varphi(x,t) = \varphi^+(x-t)\varphi^-(x+t)$, again in the sense of generators for Virasoro modules, and thus time evolution separates the components. The field-theory meaning of this decomposition as modules is that the stress-tensor has independent integer-power "holomorphic" (i.e. as function of $x-t$) and "anti-holomorphic" (i.e. as function of $x+t$) expansions with finite-order singularities. This implies that each component $\varphi^+(x)$ and $\varphi^-(x)$ commutes with energy and momentum densities at space-like distances – thus fulfilling the requirement of locality. Using this decoupling, we can formally define chiral branch point twist fields, which are defined in such a way that they cyclically permute only chiral or anti-chiral components. For example, the equal-time exchange relations for the right-moving branch-point twist field with a right-moving field φ^+ is

$$\varphi_i^+(y)\mathcal{T}^+(x) = \begin{cases} \mathcal{T}^+(x)\,\varphi_i^+(y) & (y<x) \\ \mathcal{T}^+(x)\,\varphi_{i+1}^+(y) & (x<y) \end{cases} \tag{24a}$$

while the equal-time exchange relation with a left-moving field φ^- is simply

$$\varphi_i^-(y)\mathcal{T}^+(x) = \mathcal{T}^+(x)\varphi_i^-(y). \tag{24b}$$

Similar relations hold for left-moving twist fields and for the anti-twist fields.

By considering exchange relations with the stress-energy tensor, it can immediately be seen that these chiral twist fields commute with the full energy and momentum densities of the replica (n-copy) theory. Hence, they are local fields, and one can infer from the above that these chiral twist fields must be related to the usual twist fields via its own holomorphic factorization, $\mathcal{T}(x) = \mathcal{T}^+(x)\mathcal{T}^-(x)$. In particular, their conformal dimension is given by

$$\Delta_n = \frac{c}{24}\left(n - \frac{1}{n}\right). \tag{25}$$

Note that the chiral twist fields carry spin, since for a chiral twist field the difference between its holomorphic dimension and its anti-holomorphic dimension is $\Delta \neq 0$ in general.

When chiral twist fields are brought close to each other, they may or may not have a divergence, depending on the chirality of the fields. Two fields of different chirality do not produce a divergence. For instance,

$$\mathcal{T}^+(x)\mathcal{T}^-(y) \overset{x\to y}{\sim} \mathcal{T}^+(y)\mathcal{T}^-(y) = \mathcal{T}(y). \tag{26}$$

However, fields of the same chirality do produce a divergence, for instance in the following OPE,

$$\mathcal{T}^+(x)\mathcal{T}^+(y) \overset{x\to y}{\sim} (x-y)^{\Delta_n^{(2)}-2\Delta_n}(\mathcal{T}^+)^2(y)C_{\mathcal{T}^+\mathcal{T}^+}^{(\mathcal{T}^+)^2}, \tag{27}$$

where the structure constant $C_{\mathcal{T}^+\mathcal{T}^+}^{(\mathcal{T}^+)^2}$ is a property of the CFT model under consideration, and the conformal dimension of the field $(\mathcal{T}^+)^2$, which is equal to the conformal dimension of $(\mathcal{T}^-)^2$, $(\tilde{\mathcal{T}}^+)^2$ and $(\tilde{\mathcal{T}}^-)^2$, is given by

$$\Delta_n^{(2)} := \begin{cases} \Delta_n & n \text{ odd} \\ 2\Delta_{n/2} & n \text{ even} \end{cases} \tag{28}$$

Similarly, we have the OPE

$$\mathcal{T}^+(x)\tilde{\mathcal{T}}^+(y) \overset{x\to y}{\sim} (x-y)^{-2\Delta_n}, \tag{29}$$

where the normalization in (19) was used.

3.2. *Pairings of holomorphic and anti-holomorphic fields*

It is well known that, although holomorphic factorization in CFT is true at the level of Virasoro representations – that is, the factors are local fields – it does not hold, generically, at the level of the operator algebra. That is, the OPE between fields $\varphi_i(x)$ and $\varphi_j(y)$ is generically not the product of the OPEs between their individual holomorphic, $\varphi_i^+(x)\varphi_j^+(y)$, and anti-holomorphic, $\varphi_i^-(x)\varphi_j^-(y)$, components. For instance, one may have the diagonal structure (here for spinless fields)

$$\varphi_i(x)\varphi_j(y) = \sum_k C_{ij}^k \bar{C}_{ij}^k (x-y)^{d_k-d_i-d_j}\varphi_k(y) \tag{30}$$

instead of the factorized structure

$$\varphi_i(x)\varphi_j(y) = \sum_{k,k'} C_{ij}^k \bar{C}_{ij}^{k'} (x-y)^{\Delta_k^+ + \Delta_{k'}^- - d_i - d_j}\varphi_k^+(y)\varphi_{k'}^-(y). \tag{31}$$

One may say that although holomorphic and anti-holomorphic components are local, they generically have semi-local properties with respect to the operator algebra. This generically affects the chiral twist fields that we introduced above.

It is known that the particular structure of the OPEs constitute additional data of the CFT model under consideration, which, along with the central charge, the set of modules involved and the chiral OPE coefficients, fully characterize the CFT model. This additional data may be referred to as the pairing data of the model. Because of the separation between the chiral and anti-chiral components of the stress-tensor (and of other symmetry currents), highest-weight modules always appear, in any OPE, in a factorized fashion, hence the only pairing data necessary is that identifying the pairing between modules.

The pairing of holomorphic and anti-holomorphic components is a manifestation, at the CFT level, of the fact that, at the quantum-chain level, time-evolved fields are not in general locally supported on end-points of the light-cone, but rather are supported on the full interval lying inside the light-cone. Formally, we may represent this pairing as a connection between holomorphic and anti-holomorphic components, and this connection constrains the OPEs involving the separate components.

Models in which the pairing is trivially factorized are those that are completely built out of symmetry currents: those where all representations involved are the representations associated to the symmetry algebra itself. Free-boson (harmonic chains) and free-fermion models display this property. By construction, in a model with trivially factorized pairing, the OPEs of twist fields in the replica model also trivially factorizes.

It is beyond the scope of this paper to go into any detail of the effect of the pairing data on the dynamics of entanglement. Below we make general comments on this, but mostly consider the special case of factorized pairing. However, many of our results, we expect, do not depend on the pairing data.

Remark. The pairing data of a CFT model affects n-point function calculations for $n \geq 4$; these can be calculated generically by inserting OPEs, and pairing data is necessary within this procedure. Pairing data leads to expressions of 4-point functions as particular linear combinations of products of conformal blocks. One can see, on the other hand, that 2- and 3-point functions do not depend on the pairing data.

3.3. Dynamics after a local quench

The definition of the chiral twist fields is invariant under conjugation by any unitary operator. Considering the time-evolution operator, this allows us to deduce the behavior of branch-point twist fields under time evolution. For example, evolving with the Hamiltonian H after connection, we get the following relation for right-moving fields:

$$\varphi_i^+(\tilde{y})\, e^{-iHt}\mathcal{T}^+(x)e^{iHt} = \begin{cases} e^{-iHt}\mathcal{T}^+(x)e^{iHt}\,\varphi_i^+(\tilde{y}) & (\tilde{y} < x - t) \\ e^{-iHt}\mathcal{T}^+(x)e^{iHt}\,\varphi_{i+1}^+(\tilde{y}) & (x - t < \tilde{y}) \end{cases} \tag{32}$$

where $\tilde{y} := y - t$. From this relation one can see that under time evolution with the Hamiltonian after connection, the right-moving twist field indeed evolves as $e^{-iHt}\mathcal{T}^+(x)e^{iHt} = \mathcal{T}^+(x - t)$, and the left-moving fields as $e^{-iHt}\mathcal{T}^-(x)e^{iHt} = \mathcal{T}^-(x + t)$. The same relations hold for the other twist fields defined in (17).

After time evolution, chiral twist fields are evaluated in the disconnected state $\langle\cdots\rangle_0$ defined by (6). It may be convenient to define a so-called unfolding map, in which left- and right-moving fields of the half-line are mapped to holomorphic fields on the full line, as follows:

$$\mathcal{T}^+(x) \mapsto \tau(x), \qquad \mathcal{T}^-(x) \mapsto \tilde{\tau}(-x), \qquad \tilde{\mathcal{T}}^+(x) \mapsto \tilde{\tau}(x), \qquad \tilde{\mathcal{T}}^-(x) \mapsto \tau(-x). \tag{33a}$$

The holomorphic twist fields τ and $\tilde{\tau}$ are defined on the unfolded line, and will be evaluated in thermal states as per

$$\langle\cdots\rangle^{l/r} \mapsto \langle\cdots\rangle^{\mathrm{ch}}_{\beta_{lr}}, \tag{33b}$$

where $\langle\cdots\rangle^{\mathrm{ch}}_{\beta}$ denotes the thermal expectation value taken in the holomorphic sector. The conformal dimension of these holomorphic twist fields τ and $\tilde{\tau}$ are again given by (25). Similar relations hold for the anti-twist fields.

Because of the generically nontrivial pairing data of the CFT, after time evolution, where some chiral components have evolved through the origin $x = 0$ and changed side, the expectation value in the state $\langle\cdots\rangle_0$ does not generically factorize into a product of expectation values in $\langle\cdots\rangle^{l/r}$. Indeed, pairing may imply connections between components that are positioned in different halves of the system. Hence, the holomorphic expectation values $\langle\ldots\rangle^{\mathrm{ch}}_{\beta_{lr}}$ occurring after unfolding should be understood as thermal conformal blocks, and the time-evolve correlation function is a sum of products of such blocks.

Fortunately, with factorized pairing, even after time evolution, the expectation value of chiral components in $\langle\cdots\rangle_0$ does factorize into a product expectation values in $\langle\cdots\rangle^{l/r}$. Unfolding as above, these are chiral expectation values on the line. Note that with factorized pairing, any thermal expectation value of full (holomorphic times anti-holomorphic) fields also factorizes into its chiral component, so that we have a convenient relation between the chiral expectation values in the unfolded system and full twist-field expectation values on the line:

$$\langle\tau(x)\ldots\tilde{\tau}(y)\rangle^{\mathrm{ch}}_{\beta} = \Big(\langle\mathcal{T}(x)\ldots\tilde{\mathcal{T}}(y)\rangle_{\beta}\Big)^{1/2}. \tag{34}$$

Using (8), (20) and (21), one can use these chiral twist fields to describe the dynamics of entanglement after the quench by evolving the fields under the full Hamiltonian H and then considering the time evolved fields in the disconnected system. This means that, up to certain subtleties, all twist fields that, after time evolution, are to the left of the defect should be evaluated on the half-line at temperature β_l, and all twist fields that are to the right of the defect, should be evaluated on the half-line at temperature β_r. These expressions can be simplified by unfolding the left and right systems, and one is left with products of two holomorphic expressions (conformal blocks) on the line, evaluated at different temperatures. The subtleties arise when the branch cuts emanating from the twist fields cross the point $x = 0$ separating the left and right subsystems, as we now explain.

3.4. Evolution of the entanglement entropy

As a simple example, take the entanglement entropy between a finite region $A = [u, v]$ and the rest. For reasons of simplicity, we will assume that both u and v are positive. Naively, we have

$$\operatorname{Tr}\rho_A^n(t) = c_n\delta^{2d_n}\langle\mathcal{T}(u,t)\tilde{\mathcal{T}}(v,t)\rangle_0, \tag{35}$$

where $\langle\ldots\rangle_0$ is the expectation value taken in the disconnected system and the time-evolved fields are as above. In fact, this formula might involve additional non-universal singularities. Indeed, let us express the correlation function in terms of the chiral twist fields: $\langle\mathcal{T}^+(u-t,0)\mathcal{T}^-(u+t,0)\tilde{\mathcal{T}}^+(v-t,0)\tilde{\mathcal{T}}^-(v+t)\rangle_0$. Here we have two different cuts for the left-moving fields and the right-moving fields: $A^- = [u+t, v+t]$ and $A^+ = [u-t, v-t]$, and a subtlety arises when one of the points of these regions crosses the defect. The fact that in the state ρ_0 the boundary conditions at the point of the defect is such that the two halves are separated, means that each cut extending across the defect is divided into two shorter cuts, one on each side of the defect. This is expressed by the insertion of an extra pair of twist fields, giving rise to extra divergencies that must be regularized.

To make this precise, we consider the EE at the time of the quench as the following limit,

$$\begin{aligned}\operatorname{Tr}\rho_A^n(0) &= c_n\delta^{2d_n}\langle\mathcal{T}(u,0)\tilde{\mathcal{T}}(v,0)\rangle_0\\ &= c_n\delta^{2d_n}\lim_{\varepsilon\to0}(2\varepsilon)^{2d_n}\langle\mathcal{T}(u,0)\tilde{\mathcal{T}}(t-\varepsilon,0)\mathcal{T}(t+\varepsilon,0)\tilde{\mathcal{T}}(v,0)\rangle_0,\end{aligned} \tag{36}$$

where $u < t < v$. Evolving this over a time s with the connected Hamiltonian H, this becomes

$$\begin{aligned}\operatorname{Tr}\rho_A^n(s) &= c_n\delta^{2d_n}\lim_{\varepsilon\to0}(2\varepsilon)^{2d_n}\langle\mathcal{T}(u,s)\tilde{\mathcal{T}}(t-\varepsilon,s)\mathcal{T}(t+\varepsilon,s)\tilde{\mathcal{T}}(v,s)\rangle_0\\ &= c_n\delta^{4\Delta_n}\lim_{\varepsilon\to0}(2\varepsilon)^{4\Delta_n}\langle\mathcal{T}^+(u-s,0)\mathcal{T}^-(u+s,0)\tilde{\mathcal{T}}^+(t-s-\varepsilon,0)\\ &\quad\tilde{\mathcal{T}}^-(t+s-\varepsilon,0)\mathcal{T}^+(t-s+\varepsilon,0)\mathcal{T}^-(t+s+\varepsilon,0)\tilde{\mathcal{T}}^+(v-s,0)\\ &\quad\tilde{\mathcal{T}}^-(v+s,0)\rangle_0.\end{aligned} \tag{37}$$

The expression after time evolution over a time $s = t$ with $u < t < v$ can be written as a product of expectation values for the left and the right system, with the division at 0, as in (6). We can use (6) and the OPE $\mathcal{T}^-(2t-\varepsilon)\tilde{\mathcal{T}}^-(2t+\varepsilon) \overset{\varepsilon\to0}{\sim} (2\varepsilon)^{-2\Delta_n}$ to obtain the expression

$$\begin{aligned}\operatorname{Tr}\rho_A^n(u<t<v) = c_n\delta^{4\Delta_n}\lim_{\varepsilon\to0}(2\varepsilon)^{2\Delta_n}\\ \langle\mathcal{T}^+(u-t)\tilde{\mathcal{T}}^+(-\varepsilon)\rangle_l\langle\mathcal{T}^-(u+t)\mathcal{T}^+(\varepsilon)\tilde{\mathcal{T}}^+(v-t)\tilde{\mathcal{T}}^-(v+t)\rangle_r.\end{aligned} \tag{38}$$

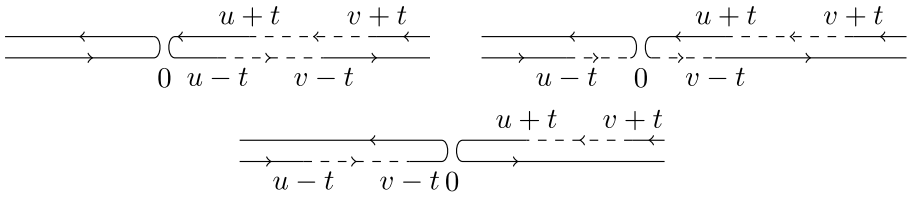

Fig. 7. EE between a part $A = [u, v]$ (with $u > 0$ and $v > 0$) and the rest, a time t after connection, with $t < u < v$ (top left), $u < t < v$ (top right) and $u < v < t$ (bottom).

As will become clear below, the expectation values in (38) are regular as $\varepsilon \to 0$. Hence we must set the remaining factor 2ε proportional to the short-distance cutoff δ. This is equivalent to reversing the limits of $\varepsilon \to 0$ and the scaling limit $\delta \to 0$. The constant of proportionality will generally depend on the number of sheets n,

$$b_n := \frac{2\varepsilon}{\delta}. \tag{39}$$

The first expectation value in (38), corresponding to the left subsystem, can be evaluated by mapping to a chiral theory on the line via the unfolding map (33). We obtain

$$\langle \mathcal{T}^+(u-t)\tilde{\mathcal{T}}^+(0)\rangle_l = \langle \tau(u)\tilde{\tau}(t)\rangle^{\mathrm{ch}}_{\beta_l}, \tag{40}$$

where the expectation value is taken on the line at inverse temperature β_l, and we have used translation invariance to shift the rhs expression over t. Using the relation (34) between the holomorphic twist fields and the full twist fields, we can relate this holomorphic expressions to a Rényi entropy of a different interval, in a system in equilibrium at a different temperature.

On the other hand, the second expectation value in (38), corresponding to the right subsystem, can be re-written as

$$\langle \mathcal{T}^-(u+t)\mathcal{T}^+(0)\tilde{\mathcal{T}}^+(v-t)\tilde{\mathcal{T}}^-(v+t)\rangle_r = \langle \mathcal{T}\left(\frac{u+t}{2}, \frac{u+t}{2}\right)\tilde{\mathcal{T}}(v,t)\rangle_r. \tag{41}$$

A physical interpretation as a Rényi entropy may be obtained by going to a Lorentz boosted frame such that both twist fields, in this frame, are evaluated on the same time slice. In this frame, the state represents a steady state with a thermal flow and with a moving boundary (intersecting the origin of space time), and the Rényi entropy is evaluated instantaneously. The boost velocity is $(t-u)/(u+t-2v)$, the resulting interval length is $D = \sqrt{ut - (u+t-2v)v/2}$, and the left-hand side of the interval is at space-time position given by $x_0 = t_0 = (u+t)(v-t)/(2D)$. Note that the boost velocity is zero at $t = u$ and is the speed of light at $t = v$.

Hence, we find that the Rényi entropy of an interval $A = [u, v]$ an intermediate time $u < t < v$ after a quench can be written in terms of equilibrium and boosted-equilibrium quantities as

$$S^{(n)}_{[u,v]}(u < t < v; \beta_l, \beta_r) = \frac{1}{2}S^{(n),\mathrm{eq}}_{[u,t]}(\beta_l) + \frac{1}{2}S^{(n),\mathrm{boost}}(\beta_r) - \frac{c'_n}{2} + \frac{d_n}{1-n}\ln b_n, \tag{42}$$

where we defined $c'_n := \ln c_n/(1-n)$, where $S^{(n),\mathrm{eq}}_C(\beta)$ denotes the Rényi entropy between a subsystem C and the rest in the system consisting of the full line, in equilibrium at inverse temperature β, and where $S^{(n),\mathrm{boost}}(\beta_r)$ denotes the Rényi entropy in the boosted state described above (which depends on u, v and t).

A simplification occurs in models with factorized pairing. The unfolding map gives

$$\langle \mathcal{T}^-(u+t)\mathcal{T}^+(\varepsilon)\tilde{\mathcal{T}}^+(v-t)\tilde{\mathcal{T}}^-(v+t)\rangle_r = \langle \tau(-v)\tilde{\tau}(-u)\tau(t+\varepsilon)\tilde{\tau}(v)\rangle^{\mathrm{ch}}_{\beta_r}, \tag{43}$$

where again we used translation invariance to shift with t. In factorized pairing models, the 4-point function of holomorphic twist fields has a direct interpretation as a Rényi entropy, using the relation (34). From this we find $S^{(n),\mathrm{boost}}(\beta_r) = S^{(n),\mathrm{eq}}_{[-v,-u]\cup[t,v]}(\beta_r)$, giving

$$S^{(n)}_{[u,v]}(u<t<v;\beta_l,\beta_r) = \frac{1}{2}S^{(n),\mathrm{eq}}_{[u,t]}(\beta_l) + \frac{1}{2}S^{(n),\mathrm{eq}}_{[-v,-u]\cup[t,v]}(\beta_r) - \frac{c'_n}{2} + \frac{d_n}{1-n}\ln b_n. \tag{44}$$

The time dependence is now fully encoded in the intervals A_j in $S^{(n),\mathrm{eq}}_{A_j}(\beta)$, with $A_1 = [u,t]$ and $A_2 = [-v,-u]\cup[t,v]$ for $\beta = \beta_{l,r}$ respectively.

The EE is obtained by taking the limit $n \to 1$, resulting in the expression

$$S_{[u,v]}(u<t<v;\beta_l,\beta_r) = \frac{1}{2}S^{\mathrm{eq}}_{[u,t]}(\beta_l) + \frac{1}{2}S^{\mathrm{boost}}(\beta_r) - \frac{c'_1}{2} - \frac{c}{12}\ln b_1, \tag{45}$$

and, with factorized pairing,

$$S_{[u,v]}(u<t<v;\beta_l,\beta_r) = \frac{1}{2}S^{\mathrm{eq}}_{[u,t]}(\beta_l) + \frac{1}{2}S^{\mathrm{eq}}_{[-v,-u]\cup[t,v]}(\beta_r) - \frac{c'_1}{2} - \frac{c}{12}\ln b_1, \tag{46}$$

where we denote with b_1 the limit $\lim_{n\to 1} b_n$.[2] The last term is equal to the boundary entropy [43]; see Appendix C.

Finally, from Fig. 7, it is clear that for late times $t > v$, the cuts do not extend across the defect, and we may simply write

$$\begin{aligned}\mathrm{Tr}\,\rho_A^n(t>v) &= c_n\delta^{4\Delta_n}\langle\mathcal{T}^+(u-t,0)\tilde{\mathcal{T}}^+(v-t,0)\rangle_l\langle\mathcal{T}^-(u+t,0)\tilde{\mathcal{T}}^-(v+t,0)\rangle_r \\ &= c_n\delta^{4\Delta_n}\langle\tau(u-t)\tilde{\tau}(v-t)\rangle^{\mathrm{ch}}_{\beta_l}\langle\tau(-v-t)\tilde{\tau}(u-t)\rangle^{\mathrm{ch}}_{\beta_r},\end{aligned} \tag{47}$$

which results in the following time-independent expression,

$$S^{(n)}_{[u,v]}(t>v;\beta_l,\beta_r) = \frac{1}{2}S^{(n),\mathrm{eq}}_{[u,v]}(\beta_l) + \frac{1}{2}S^{(n),\mathrm{eq}}_{[u,v]}(\beta_r). \tag{48}$$

We may now use similar principles in order to study the negativity.

Remark. In (38), (40) and (47), we expect factorization to occur independently of the pairing data of the CFT model, because only the identity module is involved in the two-point functions evaluated. Further, we expect the re-writing (41) to be in agreement with the original pairing between holomorphic and anti-holomorphic components imposed by the full twist fields in the original expression. This is because of the simplifications arising from taking identity modules when evaluating the limit $\varepsilon \to 0$, and when evaluating the two-point function on the left subsystem.

4. Evolution of the entanglement negativity after a local quench in the presence of an energy current

In the following, we will calculate the logarithmic negativity between two parts of equal length: $A_1 = [-\ell, 0]$ and $A_2 = [0, \ell]$. We will be considering three important time regimes: first, the time just after the quench (regime I in Fig. 8), in which the numerical results in [32]

[2] Note that we need to specify the value of b_1 as a limit, as for $n = 1$ the twist operators are just the identity operator, and do not depend on position, wherefore the exchange of limits $\delta \to 0$ and $\varepsilon \to 0$ works for any b_1.

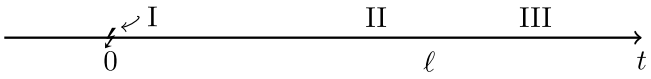

Fig. 8. We will compute the logarithmic negativity in three regimes. I: just after the quench $t \ll 1$, II: a long time after the quench, but before the steady regime $1 \ll t < \ell$ and III: in the steady state $t > \ell$.

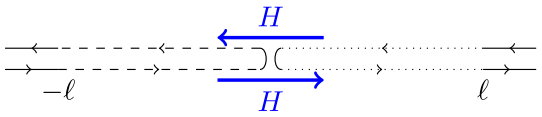

Fig. 9. The negativity between two finite parts of equal length ℓ in an infinite system at the time of the quench $t = 0$. The dashed (dotted) lines indicate that for that chiral sector, each sheet is connected with the sheet above (below). After evolution with the connected Hamiltonian H the twist fields are moved into the other system, and we must regularize the expression for the negativity.

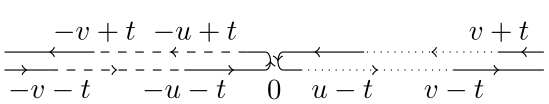

(a) Negativity after a time $t < u$.

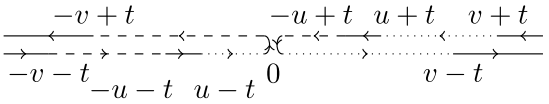

(b) Negativity after a time $u < t < v$.

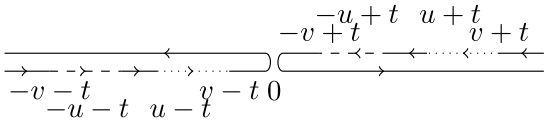

(c) Negativity after a time $t > v$.

Fig. 10. The negativity at time t between two finite parts of length $|u - v|$ evolved back to the time of the quench. On the top left (a), we have the regime $t < u$, in which there is still no entanglement. The top right picture (b) represents the case in which two cuts cross the defect. In the bottom picture (c), the cuts have moved into the different systems, and we are in the steady regime (note that for $t > v$, the negativity does not depend on t).

suggest the logarithmic negativity grows with time logarithmically. Next we consider the system in the limit $\ell \gg t \to \infty$, which would correspond to regime II in Fig. 8. From the numerical results in [32] we expect the logarithmic negativity to saturate to a constant value in this limit. Finally, when considering ℓ finite, one can study the NESS regime (regime III in Fig. 8), which actually already exists for all times $t > \ell$. From the numerics in [32], we expect that the value of the logarithmic negativity in this regime will again be constant in time, and lower than the value in regime II (Fig. 8).

Using the replica trick (21), the logarithmic negativity at the time of the quench can be found by calculating the following expression:

$$\operatorname{Tr} \rho^n_{[-\ell,0],[0,\ell]}(t=0) \propto \langle \mathcal{T}(-\ell,0)\tilde{\mathcal{T}}^2(0,0)\mathcal{T}(\ell,0)\rangle_0, \tag{49}$$

where we have used the notation $\rho_{A_1,A_2} := \rho_A^{T_2}$.

Since the expectation value $\langle \ldots \rangle_0$ is taken at the time of connection, we have to take into account that as the boundary condition changes at the connection point, we must regularize the expression. This will introduce various nonuniversal terms. Therefore, we will first calculate the following expression:

$$\operatorname{Tr} \rho^n_{A_1,A_2}(t=0) = c_n^2 \delta^{4d_n} \langle \mathcal{T}(-v,0)\tilde{\mathcal{T}}(-u,0)\tilde{\mathcal{T}}(u,0)\mathcal{T}(v,0)\rangle_0, \tag{50}$$

where here we have defined $A_1 = [-v,-u]$ and $A_2 = [u,v]$.

As for the case of the EE discussed in Section 3, the regularization may change if the expression (49) is evolved over time (Fig. 9). First, in the trivial case of $t < u$ (Fig. 10 (a)), and for the moment assuming trivial pairing data, we have:

$$\begin{aligned}&\operatorname{Tr}\rho^n_{A_1,A_2}(t<u;\beta_l,\beta_r)\\&\quad=c_n^2\delta^{4d_n}\langle\mathcal{T}^+(-v-t,0)\tilde{\mathcal{T}}^+(-u-t,0)\tilde{\mathcal{T}}^-(-u+t,0)\mathcal{T}^-(-v+t,0)\rangle_l\\&\qquad\langle\mathcal{T}^-(v+t,0)\tilde{\mathcal{T}}^-(u+t,0)\tilde{\mathcal{T}}^+(u-t,0)\mathcal{T}^+(v-t,0)\rangle_r.\end{aligned}\tag{51}$$

This can be mapped to holomorphic twist fields using (33), to give

$$\begin{aligned}\operatorname{Tr}\rho^n_{A_1,A_2}(t<u;\beta_l,\beta_r)=c_n^2\delta^{4d_n}&\langle\tau(-v-t)\tilde{\tau}(-u-t)\tau(u-t)\tilde{\tau}(v-t)\rangle^{\mathrm{ch}}_{\beta_l}\\&\langle\tilde{\tau}(-v-t)\tau(-u-t)\tilde{\tau}(u-t)\tau(v-t)\rangle^{\mathrm{ch}}_{\beta_r}.\end{aligned}\tag{52}$$

Using translation invariance of the holomorphic correlators, it is clear that this expression is independent of time. What's more, the correlators on the right-hand side can be rewritten as follows

$$c_n\delta^{2d_n}\langle\tau(-v)\tilde{\tau}(-u)\tau(u)\tilde{\tau}(v)\rangle^{\mathrm{ch}}_{\beta}=:\left(\operatorname{Tr}(\rho^{\mathrm{eq}}_{A_1\cup A_2,\emptyset})^n(\beta)\right)^{1/2},\tag{53}$$

resulting in the following relation for the logarithmic negativity

$$\mathcal{E}_{A_1,A_2}(t<u;\beta_l,\beta_r)=\frac{1}{2}\left(\mathcal{E}^{\mathrm{eq}}_{A_1\cup A_2,\emptyset}(\beta_l)+\mathcal{E}^{\mathrm{eq}}_{A_1\cup A_2,\emptyset}(\beta_r)\right)=0.\tag{54}$$

This just tells us what we already know: if you consider two intervals a distance u away from the point of connection, at a time $t < u$ after connection, the intervals have not yet had time to build up entanglement. The terms $\mathcal{E}^{\mathrm{eq}}_{\tilde{A}_1,\tilde{A}_2}(\beta)$ denote the logarithmic negativity between subsystems $\tilde{A}_1$ and $\tilde{A}_2$ for a system in equilibrium at inverse temperature β. These are calculated in an infinite system where no quench has taken place. The upshot is that we can obtain time-dependent results using equilibrium (finite temperature) expressions. However, as the intervals $\tilde{A}_1$ and $\tilde{A}_2$ change during the time evolution, the correlation functions may become more complicated.

If the expression (49) is evolved over a time $u < t < v$ (Fig. 10 (b)), extra fields must be inserted at positions $(-t-\varepsilon,t)$, $(-t+\varepsilon,t)$, $(t-\varepsilon,t)$ and $(t+\varepsilon,t)$. For that, we use the following identity:

$$\begin{aligned}&\langle\mathcal{T}(-v,t)\tilde{\mathcal{T}}(-u,t)\tilde{\mathcal{T}}(u,t)\mathcal{T}(v,t)\rangle_0\\&\quad=\lim_{\varepsilon\to0}(2\varepsilon)^{4d_n}\langle\mathcal{T}(-v,t)\tilde{\mathcal{T}}(-t-\varepsilon,t)\mathcal{T}(-t+\varepsilon,t)\tilde{\mathcal{T}}(-u,t)\tilde{\mathcal{T}}(u,t)\\&\qquad\mathcal{T}(t-\varepsilon,t)\tilde{\mathcal{T}}(t+\varepsilon,t)\mathcal{T}(v,t)\rangle_0.\end{aligned}\tag{55}$$

With this, we can express the trace using the chiral twist fields of Section 3.1, again assuming the CFT model in question has trivial pairing data:

$$\begin{aligned}&\operatorname{Tr}\rho^n_{A_1,A_2}(u<t<v;\beta_l,\beta_r)\\&\quad=c_n^2\delta^{8\Delta_n}\lim_{\varepsilon\to0}(2\varepsilon)^{8\Delta_n}\langle\mathcal{T}^+(-v-t,0)\mathcal{T}^-(-v+t,0)\tilde{\mathcal{T}}^+(-2t-\varepsilon,0)\tilde{\mathcal{T}}^-(-\varepsilon,0)\\&\qquad\mathcal{T}^+(-2t+\varepsilon,0)\tilde{\mathcal{T}}^+(-u-t,0)\tilde{\mathcal{T}}^+(u-t,0)\mathcal{T}^+(-\varepsilon,0)\rangle_l\\&\qquad\langle\mathcal{T}^-(\varepsilon,0)\tilde{\mathcal{T}}^-(-u+t,0)\tilde{\mathcal{T}}^-(u+t,0)\mathcal{T}^-(2t-\varepsilon,0)\tilde{\mathcal{T}}^-(2t+\varepsilon,0)\tilde{\mathcal{T}}^+(\varepsilon,0)\\&\qquad\mathcal{T}^-(v+t,0)\mathcal{T}^+(v-t,0)\rangle_r.\end{aligned}\tag{56}$$

Using the OPEs (29), we can simplify this expression:

$$\begin{aligned}
&\operatorname{Tr}\rho^n_{A_1,A_2}(u<t<v;\beta_l,\beta_r)\\
&\quad= c_n^2\delta^{8\Delta_n}\lim_{\varepsilon\to 0}(2\varepsilon)^{4\Delta_n}\langle\mathcal{T}^+(-v-t,0)\mathcal{T}^-(-v+t,0)\\
&\qquad\tilde{\mathcal{T}}^-(-\varepsilon,0)\tilde{\mathcal{T}}^+(-u-t,0)\tilde{\mathcal{T}}^+(u-t,0)\mathcal{T}^+(-\varepsilon,0)\rangle_l\\
&\qquad\langle\mathcal{T}^-(\varepsilon,0)\tilde{\mathcal{T}}^-(-u+t,0)\tilde{\mathcal{T}}^-(u+t,0)\tilde{\mathcal{T}}^+(\varepsilon,0)\mathcal{T}^-(v+t,0)\mathcal{T}^+(v-t,0)\rangle_r. \qquad (57)
\end{aligned}$$

After mapping this expression to an expression containing holomorphic twist fields and using translation invariance to shift by t, we get

$$\begin{aligned}
&\operatorname{Tr}\rho^n_{A_1,A_2}(u<t<v;\beta_l,\beta_r)\\
&\quad= c_n^2\delta^{8\Delta_n}\lim_{\varepsilon\to 0}(2\varepsilon)^{4\Delta_n}\langle\tau(-v)\tilde{\tau}(-u)\tilde{\tau}(u)\tau(t-\varepsilon)\tau(t+\varepsilon)\tilde{\tau}(v)\rangle^{\mathrm{ch}}_{\beta_l}\\
&\qquad\langle\tilde{\tau}(-v)\tau(-u)\tau(u)\tilde{\tau}(t-\varepsilon)\tilde{\tau}(t+\varepsilon)\tau(v)\rangle^{\mathrm{ch}}_{\beta_r}. \qquad (58)
\end{aligned}$$

Using the OPE $\tau(x)\tau(y)\sim C^{\tau^2}_{\tau\tau}(x-y)^{\Delta_n^{(2)}-2\Delta_n}\tau^2(y)$, we can write this as

$$\begin{aligned}
\operatorname{Tr}\rho^n_{A_1,A_2}(u<t<v;\beta_l,\beta_r) = c_n^2\delta^{8\Delta_n}\lim_{\varepsilon\to 0}(2\varepsilon)^{2\Delta_n^{(2)}}(C^{\tau^2}_{\tau\tau})^2\langle\tau(-v)\tilde{\tau}(-u)\tilde{\tau}(u)\tau^2(t)\tilde{\tau}(v)\rangle^{\mathrm{ch}}_{\beta_l}\\
\langle\tilde{\tau}(-v)\tau(-u)\tau(u)\tilde{\tau}^2(t)\tau(v)\rangle^{\mathrm{ch}}_{\beta_r}. \qquad (59)
\end{aligned}$$

Setting 2ε proportional to the cutoff parameter δ introduces an n-dependent constant b_n, defined in (39). This gives:

$$\begin{aligned}
\operatorname{Tr}\rho^n_{A_1,A_2}(u<t<v;\beta_l,\beta_r) = b_n^{2\Delta_n^{(2)}}c_n^2\delta^{8\Delta_n+2\Delta_n^{(2)}}(C^{\tau^2}_{\tau\tau})^2\langle\tau(-v)\tilde{\tau}(-u)\tilde{\tau}(u)\tau^2(t)\tilde{\tau}(v)\rangle^{\mathrm{ch}}_{\beta_l}\\
\langle\tilde{\tau}(-v)\tau(-u)\tau(u)\tilde{\tau}^2(t)\tau(v)\rangle^{\mathrm{ch}}_{\beta_r}. \qquad (60)
\end{aligned}$$

We observe that

$$c_n(c_n^{(2)})^{1/4}\delta^{4\Delta_n+\Delta_n^{(2)}}\langle\tau(-v)\tilde{\tau}(-u)\tilde{\tau}(u)\tau^2(t)\tilde{\tau}(v)\rangle^{\mathrm{ch}}_{\beta} =: \left(\operatorname{Tr}\rho^{n,\mathrm{eq}}_{\tilde{A}_1,\tilde{A}_2}\right)^{1/2}, \qquad (61)$$

where $\tilde{A}_1=[-v,-u]\cup[t,v]$, and $\tilde{A}_2=[u,t]$.

Taking the log of this expression, and sending $n\to 1$ from n even in (28),

$$\lim_{\substack{n\to 1\\ n\text{ even}}}\Delta_n^{(2)} = -\frac{c}{8}, \qquad (62)$$

we can express the logarithmic negativity a time $u<t<v$ after the quench for CFTs with trivial pairing in terms of the logarithmic negativity of systems in equilibrium at temperatures β_l and β_r, respectively:

$$\begin{aligned}
\mathcal{E}_{A_1,A_2}(u<t<v;\beta_l,\beta_r) = \frac{1}{2}\mathcal{E}^{\mathrm{eq}}_{\tilde{A}_1,\tilde{A}_2}(\beta_l)+\frac{1}{2}\mathcal{E}^{\mathrm{eq}}_{\tilde{A}_1,\tilde{A}_2}(\beta_r)\\
+\ln C^{\mathcal{T}^2}_{\mathcal{T}\mathcal{T}}-\ln c_{1/2}-\frac{c}{4}\ln b_1, \qquad (63)
\end{aligned}$$

where we have used $C^{\mathcal{T}^2}_{\mathcal{T}\mathcal{T}}=(C^{\tau^2}_{\tau\tau})^2$. Note that the structure constants $C^{\mathcal{T}^2}_{\mathcal{T}\mathcal{T}}$ defined in the OPE depend on n, and that in (63) the limit $n\to 1$ from even n has been taken. We will not use separate notation to indicate this. Also note that in (63) we used $c_n^{(2)}=c^2_{n/2}$ for n even. The

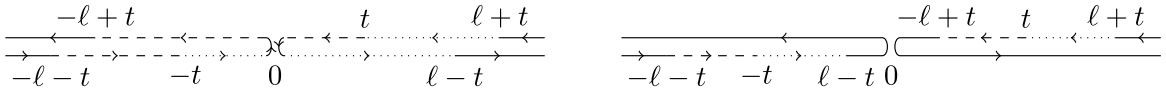

(a) Negativity after a time $t < \ell$. (b) Negativity after a time $t > \ell$.

Fig. 11. The negativity at time t between two finite parts of length ℓ evolved back to the time of the quench. On the left (a), we have the case $t < \ell$, in which two cuts cross the defect and when expressing the negativity in the disconnected system, the 3-point functions become 4-point functions. On the right (b), the cuts have moved into the different systems, and we are in the steady regime (note that for $t > \ell$, the negativity does not depend on t).

last term, $-\frac{c}{4}\ln b_1 = 3\ln g$, which is just three times the boundary entropy (see Appendix C). Again, the terms $\mathcal{E}^{\mathrm{eq}}_{\tilde{A}_1,\tilde{A}_2}(\beta)$ denote the logarithmic negativity between subsystems $\tilde{A}_1$ and $\tilde{A}_2$ for a system in equilibrium at inverse temperature β. As before, the effect of the quench is encoded in the now changed intervals $\tilde{A}_1 = [-v,-u]\cup[t,v]$ and $\tilde{A}_2 = [u,t]$.

The expression for $\operatorname{Tr}\rho^n_{A_1,A_2}(t)$ at late times $t > v$ does not need a regulator, as in that case the cuts do not extend over the connection point (see Fig. 10 (c)). We have

$$\begin{aligned}&\operatorname{Tr}\rho^n_{A_1,A_2}(t>v;\beta_l,\beta_r)\\&\quad= c_n^2\delta^{4d_n}\langle\mathcal{T}^+(-v-t,0)\tilde{\mathcal{T}}^+(-u-t,0)\tilde{\mathcal{T}}^+(u-t,0)\mathcal{T}^+(v-t,0)\rangle_l\\&\qquad\langle\mathcal{T}^-(-v+t,0)\tilde{\mathcal{T}}^-(-u+t,0)\tilde{\mathcal{T}}^-(u+t,0)\mathcal{T}^-(v+t,0)\rangle_r,\end{aligned}\tag{64}$$

which, after mapping to holomorphic twist fields and using translation invariance, becomes

$$\operatorname{Tr}\rho^n_{A_1,A_2}(t>v;\beta_l,\beta_r) = c_n^2\delta^{4d_n}\langle\tau(-v)\tilde{\tau}(-u)\tilde{\tau}(u)\tau(v)\rangle^{\mathrm{ch}}_{\beta_l}\langle\tilde{\tau}(-v)\tau(-u)\tau(u)\tilde{\tau}(v)\rangle^{\mathrm{ch}}_{\beta_r}.\tag{65}$$

This results in the following expression

$$\mathcal{E}_{A_1,A_2}(t>v;\beta_l,\beta_r) = \frac{1}{2}\mathcal{E}^{\mathrm{eq}}_{A_1,A_2}(\beta_l) + \frac{1}{2}\mathcal{E}^{\mathrm{eq}}_{A_1,A_2}(\beta_r).\tag{66}$$

From the form of (54), (63) and (66), we can conclude that for intervals $A_1 = [-v,-u]$ and $A_2 = [u,v]$ that are equidistant from the connection point and have equal length, we can always write the logarithmic negativity after the quench as the average of the logarithmic negativity for a system that is thermalized at inverse temperature β_l and one that is thermalized at temperature β_r:

$$\mathcal{E}_{[-v,-u],[u,v]}(t;\beta_l,\beta_r) = \frac{1}{2}\left(\mathcal{E}_{[-v,-u],[u,v]}(t;\beta_l) + \mathcal{E}_{[-v,-u],[u,v]}(t;\beta_r)\right).\tag{67}$$

Note that for models with trivial pairing data, this expression is valid at any time t after the quench. However, for more general CFTs we expect this to hold only for $t > v$. In the following, we will always calculate the negativity for the case $\beta_l = \beta_r = \beta$. It must therefore be noted that all our results for $t < v$ may have corrections.

Let us now specialize to the case $A_1 = [-\ell, 0]$ and $A_2 = [0,\ell]$. In this case there are two situations: $t < \ell$ and $t > \ell$ (Fig. 11). We must substitute $v = \ell$ and take the limit $u \to 0$ in the expressions (63) and (66).

In order to find the relation between the logarithmic negativity a time t after the quench and the negativity in equilibrium systems, we take the appropriate limits from the physical quantities we have computed. For instance, the equilibrium expressions are defined as

$$\mathcal{E}^{\mathrm{eq}}_{[-\ell,0],[0,\ell]}(\beta) := \lim_{\substack{u\to 0\\ v\to\ell}}\mathcal{E}^{\mathrm{eq}}_{[-v,-u],[u,v]}(\beta).\tag{68}$$

Using (68), (63) and (66), we deduce that

$$\mathcal{E}_{[-\ell,0],[0,\ell]}(t;\beta) = \lim_{\substack{u\to 0\\ v\to\ell}} \mathcal{E}_{[-v,-u],[u,v]}(t;\beta). \tag{69}$$

As a check, we may compute the relation between the two choices of intervals explicitly, and we find that irrespective of the state of the system, we get the following expression:

$$\begin{aligned}\lim_{\substack{u\to 0\\ v\to\ell}} \mathrm{Tr}(\rho_{[-v,-u],[u,v]})^n &= \lim_{\substack{u\to 0\\ v\to\ell}} c_n^2 \delta^{4d_n} \langle \mathcal{T}(-v)\tilde{\mathcal{T}}(-u)\tilde{\mathcal{T}}(u)\mathcal{T}(v)\rangle \\ &= c_n^2 C_{\tilde{\mathcal{T}}\tilde{\mathcal{T}}}^{\tilde{\mathcal{T}}^2} a_n^{-2d_n+d_n^{(2)}} \delta^{2d_n+d_n^{(2)}} \langle \mathcal{T}(-\ell)\tilde{\mathcal{T}}^2(0)\mathcal{T}(\ell)\rangle, \end{aligned} \tag{70}$$

where in the second step we used the OPE $\tilde{\mathcal{T}}(x)\tilde{\mathcal{T}}(y) \sim C_{\tilde{\mathcal{T}}\tilde{\mathcal{T}}}^{\tilde{\mathcal{T}}^2}(x-y)^{-2d_n+d_n^{(2)}}\tilde{\mathcal{T}}^2(y)$, and the constant a_1 appears when we set $(x-y)\sim a_n\delta$ in this OPE. This constant is different from b_n, since the OPE is different (it gives a different change in geometry). We note that for both equilibrium and nonequilibrium states of the system, the difference between $\mathcal{E}_{[-v,0],[0,v]}$ and the limit $u\to 0$ of $\mathcal{E}_{[-v,-u],[u,v]}$ is the same combination of constants, which on physical grounds (as asserted in (68) and (69)) we require to add up to zero:

$$\frac{c}{4}\ln a_1 + \ln c_{1/2} - \ln C_{\tilde{\mathcal{T}}\tilde{\mathcal{T}}}^{\tilde{\mathcal{T}}^2} = 0. \tag{71}$$

In the following, we will therefore be able to take $u=0$ and $v=\ell$ directly.

4.1. Early times: regimes I and II ($t<\ell$)

The expressions $\mathcal{E}^{\mathrm{eq}}_{[-\ell,0]\cup[t,\ell],[0,t]}(\beta)$ contain four-point functions:

$$\mathrm{Tr}(\rho^{\mathrm{eq}}_{[-\ell,0]\cup[t,\ell],[0,t]})^n(\beta) = c_n c_n^{(2)} \delta^{2d_n+2d_n^{(2)}} \langle \mathcal{T}(-\ell)\tilde{\mathcal{T}}^2(0)\mathcal{T}^2(t)\tilde{\mathcal{T}}(\ell)\rangle_\beta. \tag{72}$$

In this case the general result is strongly model dependent, as the expression for a four-point function contains a model-dependent function of the cross-ratio of the four coordinates. We first map this correlation function to the plane

$$\begin{aligned}&\langle \mathcal{T}(-\ell)\tilde{\mathcal{T}}^2(0)\mathcal{T}^2(t)\tilde{\mathcal{T}}(\ell)\rangle_\beta \\ &= \left(\frac{2\pi}{\beta}\right)^{2d_n+2d_n^{(2)}} (e^{2\pi t/\beta})^{d_n^{(2)}} \langle \mathcal{T}(e^{-2\pi\ell/\beta})\tilde{\mathcal{T}}^2(1)\mathcal{T}^2(e^{2\pi t/\beta})\tilde{\mathcal{T}}(e^{2\pi\ell/\beta})\rangle_{\mathbb{C}}. \end{aligned} \tag{73}$$

Using global conformal invariance, the four-point function on the plane can be brought in the following form:

$$\langle \mathcal{T}(z_1)\tilde{\mathcal{T}}^2(z_2)\mathcal{T}^2(z_3)\tilde{\mathcal{T}}(z_4)\rangle_{\mathbb{C}} = |z_{14}|^{-2d_n}|z_{23}|^{-2d_n^{(2)}}\mathcal{F}_n(\eta), \tag{74}$$

with the four-point ratio

$$\eta = \frac{z_{12}z_{34}}{z_{13}z_{24}}. \tag{75}$$

Mapping this result back to the cylinder using $w_i = \frac{\beta}{2\pi}\ln z_i$, and using

$$\lim_{\substack{n\to 1\\ n \text{ even}}} d_n = 0, \qquad \text{and} \qquad \lim_{\substack{n\to 1\\ n \text{ even}}} d_n^{(2)} = -c/4, \tag{76}$$

we can express the finite-temperature negativity between $\tilde{A}_1 = [-\ell, 0] \cup [t, \ell]$ and $\tilde{A}_2 = [0, t]$, for $t < \ell$ as follows

$$\mathcal{E}^{\text{eq}}_{[-\ell,0]\cup[t,\ell],[0,t]}(\beta) = \frac{c}{2} \ln\left(\frac{\beta}{\pi\delta} \sinh\frac{\pi t}{\beta}\right) + f\left(\frac{\sinh(\pi(\ell-t)/\beta)}{\sinh(\pi(\ell+t)/\beta)}\right) + 2\ln c_{1/2}, \quad t < \ell. \tag{77}$$

The function $f(\eta) := \lim_{\substack{n\to 1 \\ n \text{ even}}} \mathcal{F}_n(\eta)$ is model-dependent (it depends on the universality class of the CFT model). However, we may find its value for general CFT in certain limits, where the four-point function reduces to a two- or three-point function.

4.1.1. Regime I

The behavior right after the quench can be studied directly by taking the limit $t \to 0$, which corresponds to $z_3 \to z_2$ in (74), and considering the OPE

$$\tilde{\mathcal{T}}^2(x)\mathcal{T}^2(y) \overset{x\to y}{\sim} |x-y|^{-2d_n^{(2)}}. \tag{78}$$

With this, the four-point function (74) becomes

$$\langle \mathcal{T}(z_1)\tilde{\mathcal{T}}^2(z_2)\mathcal{T}^2(z_3)\tilde{\mathcal{T}}(z_4)\rangle \overset{z_2\to z_3}{\sim} |z_{23}|^{-2d_n^{(2)}} \langle \mathcal{T}(z_1)\tilde{\mathcal{T}}(z_4)\rangle. \tag{79}$$

Again mapping back to the cylinder using $z_j := \exp(2\pi w_j/\beta)$, with $w_1 = -\ell$, $w_2 = 0$, $w_3 = t$ and $w_4 = \ell$, and considering the scaling dimensions (76) in the limit $n \to 1$ from even values of n, we find that, for very early times, the behavior of the logarithmic negativity is characterized by the function

$$\mathcal{E}^{\text{eq}}_{[-\ell,0]\cup[t,\ell],[0,t]}(\beta) \sim \frac{c}{2}\ln\frac{t}{\delta} + 2\ln c_{1/2}, \qquad t \ll \text{ any other scale.} \tag{80}$$

Note that this equation only holds for t very small, but the constants in the expression are all accounted for. Using (63) to compute the logarithmic negativity after the quench, we obtain the dynamics for the negativity a very short time after the quench.

$$\mathcal{E}_{[-\ell,0],[0,\ell]}(t;\beta) \sim \frac{c}{2}\ln\frac{t}{\delta} + \ln C^{\mathcal{T}^2}_{\mathcal{T}\mathcal{T}} + \ln c_{1/2} + 3\ln g, \qquad t \ll \text{ any other scale,} \tag{81}$$

where again we note that $-\frac{c}{4}\ln b_1 = 3\ln g$ (see Appendix C), where $\ln g$ is the boundary entropy [43]. Note that although this result has been derived using the assumption of trivial pairing data, we expect this result to hold for any CFT.

4.1.2. Regime II

Another regime in which we may find a general expression is the limit $\ell \gg t \to \infty$. Note that the cross ratio in (77) depends on ℓ and t. After taking the limit $\ell \to \infty$, the cross ratio reduces to $\exp(-2\pi t/\beta)$, and the four-point function in the replica limit simplifies to

$$\lim_{\substack{n\to 1 \\ n \text{ even}}} \lim_{\ell\to\infty} \langle \mathcal{T}(-\ell)\tilde{\mathcal{T}}^2(0)\mathcal{T}^2(t)\tilde{\mathcal{T}}(\ell)\rangle_\beta = \left(\frac{\beta}{\pi}\sinh\frac{\pi t}{\beta}\right)^{c/2} \mathcal{F}_1\left(e^{-2\pi t/\beta}\right). \tag{82}$$

This gives model-dependent behavior of the logarithmic negativity as a function of time, since there is a time-dependent part in f that is dependent on the CFT model (or specifically, its universality class), and must be computed for different models, but we may study the limiting

behavior of $f(e^{-2\pi t/\beta})$ for very early or very late times. Note that we do not expect to reach the NESS regime at late times, since we consider $t < \ell$.

To characterize the behavior of $f(\eta)$ for $\eta \to 0$, we can compare the general expression for the four-point function, and take the limit $z_1 \to z_2$, so that the cross ratio $\eta \to 0$. On the other hand, we may evaluate the lhs explicitly by using the OPE

$$\mathcal{T}(z_1)\tilde{\mathcal{T}}^2(z_2) \overset{z_1\to z_2}{\sim} C^{\tilde{\mathcal{T}}}_{\mathcal{T}\tilde{\mathcal{T}}^2} |z_{12}|^{-d_n^{(2)}} \tilde{\mathcal{T}}(z_2). \tag{83}$$

By inserting an extra twist field, and comparing the expectation value of the lhs as $z_1 \to z_2$ to the expectation value of the rhs, we obtain the following relation for the structure constant $C^{\tilde{\mathcal{T}}}_{\mathcal{T}\tilde{\mathcal{T}}^2}$:

$$C^{\tilde{\mathcal{T}}}_{\mathcal{T}\tilde{\mathcal{T}}^2} = \lim_{z_1\to z_2} C_{\mathcal{T}\tilde{\mathcal{T}}^2\mathcal{T}} |z_{13}|^{-d_n^{(2)}} |z_{23}|^{d_n^{(2)}} = C_{\mathcal{T}\tilde{\mathcal{T}}^2\mathcal{T}}. \tag{84}$$

Using this OPE, we can calculate the four-point function in the limit $z_1 \to z_2$.

$$\begin{aligned}\langle \mathcal{T}(z_1)\tilde{\mathcal{T}}^2(z_2)\mathcal{T}^2(z_3)\tilde{\mathcal{T}}(z_4)\rangle &\overset{z_1\to z_2}{\sim} C^{\tilde{\mathcal{T}}}_{\mathcal{T}\tilde{\mathcal{T}}^2} |z_{12}|^{-d_n^{(2)}} \langle \tilde{\mathcal{T}}(z_2)\mathcal{T}^2(z_3)\tilde{\mathcal{T}}(z_4)\rangle \\ &= (C^{\tilde{\mathcal{T}}}_{\mathcal{T}\tilde{\mathcal{T}}^2})^2 |\eta|^{-d_n^{(2)}} |z_{23}|^{-2d_n^{(2)}} |z_{24}|^{-2d_n},\end{aligned} \tag{85}$$

where we used (84) to obtain $C_{\tilde{\mathcal{T}}\mathcal{T}^2\tilde{\mathcal{T}}} = C_{\mathcal{T}\tilde{\mathcal{T}}^2\mathcal{T}} = C^{\tilde{\mathcal{T}}}_{\mathcal{T}\tilde{\mathcal{T}}^2}$. Comparing this with (74), we see that the function $\mathcal{F}_n$ behaves in the limit $\eta \to 0$ as

$$\mathcal{F}_n(\eta) \overset{\eta\to 0}{\sim} (C^{\tilde{\mathcal{T}}}_{\mathcal{T}\tilde{\mathcal{T}}^2})^2 |\eta|^{-d_n^{(2)}}. \tag{86}$$

The result for the negativity in the limit $\ell \gg t \to \infty$ is

$$\lim_{\substack{n\to 1\\ n \text{ even}}} \lim_{\ell\gg t\to\infty} \langle \mathcal{T}(-\ell)\tilde{\mathcal{T}}^2(0)\mathcal{T}^2(t)\tilde{\mathcal{T}}(\ell)\rangle_\beta = (C^{\tilde{\mathcal{T}}}_{\mathcal{T}\tilde{\mathcal{T}}^2})^2 \left(\frac{\beta}{2\pi}\right)^{c/2}, \tag{87}$$

resulting in the following expression for the equilibrium negativity for the changed interval[3]:

$$\mathcal{E}^{\text{eq}}_{[-\infty,0]\cup[t,\infty],[0,t]}(\beta) = \frac{c}{2}\ln\frac{\beta}{2\pi\delta} + 2\ln C^{\tilde{\mathcal{T}}}_{\mathcal{T}\tilde{\mathcal{T}}^2} + 2\ln c_{1/2}, \qquad t\to\infty. \tag{88}$$

Finally, we substitute the above expression into (63) to find the logarithmic negativity in this limit, valid for CFT models with trivial pairing data:

$$\lim_{s\to\infty} \mathcal{E}_{[-\infty,0],[0,\infty]}(s;\beta) = \frac{c}{2}\ln\frac{\beta}{2\pi\delta} + 2\ln C^{\tilde{\mathcal{T}}}_{\mathcal{T}\tilde{\mathcal{T}}^2} + \ln C^{\mathcal{T}^2}_{\mathcal{T}\mathcal{T}} + \ln c_{1/2} + 3\ln g. \tag{89}$$

This is simplified by using the relation

$$C^{\tilde{\mathcal{T}}}_{\mathcal{T}\tilde{\mathcal{T}}^2} = C^{\mathcal{T}^2}_{\mathcal{T}\mathcal{T}} \tag{90}$$

proved in Appendix B. The first thing we notice is that expression (88) does not depend on t, thus confirming that the limit in (89) exists, and in regime II the logarithmic negativity reaches

[3] The expressions for the negativity in equilibrium (88) for $\ell \to \infty$, correspond to the negativity of a bipartite system at finite temperature, which was calculated in [44]. Our results agree, but we have made a different choice of function $\mathcal{F}_n(x)$.

a plateau. Unsurprisingly, the height of these plateaus decreases at higher temperatures. Another thing we may do is look at the difference of the logarithmic negativity in regime I and regime II, given by equations (81) and (89), the result is a universal function of t and the inverse temperature β:

$$\mathcal{E}_{[-\infty,0],[0,\infty]}(t;\beta) - \lim_{s\to\infty} \mathcal{E}_{[-\infty,0],[0,\infty]}(s;\beta) = \frac{c}{2}\ln\frac{2\pi t}{\beta} - 2\ln C^{\tilde{\mathcal{T}}}_{\mathcal{T}\tilde{\mathcal{T}}^2}$$
$$t \ll \text{ any other scale.} \tag{91}$$

4.2. *Late times: regime III ($t > \ell$)*

We compute the equilibrium expression for the trace:

$$\mathrm{Tr}(\rho^{\mathrm{eq}}_{[-\ell,0],[0,\ell]})^n(\beta) = c_n (c_n^{(2)})^{1/2} \delta^{2d_n + d_n^{(2)}} \langle \mathcal{T}(-\ell)\tilde{\mathcal{T}}^2(0)\mathcal{T}(\ell)\rangle_\beta. \tag{92}$$

Using the exponential map, we get the expression in terms of a correlation function on the Riemann sphere:

$$\langle \mathcal{T}(-\ell)\tilde{\mathcal{T}}^2(0)\mathcal{T}(\ell)\rangle_\beta = \left(\frac{\beta}{2\pi}\right)^{-2d_n - d_n^{(2)}} \langle \mathcal{T}(e^{-2\pi\ell/\beta})\tilde{\mathcal{T}}^2(1)\mathcal{T}(e^{2\pi\ell/\beta})\rangle_{\mathbb{C}} \tag{93}$$

Using (84), we have

$$\langle \mathcal{T}(e^{-2\pi\ell/\beta})\tilde{\mathcal{T}}^2(1)\mathcal{T}(e^{2\pi\ell/\beta})\rangle_{\mathbb{C}} = C^{\tilde{\mathcal{T}}}_{\mathcal{T}\tilde{\mathcal{T}}^2} \left(2\sinh\frac{2\pi\ell}{\beta}\right)^{-2d_n} \left(\tanh\frac{\pi\ell}{\beta}\right)^{-d_n^{(2)}}, \tag{94}$$

from which we compute the equilibrium negativity:

$$\mathcal{E}^{\mathrm{eq}}_{[-\ell,0],[0,\ell]}(\beta) = \frac{c}{4}\ln\left(\frac{\beta}{2\pi\delta}\tanh\frac{\pi\ell}{\beta}\right) + \ln C^{\tilde{\mathcal{T}}}_{\mathcal{T}\tilde{\mathcal{T}}^2} + \ln c_{1/2}. \tag{95}$$

Using (66) we find that this is equal to the NESS logarithmic negativity for $t > \ell$:

$$\mathcal{E}^{\mathrm{NESS}}_{[-\ell,0],[0,\ell]}(\beta) = \mathcal{E}_{[-\ell,0],[0,\ell]}(t > \ell;\beta) = \frac{c}{4}\ln\left(\frac{\beta}{2\pi\delta}\tanh\frac{\pi\ell}{\beta}\right) + \ln C^{\tilde{\mathcal{T}}}_{\mathcal{T}\tilde{\mathcal{T}}^2} + \ln c_{1/2}. \tag{96}$$

Note that this expression is independent of pairing data of the CFT, and therefore should hold for general CFT.

We can compare the values of this plateau (regime III, or the "thermal" regime) with the plateau in regime II (or the "prethermal" regime) by taking the limit $\ell \to \infty$ in (96). Using (90) to simplify the result in the prethermal regime, the difference between the two plateaus is

$$\lim_{s\to\infty} \mathcal{E}_{[-\infty,0],[0,\infty]}(s;\beta) - \mathcal{E}^{\mathrm{NESS}}_{[-\infty,0],[0,\infty]}(\beta) = \frac{c}{4}\ln\frac{\beta}{2\pi\delta} + 2\ln C^{\mathcal{T}^2}_{\mathcal{T}\mathcal{T}} + 3\ln g, \tag{97}$$

which is universal.

Remark. We expect the general relations (54), (63) and (66) to depend on the pairing data of the CFT model. However, the results of Section 4.1.1 are expected to hold in general, due simplifications arising when taking the limit $t \to 0$.

5. Discussion/conclusion

We have found analytical expressions for the EE and the logarithmic negativity after a local, "cut and glue"-type, quench that are valid for CFT models with trivial pairing data, as well as a few that are valid for any CFT, in certain time regimes. These expressions are in agreement with the behavior found in [32], in which the time evolution of the logarithmic negativity was studied numerically for the case of the harmonic chain. In particular, our initial logarithmic growth with t appears to agree with the behavior found in [32], as does the initial saturation in regime II, which is reached when t is large enough, but still smaller than ℓ. The results in [32] also suggest the existence of a NESS shortly after the point $t > \ell$ is reached (in our exact results this is instantaneous), whose conjectured form is confirmed by our results.

We find that for the case $t < \ell$ the universal dependence on t and ℓ of the logarithmic negativity has the same form as the logarithmic negativity in a thermal state between a region $[0, t]$ and its direct environment $[-\ell, 0] \cup [t, \ell]$, which has been considered in [44].

The appearance of the term $2 \ln C^{\tilde{\mathcal{T}}}_{\mathcal{T}\tilde{\mathcal{T}}^2}$ in the universal difference (91), in particular of the factor 2, seems to indicate the appearance, at large times t (in the limit $\ell \to \infty$), of two points around which the independent contributions to the entanglement arise. Looking at the form of the equilibrium expressions in (63) in this limit, given by (88), it is clear from the intervals $\tilde{A}_1 = [-\infty, 0] \cup [t, \infty]$, $\tilde{A}_2 = [0, t]$ that in the large t limit the same result can be obtained by using a product of two three-point functions $\langle \mathcal{T}\tilde{\mathcal{T}}^2\mathcal{T}\rangle\langle\tilde{\mathcal{T}}\mathcal{T}^2\tilde{\mathcal{T}}\rangle$, giving rise to the $2 \ln C_{\mathcal{T}\tilde{\mathcal{T}}^2\mathcal{T}}$ term (note that $C_{\tilde{\mathcal{T}}\mathcal{T}^2\tilde{\mathcal{T}}} = C_{\mathcal{T}\tilde{\mathcal{T}}^2\mathcal{T}}$). This observation on the equilibrium expression represents the fact that the negativity of an interval of length t with respect to the rest of the system at finite temperatures has, at large t, two independent contributions coming from the boundary points of an interval, due to the finite effective correlation length generated by the nonzero temperature.

We may also give a physical explanation for the relation (63) between the negativity after the quench and the equilibrium negativity. This physical explanation accounts for the equality of the universal parts: the dependence on the time, temperatures and interval lengths, up to additional non-universal constants. We take the case $u = 0$ and $v = \ell \to \infty$ for simplicity. See Fig. 12 for a pictorial representation. In this picture, one considers the creation of entangled pairs at any time before or after the quench. In the disconnected state, any particle from an entangled pair reflects at the defect. However, after connection, one of the entangled particles can move into the other subsystem. Whether this happens, depends on the time of creation, and the distance from the connection point. Using such rules, one can "count" the number of entangled pairs contributing to the entanglement between the left and right after a time t. On the other hand, one can also count the number of entangled pairs contributing to the entanglement of an interval of length t at equilibrium (without defect). A moment's thought shows that these two numbers are equal.

In our calculations we have assumed that the pairing between holomorphic and anti-holomorphic modules of the CFT is trivially factorized. This is not the case in general, and therefore the relations we have found between the logarithmic negativity after a quench and the logarithmic negativity in equilibrium do not hold in general. However, as explained, in certain time regimes the results are expected to become independent of pairing data. Further, it is possible that the above physically compelling particle-pair-creation picture could have more general validity.

A next step would be to learn more about the way in which pairing affects our computations. In particular, we would like to find limits in which the results are independent of pairing, and determine the corrections that our general relations would get for CFT models with nontrivial

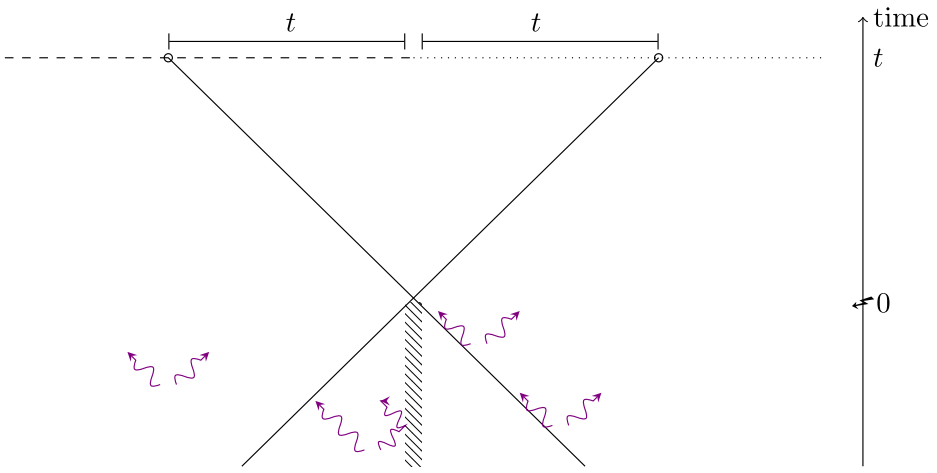

Fig. 12. A time t after the quench, we start to see an effect of two lightcones (whose size depends on the length ℓ of the intervals, so they can be infinite), one starting somewhere in the left system and one in the right, where in each lightcone there is an interval of length t in the other half of the system, which can entangle with the rest of the interval within the lightcone. If we take these two lightcones together, we end up with something looking like an interval of length t in a larger system, which accounts for the appearance of two factors of $C_{\mathcal{T}\tilde{\mathcal{T}}^2\mathcal{T}}$ at late times.

pairing data. Other interesting directions are generalizing these results to integrable QFTs, and to cases with nontrivial impurities after the connection (that situation has been studied in the recent work [45]). Another avenue would be to apply the ideas developed in this and related work to other observables. Finally, it would be extremely interesting to understand the evolution of entanglement in higher-dimensional CFT in the cut-and-glue setup, possibly using methods of gauge–gravity duality.

Acknowledgements

The authors would like to thank Pasquale Calabrese, John Cardy, Martin Plenio and Zoltan Zimboras for useful feedback.

This research has been funded in part by EPSRC, under grant code EP/J500252/1.

Appendix A. The steady-state density matrix and scattering map

Consider again the quench problem as depicted in Fig. 1, where two independently thermalized halves of the system are connected to each other and let to evolve unitarily. The steady state is reached in the region around the connection point after an infinite time evolution. More precisely, the steady-state (stationary) limit is

$$\langle \mathcal{O} \rangle_{\text{ness}} = \lim_{t\to\infty} \lim_{L\to\infty} \langle e^{iHt} \mathcal{O} e^{-iHt} \rangle_0 \tag{98}$$

where L is the total length of the system. This limit is expected to exist for $\mathcal{O}$ being any local observable or product thereof.

In [21,22], the family of observables formed by the stress-energy tensor and its descendants (the "energy sector") was considered. In CFT, this family can of course be factorized into right-movers and left-movers. It was shown that, on this family, the result of the steady-state limit can be described by a state where right-movers and left-movers are independently thermalized. That

is, if $\varphi_1^+\varphi_2^-$ is a product of right-moving and left-moving observables in the energy sector, then it was shown that

$$\langle\varphi_1^+\varphi_2^-\rangle_{\text{ness}} = \langle\varphi_1\rangle_{\beta_l}\langle\varphi_2\rangle_{\beta_r} \tag{99}$$

where $\varphi_{1,2}$ are the chiral fields corresponding to $\varphi_{1,2}^{\pm}$. This, in turn, can be interpreted as emerging from a simple density matrix:

$$\langle\mathcal{O}\rangle_{\text{ness}} = \frac{\text{Tr}\left(e^{-W}\mathcal{O}\right)}{\text{Tr}\left(e^{-W}\right)} \tag{100}$$

where

$$W = \beta_l H_+ + \beta_r H_- \tag{101}$$

and $H_\pm$ represent the total right/left-moving energies. Owing to the fact that the total energy is $H = H_+ + H_-$ and that the total momentum is $P = H_+ - H_-$, one can further re-interpret this density matrix as the boost of a thermal state [24]:

$$W = \beta_{\text{rest}}(\cosh\theta\ H - \sinh\theta\ P) \tag{102}$$

where the rest-frame inverse temperature is $\beta_{\text{rest}} = \sqrt{\beta_l\beta_r}$ and the boost velocity is $\tanh\theta = (\beta_r - \beta_l)/(\beta_r + \beta_l)$.

It is interesting to extend this family of observable and determine the form of the steady state on the extended family. One of course expects the steady state to be described, on extended families, in a similar manner as above, although the sharp light cone effect describing the instantaneous reach of the steady state in the energy sector [21,22] is not expected to hold in general.

In this section we show that the above description of the steady state stays valid on the branch-point twist fields, where the right- and left-moving factors are the right- and left-moving branch-point twist fields discussed in Section 3.

The clearest way to show this is to directly evaluate the scattering map S on branch-point twist fields. The scattering map is a map acting on observables, $\mathcal{O} \mapsto S(\mathcal{O})$, which represents the large-time forward evolution with H and backward evolution with H_0 of local observables:

$$S(\mathcal{O}) = \lim_{t\to\infty} e^{-iH_0t}e^{iHt}\mathcal{O}e^{-iHt}e^{iH_0t}. \tag{103}$$

It is a simple matter to see that it allows to write the steady state using the original state:

$$\langle\mathcal{O}\rangle_{\text{ness}} = \langle S(\mathcal{O})\rangle_0. \tag{104}$$

The observables resulting from the application of the scattering map are to be evaluated in the state $\langle\cdot\rangle_0$. In this state, the left and right regions of the system are separated. The boundary conditions for both left and right regions, at the point $x = 0$, are invariant under permutation of the replica copies. Hence, the unitary symmetry operator Z for cyclic permutation, $\varphi_i(x)Z = Z\varphi_{i+1}(x)$, can be separated into two unitary operators generating the independent symmetries on the left and the right subsystems: $Z = Z_l\,Z_r$ with

$$\varphi_i(x)Z_l = \begin{cases} Z_l\,\varphi_i(x) & (x>0) \\ Z_l\,\varphi_{i+1}(x) & (x<0) \end{cases}, \quad \varphi_i(x)Z_r = \begin{cases} Z_r\,\varphi_{i+1}(x) & (x>0) \\ Z_r\,\varphi_i(x) & (x<0) \end{cases},$$

$$Z_l^\dagger Z_l = Z_r^\dagger Z_r = \mathbf{1}.$$

For later convenience, we define the *reversed twist field*,

$$\varphi_i(y,t)\mathcal{U}(x,t) = \begin{cases} \mathcal{U}(x,t)\,\varphi_i(y,t) & (x<y) \\ \mathcal{U}(x,t)\,\varphi_{i+1}(y,t) & (y<x) \end{cases} \tag{105a}$$

with the corresponding reversed anti-twist field

$$\varphi_i(y,t)\tilde{\mathcal{U}}(x,t) = \begin{cases} \tilde{\mathcal{U}}(x,t)\,\varphi_i(y,t) & (x<y) \\ \tilde{\mathcal{U}}(x,t)\,\varphi_{i-1}(y,t) & (y<x) \end{cases} \tag{105b}$$

By definition, these are related to the normal twist fields via relations such as $\mathcal{U}(x) = Z\tilde{\mathcal{T}}(x)$, $\tilde{U}(x) = \tilde{Z}\mathcal{T}(x)$, etc., where Z and $\tilde{Z}$ are the operators that permute the sheets one way or the other (i.e. they insert a branch cut over the entire length of the system).

From these relations, it is clear that

$$\mathcal{T}(x_1)\tilde{\mathcal{T}}(x_2) = \tilde{\mathcal{U}}(x_1)\mathcal{U}(x_2) \tag{106}$$

$$\tilde{\mathcal{T}}(x_1)\mathcal{T}(x_2) = \mathcal{U}(x_1)\tilde{\mathcal{U}}(x_2). \tag{107}$$

Naturally, it is possible to identify Z_l and Z_r with appropriate regularizations of $\mathcal{U}(0^-)$ and $\mathcal{T}(0^+)$, respectively, with respect to the state $\langle\cdot\rangle_0$. For instance, $Z_r = \lim_{x\to 0^+} x^{\Delta_n}\mathcal{T}(x)$.

We will obtain the following:

$$S(\mathcal{T}^+(x)) = \begin{cases} \mathcal{U}^-(-x) & (x>0) \\ Z_l\tilde{\mathcal{U}}^+(x) & (x<0) \end{cases} \tag{108}$$

$$S(\mathcal{T}^-(x)) = \begin{cases} \mathcal{T}^-(x) & (x\geq 0) \\ Z_r\tilde{\mathcal{T}}^+(-x) & (x<0) \end{cases} \tag{109}$$

$$S(\mathcal{U}^+(x)) = \begin{cases} Z_l\tilde{\mathcal{U}}^-(-x) & (x>0) \\ \mathcal{U}^+(x) & (x\leq 0) \end{cases} \tag{110}$$

$$S(\mathcal{U}^-(x)) = \begin{cases} Z_r\tilde{\mathcal{T}}^-(x) & (x>0) \\ \mathcal{T}^+(-x) & (x\leq 0) \end{cases} \tag{111}$$

as well as similar equations with the exchange $\mathcal{T}^\pm, \mathcal{U}^\pm, Z_{l,r} \leftrightarrow \tilde{\mathcal{T}}^\pm, \tilde{\mathcal{U}}^\pm, Z_{l,r}^\dagger$.

One can interpret this map by analyzing its action on the cuts emanating from the positions of the twist fields. These cuts are to be divided into segments that fall into one of four regions: (A) left-moving fields in the left system, (B) left-moving fields in the right system, (C) right-moving fields in the left system, and (D) right-moving fields in the right system. From the above equations, we note that, essentially, the map S takes (B) and (C) into themselves, and (A) and (D) into each other.

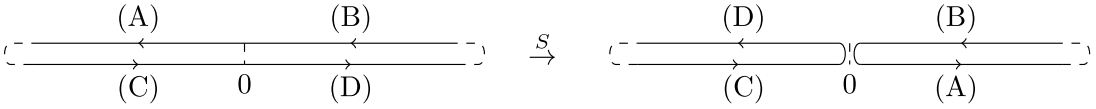

The map S above immediately implies chiral factorization in the steady state: right- and left-movers are mapped onto left- and right-subsystems, respectively, which are independently thermalized in $\langle\cdot\rangle_0$. We may now map each independent subsystem onto a chiral theory, with in particular $Z_{l,r}$ mapping to the chiral replica permutation operator Z. One can see that the composition with S is the identity operator, showing (99).

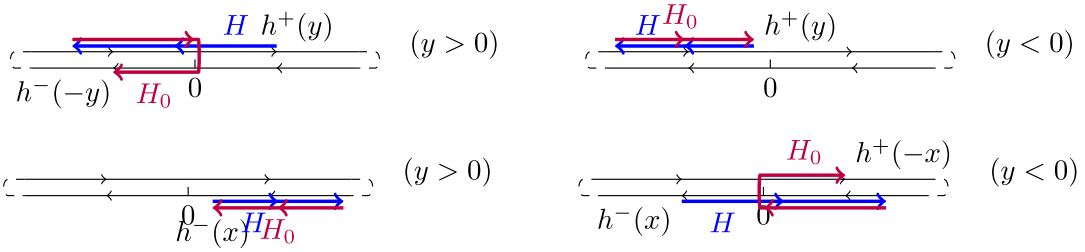

Fig. 13. The forward time evolution with H and subsequent backward time evolution with H_0 of $h^+(y)$ in equation (112) and $h^-(x)$ in equation (113) is shown.

It is then a simple matter to observe that the steady-state values of the entanglement entropy and negativity do reproduce the large-time limits evaluated by direct time evolution in the previous section.

A.1. Calculation of the scattering map

We deduce the form of $S(\mathcal{T})$ and $S(\tilde{\mathcal{T}})$ by comparing the equal-time exchange relations before and after the process of forward and backward time evolution. Consider the right- and left-moving energy densities $h^{\pm}(y)$. On these fields, the scattering map is given by [ ]

$$S(h^+(y)) = \begin{cases} h^-(-y) & (y > 0) \\ h^+(y) & (y < 0) \end{cases} \tag{112}$$

and

$$S(h^-(y)) = \begin{cases} h^-(y) & (y > 0) \\ h^+(-x) & (y < 0) \end{cases} \tag{113}$$

See Fig. 13 for a depiction of these results.

Consider the equal-time exchange relations

$$h_i^+(y)\mathcal{T}_+(0) = \begin{cases} \mathcal{T}_+(0)\, h_i^+(y) & (y < x) \\ \mathcal{T}_+(0)\, h_{i+1}^+(y). & (y > x) \end{cases} \tag{114}$$

Since the scattering (103) is a conjugation, the exchange relations are preserved. Therefore, we also have:

$$S(h_i^+(y))S(\mathcal{T}_+(x)) = \begin{cases} S(\mathcal{T}_+(x))\, S(h_i^+(y)) & (y < x) \\ S(\mathcal{T}_+(x))\, S(h_{i+1}^+(y)) & (y > x) \end{cases} \tag{115}$$

which, using (112), gives the following equations:

$$h_i^+(y)S(\mathcal{T}_+(x)) = S(\mathcal{T}_+(x))\, h_i^+(y) \qquad (y < x \;\&\; y < 0) \tag{116}$$

$$h_i^+(y)S(\mathcal{T}_+(x)) = S(\mathcal{T}_+(x))\, h_{i+1}^+(y) \qquad (y > x \;\&\; y < 0) \tag{117}$$

$$h_i^-(-y)S(\mathcal{T}_+(x)) = S(\mathcal{T}_+(x))\, h_i^-(-y) \qquad (y < x \;\&\; y > 0) \tag{118}$$

$$h_i^-(-y)S(\mathcal{T}_+(x)) = S(\mathcal{T}_+(x))\, h_{i+1}^-(-y) \qquad (y > x \;\&\; y > 0) \tag{119}$$

We can find more information on $S(\mathcal{T}_+)$ by doing the same with the exchange relations with h^-. Since $\mathcal{T}_+$ only acts as boundary-changing field on right-moving fields, these exchange relations are trivial:

$$h_i^-(y)\mathcal{T}_+(x) = \mathcal{T}_+(x)h_i^-(y). \tag{120}$$

After scattering, these are

$$h_i^-(y)S(\mathcal{T}_+(x)) = S(\mathcal{T}_+(x))h_i^-(y) \qquad (y>0) \tag{121}$$

$$h_i^+(-y)S(\mathcal{T}_+(x)) = S(\mathcal{T}_+(x))h_i^+(-y) \qquad (y<0) \tag{122}$$

Collecting these equations, we have the following exchange relations for $S(\mathcal{T}_+)$:

$$h_i^+(y)S(\mathcal{T}_+(x)) = \begin{cases} S(\mathcal{T}_+(x))h_i^+(y) & (y<x \ \&\ y<0,\ y>0) \\ S(\mathcal{T}_+(0))h_{i+1}^+(y) & (x<y<0) \end{cases} \tag{123}$$

$$h_i^-(y)S(\mathcal{T}_+(x)) = \begin{cases} S(\mathcal{T}_+(0))h_i^-(y) & (-x<y<0,\ y>0) \\ S(\mathcal{T}_+(0))h_{i+1}^-(y) & (y<-x \ \&\ y<0) \end{cases} \tag{124}$$

When $x \geq 0$, this just simplifies to:

$$h_i^+(y)S(\mathcal{T}_+(x)) = S(\mathcal{T}_+(x))h_i^+(y) \tag{125}$$

$$h_i^-(y)S(\mathcal{T}_+(x)) = \begin{cases} S(\mathcal{T}_+(x))h_i^-(y) & (-x<y) \\ S(\mathcal{T}_+(x))h_{i+1}^-(y) & (y<-x) \end{cases} \tag{126}$$

which means that:

$$S(\mathcal{T}_+(x)) = \mathcal{U}_-(-x) \qquad x \geq 0 \tag{127}$$

However, for $x<0$, we have

$$h_i^+(y)S(\mathcal{T}_+(x)) = \begin{cases} S(\mathcal{T}_+(x))h_i^+(y) & (y<x) \\ S(\mathcal{T}_+(x))h_{i+1}^+(y) & (x<y<0) \\ S(\mathcal{T}_+(x))h_i^+(y) & (y>0) \end{cases} \tag{128}$$

$$h_i^-(y)S(\mathcal{T}_+(x)) = \begin{cases} S(\mathcal{T}_+(x))h_{i+1}^-(y) & (y<0) \\ S(\mathcal{T}_+(x))h_i^-(y) & (y>0) \end{cases} \tag{129}$$

so for $x<0$ the result of $S(\mathcal{T}_+)$ is a product between $\mathcal{U}_-(0)$ and a branch cut between $x<y<0$ for the right-moving fields:

$$S(\mathcal{T}_+(x)) \propto \mathcal{U}_-(0)\mathcal{T}_+(x)\tilde{\mathcal{T}}_+(0) \qquad (x<0) \tag{130}$$

This can be re-written as

$$S(\mathcal{T}_+(x)) \propto \mathcal{U}_-(0)\tilde{\mathcal{U}}^+(x)\mathcal{U}^+(0) \propto Z_l\,\tilde{\mathcal{U}}^+(x) \qquad (x<0) \tag{131}$$

Taking into account the normalization of the field, we obtain (108).

The other relations can be obtained similarly.

Appendix B. Relations between structure constants

In this appendix we will establish general relations amongst structure constants associated with cyclic permutation twist fields (powers of the branch-point twist fields). One of these relations will be (90), needed in the main text. We will use the following notation for the fields that permute the n sheets cyclically by an amount of $i \in \{0,1,\dots,n-1\}$:

$$\sigma_i := \mathcal{T}^i. \tag{132}$$

For convenience, we extend the notation to $i \in \mathbb{N}$ by periodicity $\sigma_{i+n} = \sigma_i$.

By the fundamental properties of twist fields, the OPE $\sigma_i(x)\sigma_j(y)$ must be in the twist sector associated to $i+j$, hence

$$\sigma_i(x)\sigma_j(y) \overset{x\to y}{\sim} \frac{C^{\sigma_{i+j}}_{\sigma_i,\sigma_j}\,\sigma_{i+j}(y)}{|x-y|^{d_i+d_j-d_{i+j}}} \tag{133}$$

where d_i is the scaling dimension of σ_i. We wish to establish constraints on the structure constants $C_{i,j} := C^{\sigma_{i+j}}_{\sigma_i,\sigma_j}$.

The CFT normalization is the condition

$$C_{i,-i} = 1 \tag{134}$$

which amounts to normalizing the two-point function as

$$\langle\sigma_i(x_1)\sigma_j(x_2)\rangle = \delta_{i+j,0}\frac{1}{x_{12}^{2d_i}}. \tag{135}$$

Further, since the subgroup of cyclic permutation is abelian, we have

$$C_{i,j} = C_{j,i}. \tag{136}$$

By acting with the permutation element that inverts all sheets (this elements generates, along with cyclic permutation elements, the maximal subgroup that preserves the cyclic permutation subgroup), we also find

$$C_{-i,-j} = C_{i,j}. \tag{137}$$

With the identity element, the OPE is trivial, whence

$$C_{0,i} = 1. \tag{138}$$

In order to obtain additional information, we consider three-point functions, which are fixed by conformal invariance up to multiplicative constants:

$$\langle\sigma_i(x_1)\sigma_j(x_2)\sigma_k(x_3)\rangle = \delta_{i+j+k,0}\frac{C_{\sigma_i,\sigma_j,\sigma_{-i-j}}}{x_{12}^{d_i+d_j-d_k}x_{13}^{d_i+d_k-d_j}x_{23}^{d_j+d_k-d_i}} \tag{139}$$

From the OPE (133), we find

$$\langle\sigma_i(x_1)\sigma_j(x_2)\sigma_k(x_3)\rangle \overset{x_1\to x_2}{\sim} \frac{C_{i,j}\langle\sigma_{i+j}(x_2)\sigma_k(x_3)\rangle}{x_{12}^{d_i+d_j-d_{i+j}}} = \delta_{i+j+k,0}\frac{C_{i,j}}{x_{12}^{d_j+d_j-d_{i+j}}x_{23}^{d_{i+j}+d_k}} \tag{140}$$

and comparing with the limit $x_1\to x_2$ in (139), it is clear that $C_{\sigma_i,\sigma_j,\sigma_{-i-j}} = C_{i,j}$. Similarly,

$$\langle\sigma_i(x_1)\sigma_j(x_2)\sigma_k(x_3)\rangle \overset{x_2\to x_3}{\sim} \frac{C_{j,k}\langle\sigma_i(x_1)\sigma_{j+k}(x_3)\rangle}{x_{23}^{d_j+d_k-d_{j+k}}} = \delta_{i+j+k,0}\frac{C_{j,k}}{x_{23}^{d_j+d_k-d_{j+k}}x_{13}^{d_i+d_{j+k}}}, \tag{141}$$

wherefore $C_{\sigma_i,\sigma_j,\sigma_{-i-j}} = C_{j,-i-j}$. From these we obtain an extra constraint on the structure constants:

$$C_{i,j} = C_{j,-i-j}. \tag{142}$$

Putting $i=j=1$ in this equation, we find (90).

Finally, by factorization of the multi-sheeted theory, we also have

$$C_{i/k,j/k;n/k} = C_{i,j;n} \tag{143}$$

where we have explicitly written the number n of copies via $C_{i,j} = C_{i,j;n}$, and where k divides i, j and n.

Using these relations, one can reduce the number of unknown structure constants. For instance, for $n = 2$ we have $C_{i,j} = 1$ for all i, j. For $n = 3$, we find a single unknown structure constant, $C_{1,1} = C_{2,2}$ (the others are unity). For $n = 4$, there is also a single unknown structure constant, $C_{1,1} = C_{1,2} = C_{2,1} = C_{2,3} = C_{3,2} = C_{3,3}$ (the others are unity). The non-unity structure constants for $n = 5$ are $C_{1,1} = C_{1,3} = C_{2,4} = C_{4,4}$ and $C_{1,2} = C_{2,2} = C_{3,3} = C_{3,4}$ (up to equality under exchanging indices). For $n = 6$, the unknown are $C_{1,1} = C_{1,4} = C_{2,5} = C_{5,5}$ and $C_{1,2} = C_{1,3} = C_{2,3} = C_{3,4} = C_{3,5} = C_{4,5}$ (again up to equality under exchanging indices), $C_{2,2} = C_{4,4}$ are related to structure constants for $n = 3$, and the others are unity. The unknown structure constants must in general be determined by evaluating 4-point functions, and depend on the particular CFT model under consideration.

Appendix C. Boundary entropy

In order to find an expression for the boundary entropy introduced in [43] in terms of the nonuniversal constants appearing in our expressions for the EE and the logarithmic negativity, we must relate the EE for an interval of length ℓ on the half-line to the EE for an interval of length 2ℓ on the line, both in equilibrium. Not specifying the state of the system, we first find an expression for the trace of the system with a boundary:

$$\operatorname{Tr} \rho_{[0,\ell]}^{\text{bdry}} = c_n \delta^{2d_n} \lim_{\varepsilon\to 0} \langle \mathcal{T}(\varepsilon)\tilde{\mathcal{T}}(\ell)\rangle_{\mathbb{R}^+}. \tag{144}$$

We can compute this by unfolding (33) and using the OPE $\tilde{\tau}(-\varepsilon)\tau(\varepsilon) \sim (2\varepsilon)^{-2\Delta_n}$,

$$\lim_{\varepsilon\to 0} \langle \mathcal{T}(\varepsilon)\tilde{\mathcal{T}}(\ell)\rangle_{\mathbb{R}^+} = \lim_{\varepsilon\to 0} \langle \tau(-\ell)\tilde{\tau}(-\varepsilon)\tau(\varepsilon)\tilde{\tau}(\ell)\rangle_{\mathbb{R}}^{\text{ch}} = \lim_{\varepsilon\to 0} (2\varepsilon)^{-2\Delta_n} \langle \tau(-\ell)\tilde{\tau}(\ell)\rangle_{\mathbb{R}}^{\text{ch}}. \tag{145}$$

As discussed in Section 3, in taking the limit $\varepsilon \to 0$ we are in effect exchanging this limit with the scaling limit. In order to account for this, we define a constant $b_n := 2\varepsilon/\delta$, in terms of which the trace can be written as

$$\operatorname{Tr} \rho_{[0,\ell]}^{\text{bdry}} = c_n b_n^{-2\Delta_n} \delta^{2\Delta_n} \langle \tau(-\ell)\tilde{\tau}(\ell)\rangle^{\text{ch}} = c_n^{1/2} b_n^{-d_n} \left(\operatorname{Tr} \rho_{[-\ell,\ell]}^{\text{bulk}}\right)^{1/2}. \tag{146}$$

This leads to the relation

$$S_{[0,\ell]}^{\text{bdry}} = \frac{1}{2} S_{[-\ell,\ell]}^{\text{bulk}} + \frac{c_1'}{2} - \frac{c}{12} \ln b_1, \tag{147}$$

from which we conclude that the boundary entropy is equal to [8,46,47],

$$\ln g = -\frac{c}{12} \ln b_1. \tag{148}$$

Here we note that whenever we encounter b_1, we take this to be the limit $\lim_{n\to 1} b_n$. Recall that b_n, defined in (39), appears when taking a limit where a bulk field goes to the boundary, which amounts to exchanging limits $\delta \to 0$ and $\varepsilon \to 0$. For $n = 1$ this works for any b_1, since the branch-point twist fields are just the identity, and do not depend on position.

Appendix D. Mutual information

The mutual information between two regions A_1 and A_2 is defined as

$$I_{A_1,A_2} := S_{A_1} + S_{A_2} - S_{A_1\cup A_2}, \tag{149}$$

with S_A the EE between a region A and the rest of the system, and similarly the Rényi mutual information is defined by

$$I^{(n)}_{A_1,A_2} := S^{(n)}_{A_1} + S^{(n)}_{A_2} - S^{(n)}_{A_1\cup A_2}. \tag{150}$$

In order to find relations for the mutual information after a local quench, we first must compute relations similar to (42) and (48) but in the case of an interval $[-v,-u]$ in the left system, and the case of an interval $[-v,-u]\cup[u,v]$ in both systems. We take $u>0$ and $v>0$, as we did before. The relation for $S^{(n)}_{[-v,-u]}$ can be obtained by simply replacing $\beta_l \leftrightarrow \beta_r$ in (42) and (48). In order to find similar relations for $S^{(n)}_{[-v,-u]\cup[u,v]}$, we follow the method outlined in Section 3. First, we note that $t>v$ the cuts do not extend across the defects, wherefore the NESS result should be time independent. For times $u<t<v$, the cuts do extend across the defects, and we have to regularize the expression for the trace by inserting extra pairs of twist fields as follows:

$$\begin{aligned}
&\operatorname{Tr}\rho^n_{[-v,-u]\cup[u,v]}(u<t<v)\\
&\quad= c_n^2\delta^{4d_n}\lim_{\varepsilon\to 0}(2\varepsilon)^{4d_n}\langle\mathcal{T}(-v,t)\tilde{\mathcal{T}}(-t-\varepsilon,t)\mathcal{T}(-t+\varepsilon,t)\tilde{\mathcal{T}}(-u,t)\mathcal{T}(u,t)\tilde{\mathcal{T}}(t-\varepsilon,t)\\
&\qquad\mathcal{T}(t+\varepsilon,t)\tilde{\mathcal{T}}(v,t)\rangle_0.
\end{aligned}\tag{151}$$

Performing the time evolution on the chiral twist fields defined in Section 3 and using the necessary OPEs, we obtain

$$\begin{aligned}
&\operatorname{Tr}\rho^n_{[-v,-u]\cup[u,v]}(u<t<v)\\
&\quad= c_n^2\delta^{8\Delta_n}\lim_{\varepsilon\to 0}(2\varepsilon)^{4\Delta_n}\langle\mathcal{T}^+(-v-t,0)\mathcal{T}^-(-v+t,0)\tilde{\mathcal{T}}^+(-u-t,0)\mathcal{T}^+(u-t,0)\\
&\qquad\tilde{\mathcal{T}}^-(-\varepsilon,0)\tilde{\mathcal{T}}^+(-\varepsilon,0)\rangle_l\\
&\qquad\langle\mathcal{T}^-(\varepsilon,0)\tilde{\mathcal{T}}^-(-u+t,0)\mathcal{T}^-(u+t,0)\mathcal{T}^+(\varepsilon,0)\tilde{\mathcal{T}}^+(v-t,0)\tilde{\mathcal{T}}^-(v+t,0)\rangle_r.
\end{aligned}\tag{152}$$

After the unfolding map, this becomes

$$\begin{aligned}
&\operatorname{Tr}\rho^n_{[-v,-u]\cup[u,v]}(u<t<v)\\
&\quad= c_n^2\delta^{8\Delta_n}\lim_{\varepsilon\to 0}(2\varepsilon)^{4\Delta_n}\langle\tau(-v-t)\tilde{\tau}(-u-t)\tau(u-t)\tilde{\tau}(-\varepsilon)\tau(\varepsilon)\tilde{\tau}(v-t)\rangle^{\mathrm{ch}}_{\beta_l}\\
&\qquad\langle\tau(-v-t)\tilde{\tau}(-u-t)\tau(u-t)\tilde{\tau}(-\varepsilon)\tau(\varepsilon)\tilde{\tau}(v-t)\rangle^{\mathrm{ch}}_{\beta_r}.
\end{aligned}\tag{153}$$

We can use the OPEs again to simplify this equation further:

$$\begin{aligned}
\operatorname{Tr}\rho^n_{[-v,-u]\cup[u,v]}(u<t<v) = c_n^2\delta^{8\Delta_n}&\langle\tau(-v-t)\tilde{\tau}(-u-t)\tau(u-t)\tilde{\tau}(v-t)\rangle^{\mathrm{ch}}_{\beta_l}\\
&\langle\tau(-v-t)\tilde{\tau}(-u-t)\tau(u-t)\tilde{\tau}(v-t)\rangle^{\mathrm{ch}}_{\beta_r},
\end{aligned}\tag{154}$$

leading to the relation

$$\begin{aligned}
&\operatorname{Tr}\rho^n_{[-v,-u]\cup[u,v]}(u<t<v)\\
&\quad= \left(\operatorname{Tr}(\rho^{\mathrm{eq}}_{[-v,-u]\cup[u,v]})^n(\beta_l)\right)^{1/2}\left(\operatorname{Tr}(\rho^{\mathrm{eq}}_{[-v,-u]\cup[u,v]})^n(\beta_r)\right)^{1/2}.
\end{aligned}\tag{155}$$

Note that this relation does not depend on time. Since we also know that for times $t < u$ and $t > u$ the relation is time independent, we find that the relation between the Rényi entropy after the local quench and equilibrium quantities for two intervals of equal length, at equal distances from the point of connection, is given by

$$S^{(n)}_{[-v,-u]\cup[u,v]}(t;\beta_l,\beta_r) = \frac{1}{2}\left(S^{(n),\mathrm{eq}}_{[-v,-u]\cup[u,v]}(\beta_l) + S^{(n),\mathrm{eq}}_{[-v,-u]\cup[u,v]}(\beta_r)\right), \tag{156}$$

where, as before, we explicitly label equilibrium expressions. So the EE after a local quench between $[-v,-u]\cup[u,v]$ and its complement, does not depend on time. Using (156) and (42) (both as is and with $\beta_l \leftrightarrow \beta_r$), we have for $u < t < v$ the following relation for the Rényi mutual information:

$$\begin{aligned} I^{(n)}_{[-v,-u],[u,v]}(u<t<v;\beta_l,\beta_r) = {} & \frac{1}{2}\left(I^{(n),\mathrm{eq}}_{[u,t],[-v,-u]\cup[t,v]}(\beta_l) + I^{(n),\mathrm{eq}}_{[u,t],[-v,-u]\cup[t,v]}(\beta_r)\right) \\ & - c'_n + \frac{2d_n}{1-n}\ln b_n, \end{aligned} \tag{157}$$

with $c'_n := \ln c_n/(1-n)$. The mutual information for this time regime simplifies to

$$\begin{aligned} I_{[-v,-u],[u,v]}(u<t<v;\beta_l,\beta_r) = {} & \frac{1}{2}\left(I^{\mathrm{eq}}_{[u,t],[-v,-u]\cup[t,v]}(\beta_l) + I^{\mathrm{eq}}_{[u,t],[-v,-u]\cup[t,v]}(\beta_r)\right) \\ & + c'_1 + 2\ln g, \end{aligned} \tag{158}$$

with $\ln g$ the boundary entropy first discussed in [43], see Appendix C. In the NESS, we can use (156) together with (48) (again, for both choices of β_l, β_r) to find the simpler relation:

$$I^{(n)}_{[-v,-u],[u,v]}(t>v;\beta_l,\beta_r) = \frac{1}{2}\left(I^{(n),\mathrm{eq}}_{[-v,-u],[u,v]}(\beta_l) + I^{(n),\mathrm{eq}}_{[-v,-u],[u,v]}(\beta_r)\right), \tag{159}$$

with the mutual information given by

$$I_{[-v,-u],[u,v]}(t>v;\beta_l,\beta_r) = \frac{1}{2}\left(I^{\mathrm{eq}}_{[-v,-u],[u,v]}(\beta_l) + I^{\mathrm{eq}}_{[-v,-u],[u,v]}(\beta_r)\right). \tag{160}$$

References

[1] L. Amico, R. Fazio, A. Osterloh, V. Vedral, Entanglement in many-body systems, Rev. Mod. Phys. 80 (2008) 517–576.
[2] J. Eisert, M. Cramer, M. Plenio, Colloquium: area laws for the entanglement entropy, Rev. Mod. Phys. 82 (2010) 277–306.
[3] C. Bennett, H. Bernstein, S. Popescu, B. Schumacher, Concentrating partial entanglement by local operations, Phys. Rev. A 53 (1996) 2046–2052.
[4] D. Jonathan, M. Plenio, Entanglement-assisted local manipulation of pure quantum states, Phys. Rev. Lett. 83 (1999) 3566–3569.
[5] M.A. Nielsen, Conditions for a class of entanglement transformations, Phys. Rev. Lett. 83 (1999) 436–439.
[6] S. Turgut, Catalytic transformations for bipartite pure states, J. Phys. A 40 (40) (2007) 12185.
[7] C. Holzhey, F. Larsen, F. Wilczek, Geometric and renormalized entropy in conformal field theory, Nucl. Phys. B 424 (1994) 443–467.
[8] P. Calabrese, J. Cardy, Entanglement entropy and quantum field theory, J. Stat. Mech. 2004 (2004) P06002.
[9] G. Vidal, R. Werner, Computable measure of entanglement, Phys. Rev. A 65 (2002) 032314.
[10] M. Plenio, Logarithmic negativity: a full entanglement monotone that is not convex, Phys. Rev. Lett. 95 (2005) 090503.
[11] P. Calabrese, J. Cardy, E. Tonni, Entanglement negativity in quantum field theory, Phys. Rev. Lett. 109 (2012) 130502.

[12] P. Calabrese, J. Cardy, E. Tonni, Entanglement negativity in extended systems: a field theoretical approach, J. Stat. Mech. 2013 (2013) P02008.
[13] C. Caroli, R. Combescot, P. Nozieres, D. Saint-James, Direct calculation of the tunneling current, J. Phys. C 4 (8) (1971) 916.
[14] R. Rubin, W. Greer, Abnormal lattice thermal conductivity of a one-dimensional, harmonic, isotopically disordered crystal, J. Math. Phys. 12 (8) (1971) 1686–1701.
[15] H. Spohn, J. Lebowitz, Stationary non-equilibrium states of infinite harmonic systems, Commun. Math. Phys. 54 (2) (1977) 97–120.
[16] S. Tasaki, Nonequilibrium stationary states for a quantum 1-d conductor, in: AIP Conf. Proc., vol. 519, AIP Publishing, 2000, pp. 356–358.
[17] S. Tasaki, Nonequilibrium stationary states of noninteracting electrons in a one-dimensional lattice, Chaos Solitons Fractals 12 (2001) 2657–2674.
[18] T. Ho, H. Araki, Asymptotic time evolution of a partitioned infinite two-sided isotropic XY-chain, Proc. Steklov Inst. Math. 228 (2000) 203–216.
[19] Y. Ogata, Nonequilibrium properties in the transverse XX chain, Phys. Rev. E 66 (2002) 016135.
[20] W. Aschbacher, C.-A. Pillet, Non-equilibrium steady states of the XY chain, J. Stat. Phys. 112 (5–6) (2003) 1153–1175.
[21] D. Bernard, B. Doyon, Energy flow in non-equilibrium conformal field theory, J. Phys. A 45 (36) (2012) 362001.
[22] D. Bernard, B. Doyon, Non-equilibrium steady states in conformal field theory, Ann. Henri Poincaré (2014) 1–41.
[23] B. Doyon, M. Hoogeveen, D. Bernard, Energy flow and fluctuations in non-equilibrium conformal field theory on star graphs, J. Stat. Mech. 2014 (3) (2014) P03002.
[24] M. Bhaseen, B. Doyon, A. Lucas, K. Schalm, Energy flow in quantum critical systems far from equilibrium, Nat. Phys. (2015) 5.
[25] V. Eisler, I. Peschel, Evolution of entanglement after a local quench, J. Stat. Mech. 2007 (2007) P06005.
[26] P. Calabrese, J. Cardy, Entanglement and correlation functions following a local quench: a conformal field theory approach, J. Stat. Mech. 2007 (2007) P10004.
[27] P. Calabrese, J. Cardy, B. Doyon, Entanglement entropy in extended quantum systems, J. Phys. A 42 (2009) 500301.
[28] J.-M. Stéphan, J. Dubail, Local quantum quenches in critical one-dimensional systems: entanglement, the Loschmidt echo, and light-cone effects, J. Stat. Mech. 2011 (2011) P08019.
[29] A. Faraji Astaneh, A. Esmaeil Mosaffa, Quantum local quench, AdS/BCFT and yo-yo string, arXiv:1405.5469, 2014.
[30] C. Asplund, A. Bernamonti, Mutual information after a local quench in conformal field theory, Phys. Rev. D 89 (2014) 066015.
[31] V. Eisler, Z. Zimborás, Area-law violation for the mutual information in a nonequilibrium steady state, Phys. Rev. A 89 (2014) 032321.
[32] V. Eisler, Z. Zimboras, Entanglement negativity in the harmonic chain out of equilibrium, New J. Phys. 16 (12) (2014) 123020.
[33] J. Cardy, O. Castro-Alvaredo, B. Doyon, Form factors of branch-point twist fields in quantum integrable models and entanglement entropy, J. Stat. Phys. 130 (2007) 129–168.
[34] V. Knizhnik, Analytic fields on Riemann surfaces. II, Commun. Math. Phys. 112 (1987) 567–590.
[35] L. Dixon, D. Friedan, E. Martinec, S. Shenker, The conformal field theory of orbifolds, Nucl. Phys. B 282 (0) (1987) 13–73.
[36] X. Wen, P.-Y. Chang, S. Ryu, Entanglement negativity after a local quantum quench in conformal field theories, arXiv:1501.00568, 2015.
[37] M. Collura, D. Karevski, Quantum quench from a thermal tensor state: boundary effects and generalized Gibbs ensemble, Phys. Rev. B 89 (2014) 214308.
[38] M. Collura, G. Martelloni, Non-equilibrium transport in d-dimensional non-interacting Fermi gases, J. Stat. Mech. 2014 (2014) P08006.
[39] B. Doyon, A. Lucas, K. Schalm, M. Bhaseen, Non-equilibrium steady states in the Klein–Gordon theory, arXiv:1409.6660, 2014.
[40] A. De Luca, G. Martelloni, J. Viti, Stationary states in a free fermionic chain from the quench action method, Phys. Rev. A 91 (2015) 021603.
[41] B. Doyon, Lower bounds for ballistic current and noise in non-equilibrium quantum steady states, Nucl. Phys. B 892 (2015) 190–210.
[42] O. Castro-Alvaredo, B. Doyon, Permutation operators, entanglement entropy, and the XXZ spin chain in the limit $\delta \to -1^+$, J. Stat. Mech. 2011 (2011) P02001.

[43] I. Affleck, A. Ludwig, Universal noninteger "ground-state degeneracy" in critical quantum systems, Phys. Rev. Lett. 67 (1991) 161–164.
[44] P. Calabrese, J. Cardy, E. Tonni, Finite temperature entanglement negativity in conformal field theory, J. Phys. A 48 (1) (2015) 015006.
[45] D. Bernard, B. Doyon, J. Viti, Non-equilibrium conformal field theories with impurities, J. Phys. A 48 (5) (2015) 05FT01.
[46] N. Laflorencie, E. Sørensen, M.-S. Chang, I. Affleck, Boundary effects in the critical scaling of entanglement entropy in 1D systems, Phys. Rev. Lett. 96 (2006) 100603.
[47] H.-Q. Zhou, T. Barthel, J. Fjærestad, U. Schollwöck, Entanglement and boundary critical phenomena, Phys. Rev. A 74 (2006) 050305.

Chapter 4

Energy Current and Fluctuations

> In this chapter we will present the results of [2] and [3]. We first introduce the concept of Full Counting Statistics (FCS), and formulate a steady-state fluctuation theorem (SSFT) for the energy transfer after a thermal cut-and-glue quench. We explain how in the quantum mechanical case the quantity to consider is the energy transferred during a time interval t_0.

In Chapter 1 we introduced the fluctuation theorems (FTs) that quantify the irreversibility of a macroscopic system as a statistical effect. There are many types of FTs, depending on the system under consideration and the quantity that is fluctuating. In this thesis we consider FTs related to heat exchange between two reservoirs at different temperatures. The resulting fluctuation relations have been referred to as "exchange fluctuation theorems" [32] to distinguish them from the "work fluctuation theorems" that are the result of work performed by an external force. The first quantum exchange fluctuation theorem was put forward by Jarzynski and Wójcik [32]. It applies to two systems initially at different temperatures, $T_1 = \beta_1^{-1}$ and $T_2 = \beta_2^{-1}$, that are allowed to interact weakly during a time period Δt via a possibly time-dependent interaction. If the experiment is repeated many times, always initializing the two bodies at the specified temperatures, the observed distribution of values of q over the ensemble of repetitions satisfies [32]:

$$\frac{p(q)}{p(-q)} = e^{(\beta_1 - \beta_2)q}. \tag{4.1}$$

where $q = \Delta E_1 = -\Delta E_2$, with the second equality following from the assumed weak interaction. This situation was later generalised by [112, 113] to allow for the exchange of energy and particles between several interacting systems initially at different temperatures and chemical potentials.

One basic assumption leading to the exchange fluctuation relation, (4.1), is that the initial state is a factorised state, in which the various subsystems are uncorrelated from each other. In most experimental situations, however, unavoidable interactions between the systems would lead to some correlations and a consequent deviation from the assumed factorised state. The resulting deviation from the exchange fluctuation relation (4.1), is expected to vanish for observation times Δt larger than some characteristic time scale Δt_c, determined by the specific physical properties of the experimental setup [20, 113, 114]:

$$\frac{p(q)}{p(-q)} \overset{\Delta t \gg \Delta t_c}{\rightarrow} e^{(\beta_1 - \beta_2)q}. \tag{4.2}$$

For those large times $t \gg \Delta t_c$ a nonequilibrium steady state sets in under the condition that the reservoirs are chosen macroscopic. For this reason (4.2) is referred to as a steady state fluctuation relation (SSFT). This is in contrast to the other fluctuation relation discussed above, which instead are valid for any observation time Δt and is accordingly referred to as transient fluctuation relation. Saito and Dhar [115] provided an explicit demonstration of (4.2) for the quantum heat transfer across a harmonic chain connecting two thermal reservoirs at different temperatures.

4.1 Full Counting Statistics

The exchange FTs involve the probability distribution $p(q)$, which we define as the probability that during a certain time period Δt, q charges (which in this case means units of energy) move from the first system into the second (with $-q$ denoting the reverse process). This situation is reminiscent of a current measurement in a quantum conductor, and leads directly to the concept of full counting statistics (FCS)[1]. Full counting statistics has its roots in quantum optics [116], where the number statistics of photons is used, e. g., to characterise coherence properties of photon sources. The major step to adopt the concept to mesoscopic electron transport has been undertaken

[1] The word "full" means that the entire distribution is known, not just the average and noise.

by Levitov and Lesovik [117]. Since then the theory of FCS of charge transport in mesoscopic conductors has advanced substantially, see [118, 119].

The information contained in the probability distribution function is also contained in the cumulant generating function (CGF), defined by

$$S(\lambda) = \ln \left[\sum_q e^{i\lambda q} p(q) \right], \tag{4.3}$$

where we introduced the counting field λ. The normalisation condition requires $\sum_q p(q) = 1 \leftrightarrow S(0) = 0$. The cumulant generating function can be expanded to obtain the *cumulants* c_n,

$$S(\lambda) = \sum_{n=1}^{\infty} \frac{(i\lambda)^n}{n!} c_n, \tag{4.4}$$

which are a good measure of how far away a distribution is from being normal[2].

The heat exchange FT (4.1) translates directly into a symmetry relation for the CGF:

$$S(\lambda) = S(i(\beta_1 - \beta_2) - \lambda). \tag{4.5}$$

We are interested in discovering universal aspects of the fluctuations, which are expected to emerge at long time intervals Δt, in the NESS. We will therefore take the NESS limit described in section 1.4 and instead of the CGF, we consider the *scaled* CGF

$$F(\lambda) = \lim_{\Delta t \to \infty} \frac{1}{\Delta t} S(\lambda). \tag{4.6}$$

In analogy to (4.5), a steady-state fluctuation theorem (SSFT) for heat exchange exchange (4.2) implies a symmetry for the scaled CGF:

$$F(\lambda) = F(i(\beta_1 - \beta_2) - \lambda). \tag{4.7}$$

[2]since a normal distribution has the property that all cumulants of order higher than two are identically zero

4.2 FCS after a thermal cut-and-glue quench

4.2.1 Two-time projective measurement

In order to study the total energy transferred $E(\Delta t)$ over a large period of time Δt in a quantum mechanical setting, we must properly define how we measure the values of $E(\Delta t)$ within a quantum measurement protocol. One way of doing this would be by continuously measuring the local current over a long time Δt. This would have to be done via an indirect measurement, so as not to have a 'quantum Zeno' effect, in which the state is continuously influenced by the measurement, 'freezing' the current to a certain value. Another protocol to define the transferred charge between two reservoirs during a time Δt, which we will use, is taking two projective measurements at different times, where the energy difference between the two halves is measured. More precisely, this is done by first performing a measurement at an initial time $t = 0$, letting the system evolve, and then measuring again at a later time $t = \Delta t$. Let Q be the charge operator[3], and P_q the operator that projects onto an eigenspace of Q with eigenvalue q. Taking ρ_0 to be the density matrix[4] at time 0, the joint probability of measuring a certain eigenvalue q_0 at time $t = 0$ and another eigenvalue $q_{\Delta t}$ at time Δt is given by

$$p[q_{\Delta t}, q_0] = \mathrm{Tr}\left\{P_{q_{\Delta t}} U_{\Delta t} P_{q_0} \rho_0 P_{q_0} U_{\Delta t}^{-1} P_{q_{\Delta t}}\right\}. \tag{4.8}$$

From this, the probability distribution for the difference $\Delta q = q_{\Delta t} - q_0$ between the output of the two measurements can be obtained:

$$p(\Delta q) = \sum_{q_{\Delta t}, q_0} \delta\left(\Delta q - (q_{\Delta t} - q_0)\right) p[q_{\Delta t}, q_0]. \tag{4.9}$$

In (4.8), what state the measurements are performed in is determined by the initial density matrix ρ_0, and the time Δt over which the state is evolved in between measurements. In general, it is not easy to evaluate (4.8) as it may not be possible to find an exact formula for the density matrix. For the case of the energy FCS after the thermal

[3] The charge operator needs to be suitably defined. For instance, in case of energy transfer between two reservoirs, a suitable definition might be $Q := H_l - H_r$, where $H_{l/r}$ measures the energy of the left/right reservoir.

[4] we will ignore a normalisation term, or simply assume ρ_0 to be normalised.

cut-and-glue quench it has been proved in the critical case [1] that one can take a suitable limit (see section 1.4) to reach a non-equilibrium steady state (NESS), in which the density matrix has a simple form.

For the thermal cut-and-glue quench, the first measurement is taken at the time of connection, so that the density matrix is that of the disconnected systems. After a long time evolution, the system is expected to be in a NESS when the second measurement is performed. In case of electron FCS, it has been shown [120] that taking the first measurement in the disconnected state and the second in the steady state is the same as taking both measurements in the steady state (but with the same difference). This is expected to be due to the discreteness of the electric charge. In case of the energy FCS, it is not known how to compute the large deviation function in case where both projections are done in the steady state. Generally, the first projective measurement is taken before connection, and the second in the steady state.

4.2.2 Previous results

Our results generalise and supplement the proof for the results in [1], of which we will here briefly summarise the most relevant ones. For the thermal cut-and-glue quench between two CFTs thermalized at temperatures β_l and β_r, the authors considered the current and fluctuations of the charge $Q = \frac{1}{2}(H_l - H_r)$, which is the energy difference between the left and right subsystems. The heat current at criticality has the form

$$J = \frac{\pi c}{12}\left(T_l^2 - T_r^2\right), \tag{4.10}$$

which depends only on the central charge of the CFT, c, and the two temperatures. Note that this current is of the form

$$J(T_l, T_r) = f(T_l) - f(T_r), \tag{4.11}$$

which we will refer to as 'additive', since it has the following property:

$$J(T_1, T_2) + J(T_2, T_3) - J(T_1, T_3) = 0. \tag{4.12}$$

In [121], it was

The scaled CGF (4.6) was found to be

$$F(\lambda) = \frac{i\lambda\pi c}{12}\left(\frac{1}{\beta_r(\beta_r - i\lambda)} - \frac{1}{\beta_l(\beta_l + i\lambda)}\right), \tag{4.13}$$

which means the cumulants are

$$C_n = \frac{\pi c n!}{12}\left(T_l^{n+1} + (-1)^n T_r^{n+1}\right). \tag{4.14}$$

This is also very universal, depending only on the CFT central charge and universal constants. It depends among other things on the assumption that the Fluctuation Theorem (4.7) holds. Further proof was given in [73] and in [2], included in this chapter.

In [69] it was further shown that in any system with pure energy transmission (i.e. $QS = -SQ$, with S the system's scattering operator), one can evaluate the cumulant generating function solely from an expression of the current in which the inverse temperatures β_l, β_r have been shifted by a parameter z. This gives us the *extended fluctuation relation*:

$$\frac{dF(z)}{dz} = J(\beta_l - z, \beta_r + z) \quad \leftrightarrow F(z) = \int_0^z dz'\, J(\beta_l - z', \beta_r + z'). \tag{4.15}$$

The scaled cumulants can then be obtained by taking derivatives of the current with respect to z, and set $z = 0$:

$$C_{n+1} = \frac{d^n}{dz^n} J(\beta_l - z, \beta_r + z)|_{z=0}. \tag{4.16}$$

4.3 Generalizing to an N-junction

We generalize the exact result for the scaled cumulant generating function in the steady state of [1] to the case of a junction of N critical slabs with edge currents, connected in such a way that the edge currents of each leg can only flow into the next leg.

The first paper featured in this chapter [2], is the generalisation of the results of Bernard and Doyon [1] to a system where the number of baths can be large, and all the baths are connected at one point. Thus, the setup is that of N identical 1+1 dimensional Conformal Field Theories (CFT) on a star graph, which is a model for a junction of several quantum wires. We find the large deviation function for steady energy transfers

and associated Fluctuation Theorems that are a generalisation of that found in [1], and further confirmed the physical interpretation in terms of a Poisson process. We have written the results in [2], in which we also introduced new algebraic methods. The results are valid for any CFT: we have found a great starting point for exploring all systems that have quantum critical points. As an application of these results, quantum wire junctions have been intensively studied theoretically and experimentally since these are building blocks for quantum circuits (see [2] for references).

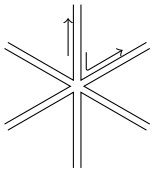

FIGURE 4.1: After connecting the 1d systems, the right-moving fields and the left-moving fields of one leg of the graph are connected to different legs. In this picture, a double line is one quantum system, where one line represents the right-moving fields, and the other the left-moving fields.

More precisely, we consider N identical 1d CFTs that were initially thermalised at different temperatures and connected sequentially in such a way that the right-moving fields and the left-moving fields are connected to different legs (for more details and some pictures, see [2]). After connection, the new Hamiltonian

$$H = \sum_{j=1}^{N} H_0^{(j)} + \Delta H \tag{4.17}$$

contains the disconnected Hamiltonians $H_0^{(j)}$ of the subsystems, and an extra term ΔH, whose form is unknown[5]. However, we do know the effect of this term as a change in boundary (in this case, vertex) conditions. After letting the connected systems evolve unitarily with the full Hamiltonian H, we expect a growing region around the vertex to reach a steady state. In order to have an infinitely large region that is in a steady state, we take the limit that this time over which we evolve goes to infinity. Note that this only works if the length of the 1d systems is also infinite[6].

[5] if we consider our systems as the scaling limit of a discrete system (at criticality), such as a spin chain or a harmonic chain, the term ΔH represents for instance an extra link connecting the different chains in the star graph. In the scaling limit, the contribution of this link to the energy of the total system vanishes. Since we are interested in universal behaviour, we can neglect the contribution of this term to the energy (but we cannot neglect its contribution to the time evolution).

[6] there are some subtleties with these limits, which are discussed in [2]

In order to use the operator formalism of quantum mechanics to calculate expectation values algebraically, we need to define a vacuum state, and express the quantities that we want to calculate in terms of generators of the conformal transformations, which satisfy a Virasoro algebra,

$$[L_m, L_n] = (m-n)L_{m+n} + \frac{c}{12}(m^3 - m)\delta_{m+n,0}, \tag{4.18}$$

where m and n are integers, and c is the central charge of the CFT. In order to define these, one needs the spatial direction to have a finite length, so that there are discrete levels. However, our systems must be infinite to be able to reach a steady state.[7] Therefore, we need to calculate expectation values for systems of finite length, and then take the limit of the length going to infinity. Note that we have to take this large system size limit before we take the long-time limit in order to describe a steady state.

An interesting result in itself is the calculation of the large volume[8] limit of expectation values of (products of) Virasoro generators. It turns out that (up to terms that disappear after integration) one can calculate these using an auxiliary 'continuous' algebra,

$$[a_p, a_{p'}] = (p-p')a_{p+p'} + \left(2p\,k + \tfrac{c}{12}p^3\right)\delta(p+p') \tag{4.19}$$

where the index p of the Virasoro generator is not a discrete number, but a continuous variable. With appropriate choices of k, and of the state, the averages calculated using these generators give the same results as the averages of the Virasoro generators in the limit of infinitely long systems[9]. Calculating quantum averages in this continuous algebra is easier, as simplifications that occur in the large volume limit for averages of the Virasoro algebra are already taken into account. This way of dealing with the large system size limit is different from the way it was dealt with in [1, 120], and has two advantages: firstly, it provides an extra argument for the universality of the results, since the two papers have used different methods for regularising the large p divergences. Secondly, the method we developed is a very direct method of dealing with infinite volume Virasoro algebra, and may be applied to other systems out of equilibrium. The

[7] Recall that we are not in equilibrium, and cannot map our system to a Euclidean theory. The choice of space and time directions has already been made, so the trick of radial quantisation does not work.

[8] large system length

[9] there are some subtleties, explained in section 5 of [2]

algebraic Virasoro method also fills a hole in the derivation of [120] and therefore gives the first full derivation of the scaled cumulant generating function in CFT.

Defining a 'charge' as a weighted sum over the energies in the different legs of the star graph,

$$Q := \sum_{j=1}^{N} \alpha_j H^{(j)}, \tag{4.20}$$

we calculate the Full Counting Statistics of this charge by performing a projective measurement at the time of connection, and again at a time t[10], which is sent to infinity. The steady current is found to generalise the form of the current found in [1] (in which the case $N = 2$ and $\alpha_{j+1} = 1/2 = -\alpha_j$ was considered). The current is of the form

$$J = \frac{\pi c}{12} \sum_{j=1}^{N} \frac{\Delta\alpha_j}{\beta_j^2}, \tag{4.21}$$

where c is the central charge of the CFT describing the critical 1d systems, and $\Delta\alpha_j := \alpha_{j+1} - \alpha_j$ is the difference in weight of the $j+1$-st leg and the j-th leg. An exact equation for the scaled CGF[11] (4.6) is also found to generalise the results from [1]

$$F(\lambda) = \frac{i\lambda\pi c}{12} \sum_{j=1}^{N} \frac{\Delta\alpha_j}{\beta_j(\beta_j - i\Delta\alpha_j\lambda)}, \tag{4.22}$$

which satisfies [2] the following symmetry relation:

$$F(\omega_1 - i\beta_1, \ldots, \omega_N - i\beta_N) \quad \text{is symmetric under permutations of } \omega_1, \ldots, \omega_N \tag{4.23}$$

with $\omega_j := \lambda\Delta\alpha_j$. Such a symmetry relation of the scaled CGF implies [20] a steady state Fluctuation Theorem. This is consistent with the physical picture of purely Poissonian long-time energy transfer [1] where in this case, due to the separation into the $H^{(j,j+1)}$ subsystems in the steady state, $F(\lambda)$ describes N independent energy transfer processes. Each energy transfer process can be seen as a family of independent Poisson processes, one for each value of the transferred energy, weighed by the Maxwell-Boltzmann factor $e^{-\beta_j E}$.

[10] in between the two measurements, the system evolves unitarily

[11] note that in our paper we call this the long-time cumulant generating function

4.4 Generalising to massive IQFT

Another generalisation we have made to the setup of [1] is a perturbation away from criticality, in such a way that the resulting system can be described with a relativistic quantum field theory that is integrable. In the paper [3], included in this chapter, we present analytical work, generalising the Thermodynamic Bethe Ansatz methods in [122], to find a low-temperature expansion, and a high-temperature expansion[12]. For specific models, we have solved the resulting TBA equations numerically in order to calculate the current and higher order cumulants. We obtain for the first time the exact energy current and scaled cumulant generating function (CGF) in interacting integrable models. We find that the scaled CGF in the NESS can be described by a set of independent Poisson processes. We furthermore show that, unlike in the critical case, the off-critical current is not additive, i.e. we cannot write $J(T_l, T_r) = f(T_l) - f(T_r)$ for some function $f(T)$ when the system is not exactly at a critical point.

We consider a relativistic QFT model with a spectrum of ℓ particle types with masses $m_1, \ldots, m_\ell$:

$$|\text{vac}\rangle, \quad |\theta_1, \ldots, \theta_n\rangle_{i_1,\ldots,i_n} : \quad \theta_1 > \cdots > \theta_n \tag{4.24}$$

The steady state ρ_{stat} is constructed in the following way:

$$\rho_{\text{stat}}|\text{vac}\rangle = 1, \tag{4.25}$$

and

$$\rho_{\text{stat}}|\theta_1, \ldots, \theta_n\rangle_{i_1,\ldots,i_n} = e^{-\sum_k W_{i_k}(\theta_k)}|\theta_1, \ldots, \theta_n\rangle_{i_1,\ldots,i_n}, \tag{4.26}$$

where

$$W_i(\theta) = m_i \cosh\theta \begin{cases} \beta_l & (\theta > 0) \\ \beta_r & (\theta < 0) \end{cases} \tag{4.27}$$

A physical interpretation for this is as the long-time evolution of the initial density matrix ρ_0

$$\rho_{\text{stat}} = \lim_{t\to\infty} e^{-iHt}\rho_0 e^{iHt}. \tag{4.28}$$

[12] which agrees in the large-temperature limit with the CFT results for the current in [1]

Considering the case of a general integrable relativistic QFT, under the assumption that there is no 'back-scattering' (i.e. the scattering matrix is diagonal, and particle scattering can only result in an additional phase), we found the following TBA equations for the current in the non equilibrium steady state, which we will refer to as the NESSTBA equations:

$$J(\beta_l, \beta_r) = \sum_{i=1}^{\ell} \int_{-\infty}^{\infty} \frac{d\theta}{2\pi} \frac{m_i \cosh\theta \, x_i}{1 + e^{\epsilon_i(\theta)}} \tag{4.29a}$$

$$x_i = m_i \sinh\theta + \sum_{j=1}^{\ell} \int_{-\infty}^{\infty} \frac{d\theta'}{2\pi} \frac{\varphi_{ij}(\theta - \theta') x_j(\theta')}{1 + e^{\epsilon_j(\theta')}} \tag{4.29b}$$

$$\epsilon_i(\theta) = W_i(\theta) - \sum_{j=1}^{\ell} \int_{-\infty}^{\infty} \frac{d\theta'}{2\pi} \varphi_{ij}(\theta - \theta') \log\left(1 + e^{-\epsilon_j(\theta')}\right), \tag{4.29c}$$

where $\epsilon(\theta)$ is the pseudo-energy and x_i is the 'dressed' momentum at rapidity θ.

We verify that the high temperature expansion of (4.29a) reproduces the CFT result of [1, 73], with the correct central charge. Furthermore, for integrable systems, the extended fluctuation relations (4.15) [69] can be used to find an expression for the exact scaled CGF using the above equations (4.29):

$$F(z) = \sum_{i=1}^{\ell} \int_{-\infty}^{\infty} \frac{d\theta}{2\pi} m_i \cosh\theta \int_0^z dz' \frac{x_i(\theta, z')}{1 + e^{\epsilon_i(\theta, z')}} \tag{4.30a}$$

$$x_i(\theta, z) = m_i \sinh\theta + \sum_{j=1}^{\ell} \int_{-\infty}^{\infty} \frac{d\theta'}{2\pi} \frac{\varphi_{ij}(\theta - \theta') x_j(\theta', z)}{1 + e^{\epsilon_j(\theta', z)}} \tag{4.30b}$$

$$\epsilon_i(\theta, z) = W_i(\theta) + z\mathrm{sgn}(\theta)\, m_i \cosh\theta - \sum_{j=1}^{\ell} \int_{-\infty}^{\infty} \frac{d\theta'}{2\pi} \varphi_{ij}(\theta - \theta') \log\left(1 + e^{-\epsilon_j(\theta', z)}\right). \tag{4.30c}$$

We further study the behaviour of the energy current and the cumulants for the sine-Gordon model, the sinh-Gordon model and the roaming trajectories model. This is done by solving the NESSTBA equations (4.29) and (4.30) numerically. The results are presented in paper [3], which is the last paper in this chapter. We confirm that the normalised current,

$$c_1(T_l, T_r) := \frac{12\, J(T_l^{-1}, T_r^{-1})}{\pi(T_l^2 - T_r^{-2})} = \frac{6}{\pi^2(T_l^2 - T_r^2)} \sum_{i=1}^{\ell} \int_{-\infty}^{\infty} d\theta\, m_i \cosh\theta \frac{x_i(\theta)}{1 + e^{\epsilon_i(\theta)}}, \tag{4.31}$$

has the correct behaviour to be a c-function[13], i.e. it increases monotonically with the energy scale, and at the critical points, it takes the values of the central charge of the corresponding CFTs. Furthermore, we construct similar normalised cumulants, and find that these behave as a family of c-functions[14] c_n, which depend only on the dimensionless variables T_l/m, T_r/m, with m the mass scale (for instance the mass of the lightest particle). This implies that the cumulants themselves behave as

$$\frac{d}{dm}C_n \leq 0, \tag{4.32}$$

which means that as the mass scale is decreased, the average energy transferred increases, and the fluctuations are stronger. A quasi-particle picture is that when lowering the mass scale whilst keeping the temperature constant, more quasi-particles can be created and thus we make more energy carriers available. This indeed leads one to expect a higher energy current, as the situation is similar to that of lowering the resistance while keeping the voltage the same in an electric circuit. In the limit of zero gap, as $m \to 0$, one expects to recover the CFT result (4.14), providing us with exact upper bounds on the cumulants, given by the cumulants of the UV fixed point:

$$C_n \leq \frac{\pi c n!}{12}\left(T_l^{n+1} + (-1)^n T_r^{n+1}\right). \tag{4.33}$$

We expect these results to hold in any integrable model with diagonal scattering, and possibly much more generally.

As mentioned above, another question we considered is whether the description of the scaled CGF as Poisson processes is still valid for massive integrable QFT. We verified that the scaled cumulant generating function can be seen as that of a family of independent Poisson processes, one for every value of the transferred energy. Hence, the complete, large-time scaled statistics of the energy transfer is that of independent, classical energy packets jumping towards the right or left in a Poissonian fashion with weight $\omega(q)$. We have evaluated $\omega(q)$ numerically for the sinh-Gordon and roaming trajectories models,

[13] A c-function [77] is a function of the energy scale (some physical quantity such as the temperature or the distance in a correlation function), or of the position on a renormalisation group (RG) trajectory, which represents well the effective number of degrees of freedom at this scale or at that point on the trajectory.

[14] Note that these functions are *non-equilibrium* c-functions, defined with respect to physical quantities that characterise a non-equilibrium steady state.

thus verifying that it is nonnegative. The Poisson process description may be seen as an improvement on the idea behind the Landauer formula for non-equilibrium currents.

Finally, as mentioned earlier, we consider the question whether additivity holds away from criticality. As observed in [121], additivity, or the existence of some function f as defined in (4.11), implies that the non-equilibrium current is completely determined by the linear conductance in equilibrium. If the additivity property (4.12) were to hold for systems that cannot be described by a CFT, as was conjectured for general QFT in [74], and for which numerical evidence for the XXZ spin chain was given in [121], this could have deep and important physical consequences. However, our numerical results suggest that the current away from the critical points is not of the form (4.11), i.e. that it does not satisfy the additivity property in general: the non-equilibrium current is not determined by the equilibrium conductance. But, as we observe in the sine-Gordon model, the breaking of additivity may be very small. This is important, because the numerical analysis of [121], from which it was concluded that additivity exactly held, is not expected to reach the accuracy necessary to detect such small effects. It is in any case rather interesting that the results of [121] and our present results indicate that additivity may be approximately satisfied in many cases.

Personal contributions

The first paper that is included in this chapter, [2], was the result of discussions between all the authors. The calculations were done by the first two authors. The second paper that is included here, [3], is a result of collaboration and discussions between all the authors. My personal contributions were mostly in the form of numerical solutions of the TBA equations for the current and certain higher order cumulants, and specifically, the plots that were used to prove that the current is not additive when the system is not critical.

Journal of Statistical Mechanics: Theory and Experiment
An IOP and SISSA journal

Energy flow and fluctuations in non-equilibrium conformal field theory on star graphs

Benjamin Doyon[1], **Marianne Hoogeveen**[1] **and Denis Bernard**[2]

[1] Department of Mathematics, King's College London, London, UK
[2] Laboratoire de Physique Théorique de l'ENS, CNRS and Ecole Normale Supérieure de Paris, France
E-mail: benjamin.doyon@kcl.ac.uk, marianne.hoogeveen@kcl.ac.uk and denis.bernard@ens.fr

Received 5 November 2013
Accepted for publication 20 January 2013
Published 11 March 2014

Online at stacks.iop.org/JSTAT/2014/P03002
doi:10.1088/1742-5468/2014/03/P03002

Abstract. We consider non-equilibrium quantum steady states in conformal field theory (CFT) on star-graph configurations, with a particular, simple connection condition at the vertex of the graph. These steady states occur after a large time as a result of initially thermalizing the legs of the graph at different temperatures, and carry energy flows. Using purely Virasoro algebraic calculations we evaluate the exact scaled cumulant generating function for these flows. We show that this function satisfies a generalization of the usual non-equilibrium fluctuation relations. This extends results by two of the authors to the case of more than two legs. It also provides an alternative derivation centered on Virasoro algebra operators rather than local fields, hence an alternative regularization scheme, thus confirming the validity and universality of the scaled cumulant generating function. Our derivation shows how the usual Virasoro algebra leads, in large volumes, to a continuous-index Virasoro algebra for which we develop diagrammatic principles, which may be of interest in other non-equilibrium contexts as well. Finally, our results shed light on the Poisson-process interpretation of the long-time energy transfer in CFT.

Keywords: conformal field theory, conformal field theory (theory), exact results, quantum transport in one dimension

 1742-5468/14/P03002+33$33.00

Contents

1. Introduction

There is currently great interest in the thermodynamics of quantum systems out of equilibrium. This has to do in part with the general need to find a framework that extends equilibrium thermodynamics to far-from-equilibrium situations [1], and in part with the recent experimental advances which make it possible to prepare quantum systems in non-equilibrium states in a controlled way, and verify fluctuation relations experimentally [2]–[6]. In the context of non-equilibrium quantum steady states, where there is transfer of energy, charge, particles, etc, one of the objects of interest is the scaled cumulant generating function (the Legendre transform of the large deviation function), see for instance the review [7]. This characterizes the fluctuations of these transfers measured over a large time period, and encodes many properties of their non-equilibrium statistics.

doi:10.1088/1742-5468/2014/03/P03002

J. Stat. Mech. (2014) P03002

Calculating it exactly in model systems and obtaining the associated fluctuation relations are important steps in developing the general theory of non-equilibrium steady states.

Recently, a step in this direction was achieved by calculating exactly the scaled cumulant generating function in non-equilibrium conformal field theory (NECFT) [8, 9], for energy and charge transfer. The setup consisted of two systems (acting as baths), initially thermalized at different temperatures and chemical potentials, which were connected to form a homogeneous system, so that a steady state is established at late times. Besides deriving the non-equilibrium density matrix and proving an exact nontrivial formula for the cumulant generating function in this relatively simple situation of NECFT, two claims were made. Firstly, it was claimed (with justifications) in [8, 9] that this formula is *universal*. That is, it gives the correct scaled cumulant generating function for any quantum critical system[3], prepared in the way described above, at small temperatures and chemical potentials[4]. This is a nontrivial statement, meaning that, for the first time, the exact long-time fluctuation statistics were obtained for both energy and charge transfer for many families of quantum systems, even with very strong interactions. The only parameter needed, that encodes the interaction, is the central charge. The NECFT universal average current was recently confirmed numerically [10] in a particular critical quantum model. It was also observed in [8] that the long-time energy transfer statistics is purely Poissonian, leading to the claim that the natural right-moving and left-moving energy carriers behave over a long time like ensembles of Poissonian particles.

The objective of the present paper is two-fold. Firstly, we generalize the results of [8] to non-equilibrium energy flows amongst any number of baths, connected to each other at one point in a star-graph configuration. We obtain the density matrix and derive the exact universal scaled cumulant generating function (which we will sometimes refer to as the full counting statistics) in NECFT under a simple connection condition at the vertex of the graph. Our results are a simple generalization of those of [8], and we find a generalization of the standard fluctuation relations to this many-leg case. There has been a lot of activity in the study of such 'quantum graphs' (see for instance [11] for a review, and [12]–[19] for condensed matter applications). Recently, certain quantum field theory methods and concepts have been introduced (see for example [20]–[26]) and studies have looked at far-from-equilibrium quantities in various types of quantum graphs [16], [27]–[29]. However, to our knowledge no exact cumulant generating function has been derived yet, and most of these studies are restricted to free propagation in the legs of the graph (e.g. Luttinger liquids), concentrating on the nontrivial scattering at vertices (see for instance the methods developed in [30]). By contrast our results apply to general CFT in the legs, possibly representing strongly interacting critical systems, albeit with simple vertex scattering.

Secondly, we develop a new method for deriving the scaled cumulant generating function. Some of the problems in using conformal field theory (CFT) methods in NECFT are that (1) in order to describe baths, the systems must be of infinite length, and (2) there is (yet) no simple Euclidean-space geometry to re-interpret out-of-equilibrium states and their fluctuations, so that we have a truly real-time problem where the quantization

[3] With dynamical critical exponent $z = 1$.

[4] There are subtleties regarding the interplay between the large-t limit and the scaling limit. These are discussed in [9].

scheme is fixed *a priori*. This hampers the use of standard techniques based on the Virasoro algebra and its representations, which usually require the choice of a quantization scheme where space is compact. This problem was circumvented in [8] by concentrating on the algebra of local fields on the line. Here we attack the problem directly, and develop a method to calculate quantum averages of Virasoro generators in the limit where the length of the system goes to infinity. To that end, we study a continuous-index Virasoro algebra and develop associated diagrammatic principles. This algebraic method could find applications in other contexts, for instance in the study of non-equilibrium steady states in NECFT with nontrivial impurities (impurities are usually described in terms of the Virasoro algebra), or in quantum quenches.

Besides obtaining the non-equilibrium density matrix and deriving the exact scaled cumulant generating function in NECFT with the present simple star-graph configuration, our results provide further evidence for the two claims mentioned above. Indeed, within our new calculation method, there is a natural UV regularization scheme, closely linked to the usual UV regularization of quantum field theory, but different from that used in [9]. Since our results agree with those of [8, 9] in the two-leg case, this provides further confirmation of the expected independence from the regularization scheme, and consequently universality (although it is not a full proof or a full analysis of the effect of irrelevant operators). Also, our cumulant generating function has a clear Poisson-process interpretation, further confirming the interpretation of [8].

The paper is organized as follows. In section 2, we describe precisely the system under consideration and obtain the non-equilibrium density matrix. In section 3, we describe our main results and discuss their meaning. In section 4, we develop some aspects of the continuous Virasoro algebra; in particular, we study the diagrams used to evaluate averages. In section 5 we evaluate the full counting statistics. Finally, in section 6, we provide concluding remarks.

2. A non-equilibrium steady state on a star graph

Consider a number N of identical, decoupled one-dimensional quantum systems, each of length $R/2$ and at criticality, thermalized at inverse temperatures $\beta_1, \ldots, \beta_N$. Assume that the temperatures are small as compared with the microscopic energy scale J (the typical energy of a link in a quantum chain, for instance), $k_{\mathrm{B}}T \ll J$. Then the physics of each quantum system can be described by a conformal field theory (CFT) with some central charge c. In particular, the boundaries are also conformal. Since the systems are described by a CFT, the energy and momentum densities (and their descendants) in the bulk, separate into left- and right-movers. We arrange the systems radially, forming the legs (or edges) of a star graph (N legs meeting at a single vertex); then it is clearer to call the fields incoming or outgoing, where incoming fields are the fields that move towards the vertex, and outgoing are those that move away from the vertex. We will denote them by $h_j^{\mathrm{in/out}}$, respectively, so that the energy density is $h_j^{\mathrm{in}} + h_j^{\mathrm{out}}$ and the (inward) momentum density is $h_j^{\mathrm{in}} - h_j^{\mathrm{out}}$ in leg j. Thanks to the conformal boundary conditions, at the boundaries of each system, we have reflective conditions for the densities $h_j^{\mathrm{in/out}}$ [31]. For example, incoming fields become outgoing fields moving at the same speed upon

reaching the innermost boundaries of the systems, which are located at the vertex of the star graph.

At some time $-t_0 < 0$ in the far past, the independently thermalized systems are all connected at the vertex. There are several ways of making this connection; in this paper the connection is assumed to be made in such a way that the incoming and the outgoing fields on one leg are connected to different legs. More precisely, the incoming fields of the jth leg, when they reach the vertex, move into the $j+1$th leg (mod N), where they become outgoing fields[5]. One way to think of this connection, where incoming and outgoing fields move into different legs, is by considering these fields as the edge currents of a set of N very long and narrow quantum Hall slabs arranged into a star graph.

After the systems are connected, the new total system is evolved unitarily. Then, energy will begin to flow from higher-temperature regions to lower-temperature regions. If we let the system evolve for a long enough time, we expect the system to reach a steady state. More precisely, in order for the system to be in a steady state at time $t = 0$, we must take the length R to infinity before we take the limit $t_0 \to \infty$. This ensures that the legs of the graph act as reservoirs at different temperatures, and that any finite part of the system around the vertex can be seen as an open system. Indeed, waves emanating from the vertex will not have time to bounce back at outer boundaries, and hence will effectively be absorbed by the legs; waves incoming to the vertex can only come from deep inside the legs, carrying the information of the initial thermalization. We will call this limit, $\lim_{R\gg t_0\to\infty}$, the steady-state limit, and what we mean by the system reaching a steady state is the existence of the limit on averages,

$$\lim_{t_0\to\infty}\lim_{R\to\infty}\langle\cdots\rangle_{R,t_0} = \langle\cdots\rangle^{\mathrm{stat}}, \tag{1}$$

where $\langle\cdots\rangle_{R,t_0}$ represents the average in the finite-R star graph a length of time t_0 after the connection has been made. Since it is only finite parts around the vertex that are expected to possess a steady-state limit, for the system to be said to reach a steady state we only impose this limit to exist whenever the ellipses $\cdots$ are replaced by operators supported in finite regions around the vertex; and in fact, we will here only look at operators in the same Virasoro sector as that of the energy and momentum densities. We expect there to be a steady energy current flowing, so that, in particular, the steady-state average of the energy current observable (the momentum density) should be finite and nonzero. Note that any finite region around the vertex, no matter how large, will be in a steady state in this limit. What effectively happens in the steady-state limit, is that the region in which we have a steady energy current becomes infinitely large, and that the thermal baths are pushed to infinity.

The distance along any one of the N legs is parametrized by $x \in [0, R/2]$. Before the connection, the continuity conditions for the incoming and outgoing densities $h^{\mathrm{in/out}}(x)$ are

$$h_j^{\mathrm{in}}(0) = h_j^{\mathrm{out}}(0), \qquad h_j^{\mathrm{out}}\left(\frac{R}{2}\right) = h_j^{\mathrm{in}}\left(\frac{R}{2}\right) \tag{2}$$

[5] Under these new vertex conditions, one might represent the system after the connection as a chiral theory on a large circle divided into N segments, where each segment corresponds to one leg of the graph. However, it turns out that this picture is not convenient when taking the steady-state limit.

and after the connection, these conditions are changed to

$$h_j^{\rm in}(0) = h_{j+1}^{\rm out}(0), \qquad h_j^{\rm out}\left(\frac{R}{2}\right) = h_j^{\rm in}\left(\frac{R}{2}\right) \tag{3}$$

where here and in the following we understand that leg indices are defined mod (N).

The former set of continuity conditions holds under time evolution of the disconnected system, and in averages with the initial state where each system is independently thermalized. The latter set holds under time evolution of the connected system, and, as it will turn out, the part of it at $x = 0$ holds in the steady-state average (the part of it at $x = R/2$ does not make sense because in the steady state R has been sent to infinity, and we only get averages of local operators around the vertex).

Let us denote by $H_0^{(j)}, j = 1, \ldots, N$ the Hamiltonians of the disconnected systems on the legs of the graph. Then the initial density matrix is

$$\rho_0 = \mathfrak{n}\left[\mathrm{e}^{-\sum_{j=1}^N \beta_j H_0^{(j)}}\right]$$

where here and below we use the notation $\mathfrak{n}[\rho] = \rho/\mathrm{Tr}(\rho)$. This density matrix is invariant under the disconnected-system evolution Hamiltonian $H_0 = \sum_{j=1}^N H_0^{(j)}$. Assuming that $R \gg x, |t| > 0$, the H_0-evolution, taking into account equation (2), is given by

$$\mathrm{e}^{\mathrm{i}H_0 t} h_j^{\rm out}(x) \mathrm{e}^{-\mathrm{i}H_0 t} = \begin{cases} h_j^{\rm out}(x-t) & x - t > 0 \\ h_j^{\rm in}(t-x) & x - t < 0 \end{cases} \tag{4}$$

$$\mathrm{e}^{\mathrm{i}H_0 t} h_j^{\rm in}(x) \mathrm{e}^{-\mathrm{i}H_0 t} = \begin{cases} h_j^{\rm in}(x+t) & x + t > 0 \\ h_j^{\rm out}(-(x+t)) & x + t < 0. \end{cases} \tag{5}$$

On the other hand, let us denote by H the Hamiltonian of the connected, total system. The H-evolution, which takes into account the continuity condition (3) at the vertex and assuming again that $R \gg x, |t| > 0$, is given by

$$\mathrm{e}^{\mathrm{i}Ht} h_j^{\rm out}(x) \mathrm{e}^{-\mathrm{i}Ht} = \begin{cases} h_j^{\rm out}(x-t) & x - t > 0 \\ h_{j-1}^{\rm in}(t-x) & x - t < 0 \end{cases} \tag{6}$$

$$\mathrm{e}^{\mathrm{i}Ht} h_j^{\rm in}(x) \mathrm{e}^{-\mathrm{i}Ht} = \begin{cases} h_j^{\rm in}(x+t) & x + t > 0 \\ h_{j+1}^{\rm out}(-(x+t)) & x + t < 0. \end{cases} \tag{7}$$

The average in (1) can be written in terms of H and ρ_0 as follows:

$$\langle \cdots \rangle_{R,t_0} = \mathrm{Tr}\left(\mathrm{e}^{-\mathrm{i}Ht_0} \rho_0 \mathrm{e}^{\mathrm{i}Ht_0} \cdots\right).$$

Further, the steady state (1) is invariant under the H-evolution, as we will show.

It is clear that in the initial density matrix ρ_0, the system decouples into its subsystems with Hamiltonians $H_0^{(j)}, j = 1, \ldots, N$ on the various legs of the graph. For instance,

$$\left\langle \prod_{j=1}^N h_j^{\rm in}(x_j) h_j^{\rm out}(y_j) \right\rangle_{R,0} = \prod_{j=1}^N \langle h_j^{\rm in}(x_j) h_j^{\rm out}(y_j) \rangle_{R,0}.$$

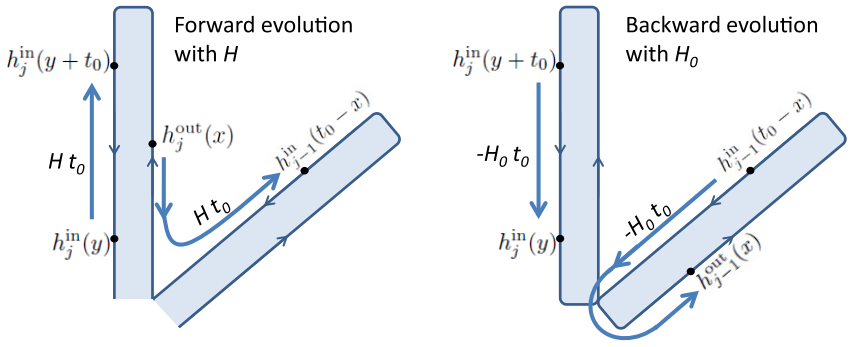

Figure 1. The forward time evolution with H and subsequent backward time evolution with H_0 of $h_j^{\rm in}(y)$ in equation (10) and $h_j^{\rm out}(x)$ in equation (11) is shown, focusing only on the jth and $j-1$th legs of the star graph. This shows that measuring $h_j^{\rm in}$ and $h_j^{\rm out}$ in the steady state corresponds to measuring $h_j^{\rm in}$ and $h_{j-1}^{\rm out}$ in the disconnected system, respectively.

In the steady-state limit, it turns out that the system again decouples, but not into the separate legs of the graph. It rather decouples into N subsystems, for $j=1,\dots,N$, where in each subsystem $h_j^{\rm in}$ and $h_{j+1}^{\rm out}$ are coupled to each other, in particular satisfying the first equation of (3).

Let us now construct explicitly the steady state from (1) using the above considerations, and see explicitly the H-invariance and the decoupling mentioned. This follows the methods of [8, 9]. Assuming that $R \gg t_0 \gg x > 0$, we have

$$\mathrm{e}^{\mathrm{i}Ht_0} h_j^{\rm in}(x) \mathrm{e}^{-\mathrm{i}Ht_0} = h_j^{\rm in}(x+t_0) \tag{8}$$

$$\mathrm{e}^{\mathrm{i}Ht_0} h_j^{\rm out}(x) \mathrm{e}^{-\mathrm{i}Ht_0} = h_{j-1}^{\rm in}(-x+t_0). \tag{9}$$

Evolving the result backward with H_0 then gives

$$\mathrm{e}^{-\mathrm{i}H_0t_0}\mathrm{e}^{\mathrm{i}Ht_0} h_j^{\rm in}(x) \mathrm{e}^{-\mathrm{i}Ht_0}\mathrm{e}^{\mathrm{i}H_0t_0} = h_j^{\rm in}(x) \tag{10}$$

$$\mathrm{e}^{-\mathrm{i}H_0t_0}\mathrm{e}^{\mathrm{i}Ht_0} h_j^{\rm out}(x) \mathrm{e}^{-\mathrm{i}Ht_0}\mathrm{e}^{\mathrm{i}H_0t_0} = h_{j-1}^{\rm out}(x). \tag{11}$$

The above process of forward evolution with H until the time of connection, and subsequent backward evolution with H_0, is visualized in figure 1

For definiteness, let us consider the observable $\prod_{j=1}^N h_j^{\rm in}(x_j) h_j^{\rm out}(y_j)$. Using the fact that ρ_0 is H_0-invariant and the above equations, we then obtain

$$\lim_{R\gg t_0\to\infty} \left\langle \prod_{j=1}^N h_j^{\rm in}(x_j) h_j^{\rm out}(y_j) \right\rangle_{R,t_0} = \left\langle \prod_{j=1}^N h_j^{\rm in}(x_j) h_{j-1}^{\rm out}(y_j) \right\rangle_{\infty,0}. \tag{12}$$

This expression is factorized, but the factorization is not in terms of legs. In order to find a steady state that reproduces the above relation, let us introduce the Hamiltonians $H^{(j,j+1)}$, $j=1,\dots,N$, which mutually commute and which couple together $h_j^{\rm in}$ with $h_{j+1}^{\rm out}$ in the same way $H_0^{(j)}$ couple together $h_j^{\rm in}$ with $h_j^{\rm out}$. It is convenient for our later derivations

to consider these Hamiltonians, like the Hamiltonians $H_0^{(j)}$, with R finite. This means that with $H^{(j,j+1)}$ the continuity conditions are

$$h_j^{\text{in}}(0) = h_{j+1}^{\text{out}}(0), \qquad h_{j+1}^{\text{out}}\left(\frac{R}{2}\right) = h_j^{\text{in}}\left(\frac{R}{2}\right), \tag{13}$$

paralleling (2). Then we may define

$$\rho_{\text{stat}} = \mathfrak{n}\left[\mathrm{e}^{-\sum_{j=1}^{N}\beta_j H^{(j,j+1)}}\right]. \tag{14}$$

We see that any average of an operator $\mathcal{O}$ with the density matrix ρ_0 is equal to the average of a modified operator $\tilde{\mathcal{O}}$ with the density matrix ρ_{stat}, where $\tilde{\mathcal{O}}$ is obtained by replacing every h_j^{out} by h_{j+1}^{out}. Hence we see that the density matrix (14) gives rise to the steady-state average,

$$\langle\cdots\rangle_{\text{stat}} := \lim_{R\to\infty} \operatorname{Tr}\left(\rho_{\text{stat}}\cdots\right), \tag{15}$$

as (12) then implies

$$\lim_{R\gg t_0\to\infty}\left\langle\prod_{j=1}^{N} h_j^{\text{in}}(x_j)h_j^{\text{out}}(y_j)\right\rangle_{R,t_0} = \left\langle\prod_{j=1}^{N} h_j^{\text{in}}(x_j)h_j^{\text{out}}(y_j)\right\rangle_{\text{stat}}. \tag{16}$$

A similar derivation holds for any other finite product of fields. Since the Hamiltonians $H^{(j,j+1)}$ commute, this shows the factorization mentioned above. The result below of a nonzero energy current then confirms that this is a non-equilibrium steady state.

A picture representing, side by side, the physical situation after connection, and the Hamiltonians $H^{(j,j+1)}$ used in the construction of the steady-state density matrix, is shown in figures 2 and 3.

In the $H^{(j,j+1)}$ subsystems, it is simpler to work with 'right-moving' fields only, which are the incoming fields from one leg and the outgoing fields into the next leg. We will label these by the two legs on which they move, and make the following identification:

$$h^{(j,j+1)}(x) := \begin{cases} h_j^{\text{in}}(-x) & x < 0 \\ h_{j+1}^{\text{out}}(x) & x \geq 0 \end{cases}, \qquad x \in \left[-\frac{R}{2}, \frac{R}{2}\right]. \tag{17}$$

With these new fields, the time evolution is now simply

$$\mathrm{e}^{\mathrm{i}Ht}h^{(j,j+1)}(x)\mathrm{e}^{-\mathrm{i}Ht} = h^{(j,j+1)}(x-t), \qquad x,t \ll R \tag{18}$$

and $h^{(j,j+1)}(x)$ is continuous.

Remark 2.1. It is important to note that the connected-system Hamiltonian H *does not* commute with $H^{(j,j+1)}$. However, thanks to the agreement between the first equations of (3) and (13), the evolution with H by a time t on fields at x, for any $R \gg |t|, x > 0$, is exactly in agreement with the evolution with $\sum_{j=1}^{N} H^{(j,j+1)}$:

$$H = \sum_{j=1}^{N} H^{(j,j+1)} \qquad \text{as evolution operators on fields a finite distance from the vertex.}$$

Since $\sum_{j=1}^{N} H^{(j,j+1)}$ commutes with ρ_{stat}, this implies that the steady-state average $\langle\cdots\rangle_{\text{stat}}$ (defined only for products of local fields a finite distance from the vertex) is H-invariant, as claimed above.

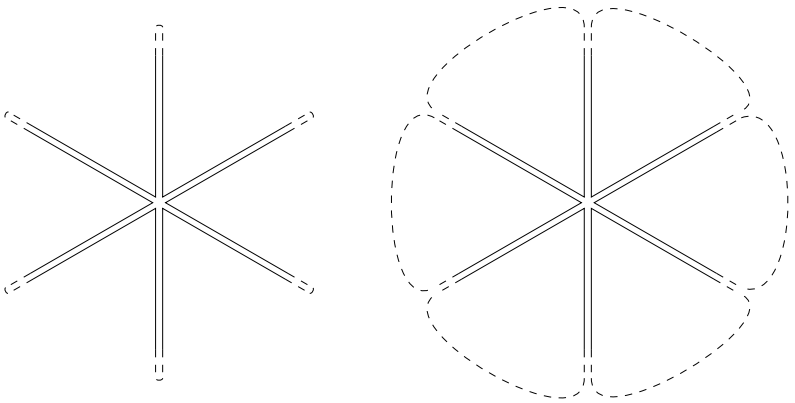

Figure 2. Two pictures indicating the different continuity conditions with dashed lines. On the left, the physical situation at finite R after the connection: several heat baths connected at a point, with continuity conditions (3). On the right, how expectation values are calculated using the fact that in the steady-state limit the system decouples into subsystems as in this picture, corresponding to the continuity conditions (13).

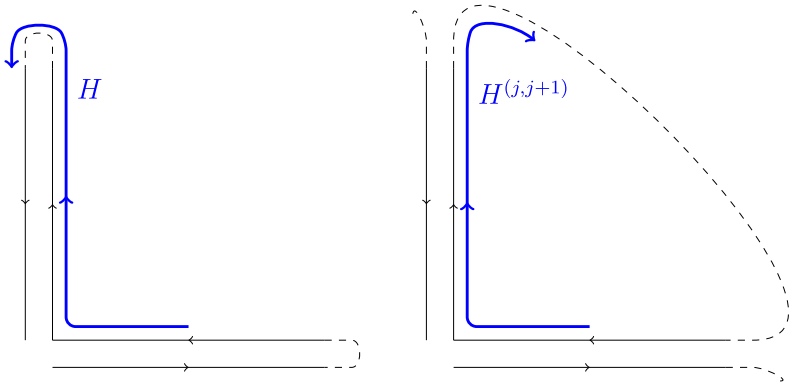

Figure 3. A closer look at the different continuity conditions illustrated in figure 2. In the left picture, the Hamiltonian H represents evolution along the path going around the graph. On the right, the Hamiltonians $H^{(j,j+1)}$ represent evolutions along the distinct paths. These two time evolutions are the same for fields near the vertex.

3. Results and discussion

We now state our main results concerning the energy current and its fluctuations in the steady state described in section 2.

Consider a charge

$$Q = \sum_{j=1}^{N} \alpha_j H_0^{(j)},$$

the weighted sum of the energies in the various legs of the star graph[6]. The time derivative of Q is the associated 'energy current' operator, $\mathcal{J} := i[H, Q] = \sum_{j=1}^{N} \alpha_j (h_j^{\text{out}}(0) - h_j^{\text{in}}(0))$, which is the weighted sum of the momentum densities on the various legs of the graph. It is local, hence it has a well-defined steady-state average $J = \langle \mathcal{J} \rangle_{\text{stat}} = i\langle [H, Q] \rangle_{\text{stat}}$. Note that this steady-state average does not necessarily vanish because Q itself is not a local operator.

3.1. Average current

The average current is in fact simple to evaluate using standard CFT techniques (see for instance [34]) which give the result $\langle h^{(j,j+1)} \rangle_{\text{stat}} = \pi c/(12\beta_j^2)$. Hence:

$$J = \frac{\pi c}{12} \sum_{j=1}^{N} \frac{\Delta\alpha_j}{\beta_j^2} \tag{19}$$

where $\Delta\alpha_j := \alpha_{j+1} - \alpha_j$. This generalizes the result of [8], where the case $N = 2$ and $\alpha_1 = -\alpha_2 = 1/2$ was considered. This is in agreement with the simple picture according to which energy flows from leg j to leg $j + 1$ with the information of the asymptotic thermal bath of leg j, with a current $\pi c/(12\beta_j^2)$.

The charge and energy current has been calculated via a scattering state approach in [27, 29] in the context of free fermion and Luttinger liquid models for more general continuity conditions at the vertex, where the systems also have a set of chemical potentials. As an example, for a system of Dirac fermions (with central charge $c = 1$) the energy current from one leg into the vertex (hence into all other legs) was calculated. Our result agrees with the result found in [27, 29] for a critical system with our sequential boundary conditions and all the chemical potentials set to zero. For more details, see appendix A.

3.2. Current fluctuations

The energy current fluctuations can also be evaluated within our framework. There are various ways of defining these fluctuations. We will consider the setup [7] where the charge Q is first quantum-mechanically measured (von Neumann measurement) at the contact time $-t_0$, and then measured at time 0. The cumulants of the difference $\Delta_{t_0} Q$ of the measured values are then evaluated in the steady-state limit (where in particular t_0 becomes infinite). We find that all cumulants diverge linearly in t_0, and we obtain the exact coefficients of this divergence for all cumulants. These can be organized into the coefficients of the Taylor expansion in $\mathrm{i}\lambda$ of the scaled cumulant generating function $F(\lambda)$, which is the Legendre transform of the large deviation function. As was shown in [9] (this was the case for $N = 2$, but the proof is easily generalizable to all N), the result of these operations can be represented by the formula

$$F(\lambda) = \lim_{t\to\infty} \frac{1}{t} \log \langle \mathrm{e}^{\mathrm{i}\lambda Q(t)} \mathrm{e}^{-\mathrm{i}\lambda Q} \rangle_{\text{stat}} \tag{20}$$

[6] We keep the weights α_j general in our results, which, as it turns out, does not complicate the calculations. For one thing, this allows one to look at energy transfer between any two parts of the system by choosing appropriate values of the weights α_j.

where $Q(t) = \mathrm{e}^{\mathrm{i}Ht}Q\mathrm{e}^{-\mathrm{i}Ht}$. This is of the same form as the standard expression for the so-called full counting statistics of charge transfer, which was first obtained within the context of indirect measurements, instead of the two-time von Neumann measurement protocol we discuss above, in free fermion models in [32]. In fact, we will show that formula (20) is equivalent to the simpler, 'naive' expression

$$F(\lambda) = \lim_{t\to\infty} \frac{1}{t} \log\langle \mathrm{e}^{\mathrm{i}\lambda(Q(t)-Q)}\rangle_{\mathrm{stat}}. \tag{21}$$

This, for instance, immediately implies that the second order in $\mathrm{i}\lambda$, which is the noise (made up of the thermal noise and the so-called shot noise), takes the familiar form:

$$F(\lambda) = \mathrm{i}\lambda J + \frac{(\mathrm{i}\lambda)^2}{2}\int_0^\infty \mathrm{d}t\ \left(\langle\{\mathcal{J}(t),\mathcal{J}(0)\}\rangle_{\mathrm{stat}} - 2J^2\right) + \cdots. \tag{22}$$

Further, using the time evolution equations of section 2, one finds that

$$\Delta_t Q := Q(t) - Q = \sum_j \Delta\alpha_j \int_0^t \mathrm{d}x\, h_j^{\mathrm{in}}(x). \tag{23}$$

Hence, the function $F(\lambda)$ can also be interpreted as the generating function for large-L cumulants of the weighted sum, over the legs of the graph, of the incoming energies $\int_0^L \mathrm{d}x\, h_j^{\mathrm{in}}(x)$ on intervals of lengths L. In contrast with the initial two-measurement description, in this interpretation, these incoming energies are now measured in single von Neumann measurements.

We find the following exact expression for $F(\lambda)$:

$$F(\lambda) = \frac{\mathrm{i}\lambda\pi c}{12}\sum_{j=1}^{N} \frac{\Delta\alpha_j}{\beta_j(\beta_j - \mathrm{i}\Delta\alpha_j\lambda)}, \tag{24}$$

generalizing the result of [8] to higher N and to different charges Q (different weighted sums). Specializing to the case where the charge measured is the energy difference between two contiguous parts of the star graph $Q = \frac{1}{2}(H_{\mathrm{part1}} - H_{\mathrm{part2}})$, the cumulant generating function simplifies to:

$$F(\lambda) = \frac{\mathrm{i}\lambda\pi c}{12}\left(\frac{1}{\beta_m(\beta_m - \mathrm{i}\lambda)} - \frac{1}{\beta_n(\beta_n + \mathrm{i}\lambda)}\right) \tag{25}$$

where m and n are the legs just after which the sign of the weight changes from minus to plus and from plus to minus, respectively. This result is identical in form to the case $N = 2$.

3.3. Fluctuation relations and Poisson processes

The function (25) satisfies the usual symmetry relation (or fluctuation relation) found in bipartite systems,

$$F(\mathrm{i}(\beta_n - \beta_m) - \lambda) = F(\lambda). \tag{26}$$

This is a standard relation in the context of non-equilibrium steady states, and is characteristic of an exponentially decaying ratio of probabilities for energy transfer from the lower-temperature (larger β) region and energy transfer from the higher-temperature (smaller β) region [7], over large periods of time. That is, let $P_{(2\,\mathrm{parts})}(q)$ be the probability that $\Delta_{t_0} Q = q$ for this particular choice of weights α_j. Then (26) is equivalent to a so-called *steady-state* fluctuation theorem:

$$P_{(2\,\mathrm{parts})}(q) \sim \mathrm{e}^{(\beta_n-\beta_m)q} P_{(2\,\mathrm{parts})}(-q) \tag{27}$$

where '$\sim$' indicates that the fluctuation relation holds only at large t_0 and accordingly large q.

In general, however, the cumulant generating function (24) does not satisfy such a simple symmetry relation involving a shift in λ only. Yet there is a simple physical picture behind formula (24), and a generalized symmetry relation that agrees with this picture. Denoting $\omega_j := \lambda \Delta\alpha_j$, with $j = 1, \ldots, N$, the symmetry relation is:

$$F(\omega_1 - \mathrm{i}\beta_1, \ldots, \omega_N - \mathrm{i}\beta_N) \qquad \text{is symmetric under permutations of } \omega_1, \ldots, \omega_N. \tag{28}$$

Indeed, we observe that our exact formula (24) satisfies (28):

$$F(\omega_1 - \mathrm{i}\beta_1, \ldots, \omega_N - \mathrm{i}\beta_N) = -\frac{\pi c}{12} \sum_j \left(\frac{1}{\beta_j} + \frac{1}{\mathrm{i}\omega_j} \right). \tag{29}$$

The physical picture is as follows. Due to the separation of the stationary state into the $H^{(j,j+1)}$ subsystems, we expect $F(\lambda)$ in general to correspond to a set of N independent processes whereby energy is transferred from leg j to leg $j+1$, with $j = 1, \ldots, N$. Let $P^{(j,j+1)}(r)$ be the probability that an energy $r > 0$ be transferred from leg j to leg $j+1$ in such a process (this energy is always positive thanks to our choice of continuity conditions at the vertex). Further, let us denote by $P_{\Delta\alpha_1,\ldots,\Delta\alpha_N}(q)$ the probability that $\Delta_{t_0} Q = q$ for general weights α_j (it depends only on the weight differences $\Delta\alpha_j$). We have in particular $\mathrm{e}^{t_0 F(\lambda)} = \int \mathrm{d}q\, \mathrm{e}^{\mathrm{i}\lambda q} P_{\Delta\alpha_1,\ldots,\Delta\alpha_N}(q)$. Then we expect that at large t_0, we have

$$P_{\Delta\alpha_1,\ldots,\Delta\alpha_N}(q) \sim \int_{q=\sum_j \Delta\alpha_j r_j} \prod_j \mathrm{d}r_j\, P^{(j,j+1)}(r_j). \tag{30}$$

Furthermore, we expect the independent $j \to j+1$ processes to be related to each other via a similar fluctuation relation as (27):

$$\mathrm{e}^{\beta_j r} P^{(j,j+1)}(r) \sim \mathrm{e}^{\beta_k r} P^{(k,k+1)}(r) \qquad \forall \quad j,k. \tag{31}$$

We can verify that in the 2-part case discussed above, we do recover (27):

$$\begin{aligned} \mathrm{e}^{\beta_m q} P_{(2\,\mathrm{parts})}(q) &\sim \int_{q=r_m-r_n} \mathrm{d}r_m\, \mathrm{d}r_n\, \mathrm{e}^{\beta_m(r_m-r_n)} P^{(m,m+1)}(r_m) P^{(n,n+1)}(r_n) \\ &\sim \int_{q=r_m-r_n} \mathrm{d}r_m\, \mathrm{d}r_n\, \mathrm{e}^{\beta_n(r_m-r_n)} P^{(n,n+1)}(r_m) P^{(m,m+1)}(r_n) \end{aligned}$$

doi:10.1088/1742-5468/2014/03/P03002

$$= \int_{-q=r_m-r_n} \mathrm{d}r_m \mathrm{d}r_n \, \mathrm{e}^{\beta_n(r_n-r_m)} P^{(n,n+1)}(r_n) P^{(m,m+1)}(r_m)$$

$$\sim \mathrm{e}^{\beta_n q} P_{(2\,\mathrm{parts})}(-q).$$

What's more, this picture implies the generalized symmetry relation (28) for $F(\lambda)$. This is simple to see from

$$\mathrm{e}^{t_0 F(\omega_1,\ldots,\omega_N)} \sim \int \prod_j \mathrm{d}r_j \, \mathrm{e}^{\mathrm{i}\omega_j r_j} P^{(j,j+1)}(r_j) \tag{32}$$

and using (31).

Hence, our result for the large-time cumulant generating function is indeed in agreement with the proposed picture.

Consider the conditions that (i) $F(\lambda)$ separates into a sum over j of a two-variable function of $\omega_j := \lambda\Delta\alpha_j$ and β_j; (ii) $F(\lambda)$ is a homogeneous function of ω_j and β_j of degree -1; (iii) $F(0) = 0$; and (iv) the symmetry relation (28) holds. We observe that these conditions are sufficient to fully fix the function $F(\lambda)$ to the form (24), up to an overall normalization. Indeed, the first condition says that $F(\lambda) = \sum_j f(\omega_j, \beta_j)$. Let us denote $\tilde{f}(\omega, \beta) = f(\omega - \mathrm{i}\beta, \beta)$. Then the fourth condition implies that $\tilde{f}(\omega, \beta) = \tilde{f}_1(\omega) + \tilde{f}_2(\beta)$. By the second condition, we then have $\tilde{f}_1(\omega) = a_1/(\mathrm{i}\omega)$ and $\tilde{f}_2(\beta) = a_2/\beta$. Further, the third condition says that $\tilde{f}(\mathrm{i}\beta, \beta) = 0$, which gives $a_1 = a_2$. Hence we indeed find the right-hand side of (29) for $\sum_j \tilde{f}_j(\omega_j, \beta_j)$ up to a normalization, which completes the proof. Condition (i) is a consequence of the factorization of the stationary density matrix (14) and of (23) and (22). Condition (ii) is a consequence of scale invariance, and condition (iii) of the basic definition of the generating function. Hence, along with basic properties of CFT, the symmetry relation (28) fully fixes the cumulant generating function $F(\lambda)$. This generalizes what was observed in [8] in the case $N = 2$.

We finally note that the independent processes of energy transfer from legs j and $j + 1$, with probabilities $P^{(j,j+1)}(q)$, in the asymptotic regime $t_0 \to \infty$, can be uniquely identified. Indeed, we can interpret $F(\lambda)$ as describing the cumulants of a random variable q coming from classical processes as follows: at each interface $j \to j + 1$, there is a family of independent Poisson processes parametrized by $r > 0$, with intensities $\mathrm{e}^{-\beta_j r}$, each contributing to the random variable q a value $\Delta\alpha_j r$. This is again a generalization of what was observed in [8] in the case $N = 2$, and further confirms that for large energy transfers, CFT is equivalently described by replacing right-movers and left-movers by independent carriers of energy units, distributed according to the appropriate density of state, jumping towards the right and left, respectively, in a Poissonian fashion.

4. The continuous Virasoro algebra and its diagrams

Our strategy to prove the form (24) of the cumulant generating function will be an analysis of (20) as a series expansion in $\mathrm{i}\lambda$, along with the use of the Virasoro algebra at the basis of CFT. This algebraic analysis provides an alternative to the local-variable analysis used in [9] in order to prove (24) in the case $N = 2$ (and for $\alpha_1 = -\alpha_2 = 1/2$). The Virasoro algebra occurs as a natural algebra in the quantization of CFT on the circle or on segments

(or in radial quantization). Of course, in the construction discussed in section 2, we have instead, after the connection, the star-graph geometry; yet the usual notions of CFT on segments of lengths $R/2$ can still be used.

A complete analysis of the quench using the standard formulation of the Virasoro algebra would be interesting. Some initial ideas are presented in appendix B, where it turns out we obtain the expected value of the holomorphic dimension of the branch-point twist field [35], which is used in entanglement entropy.

However, in the establishment of the steady state through the steady-state limit (1), the large-R limit needs to be taken before the time evolution can be analyzed. The large-R limit of the quantization on the circle or on segments gives rise to the quantization on the line or the semi-line (depending on how exactly the limit is taken). In this quantization space, the Virasoro algebra is no longer a natural algebra. At equilibrium, one can circumvent this problem, as one knows the Euclidean geometry describing the large-R limit: either a cylinder, infinite or semi-infinite (at finite temperature, with the circumference equal to the inverse temperature), or the plane or half-plane (at zero temperature). In these cases, either using the quantization on the circle or radial quantization, one can still make use of the Virasoro algebra. However, out of equilibrium, there is not yet a clear Euclidean geometric picture; hence one needs to keep the quantization on the line or the semi-line (here, appropriately tailored to the graph geometry), whence one loses the Virasoro algebra.

The natural algebraic structure that emerges in the large-R limit is that which one may refer to as the *continuous Virasoro algebra*. This is an algebra similar to the Virasoro algebra, but with a continuous index. The algebraic structure is rather simple, but its connection to the result of the large-R limit of the Virasoro algebra present some subtleties. Its representation theory also presents many subtleties, which we will not address here. We present instead basic aspects of this algebra and the diagrams used to evaluate certain traces of products of algebra elements, which we will need in the next section.

4.1. Definitions

Consider a Lie algebra with a continuous basis

$$\{a_p : p \in \mathbb{R}\} \tag{33}$$

satisfying the following commutation relations

$$[a_p, a_q] = (p-q)a_{p+q} + \left(2p\,k + \frac{c}{12}p^3\right)\delta(p+q) \tag{34}$$

where[7] $k, c \in \mathbb{R}$. For a fixed c, the algebras corresponding to different values of k are isomorphic: a simple change of basis $\tilde{a}_p = a_p + k\delta(p)$ makes the linear-in-p term vanish. However, it is convenient for us to keep this term. Given an appropriate highest-weight representation of this algebra, where a_0 is diagonalizable and with eigenvalues that are bounded from below, we may define a state by the following ratio of traces

$$\langle \cdots \rangle_\beta \equiv \frac{\mathrm{Tr}\left(\mathrm{e}^{-2\pi\beta a_0} \cdots\right)}{\mathrm{Tr}\left(\mathrm{e}^{-2\pi\beta a_0}\right)} \tag{35}$$

[7] Instead of seeing k, c as numbers, we could also see them as additional central elements; but in the representation we will need these simply take fixed values.

where $\cdots$ represents some product of the generators a_p, and $\beta > 0$ is some parameter. A simple calculation using (34), and assuming that the cyclic property of the trace holds,

$$\langle a_p \rangle_\beta = \frac{\mathrm{Tr}\left(\mathrm{e}^{-2\pi\beta a_0} a_p\right)}{\mathrm{Tr}\left(\mathrm{e}^{-2\pi\beta a_0}\right)} = \frac{\mathrm{Tr}\left(a_p \mathrm{e}^{-2\pi\beta a_0}\right)}{\mathrm{Tr}\left(\mathrm{e}^{-2\pi\beta a_0}\right)} = \mathrm{e}^{-2\pi\beta p}\langle a_p \rangle_\beta = 0 \qquad \text{for } p \neq 0,$$

shows that we must have

$$\langle a_p \rangle_\beta = B\,\delta(p) \tag{36}$$

for some number B. With an appropriate choice of basis, it is possible to impose

$$B = 0.$$

With this condition, the basis is completely fixed (albeit in a state-dependent way) and in particular k in (34) is unambiguous. Below we will have a representation where, with the condition $B = 0$,

$$k = k(\beta) := \frac{c}{24\beta^2}. \tag{37}$$

We can then calculate expectation values of products of more than one generator, again using the cyclic property of the trace along with the algebra relations. For example,

$$\begin{aligned}\langle a_{p_1} a_{p_2} \rangle_\beta &= \frac{\mathrm{Tr}(\mathrm{e}^{-2\pi\beta a_0} a_{p_1} a_{p_2})}{\mathrm{Tr}(\mathrm{e}^{-2\pi\beta a_0})} = \frac{\mathrm{Tr}(a_{p_2} \mathrm{e}^{-2\pi\beta a_0} a_{p_1})}{\mathrm{Tr}(\mathrm{e}^{-2\pi\beta a_0})} \\ &= \mathrm{e}^{-2\pi\beta p_2}\langle a_{p_2} a_{p_1} \rangle_\beta = \frac{1}{\mathrm{e}^{2\pi\beta p_2} - 1}\langle [a_{p_2}, a_{p_1}] \rangle_\beta \\ &= \frac{1}{\mathrm{e}^{2\pi\beta p_2} - 1}\left(2p_2\, k(\beta) + \frac{c}{12} p_2^3\right)\delta(p_1 + p_2).\end{aligned} \tag{38}$$

4.2. Diagrams

Expectation values of products of several generators a_p can be calculated similarly using the cyclic property of traces on, for instance, the rightmost generator, giving

$$\langle a_{p_1} \cdots a_{p_M} \rangle_\beta = \frac{1}{\mathrm{e}^{2\pi\beta p_M} - 1} \sum_{j=1}^{M-1} \langle a_{p_1} \cdots [a_{p_M}, a_{p_j}] \cdots a_{p_{M-1}} \rangle_\beta. \tag{39}$$

One obtains a recursion relation for these expectation values by using (34) for the commutator. There are two terms occurring: the first is proportional to the generator $a_{p_j + p_M}$, and the second is the central term, with a delta function factor $\delta(p_j + p_M)$. We may represent these two contributions using the following diagrams:

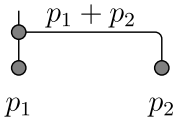

$$= \frac{p_2 - p_1}{e^{2\pi\beta p_2} - 1} \tag{40a}$$

$$= \frac{1}{e^{2\pi\beta p_2} - 1}\left(2p_2\, k(\beta) + \tfrac{c}{12} p_2^3\right)\delta(p_1 + p_2). \tag{40b}$$

Repeating the process, we obtain the expectation value as a sum of diagrams constructed according to the following rules:

(1) Start with a horizontal alignment of 'open dots' carrying momenta $p_1, \ldots, p_M$, for instance

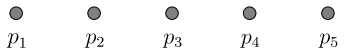

(2) Connect the rightmost dot with a dot to its left, using either the vertex (40*a*) or the cap (40*b*). The use of the vertex (40*a*) leaves an open dot at the horizontal position of the leftmost dot in the connected pair, and at one vertical step higher, carrying the sum of momenta of the connected dots. The use of the cap (40*b*) closes both dots connected. If there are only two open dots, use only (40*b*).

(3) Repeat the previous step with the remaining open dots, one vertical step higher.

(4) Finish when there are no remaining open dots.

Note that we do not allow for diagrams with a single open dot; this corresponds to our choice of basis according to which $\langle a_p \rangle = 0$. As an example, two diagrams contributing to the expectation value $\langle a_{p_1} a_{p_2} a_{p_3} a_{p_4} a_{p_5} \rangle_\beta$ are

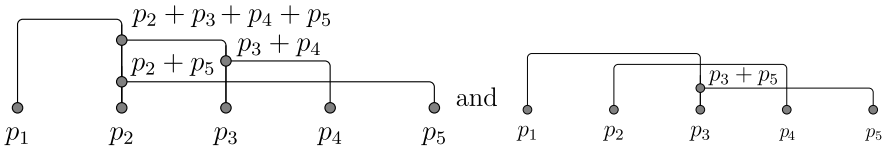

The first diagram corresponds to the term

$$\frac{p_5-p_2}{\mathrm{e}^{2\pi\beta p_5}-1}\frac{p_4-p_3}{\mathrm{e}^{2\pi\beta p_4}-1}\frac{p_3+p_4-(p_2+p_5)}{\mathrm{e}^{2\pi\beta(p_3+p_4)}-1} \times \frac{2(p_2+p_3+p_4+p_5)k(\beta)+(c/12)(p_2+p_3+p_4+p_5)^3}{\mathrm{e}^{2\pi\beta(p_2+p_3+p_4+p_5)}-1} \times \delta(p_1+p_2+p_3+p_4+p_5), \tag{41}$$

and the second diagram corresponds to the term

$$\frac{p_5-p_3}{\mathrm{e}^{2\pi\beta p_5}-1}\frac{2(p_3+p_5)k(\beta)+(c/12)(p_3+p_5)^3}{\mathrm{e}^{2\pi\beta(p_3+p_5)}-1}\delta(p_1+p_3+p_5) \times \frac{2p_4\,k(\beta)+(c/12)p_4^3}{\mathrm{e}^{2\pi\beta p_4}-1}\delta(p_2+p_4). \tag{42}$$

Note that the second diagram can be written as a product of two separate diagrams

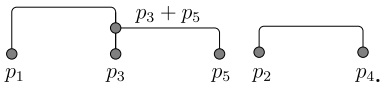

We will call a diagram 'connected' if there is a connected path between all initial dots; otherwise it is 'disconnected'. Above, the first diagram is connected, while the second is disconnected. It is clear, from our diagrammatic rules, that a disconnected diagram can always be written as a product of connected diagrams. Note also that the value of the

J. Stat. Mech. (2014) P03002

momentum is conserved at each three-leg vertex introduced by the first type of connection (40*a*), and that the second type of connection (40*b*) produces a factor of a delta function that sets the sum of the momenta to zero. Hence, the set of momenta in every connected diagram is constrained to sum to zero, but has no other constraint.

As another example, the full expression for the expectation value $\langle a_{p_1} a_{p_2} a_{p_3} a_{p_4} \rangle_\beta$ is

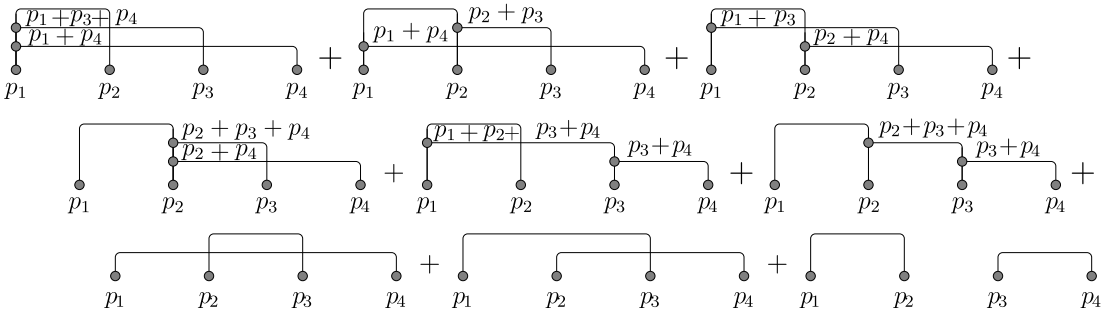

(43)

We finally note that diagrams obtained according the above rules have a nice dynamic interpretation. Indeed, we imagine starting with N particles, carrying conserved quantities p_j, which can only move left, such that two particles can either jump through each other without interacting, or interact with each other by forming a bound state (a new particle) or by annihilating each other. Observing diagrams from bottom to top and interpreting them as world-lines, with time increasing upwards, the rules above give rise to all possible inequivalent events for this dynamics with the further constraint that the rightmost particle always interact first.

4.3. A combinatoric formula

We now show that our rules for constructing diagrams imply that every expectation value can be written as a sum over all partitions of the initial set of momenta, where each term in the sum is the product over all subsets forming the partition, of the sum of all connected diagrams associated to the subset. That is, let $P = (p_1, \ldots, p_M)$ be a list of momenta, and for any ordered sublist $s \subset P$ (i.e. any sublist $(p_{j_1}, \ldots, p_{j_m})$ with $j_1 < \cdots < j_m$), let us denote by $C(s)$ the sum of all diagrams associated with s constructed according to the rules above and which are connected. Then we show that

$$\langle a_{p_1} \cdots a_{p_M} \rangle_\beta = \sum_S C(s_1) \cdots C(s_n) \tag{44}$$

where the sum is over the partitions $S = \{s_1, \ldots, s_n\}$ of P:

$$s_1 \subset P, \ldots, s_n \subset P, \qquad \bigcup_i s_i = P, \qquad s_i \cap s_j = \emptyset \quad (i \neq j). \tag{45}$$

Let us call 'admissible' a diagram based on a list s of momenta, which satisfies our rules for diagram construction. Let us denote by D_P the set of all admissible diagrams based on P, by D_s^C the set of all admissible connected diagrams based on the ordered sublist s of P, and by $\tilde{D}_P = \cup_S D_{s_1}^C \cdots D_{s_n}^C$ the set of all products (juxtapositions) of connected admissible diagrams based on all partitions S of P. In order to show (44), we

only need to show $D_P = \tilde{D}_P$. The proof is in three steps. First, we show that the connected factors in every admissible diagram are themselves admissible diagrams, based on the list of momenta which they connect. Second, we show that every admissible diagram based on P is a product of connected factors based on a partition S of P. These first two points show that $D_P \subset \tilde{D}_P$. Last, we show that every product of connected admissible diagrams based on a partition S of P is an admissible diagram based on P. This shows $\tilde{D}_P \subset D_P$, proving the equality.

Given a pair of dots that are connected either with (40*a*) or with (40*b*), we will refer to its horizontal position as the horizontal position of the rightmost member of the pair, and to its vertical position as the height of the flat horizontal part of the diagram component (40*a*) or (40*b*). Then, we remark the following.

Remark 4.1. The set of all diagrams formed using our rules is the set of all diagrams obtained from the basic components (40*a*) and (40*b*), under the unique additional condition that the bottom-to-top ordering of the vertical positions of the connections be in agreement with the right-to-left ordering of their horizontal positions.

Indeed, it is clear that the rules provide diagrams that satisfy the additional condition of this remark. Further, given a diagram that does satisfy it, we may scan the rightmost members of the connected pairs from the right to the left; we observe that under such a scan the connections exactly agree with the rules.

For the first step of the proof of (44), let us consider a connected factor, and the initial dots that are being connected within the factor. These correspond to an ordered sublist s of the initial list P, and are horizontally aligned and ordered. Then, according to Remark 4.1, the bottom-to-top ordering of the connections within the factor are in agreement with the right-to-left ordering of the right-members of the connected pairs within the factor; again according to Remark 4.1, this implies that a connected factor is an admissible diagram.

The second step is simply a consequence of the fact that given an admissible diagram, the relation according to which two elements of P belong to the same connected factor is an equivalence relation.

The last step is based on the simple observation that within a connected admissible diagram, it is aways possible to move the connections vertically so as to space them out, keeping their order the same. Consider a partition S of P and a product of connected admissible diagrams based on S. Let us draw the product of diagrams with the original dots corresponding to P in ordered horizontal alignment. Let us scan the rightmost members of the connected pairs in the full diagram from the right to the left. Going through connected pairs in a connected factor we observe the correct vertical ordering of the connections. As we go from a pair in a connected factor to a new pair in a new connected factor, we impose the correct vertical ordering by moving up all connections of the new connected factor at or above the level of the new pair. This does not affect connections in other connected factors. At the end of this process, the additional condition of Remark 4.1 is satisfied for the full diagram, hence the diagram is admissible.

doi:10.1088/1742-5468/2014/03/P03002

5. Full counting statistics

In this section we calculate the full counting statistics (20), proving formula (24). First, we show that the large-R limit of the average in the formula (20) can be calculated using the continuous Virasoro algebra introduced in section 4. With that, it is clear that after taking the logarithm, only the connected diagrams survive thanks to (44). Then, we show that in the large-t limit, these connected diagrams have a simple dependence on the number of generators, and resumming the orders of λ, we end up with the desired expression (24).

5.1. Full counting statistics in terms of Virasoro algebra

As explained in section 2, in the steady-state limit, the system factorizes into subsystems described by the Hamiltonians $H^{(j,j+1)}$, so that expectation values for local fields can be calculated using the steady-state density matrix (14), see figure 2. By rewriting the product of exponentials in (20) as

$$\mathrm{e}^{\mathrm{i}\lambda Q(t)}\mathrm{e}^{-\mathrm{i}\lambda Q} = \mathrm{e}^{\mathrm{i}\lambda Q+\mathrm{i}\lambda\Delta_t Q}\mathrm{e}^{-\mathrm{i}\lambda Q} = \mathcal{P}\exp\left(\mathrm{i}\int_0^\lambda \mathrm{d}\lambda'\,\Delta_t Q(\lambda')\right), \tag{46}$$

we see that we need to evaluate steady-state averages of $\Delta_t Q = Q(t) - Q$ evolved with Q:

$$\Delta_t Q(\lambda') := \mathrm{e}^{\mathrm{i}\lambda' Q}\Delta_t Q\mathrm{e}^{-\mathrm{i}\lambda' Q}, \tag{47}$$

and ordered products thereof. The quantity $\Delta_t Q$ was shown in (23) to depend only on the incoming fields h_j^{in}, for $j = 1, \ldots, N$. Using (17), we can replace these with the chiral fields $h^{(j,j+1)}$, and write:

$$\Delta_t Q = \sum_{j=1}^{N} \Delta\alpha_j \int_0^t \mathrm{d}x\, h^{(j,j+1)}(-x). \tag{48}$$

Recall that $\mathrm{i}[H_0^j, h_{j'}^{\mathrm{in}}(x)] = \delta_{j,j'}\partial_x h_j^{\mathrm{in}}(x)$. Since also $\mathrm{i}[H^{(j,j+1)}, h^{(j',j'+1)}(-x)] = \delta_{j,j'}\partial_x \big(h^{(j',j'+1)}(-x)\big)$, the action of $Q = \sum_j \alpha_j H_0^j$ on $\Delta_t Q$ is the same as the action of $\sum_j \alpha_j H^{(j,j+1)}$. Therefore, in (47), we can make the following replacement:

$$Q \mapsto \sum_{j=1}^{N} \alpha_j H^{(j,j+1)}.$$

Hence, the Q-evolution of 'time' λ is the same as a H-evolution where fields are evolved over a time $\lambda\alpha_j$, which depends on the leg the fields are on. The above results mean that the path-ordered exponential in (46) actually *factorizes* amongst the subsystems $H^{(j,j+1)}$, as does the stationary density matrix (14). Hence the average in (20) is a sum of terms of similar form. In order to evaluate these terms, we need to introduce the appropriate algebraic setup.

The expression (46) is plagued by UV divergences coming from local operators $h^{(j,j+1)}(x)$ at coinciding positions. We will use an explicit regularization below.

J. Stat. Mech. (2014) P03002

As is well known (see for instance the book [34]), the algebraic setup underlying CFT is based on the Virasoro algebra. This means that we can calculate the expectation value in (20) using N commuting copies of a Virasoro algebra, $L_n^{(j,j+1)}$, $n \in \mathbb{Z}$, $j = 1, \ldots, N$:

$$[L_m^{(j,j+1)}, L_n^{(j,j+1)}] = (m-n)L_{m+n}^{(j,j+1)} + \frac{c}{12}(n^3 - n)\delta_{m+n,0}. \tag{49}$$

There is one copy for the chiral fields in each subsystem $(j, j+1)$, living on the line segment $[-R/2, R/2]$ with the endpoints identified (see figure 2). In terms of this algebra, the energy density operator and the Hamiltonian are given by

$$h^{(j,j+1)}(x) = \frac{2\pi}{R^2}\left(\sum_{n=-\mathcal{N}}^{\mathcal{N}} L_n^{(j,j+1)} \mathrm{e}^{2\pi \mathrm{i} n x/R} - \frac{c}{24}\right), \qquad H^{(j,j+1)} = \frac{2\pi}{R}\left(L_0^{(j,j+1)} - \frac{c}{24}\right), \tag{50}$$

and the steady-state density matrix takes the following form:

$$\rho_{\mathrm{stat}} = \lim_{R\to\infty} \mathfrak{n}\left[\mathrm{e}^{-\sum_j \beta_j (2\pi/R) L_0^{(j,j+1)}}\right]. \tag{51}$$

In (50) we have used an explicit UV regularization by summing over a finite number of modes $L_n^{(j,j+1)}$. This is equivalent to smearing out the local densities $h^{(j,j+1)}(x)$.

Note that the constant terms in (50) cancel out and play no role in the considerations below. Performing the integral over x, we have, from (48),

$$\Delta_t Q = \frac{2\pi}{R^2}\sum_{j=1}^{N}\Delta\alpha_j \sum_{n=-\mathcal{N}}^{\mathcal{N}} L_n^{(j,j+1)} \int_{-t}^{0} \mathrm{d}x\, \mathrm{e}^{2\pi \mathrm{i} n x/R} = \sum_{j=1}^{N}\Delta\alpha_j \left(\tilde{S}^j + S^j\right), \tag{52}$$

with

$$\tilde{S}^j := \frac{2\pi t}{R^2} L_0^{(j,j+1)}, \qquad S^j := \frac{2}{R}\sum_{\substack{n=-\mathcal{N},\\ n\neq 0}}^{\mathcal{N}} L_n^{(j,j+1)} \mathrm{e}^{-\mathrm{i}\pi n t/R} \frac{\sin(\pi n t/R)}{n}. \tag{53}$$

The Q-evolution in the path-ordered exponential does not affect $\tilde{S}^j$, since $[Q, \tilde{S}^j] = 0$. However, S^j is affected by the action of Q. Using

$$\mathrm{e}^{\mathrm{i}\lambda'\alpha_j (2\pi/R) L_0^{(j,j+1)}} L_n^{(j,j+1)} \mathrm{e}^{-\mathrm{i}\lambda'\alpha_j (2\pi/R) L_0^{(j,j+1)}} = L_n^{(j,j+1)} \mathrm{e}^{-\mathrm{i}\lambda'\alpha_j (2\pi/R) n},$$

we can write the Q-evolution of a 'time' λ' as a shift of the time variable appearing in the exponential in (53) of twice the value $\lambda'\alpha_j$, replacing S^j with $S^j_{\lambda'\alpha_j}$, where

$$S^j_\tau := \sum_{\substack{n=-\mathcal{N},\\ n\neq 0}}^{\mathcal{N}} L_n^{(j,j+1)} \mathrm{e}^{-\mathrm{i}\pi n (t+2\tau)/R} \frac{\sin(\pi n t/R)}{n}. \tag{54}$$

Then, the factorized form of the path-ordered exponential in (46) is, after changing variable to $\tau = \lambda'\alpha_j$ for convenience,

$$\mathcal{P}\exp\left(\mathrm{i}\int_0^\lambda \mathrm{d}\lambda'\, \Delta_t Q(\lambda')\right) = \prod_{j=1}^{N} \mathcal{P}\exp\left(\frac{\mathrm{i}\Delta\alpha_j}{\alpha_j}\int_0^{\lambda\alpha_j} \mathrm{d}\tau\, (\tilde{S}^j + S^j_\tau)\right). \tag{55}$$

Taking the log, (20) gives a sum over the legs,

$$F(\lambda) = \sum_{j=1}^{N} f(\alpha_j, \Delta\alpha_j, \beta_j, \lambda) \tag{56}$$

with

$$f(\alpha, \Delta\alpha, \beta, \lambda) := \lim_{t\to\infty} \frac{1}{t} \log \lim_{R\to\infty} \left\langle \mathcal{P} \exp\left(\frac{\mathrm{i}\Delta\alpha}{\alpha} \int_0^{\lambda\alpha} \mathrm{d}\tau \, (\tilde{S} + S_\tau) \right) \right\rangle_{\beta,R}. \tag{57}$$

Since the form of this expression is identical for each subsystem $(j, j+1)$, we here and below use a single copy of the Virasoro algebra (49), denoted L_n, $n \in \mathbb{Z}$, and similarly we drop the superscripts j on $\tilde{S}$ and S. Here, the average $\langle \cdots \rangle_{\beta,R}$ is the trace over a representation of this single copy of the Virasoro algebra, with density matrix $\mathfrak{n}[\exp(-\beta(2\pi/R)L_0)]$:

$$\langle \cdots \rangle_{\beta,R} := \mathrm{Tr}\left(\mathfrak{n}\left[\mathrm{e}^{-\beta(2\pi/R)L_0} \right] \cdots \right).$$

Expanding the path-ordered exponential in (57) and taking the average, we get a sum over $m \geq 0$ of

$$\left(\frac{\mathrm{i}\Delta\alpha}{\alpha} \right)^m \int_0^{\lambda\alpha} \mathrm{d}\tau_1 \cdots \int_0^{\tau_{m-1}} \mathrm{d}\tau_m \, \langle (\tilde{S} + S_{\tau_1}) \cdots (\tilde{S} + S_{\tau_m}) \rangle_{\beta,R}. \tag{58}$$

In the following we will show that the limit $R \to \infty$ of these averages can be calculated using the continuous Virasoro algebra of section 4, with the value (37) of k.

5.2. Expectation values in the large-R limit

We now show that the large-R limit of a product of Virasoro generators can be calculated using the continuous algebra of section 4. We will proceed by showing first that this is the case for an expectation value of two generators, and then by induction that it holds for any number of generators.

It turns out that in the large-R limit we should take the UV regularization $\mathcal{N}$ to grow proportionally to R, thus introducing a fixed energy cutoff Λ, given by $\mathcal{N} = \Lambda R$.

In order to make the connection to the continuous algebra clear, we will make use of the following notation,

$$p_i := \frac{n_i}{R}, \qquad a^{(R)}_{p_i} := \frac{L_{n_i}}{R}(1 - \delta_{n_i,0}), \qquad A^{(R)} := \frac{L_0}{R^2}, \qquad \delta^{(R)}(p_i - p_j) := R\delta_{n_i,n_j}, \tag{59}$$

where the label (R) indicates that these quantities are defined for finite system size R. Note in particular that, according to our definition, $a^{(R)}_0 = 0$, which is for convenience.

In (58), we see that we need averages of products of $\tilde{S}$ and S_τ. The latter is a sum over $n \neq 0$, the former contains L_0 only. Hence, we are interested in evaluating sums over $n_i \in \mathbb{Z}$ of averages of products of operators $a^{(R)}_{p_i}$ and operators $A^{(R)}$ (the condition $n_i \neq 0$ is already implemented in the definition of $a^{(R)}_{p_i}$). We will evaluate these sums, in the large-R limit, as integrals over continuous momenta p_i of averages of operators a_{p_i} in the continuous Virasoro algebra developed in section 4. More precisely, we will show that

J. Stat. Mech. (2014) P03002

the following is true, for every $M \geq 0$, every $\ell \geq 0$ and every continuous function f of the momenta (on the left-hand side, $p_i = n_i/R$ with $n_i \in \mathbb{Z}$; on the right-hand side, $p_i \in \mathbb{R}$; we use the notation $\mathbf{p} = (p_1, \ldots, p_M)$):

$$\lim_{R\to\infty} \sum_{\mathbf{p}=-\Lambda}^{\Lambda} f(\mathbf{p}) \langle a_{p_1}^{(R)} \cdots a_{p_M}^{(R)} \rangle_{\beta,R} = \int_{-\Lambda}^{\Lambda} \mathrm{d}^M p\, f(\mathbf{p}) \langle a_{p_1} \cdots a_{p_M} \rangle_\beta \tag{60a}$$

$$\lim_{R\to\infty} \sum_{\mathbf{p}=-\Lambda}^{\Lambda} f(\mathbf{p}) \langle (A^{(R)})^\ell a_{p_1}^{(R)} \cdots a_{p_M}^{(R)} \rangle_{\beta,R} = (k(\beta))^\ell \int_{-\Lambda}^{\Lambda} \mathrm{d}^M p\, f(\mathbf{p}) \langle a_{p_1} \cdots a_{p_M} \rangle_\beta, \tag{60b}$$

as well as similar statements to (60*b*), but with $A^{(R)}$ operators in all possible positions in the average on the left-hand side. On the right-hand side of (60), the averages are calculated using the continuous Virasoro algebra of section 4 with $k = k(\beta)$. Recall that $k(\beta)$, defined in (37), equals $c/(24\beta^2)$. This is the expectation value of the operator $A^{(R)}$ in the large-R limit (see for instance [34]):

$$\lim_{R\to\infty} \langle A^{(R)} \rangle_{\beta,R} = \frac{c}{24\beta^2}. \tag{61}$$

The statement (62*b*), and its relative with different positions of $A^{(R)}$, can be interpreted by saying that the operator $A^{(R)}$ tends, in the infinite-R limit, to a central element, which assumes a fixed, state-dependent value.

Defining $a_p^{(R)}$ as being zero at $p = 0$ is appropriate because it automatically implements the condition $n \neq 0$ in the sum defining S_τ. Also, we note that the large-R limit of L_0/R diverges: it is the operator that measures the energy in the system. The quantity proportional to L_0 and that has a finite large-R limit is $A^{(R)}$, which corresponds to the energy density.

The induction proof that we present below is an induction on M. We will assume that

$$\lim_{R\to\infty} \langle a_{p_1}^{(R)} \cdots a_{p_M}^{(R)} \rangle_{\beta,R} \doteq \langle a_{p_1} \cdots a_{p_M} \rangle_\beta \tag{62a}$$

$$\lim_{R\to\infty} \langle (A^{(R)})^\ell a_{p_1}^{(R)} \cdots a_{p_M}^{(R)} \rangle_{\beta,R} \doteq (k(\beta))^\ell \langle a_{p_1} \cdots a_{p_M} \rangle_\beta, \tag{62b}$$

holds for some M and for all $\ell \geq 0$ (as well as similar equations to (62*b*) but with the $A^{(R)}$ operators in different positions), and show that this implies the same for $M + 1$. We will also show that this holds for $M = 2$. Here the equations are understood as distributions, in the sense of (60), which we represent by the equality symbol '$\doteq$'. In practice, this means that the limits on the left-hand sides are taken with fixed p_i, terms giving zero under integration on the right-hand sides are neglected, and the distribution relation

$$\delta^{(R)}(p_i - p_j) \to \delta(p_i - p_j) \tag{63}$$

is used. The passage from (62) to (60) is then simply done by using the relation

$$\sum_{\substack{n=-\Lambda R,\\ n\neq 0}}^{\Lambda R} \frac{1}{R} \to \int_{-\Lambda}^{\Lambda} \mathrm{d}p.$$

For lightness of notation we will omit the explicit integration boundaries below.

5.2.1. Proof at order 2. The left-hand side of (62*a*) for the case $M = 2$ can be written in terms of Virasoro generators, using the definitions (59) and assuming for now $p_1 \neq 0$ and $p_2 \neq 0$:

$$\langle a_{p_1}^{(R)} a_{p_2}^{(R)} \rangle_{\beta,R} = \frac{1}{R^2} \langle L_{n_1} L_{n_2} \rangle_{\beta,R} = \frac{1}{R^2} \frac{\mathrm{Tr}(\mathrm{e}^{-\beta(2\pi/R)L_0} L_{n_1} L_{n_2})}{\mathrm{Tr}(\mathrm{e}^{-\beta(2\pi/R)L_0})}.$$

Making use of the cyclicity of the trace and the Virasoro algebra, in particular the exchange relation

$$L_n \mathrm{e}^{-(2\pi\beta/R)L_0} = \mathrm{e}^{-(2\pi\beta/R)n} \mathrm{e}^{-(2\pi\beta/R)L_0} L_n, \tag{64}$$

the result is

$$\langle L_{n_1} L_{n_2} \rangle_{\beta,R} = \frac{1}{\mathrm{e}^{2\pi\beta n_2/R} - 1} \left((n_2 - n_1) \langle L_{n_1+n_2} \rangle_{\beta,R} + \frac{c}{12} (n_2^3 - n_2) \delta_{n_1+n_2,0} \right).$$

Because $\langle L_n \rangle_{\beta,R} = 0$ for $n \neq 0$, we can write the average of two generators as

$$\langle L_{n_1} L_{n_2} \rangle_{\beta,R} = \frac{1}{\mathrm{e}^{2\pi\beta n_2/R} - 1} \left(2n_2 \langle L_0 \rangle_{\beta,R} + \frac{c}{12} (n_2^3 - n_2) \right) \delta_{n_1+n_2,0},$$

which we can express back in terms of the quantities $A^{(R)}$, $a_p^{(R)}$, p and $\delta^{(R)}(p)$ using (59):

$$\langle a_{p_1}^{(R)} a_{p_2}^{(R)} \rangle_{\beta,R} = \frac{1}{\mathrm{e}^{2\pi\beta p_2} - 1} \left(2p_2 \langle A^{(R)} \rangle_{\beta,R} + \frac{c}{12} \left(p_2^3 + \frac{p_2}{R^2} \right) \right) \delta^{(R)}(p_1 + p_2). \tag{65}$$

Taking the limit $R \to \infty$ and using the delta function limit (63) and the expectation value of $A^{(R)}$ (61), we find

$$\lim_{R\to\infty} \langle a_{p_1}^{(R)} a_{p_2}^{(R)} \rangle_{\beta,R} \doteq \frac{1}{\mathrm{e}^{2\pi\beta p_2} - 1} \left(2p_2 \frac{c}{24\beta^2} + \frac{c}{12} p_2^3 \right) \delta(p_1 + p_2).$$

This is in fact true for general p_1 and p_2, noting that although for $p_1 = p_2 = 0$ the left-hand side is zero and the right-hand side is not, the difference does integrate to zero. The right-hand side corresponds to the value one would obtain by evaluating $\langle a_{p_1} a_{p_2} \rangle_\beta$ using the diagram rules in section 4 for the choice $k = c/(24\beta^2)$. This shows (62*a*) for $M = 2$.

Let us now show (62*b*) for $M = 2$. Starting with $\ell = 1$, we can write the insertion of $A^{(R)}$ in terms of the Virasoro generators as

$$\langle A^{(R)} a_{p_1}^{(R)} a_{p_2}^{(R)} \rangle_{\beta,R} = \frac{1}{R^2} \langle L_0 \, a_{p_1}^{(R)} a_{p_2}^{(R)} \rangle_{\beta,R}.$$

In general, inserting an extra L_0 in an average of an operator $\mathcal{O}$ can be done by differentiating with respect to β,

$$\frac{\partial}{\partial\beta} \langle \mathcal{O} \rangle_{\beta,R} = -\frac{2\pi}{R} \langle L_0 \mathcal{O} \rangle_{\beta,R} + \frac{2\pi}{R} \langle L_0 \rangle \langle \mathcal{O} \rangle_{\beta,R}. \tag{66}$$

Hence, the insertion of $A^{(R)}$ is equivalent to the application of a differential operator:

$$\langle A^{(R)} \mathcal{O} \rangle_{\beta,R} = \left(\langle A^{(R)} \rangle_{\beta,R} - \frac{1}{2\pi R} \frac{\partial}{\partial\beta} \right) \langle \mathcal{O} \rangle_{\beta,R}. \tag{67}$$

J. Stat. Mech. (2014) P03002

Specializing to the case $\mathcal{O} = a^{(R)}_{p_1} a^{(R)}_{p_2}$ and looking at (65), one can see that the large-R limit commutes with the $\partial/\partial\beta$ derivative (in (65), a careful analysis is necessary in order to see this on the average $\langle A^{(R)}\rangle_{\beta,R}$, which is beyond the scope of this paper). Hence the last term on the right-hand side above vanishes in the limit, which shows (62*b*) using (61). Insertions of $\ell > 1$ operators $A^{(R)}$ are obtained similarly by multiple applications of the differential operator. Furthermore, the fact that the position of $A^{(R)}$ is unimportant is an immediate consequence of the commutation relation

$$[a^{(R)}_p, A^{(R)}] = \frac{p}{R} a^{(R)}_p \to 0 \qquad \text{as } R \to \infty \tag{68}$$

where the large-R limit is taken inside averages and with fixed p, as above.

5.2.2. The induction step. In order to prove that (62*a*) holds for all values of M, we must now prove the induction step: if (62*a*) holds up to some number M of generators, it must also hold for $M+1$ generators.

The finite-R expectation value of $M+1$ operators, again assuming all p_is different from zero,

$$\langle a^{(R)}_{p_1} \cdots a^{(R)}_{p_{M+1}} \rangle_{\beta,R} = \frac{1}{R^{M+1}} \langle L_{n_1} \cdots L_{n_{M+1}} \rangle_{\beta,R},$$

can be calculated in terms of expectation values with M and $M-1$ operators using cyclicity of the trace and (64) in order to bring $L_{n_{M+1}}$ cyclically through all other operators. This gives

$$\begin{aligned}
\langle L_{n_1} \cdots L_{n_{M+1}} \rangle &= \frac{1}{\mathrm{e}^{2\pi\beta n_{M+1}/R} - 1} \sum_{i=1}^{M} \langle L_{n_1} \cdots [L_{n_{M+1}}, L_{n_i}] \cdots L_{n_M} \rangle \\
&= \frac{1}{\mathrm{e}^{2\pi\beta n_{M+1}/R} - 1} \sum_{j=1}^{M} \Bigg[(n_{M+1} - n_i) \langle L_{n_1} \cdots L_{n_i + n_{M+1}} \cdots L_{n_M} \rangle \\
&\quad \times (1 - \delta_{n_i + n_{M+1}, 0}) + \Bigg(2n_{M+1} \langle L_{n_1} \cdots L_0 \cdots L_{n_M} \rangle \\
&\quad + \frac{c}{12} (n^3_{M+1} - n_{M+1}) \langle L_{n_1} \cdots \widehat{L_{n_i}} \cdots L_{n_M} \rangle \Bigg) \delta_{n_i + n_{M+1}, 0} \Bigg],
\end{aligned}$$

where in the last line we separated the case where the n_i and n_{M+1} add up to zero (and the hat indicates that the factor is omitted). Using (59), this can be re-written as

$$\begin{aligned}
\langle a^{(R)}_{p_1} \cdots a^{(R)}_{p_{M+1}} \rangle_{\beta,R} = \frac{1}{\mathrm{e}^{2\pi\beta p_{M+1}} - 1} \sum_{i=1}^{M} \Bigg[& (p_{M+1} - p_i) \langle a^{(R)}_{p_1} \cdots a^{(R)}_{p_i + p_{M+1}} \cdots a^{(R)}_{p_M} \rangle_{\beta,R} \\
& + 2p_{M+1} \langle a^{(R)}_{p_1} \cdots A^{(R)} \cdots a^{(R)}_{p_M} \rangle_{\beta,R} \\
& + \frac{c}{12} \left(p^3_{M+1} - \frac{p_{M+1}}{R^2} \right) \langle a^{(R)}_{p_1} \cdots \widehat{a^{(R)}_{p_i}} \cdots a^{(R)}_{p_M} \rangle_{\beta,R} \, \delta^{(R)}(p_i + p_{M+1}) \Bigg]
\end{aligned} \tag{69}$$

and from the induction assumption expressed in (62), we can immediately evaluate the large-R limit:

$$\lim_{R\to\infty}\langle a^{(R)}_{p_1}\cdots a^{(R)}_{p_{M+1}}\rangle \doteq \frac{1}{\mathrm{e}^{2\pi\beta p_{M+1}}-1}\sum_{i=1}^{M}\Bigg[(p_{M+1}-p_i)\langle a_{p_1}\cdots a_{p_i+p_{M+1}}\cdots a_{p_M}\rangle_\beta + \left(2p_{M+1}k(\beta)+\frac{c}{12}p_{M+1}^3\right)\langle a_{p_1}\cdots\widehat{a_{p_i}}\cdots a_{p_M}\rangle_\beta\,\delta(p_i+p_{M+1})\Bigg]. \tag{70}$$

This is exactly the induction step (39) (along with (34) and (37)) used in order to evaluate averages in the continuous Virasoro algebra. Again this holds for general p_is, noting that at $p_i = 0$ the difference between the left- and right-hand sides are terms that integrate to zero. This shows (62*a*) for $M \mapsto M+1$.

In order to show (62*b*) (and similar equations with the operators $A^{(R)}$ at different positions), one may use again a derivative argument based on (67), and the vanishing, in the large-R limit, of the commutator (68). The fact that the large-R limit commutes with the derivative operator $\partial/\partial\beta$ can be seen recursively from (69), using the observation that this fact was true in the case $M = 2$ and using (67) (and again, at every step it is necessary to use this nontrivial fact on the expectation value $\langle A^{(R)}\rangle_{\beta,R}$).

5.3. Large-t limit

We can now use the results (60) in order to calculate the expectations that appear in the expansion (58). Writing S_τ and $\tilde{S}$ in terms of $A^{(R)}$ and $a^{(R)}_p$ following (59), where $p = n/R$ takes discrete values, we find

$$\tilde{S} = \frac{2\pi t}{R^2}L_0 = 2\pi t\,A^{(R)} \tag{71a}$$

$$S_\tau = \frac{2}{R}\sum_{n\neq 0}L_n\mathrm{e}^{-\mathrm{i}\pi n(t+2\tau)/R}\frac{\sin(\pi nt/R)}{n} = \frac{2}{R}\sum_{p}a^{(R)}_p\mathrm{e}^{-\mathrm{i}\pi p(t+2\tau)}\frac{\sin(\pi pt)}{p}. \tag{71b}$$

Equation (60*a*) then implies that we can express the large-R limit of expectation values of products of S_τ in terms of the continuous algebra,

$$\lim_{R\to\infty}\langle S_{\tau_1}\cdots S_{\tau_M}\rangle_{\beta,R} = 2^M\int \mathrm{d}^M p\,\langle a_{p_1}\cdots a_{p_M}\rangle_\beta\prod_{i=1}^{M}\mathrm{e}^{-\mathrm{i}\pi p_i(t+2\tau_i)}\frac{\sin(\pi p_i t)}{p_i}. \tag{72}$$

Further, equation (60*b*) and its relatives, i.e. the statement that in the large-R limit, $A^{(R)}$ becomes central and assumes the fixed value $k(\beta)$, implies that in the large-R limit, $\tilde{S}$ factorizes and can be treated as the number $2\pi t\,k(\beta)$. Therefore, the large-R limit of the

expectation value in (57) can be written as

$$\lim_{R\to\infty}\left\langle \mathcal{P}\exp\left(\frac{\mathrm{i}\Delta\alpha}{\alpha}\int_0^{\lambda\alpha}\mathrm{d}\tau\,(\tilde{S}+S_\tau)\right)\right\rangle_{\beta,R}$$
$$=\mathrm{e}^{2\pi\mathrm{i}t\,k(\beta)\,\Delta\alpha\,\lambda}\sum_{M=0}^{\infty}\left(\frac{2\mathrm{i}\Delta\alpha}{\alpha}\right)^M\int\mathrm{d}^M p\,\langle a_{p_1}\cdots a_{p_M}\rangle_\beta$$
$$\times\prod_{i=1}^{M}\int_0^{\tau_{i-1}}\mathrm{d}\tau_j\,\mathrm{e}^{-\mathrm{i}\pi p_i(t+2\tau_i)}\frac{\sin(\pi p_i t)}{p_i}, \tag{73}$$

with $\tau_0 := \lambda\alpha$.

In order to calculate the large-time cumulant generating function (57), we take the logarithm of the above expression. Recall the combinatoric formula (44): an expectation $\langle a_{p_1}\cdots a_{p_M}\rangle_\beta$ is a sum over partitions S of the list of momenta $(p_1,\ldots,p_M)$, of products over the partition's parts $s\in S, s\subset(p_1,\ldots,p_M)$, of sums $C(s)$ of connected diagrams linking the momenta in s. Then by standard combinatoric arguments, the logarithm of (73) is a series formed by the connected averages $\langle a_{p_1}\cdots a_{p_M}\rangle_\beta^{\mathrm{conn}} := C(p_1,\ldots,p_M)$ evaluated by summing over the connected diagrams. From (57) and (73), we have

$$f(\alpha,\Delta\alpha,\beta,\lambda)=2\pi\mathrm{i}\,k(\beta)\,\Delta\alpha\,\lambda$$
$$+\lim_{t\to\infty}\frac{1}{t}\sum_{M=2}^{\infty}\left(\frac{2\mathrm{i}\Delta\alpha}{\alpha}\right)^M\int\mathrm{d}^M p\,\langle a_{p_1}\cdots a_{p_M}\rangle_\beta^{\mathrm{conn}}$$
$$\times\prod_{i=1}^{M}\int_0^{\tau_{i-1}}\mathrm{d}\tau_i\,\mathrm{e}^{-\mathrm{i}\pi p_i(t+2\tau_i)}\frac{\sin(\pi p_i t)}{p_i}. \tag{74}$$

Every connected diagram γ with M momenta contains exactly one overall delta function $\delta(p_1+\cdots+p_M)$, and can be written in the form

$$G_M^\gamma(\mathbf{p})\,\delta(p_1+\cdots+p_M), \tag{75}$$

where G_M^γ, defined on the hyperplane $p_1+\cdots+p_M=0$, is an entire function of the momenta except for simple poles when seen as a function of the sum of any subset of the momenta (as is clear from the diagram rules (40*a*) and (40*b*)). Hence also connected averages have this form,

$$\langle a_{p_1}\cdots a_{p_M}\rangle_\beta^{\mathrm{conn}}=\left(\sum_\gamma G_M^\gamma(\mathbf{p})\right)\delta(p_1+\cdots+p_M)=:G_M(\mathbf{p})\,\delta(p_1+\cdots+p_M)$$
$$(M\geq 2). \tag{76}$$

Taking into account this form, we may evaluate the large-time limit on the right-hand side of (74) using the formula (see e.g. [33])

$$\lim_{t\to\infty}\frac{1}{t}\int\mathrm{d}^M p\,g(\mathbf{p})\left(\prod_{i=1}^{M}\frac{\sin(\pi p_i t)}{\pi p_i}\right)\delta(p_1+\cdots+p_M)=g(0,\ldots,0), \tag{77}$$

which gives rise to

$$f(\alpha,\Delta\alpha,\beta,\lambda) = 2\pi\mathrm{i}\,k(\beta)\,\Delta\alpha\,\lambda + \sum_{M=2}^{\infty}\left(\frac{2\pi\mathrm{i}\Delta\alpha}{\alpha}\right)^M G_M(0,\ldots,0)\prod_{i=1}^{M}\int_0^{\tau_{i-1}}\mathrm{d}\tau_i$$
$$= 2\pi\mathrm{i}\,k(\beta)\,\Delta\alpha\,\lambda + \sum_{M=2}^{\infty}\frac{(2\pi\mathrm{i}\,\Delta\alpha\,\lambda)^M}{M!}G_M(0,\ldots,0). \tag{78}$$

Hence, we need to evaluate $G_M(0,\ldots,0)$. Although each $G_M^\gamma(\mathbf{p})$ has poles which make its value at $p_1 = \cdots = p_M = 0$ ill-defined (the limit of $G_M^\gamma(\mathbf{p})$ when $\mathbf{p}\to(0,\ldots,0)$ does not exist), the sum of all connected diagrams is well defined at zero momenta. The value of $G_M(0,\ldots,0)$ can be calculated as follows. Consider the operators $\tilde{a}_p := a_p + k(\beta)\delta(p)$. These satisfy commutation relations with a central term that does not contain the term linear in p, that is $[a_p, a_q] = (p-q)+(c/12)p^3\,\delta(p+q)$. Hence, these operators are explicitly independent of β, and they have a nonzero one-point average given by $\langle\tilde{a}_p\rangle_\beta = k(\beta)\delta(p)$. Consider the connected averages $\langle\tilde{a}_{p_1}\cdots\tilde{a}_{p_M}\rangle_\beta^{\mathrm{conn}}$, defined combinatorially as usual. The insertion of an operator $\tilde{a}_0$ can be obtained simply by differentiating with respect to β:

$$\langle\tilde{a}_{p_1}\cdots\tilde{a}_{p_M}\tilde{a}_0\rangle_\beta^{\mathrm{conn}} = -\frac{1}{2\pi}\frac{\partial}{\partial\beta}\langle\tilde{a}_{p_1}\cdots\tilde{a}_{p_M}\rangle_\beta^{\mathrm{conn}}$$

for any $M \geq 1$. Since we take connected averages, the shift of the expectation value is irrelevant whenever the number of operators is greater than or equal to two: $\langle\tilde{a}_{p_1}\cdots\tilde{a}_{p_M}\rangle_\beta^{\mathrm{conn}} = \langle a_{p_1}\cdots a_{p_M}\rangle_\beta^{\mathrm{conn}}$ for all $M \geq 2$. Hence, we find the recursion relation

$$G_M(0,\ldots,0) = -\frac{1}{2\pi}\frac{\partial}{\partial\beta}G_{M-1}(0,\ldots,0),$$

which holds for all $M \geq 2$ if we define $G_1(0) := k(\beta)$. Using (37), this gives

$$G_M(0,\ldots,0) = \frac{M!\,k(\beta)}{(2\pi\beta)^{M-1}}.$$

Hence, putting this in (78), we find

$$f(\alpha,\Delta\alpha,\beta,\lambda) = 2\pi\beta\,k(\beta)\sum_{M=1}^{\infty}\left(\frac{\mathrm{i}\,\Delta\alpha\,\lambda}{\beta}\right)^M = \frac{2\pi\mathrm{i}\,\beta\,k(\beta)\,\Delta\alpha\,\lambda}{\beta - \mathrm{i}\,\Delta\alpha\,\lambda}.$$

With (56) and (37), this indeed reproduces (24).

Finally, we observe that the function $f(\alpha,\Delta\alpha,\beta,\lambda)$ is in fact independent of α. Hence, seeing our initial expression (46) as a function of α_j and $\Delta\alpha_j$ in the form

$$\mathcal{P}\exp\left(\mathrm{i}\int_0^\lambda \mathrm{d}\lambda' \mathrm{e}^{\mathrm{i}\lambda' Q(\{\alpha\})}(\Delta_t Q)(\{\Delta\alpha\})\mathrm{e}^{-\mathrm{i}\lambda' Q(\{\alpha\})}\right),$$

we conclude that the same result for the full counting statistics is obtained by setting $\alpha_j = 0$ in this expression. But setting $\alpha_j = 0$ means setting $Q = 0$, and the exponential becomes simply $\mathrm{e}^{\mathrm{i}\lambda\Delta_t Q}$, so that we have shown that the expression (21) indeed gives the same result.

doi:10.1088/1742-5468/2014/03/P03002

5.4. UV regularization

In the above derivation, we omitted the explicit momentum cutoff Λ in our integrals. These cutoffs are necessary because the expression (72), for the large-R limit of expectation values at finite time t, is a multiple momentum integral that is divergent at large momenta. In fact, as we mentioned, even before taking the large-R limit, at each order in λ, the average of $e^{i\lambda Q(t)}e^{-i\lambda Q}$, written in terms of sums over Virasoro indices n_i of averages of Virasoro generators through (55), (53) and (54), is divergent at large values of n_i. These divergences are expected, as we are effectively evaluating exponentials of local fields (integrated over finite regions) in a quantum field theory. Hence, in order to make our calculations finite, we need a UV regularization. A natural way of regularizing is to modify the expression of the local fields needed, $h^{(j,j+1)}(x)$: as was done above, one may simply sum over indices $n \in \mathbb{Z} \cap [-\mathcal{N}, \mathcal{N}]$ in (50), with $\mathcal{N} > 0$ finite. Then the finite-R average of $e^{i\lambda Q(t)}e^{-i\lambda Q}$, which is the average of path-ordered exponential (55), is finite order by order in λ. At large R, however, we need to make sure that the UV regularization, which should be an energy, behaves correctly: what needs to be fixed is not the range of the dimensionless indices n, but rather the range of the momenta p. That is, we take $\mathcal{N} = \Lambda R$ with Λ a fixed quantity with dimensions of energy. Then, the regularization translates into limiting the multiple momentum integral to the range $p_i \in [-\Lambda, \Lambda]$ in (72), which is indeed finite. The large-t limit can then be taken, which kills the integral and constrains the values of the momenta to 0. Hence, after the large-t limit is taken, the result is explicitly independent of Λ: the UV regularization can be taken to infinity.

These considerations, and our proof above, gives further confirmation of the claim made in [8, 9] that the result for the full counting statistics of the energy flow in CFT is universal (although it is not a proof and does not fully address the problem of irrelevant operators). Indeed, we have here a very different regularization scheme (perhaps more standard) from that used in [9], yet we find the same result.

The present considerations can also be translated into an intuition as to how the special steady-state limit, $R \to \infty$ followed by $t \to \infty$, behaves in terms of the Virasoro modes in CFT. Indeed, as we mentioned, the present formulation is equivalent to a two-time measurement where the first measurement is at the connection time. Hence, although the parameter R we used was an 'artifact' in order to construct the steady-state density matrix, it can be interpreted as the length of the physical system; and the time t between the two measurements can be interpreted as the time the system has evolved towards the steady state. Then, the way we took the $R \to \infty$ limit indicates that the large-volume physics occurs at very large modes, $n \sim pR$ with fixed momenta p, and the result of the $t \to \infty$ limit indicates that the large-time limit is dominated by very small values of momenta p.

6. Conclusion

We have evaluated the scaled cumulant generating function for the energy transfer in NECFT on a star graph with temperature imbalances amongst the legs of the graph, and a simple connection condition at the vertex. We introduced new techniques in order to perform the calculation, in particular studying a continuous version of the Virasoro

doi:10.1088/1742-5468/2014/03/P03002

J. Stat. Mech. (2014) P03002

algebra and the associated diagrams. This generalizes the NECFT results of [8, 9] to the star-graph configuration, and agrees, in the particular case of unit central charge, with previously obtained results concerning free bosons (Luttinger liquids) [29] and free Dirac fermions [27] on star graphs. Our results further confirm the universality of the NECFT full counting statistics, as well as the Poisson-process picture underlying long-time energy transfer in NECFT.

There are interesting open problems that the techniques of the present paper may help address. An immediate question concerns the energy or charge transfer in the cases of a nontrivial but conformal impurity at the vertex of the graph. Since impurities are usually described algebraically in CFT, it is possible that the present Virasoro algebraic methods may be of use in order to make progress. Another set of non-equilibrium problems that are of current interest are those where parameters of a system are suddenly changed and the system then allowed to evolve. It is expected that the result at large time is a so-called 'generalized Gibbs ensemble', described by a nontrivial density matrix. The techniques developed here may help in evaluating averages in such density matrices. Finally, it would also be interesting to generalize the present ideas to non-conformal (say integrable) situations, for instance with conformal baths and a non-conformal integrable impurity (like the multi-channel Kondo model).

Appendix A. Comparison with other results

We compare our results for the energy current with the results obtained in [27], where the steady charge and energy current were obtained for a quantum wire junction (both relativistic and nonrelativistic). The quantum junction is modeled by a star graph where fields living on one of the legs that are incoming to the vertex have an associated temperature and chemical potential determined by the leg. The charge and energy exchange are modeled by pointlike interactions in the vertex; for comparison with our results, we take these to be scale-invariant. In the notation of [27] this means the scattering matrix takes the form

$$\mathbb{S}_{\rm inv} = \theta(k)\mathbb{U} + \theta(-k)\mathbb{U}^{-1}, \tag{A.1}$$

where in [27] the matrix $\mathbb{U}$ is an arbitrary unitary $N \times N$ matrix, representing the vertex conditions for positive or negative values of the parameter k (which plays the role of a momentum). We note that the diagonal elements are reflection at the vertex, and the off-diagonal element $\mathbb{S}_{ij}$ is the transmission amplitude from the ith leg to the jth leg. This means that the vertex conditions of the present work correspond to the following choice for $\mathbb{U}$,

$$\mathbb{U}_{ij} = \gamma_{i-1}\,\delta_{j,i-1}, \qquad \mathbb{U}^{-1}_{ij} = \gamma_i^{-1}\delta_{j,i+1}, \tag{A.2}$$

where $\{\gamma_1, \ldots, \gamma_{N-1}\}$ are complex numbers that have to satisfy the requirement

$$\gamma_j^{-1} = \gamma_j^*. \tag{A.3}$$

The energy flow from the ith leg into the vertex at criticality is given by

$$\mathcal{T}_i(\beta,\mu,\tilde{\mu}) = \frac{1}{2\pi}\sum_{j=1}^{N}\left(|\mathbb{U}_{ij}|^2-\delta_{ij}\right)\frac{1}{\beta_j^2}\left[\mathrm{Li}_2\left(-\mathrm{e}^{-\beta_j\mu_j}\right)+\mathrm{Li}_2\left(-\mathrm{e}^{-\beta_j\tilde{\mu}_j}\right)\right]. \quad \text{(A.4)}$$

With $\mathrm{Li}_2(x)$ known as the dilogarithm (or Spence function $\mathrm{Sp}(x)$). Since we assume that the chemical potentials for the (anti)particles are all equal, we may take them to zero, and the terms between square brackets become:

$$\mathrm{Li}_2\left(-\mathrm{e}^{-\beta_j\mu_j}\right)+\mathrm{Li}_2\left(-\mathrm{e}^{-\beta_j\tilde{\mu}_j}\right)\Big|_{\mu,\tilde{\mu}=0} = 2\mathrm{Li}_2(-1) = -\frac{2\pi^2}{12}. \quad \text{(A.5)}$$

The heat flow for zero chemical potential is given by

$$\mathcal{T}_i(\beta) = \frac{\pi}{12}\sum_{j=1}^{N}\left(\delta_{ij}-|\mathbb{U}_{ij}|^2\right)\frac{1}{\beta_j^2}. \quad \text{(A.6)}$$

For our example of sequentially connected CFTs, we have

$$|\mathbb{U}_{ij}|^2 = \mathbb{U}^*_{ij}\mathbb{U}_{ij} = \gamma^*_{i-1}\gamma_{i-1}\delta_{j,i-1} = \gamma^{-1}_{i-1}\gamma_{i-1}\delta_{j,i-1} = \delta_{j,i-1}, \quad \text{(A.7)}$$

so the heat flow at criticality from the ith leg into the $i+1$th leg is given by

$$\mathcal{T}_i(\beta) = \frac{\pi}{12}\left(\frac{1}{\beta_i^2}-\frac{1}{\beta_{i-1}^2}\right). \quad \text{(A.8)}$$

Summing over all legs, and giving each contribution a weight $\Delta\alpha_i$, it is easy to see that this agrees with our result (19), with a choice of the central charge $c = 1$.

Appendix B. An operator interpretation of the change of connection at the vertex of the graph

At the time $-t_0$ when the N separate systems are connected as represented in figure 2, there is a drastic change in the dynamics. Such changes of boundary or 'impurity' conditions are often represented in CFT as insertions of particular local fields at the position of the impurity. Although this picture is a Euclidean one, and does not seem to be directly applicable to the calculation of quantities in the non-equilibrium steady state, it may be of use in evaluating overlaps between Hamiltonian eigenstates before and after the connection.

In the present context, there is a very natural interpretation of the impurity changing operator. Indeed, before the connection we have N independent chiral copies of a CFT model, while at the moment of the connection, these copies are connected to each other in a sequential way. Geometrically, this means that at the time of the connection there is a branch point. Hence, the impurity condition changing operator should be the branch-point twist field, a twist field associated with the $\mathbb{Z}_N$ symmetry of any model composed of N independent copies. An elegant derivation of its scaling dimension was found in [35] in the context of evaluating the entanglement entropy in CFT.

J. Stat. Mech. (2014) P03002

This can be confirmed by analyzing the shift of L_0-eigenvalues produced by the connection, which should be related to the dimension of the branch-point twist field. This shift is easily calculated as follows. Consider the total energy before and after the connection. Before the connection, there are N independent Virasoro algebras, $L_n^{(j)}$, $n \in \mathbb{Z}$, representing the single chiral fields running around each leg of the graph. In each leg j, a single chiral field is used, as is standard in boundary CFT, to represent both $h_j^{\rm in}(x)$ and $h_j^{\rm out}(x)$ and the reflecting boundary conditions at $x = 0$ and $x = R$. After the connection, there is a single Virasoro algebra $L_n, n \in \mathbb{Z}$, representing the single chiral field running around the whole graph, see the left part of figure 2. This single chiral field now represents all of the fields $h_j^{\rm in}(x)$ and $h_j^{\rm out}(x)$, for $j = 1, \ldots, N$, as well as the special connection at the vertex of the graph. Denoting $\tilde{L}_n = L_n - (c/24)\delta_{n,0}$ and $\tilde{L}_n^{(j)} = L_n^{(j)} - (c/24)\delta_{n,0}$, the energy before the connection is the sum of those of the N separate systems, each of length R:

$$\frac{2\pi}{R}\sum_{j=1}^{N}\tilde{L}_0^{(j)}.$$

After the connection, the energy is that of a single system, but of length NR,

$$\frac{2\pi}{NR}\tilde{L}_0.$$

Since the connection only changes the energy by an infinitesimal amount, these should be equal,

$$\frac{1}{N}L_0 + \frac{c}{24}\left(N - \frac{1}{N}\right) = \sum_{j=1}^{N} L_0^{(j)}. \tag{B.1}$$

Hence, the eigenvalues of $\sum_{j=1}^{N} L_0^{(j)}$, in the initial system, are shifted by $d := (c/24)\,(N - (1/N))$ as compared to the eigenvalues of $(1/N)L_0$ (the $1/N$ scaling simply represents the change of length). The number d is indeed the holomorphic dimension of the branch-point twist field [35].

Relation (B.1) is one of an infinity of relations amongst the Virasoro generators before and after the connection. These relations can be obtained as follows. Consider a local right-moving energy density $h_+(z)$, for $z \in [0, NR]$ running over the chiral paths of all legs of the graph. Before the connection, $h_+(z)$ is interpreted as representing the chiral fields in all separate legs, with each leg corresponding to an interval $z \in [jR, (j+1)R]$ of length R, and with periodicity given by identifying the points $z = j$ and $z = j + R$, for $j = 0, \ldots, N-1$. After the connection, the same field $h_+(z)$ is now interpreted as representing a single chiral field on the interval of length NR, with periodicity where the point 0 is identified with the point NR. The field $h_+(x)$ can then be written in two different ways:

$$\begin{aligned} h_+(z) &= \frac{2\pi}{R^2}\left(-\frac{c}{24} + \sum_{n\in\mathbb{Z}} L_n^{(j)} \mathrm{e}^{2\pi \mathrm{i} n z/R}\right)\Theta\,(jR \le z < (j+1)R) \\ &= \frac{2\pi}{R^2}\left(-\frac{c}{24} + \sum_{n\in\mathbb{Z}} L_n \mathrm{e}^{2\pi \mathrm{i} n z/(NR)}\right) \end{aligned}$$

where $\Theta(\cdots)$ is unity if the condition $\cdots$ is satisfied, and zero otherwise. The equality between these two expressions gives rise to an infinity of relations between L_n and $L_n^{(j)}$. In particular, one family of such relations is

$$\frac{1}{N}L_{Nk} + \frac{c}{24}\left(N - \frac{1}{N}\right)\delta_{k,0} = \sum_{j=1}^{N} L_k^{(j)}, \qquad k \in \mathbb{Z}$$

which generalizes (B.1). It is indeed a simple matter to check that both sides are generators that satisfy the Virasoro algebra commutation relations with central charge Nc.

References

[1] Zwanzig R, 2001 *Nonequilibrium Statistical Mechanics* (Oxford: Oxford University Press)
[2] Utsumi Y, Golubev D, Marthaler M, Saito K, Fujisawa T and Schön G, *Bidirectional single-electron counting and the fluctuation theorem*, 2010 *Phys. Rev.* B **81** 125331
[3] Nakamura S *et al*, *Nonequilibrium fluctuation relations in a quantum coherent conductor*, 2010 *Phys. Rev. Lett.* **104** 080602
[4] Nakamura S *et al*, *Fluctuation theorem and microreversibility in a quantum coherent conductor*, 2011 *Phys. Rev.* B **83** 155431
[5] Sánchez R and Büttiker M, *Detection of single-electron heat transfer statistics*, 2012 *Europhys. Lett.* **100** 47008
[6] Saira O-P, Yoon Y, Tanttu T, Möttönen M, Averin D and Pekola J, *Test of the Jarzynski and Crooks fluctuation relations in an electronic system*, 2012 *Phys. Rev. Lett.* **109** 180601
[7] Esposito M, Harbola U and Mukamel S, *Nonequilibrium fluctuations, fluctuation theorems, and counting statistics in quantum systems*, 2009 *Rev. Mod. Phys.* **81** 1665
[8] Bernard D and Doyon B, *Energy flow in non-equilibrium conformal field theory*, 2012 *J. Phys. A: Math. Theor.* **45** 362001
[9] Bernard D and Doyon B, *Non-equilibrium steady-states in conformal field theory*, 2013 *Ann. Henri Poincaré* doi:10.1007/s00023-014-0314-8
[10] Karrasch C, Ilan R and Moore J E, *Nonequilibrium thermal transport and its relation to linear response*, 2013 *Phys. Rev.* B **88** 195129
[11] Kuchment P, *Quantum graphs: an introduction and a brief survey*, 2008 *Comput. Struct.* **104–105** 13
[12] Nayak C, Fisher M, Ludwig A and Lin H-H, *Resonant multi-lead point-contact tunneling*, 1999 *Phys. Rev.* B **59** 15694
[13] Oshikawa M, Chamon C and Affleck I, *Junctions of three quantum wires*, 2006 *J. Stat. Mech.* P02008
[14] Hou C-Y, Kim E-A and Chamon C, *Corner junction as a probe of helical edge states*, 2009 *Phys. Rev. Lett.* **102** 076602
[15] Agarwal A, Das S, Rao S and Sen D, *Enhancement of tunneling density of states at a junction of three Luttinger liquid wires*, 2009 *Phys. Rev. Lett.* **103** 026401
[16] Safi I, Devillard P and Martin T, *Partition noise and statistics in the fractional quantum Hall effect*, 2001 *Phys. Rev. Lett.* **86** 4628
[17] Béri B and Cooper N R, *Topological Kondo effect with Majorana fermions*, 2012 *Phys. Rev. Lett.* **109** 156803
[18] Tsvelik A M, *Majorana fermion realization of a two-channel Kondo effect in a junction of three quantum Ising chains*, 2013 *Phys. Rev. Lett.* **110** 147202
[19] Crampé N and Trombettoni A, *Quantum spins on star graphs and the Kondo model*, 2013 *Nucl. Phys.* B **871** 526 [FS]
[20] Friedan D, *Entropy flow in near-critical quantum circuits*, 2005 arXiv:cond-mat/0505084
Friedan D, *Entropy flow through near-critical quantum junctions*, 2005 arXiv:cond-mat/0505085
[21] Das S, Rao S and Sen D, *Interedge interactions and fixed points at a junction of quantum Hall line junctions*, 2006 *Phys. Rev.* B **74** 045322
[22] Bellazzini B and Mintchev M, *Quantum fields on star graphs*, 2006 *J. Phys. A: Math. Gen.* **39** 11101
[23] Bellazzini B, Mintchev M and Sorba P, *Bosonization and scale invariance on quantum wires*, 2007 *J. Phys. A: Math. Theor.* **40** 2485

[24] Bellazzini B, Burrello M, Mintchev M and Sorba P, *Quantum field theory on star graphs*, 2008 *Analysis on Graphs and Its Applications (Proc. Symp. Pure Math.* vol 77) ed P Exner *et al* p 639 (arXiv:0801.2852)
[25] Ragoucy E, *Quantum field theory on quantum graphs and application to their conductance*, 2009 *J. Phys. A: Math. Theor.* **42** 295205
[26] Rahmani A, Hou C-Y, Feiguin A, Oshikawa M, Chamon C and Affleck I, *General method for calculating the universal conductance of strongly correlated junctions of multiple quantum wires*, 2012 *Phys. Rev.* B **85** 045120
[27] Mintchev M, *Non-equilibrium steady states of quantum systems on star graphs*, 2011 *J. Phys. A: Math. Theor.* **44** 415201
[28] Caudrelier V, Mintchev M and Ragoucy E, *Quantum wire network with magnetic flux*, 2013 *Phys. Lett.* A **377** 1788
[29] Mintchev M and Sorba P, *Luttinger liquid in non-equilibrium steady state*, 2013 *J. Phys. A: Math. Theor.* **46** 095006
[30] Caudrelier V and Ragoucy E, *Direct computation of scattering matrices for general quantum graphs*, 2009 *Nucl. Phys.* N **828** 515
[31] Cardy J, *Conformal invariance and surface critical behavior*, 1984 *Nucl. Phys.* B **240** 514 [FS12]
[32] Levitov L S and Lesovik G B, *Charge distribution in quantum shot noise*, 1993 *JETP Lett.* **58** 230
[33] Bernard D and Doyon B, *Full counting statistics in the resonant-level model*, 2012 *J. Math. Phys.* **53** 2302
[34] Di Francesco P, Mathieu P and Senechal S, 1997 *Conformal Field Theory* (Berlin: Springer)
[35] Calabrese P and Cardy J L, *Entanglement entropy and quantum field theory*, 2004 *J. Stat. Mech.* P06002

J. Stat. Mech. (2014) P03002

Journal of Statistical Mechanics: Theory and Experiment
An IOP and SISSA journal

Thermodynamic Bethe ansatz for non-equilibrium steady states: exact energy current and fluctuations in integrable QFT

Olalla Castro-Alvaredo[1], Yixiong Chen[2], Benjamin Doyon[2] and Marianne Hoogeveen[2]

[1] Department of Mathematics, City University London, Northampton Square EC1V 0HB, UK
[2] Department of Mathematics, King's College London, Strand WC2R 2LS, UK
E-mail: o.castro-alvaredo@city.ac.uk, yixiong.chen@kcl.ac.uk, benjamin.doyon@kcl.ac.uk and marianne.hoogeveen@kcl.ac.uk

Received 8 November 2013
Accepted for publication 25 January 2014
Published 20 March 2014

Online at stacks.iop.org/JSTAT/2014/P03011
doi:10.1088/1742-5468/2014/03/P03011

Abstract. We evaluate the exact energy current and scaled cumulant generating function (related to the large-deviation function) in non-equilibrium steady states with energy flow, in any integrable model of relativistic quantum field theory (IQFT) with diagonal scattering. Our derivations are based on various recent results of Bernard and Doyon. The steady states are built by connecting homogeneously two infinite halves of the system thermalized at different temperatures $T_{\rm l}$, $T_{\rm r}$, and waiting for a long time. We evaluate the current $J(T_{\rm l}, T_{\rm r})$ using the exact QFT density matrix describing these non-equilibrium steady states and using Zamolodchikov's method of the thermodynamic Bethe ansatz (TBA). The scaled cumulant generating function is obtained from the extended fluctuation relations which hold in integrable models. We verify our formula in particular by showing that the conformal field theory (CFT) result is obtained in the high-temperature limit. We analyze numerically our non-equilibrium steady-state TBA equations for three models: the sinh-Gordon model, the roaming trajectories model, and the sine-Gordon model at a particular reflectionless point. Based on the numerics, we conjecture that an infinite family of non-equilibrium

 1742-5468/14/P03011+57$33.00

J. Stat. Mech. (2014) P03011

c-functions, associated with the scaled cumulants, can be defined, which we interpret physically. We study the full scaled distribution function and find that it can be described by a set of independent Poisson processes. Finally, we show that the 'additivity' property of the current, which is known to hold in CFT and was proposed to hold more generally, does not hold in general IQFT—that is, $J(T_\mathrm{l}, T_\mathrm{r})$ is not of the form $f(T_\mathrm{l}) - f(T_\mathrm{r})$.

Keywords: integrable quantum field theory, thermodynamic Bethe ansatz, large deviations in non-equilibrium systems, quantum transport

ArXiv ePrint: 1310.4779

Contents

1. Introduction

In recent years, there has been a surge of interest in the study of the thermodynamics of quantum systems out of equilibrium (for reviews, see [1, 2]). In part this is due to the recent advances in experimental techniques, making it possible to drive quantum systems away from equilibrium in a controlled way, and to study their non-equilibrium properties, see for instance [3]–[8]. This is also due to theoretical advances which include the discovery of several types of fluctuation theorems, generalizing the fluctuation-dissipation theorem [9] to systems far from equilibrium (see [1, 2] for extensive discussions). These fluctuation theorems express 'universal' properties of certain distribution functions. In non-equilibrium steady states, where constant flows of particles, charge or energy exist, one object of interest is the scaled cumulant generating function (SCGF)[3]. The SCGF fully characterizes the statistics of the transferred quantity at large times. Fluctuation theorems are symmetry relations for the SCGF; see for instance [10]–[15] concerning the energy-flow SCGF.

In this manuscript we obtain for the first time the exact non-equilibrium current and SCGF for energy transfer in a wide family of integrable models. For this purpose, we propose, develop and test a new approach to the study of quantum integrable models in non-equilibrium steady states, concentrating on the study of non-equilibrium energy flows. We take the setup where two Hamiltonian reservoirs at different temperatures are connected homogeneously to each other (local quantum quench), so that at large times an energy current be established. We consider the scaling limit: the quantum system is assumed to be in the universal regime near a quantum critical point (with unit dynamical exponent), with a mass gap and the driving temperatures assumed to be much smaller than any microscopic energy scale. This regime is described by massive quantum field theory (QFT). Our results are the first exact results for the energy SCGF and most general results for the energy current in non-critical models that cannot be described by free particles.

Integrability occurs when enough additional symmetries render the model exactly solvable [16, 17]. Exact solvability means that in principle all energy eigenstates

[3] This is related to the large-deviation function, commonly used in large-deviation theory, by a Legendre transform.

and eigenvalues, and correlation functions of local operators, can be obtained non-perturbatively. Integrability has enjoyed much success over the past four decades. For integrable quantum spin chains, several very effective approaches exist, such as the algebraic Bethe ansatz (see e.g. [18]). For integrable massive quantum field theories (IQFTs) the problem of computing scattering amplitudes and vacuum correlation functions of local fields has been solved for many models using factorized scattering theory [19]–[24]. Factorized scattering and Bethe ansatz ideas led to a very successful approach for the study of the equilibrium thermodynamic properties of integrable models proposed by Zamolodchikov [25], known as the thermodynamic Bethe ansatz (TBA) approach. Other exact methods are based on free-fermion techniques (Clifford algebras), and the universal regime of exactly gapless quantum models is described by conformal field theory (CFT), for which a very wide variety of exact techniques are available [26, 27].

Using some of such techniques, exact results for the SCGF in non-equilibrium integrable quantum systems have been obtained in the past, especially for charge flows, in which case the SCGF is referred to as the 'full-counting statistics'. The first exact formula in free-fermion models was obtained by Lesovik and Levitov in [28, 29] and further studied in other works [30]–[33]. Other exact formulas were obtained in Luttinger liquids, which are particular models of CFT, in [34], and in the low-temperature universal regime of quantum critical models in [35] using general CFT. In certain integrable interacting impurity models, the SCGF was obtained in [36, 37] using TBA-like ideas. Exact charge current and shot noise (zero-temperature second cumulant) studies have also been done from similar ideas before in a variety of integrable models and with a variety of techniques, see for instance [38]–[50].

However, for energy flows, exact results for currents in interacting models and for SCGF in general are more recent. As far as we are aware, the first exact SCGF was obtained for a chain of quantum harmonic oscillators in [51]. Exact results for the energy current and SCGF in the low-temperature universal regime of general quantum critical models were obtained very recently in [52, 35] using CFT, and for the quantum Ising chain in a magnetic field in [53] using free-fermion techniques (results also exist for energy flows in more general 'star-graph' configurations, see for instance [54]–[56]).

There are in fact many ways of theoretically constructing a non-equilibrium steady state (see [57] for a discussion); the aforementioned results involve a variety of setups. The Hamiltonian-reservoir setup considered here is an old idea going back, in the quantum realm, to Keldysh [58] and Caroli *et al* [59], and studied in detail classically in [60]. For energy flows, it was rigorously analyzed in the XX and XY models in [61, 62], partly from general results in [63, 64], where the resulting non-equilibrium density matrix was constructed[4]. Similarly, non-equilibrium energy flows were studied in CFT in [52, 35, 56]. The energy-flow non-equilibrium density matrix of the Hamiltonian setup in general massive QFT was proposed and derived in [52, 68]. Further, other rigorous works considered non-equilibrium steady states and other non-equilibrium situations in free-fermion models such as the XX or XY model, see e.g. [69]–[71].

[4] The idea of a density matrix for representing a steady state has arisen many times in the past, both in physics and mathematics literature, see for instance [65, 63, 66, 67].

J. Stat. Mech. (2014) P03011

We present here a generalization of the TBA approach to non-equilibrium steady-states energy flows with Hamiltonian reservoirs: the NESSTBA approach. We base our derivation on the exact massive QFT density matrix derived in [68]. We deduce a set of coupled integral equations which are analogous to the standard TBA equations up to some crucial modifications. Solutions to these equations give the exact energy current. All the exact cumulants are then obtained from the extended fluctuation relation that was derived in [15]. We illustrate the working of our approach by numerically evaluating the current and some of the cumulants in three different models: the sinh-Gordon model, the roaming trajectories model, and the sine-Gordon model at the simplest nontrivial reflectionless point. Our work can be seen as a generalization of the CFT results of [52] to IQFTs. In particular, as a consistency check we show that our formulation indeed leads to the known CFT result for the current and SCGF when both right and left temperatures are very high as compared to the gap.

The analysis of our results bring out three interesting observations. First, we find a family of non-equilibrium analogues of Zamolodchikov's c-functions [25], in terms of the current and all higher cumulants. We numerically verify that our non-equilibrium c-functions are monotonic along RG trajectories, and equal to the central charge at fixed points. Hence, following the usual wisdom, they are (non-equilibrium) measures of the number of degrees of freedom as functions of the energy scale. Our c-functions in turn give rise to exact upper bounds on the current and all higher cumulants. Second, we show numerically that the process of energy transfer can be understood, in its large-time regime, as a family of independent Poisson processes, one for each energy value and direction of transfer. This generalizes nontrivially what was observed in CFT in [52]. It indicates that the generalization of the usual Landauer form of the conductance to the full out-of-equilibrium statistics is not straightforward: the weights of the Poisson processes are *not* simply related to the state density and occupation (contrary to the CFT case). Finally, it is known that in CFT the current is *additive* [52]: it satisfies $J(\beta_1, \beta_2) + J(\beta_2, \beta_3) + J(\beta_3, \beta_1) = 0$ (where β_i are inverse temperatures), equivalently $J(\beta_l, \beta_r) = f(\beta_l) - f(\beta_r)$ for some function f. This was suggested to hold more generally from various arguments [72, 68], most importantly including DMRG numerics [72]. We provide a proof that additivity does not hold in a large family of IQFT (including the three models we consider), a fact which is explained via the nontrivial relationship between state occupation and state density in interacting models. This result is not in disagreement with the DMRG numerics.

The paper is organized as follows: In section 2 we describe the physical situation and give the density matrix that describes the non-equilibrium steady state. We also give an overview of some existing results which we will use. In section 3 we derive the NESSTBA equations. In section 4 we introduce the integrable models that we will consider. In section 5 we present numerical results for the current and the L-functions of these models. In section 6 we introduce a family of c-functions that can be obtained by normalizing higher order cumulants, and present numerical evidence of their monotonicity. We discuss the physical implications of this property. In section 7 we provide evidence of the Poissonian nature of the energy transfer process. In section 8 we test the additivity property of the current and show that it is non-additive for three different integrable models. We provide a general argument as well as a mathematical proof as to why this must be the

doi:10.1088/1742-5468/2014/03/P03011

case for IQFTs. Finally, we present our conclusions in section 9. Various derivations, proofs, particular limits and consistency checks of our formulation are presented in appendices A–E.

2. Physical situation and overview of relevant previous results

2.1. Physical description

Consider a homogeneous open quantum chain of length L with local interactions. Suppose it is initially broken into two contiguous halves of lengths $L/2$ with commuting Hamiltonians $H_{\rm l}^L$ and $H_{\rm r}^L$ (for instance, some links are broken near some site, so that the two halves do not interact with each other). The two halves are independently thermalized at temperatures[5] $T_{\rm l} = \beta_{\rm l}^{-1}$ and $T_{\rm r} = \beta_{\rm r}^{-1}$ respectively (left and right), so that the system is described by the density matrix $\rho_0 = \mathrm{e}^{-\beta_{\rm l} H_{\rm l}^L - \beta_{\rm r} H_{\rm r}^L}$. At time 0 the two halves are connected in order to form the original homogeneous quantum chain of length L, with Hamiltonian $H^L = H_{\rm l}^L + H_{\rm r}^L + \delta H$. Here δH represents the connection energy between the two halves, which must be local, i.e. involving only a few sites around the connection point, and which we assume to be independent of L. The system is then allowed to H-evolve unitarily until time t. One can view this situation as starting with a profile of temperature on the full quantum chain that has a step change around one site, with $T_{\rm l}$ on its left and $T_{\rm r}$ on its right, and then evolving unitarily from this profile—this point of view requires the notion of a local temperature, which we do not discuss here.

Averages of observables $\mathcal{O}$ at time t are described by

$$\langle \mathcal{O} \rangle(L;t) = \mathrm{Tr}\left(\mathrm{e}^{-\mathrm{i}tH^L}\, \mathfrak{n}[\rho_0]\, \mathrm{e}^{\mathrm{i}tH^L}\, \mathcal{O} \right), \qquad \rho_0 = \mathrm{e}^{-\beta_{\rm l} H_{\rm l}^L - \beta_{\rm r} H_{\rm r}^L} \tag{1}$$

where here and below we use $\mathfrak{n}[\rho] = \rho/\mathrm{Tr}(\rho)$. The *steady-state limit* is the limit $L \to \infty$ followed by $t \to \infty$ of such an average, with the observation length ℓ kept fixed, see figure 1 (below we will denote by H, $H_{\rm l}$ and $H_{\rm r}$ the $L \to \infty$ limits, when it makes sense, of the operators H^L, $H_{\rm l}^L$ and $H_{\rm r}^L$ respectively). The observation length is the length of the region over which lie the support of $\mathcal{O}$ and the contact point $x = 0$.

If this limit exists, then we say that the system reaches a steady state with respect to the observable $\mathcal{O}$:

$$\langle \mathcal{O} \rangle_{\rm stat} := \lim_{t\to\infty} \lim_{L\to\infty} \langle \mathcal{O} \rangle(L;t). \tag{2}$$

For local observables, we expect the steady-state limit to exist thanks to the locality of the Hamiltonians. Physically, this is because we expect the two infinite ($L \to \infty$) halves of the system to play the role, at large enough times, of far thermal reservoirs, able to absorb and emit independent thermalized excitations unboundedly for all times $t \ll L/v$, where v is a propagation velocity. Indeed for such times, excitations do not have time to bounce off the far endpoints and thus create non-thermal correlations or be re-emitted.

[5] In this paper we set $k_{\rm B} = 1$ and $\hbar = 1$.

J. Stat. Mech. (2014) P03011

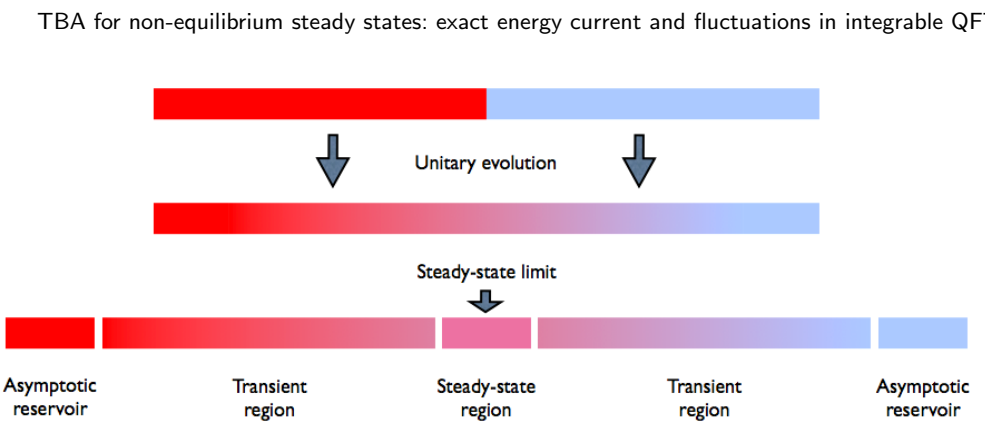

Figure 1. The steady state is established by connecting two halves of the system that have been independently thermalized, and letting them evolve unitarily for a time t. After a long time and in a very large system, there will be asymptotically far hot and cold reservoirs which have not yet received any excitation from the connection point, two transient regions, and the steady-state region (the region described by the steady-state limit). In integrable massive QFT, excitations scatter elastically, and different points in the transient regions will receive excitations at different times depending on the excitation's velocity. Hence the transient regions should be of lengths scaling proportionally to t. There is no prediction for the length of the steady-state region, which may be observable-dependent and which may scale slower than Ct for every $C > 0$. The only requirement is that every point a finite distance away from the connection point will converge to the steady state.

Then, observing only locally, the detailed reservoir information is lost and we only see the steady state. In particular, the energy current observable

$$\mathcal{J} := \frac{\mathrm{i}}{2}[H^L, H^L_{\mathrm{r}} - H^L_{\mathrm{l}}] = \frac{\mathrm{i}}{2}[\delta H, H^L_{\mathrm{r}} - H^L_{\mathrm{l}}] \tag{3}$$

is local (and independent of L) thanks to the locality of δH, hence the system should reach a steady state with respect to the energy current.

The first detailed study of this steady-state limit appeared for classical harmonic oscillators in [60]. In quantum systems, similar steady-state limits were discussed and shown to exist in quantum models under certain conditions in [63] and, more particularly, in the XY model in [61, 62]; in the context of charge transfer in the Kondo model in [67] and in the resonant-level model in [73, 33]; and in the context of energy and charge transfer in conformal models in [52, 35].

As was discussed in many works, the effect of the connection will propagate from the center outwards as time evolves, so that the effective reservoirs, i.e. the regions which are still thermal, will be situated further and further away from the connection point; specifically, the temperature profile will become flat. This holds true in general local models, not just in CFT (although there are differences in the details). Hence, if energy transport is purely diffusive, then the steady-state current should be zero (by Fourier's law). However, if the initial temperatures are different and the energy propagation in the system has a ballistic component, then we expect that the steady-state limit will support an energy flow, $\langle \mathcal{J} \rangle_{\mathrm{stat}} \neq 0$: it is then a nontrivial non-equilibrium steady state.

doi:10.1088/1742-5468/2014/03/P03011

It is expected that any integrable system will display a ballistic component to the energy transport: the conserved charges give enough constraints to counteract diffusion [74]–[76]. In particular, the conserved charge associated with the energy current is usually one of the first nontrivial 'higher' conserved charges in integrable quantum spin chains.

Remark 2.1. In CFT and QFT, the momentum is always conserved; hence, as explicitly shown in [52, 35] in CFT, the steady-state limit exists and supports a nonzero energy flow. This means that in the scaling limit (low-temperature, small-gap universal regime) of any quantum chain (with unit dynamical exponent), integrable or not, the steady-state limit should exist (we refer to [35, 68] for a discussion of the interplay between the steady-state limit and the scaling limit). This was indeed observed using DMRG numerics for a particular non-integrable quantum chain in [72]. Of course, in any quantum chain, the nonzero temperatures and, possibly, nonzero gap mean that the system is never exactly in the scaling limit. Hence, if the microscopic system is not integrable, there may be some large, non-universal time scale where non-integrability 'kicks-off' and the current starts to decrease. An interesting open question is the nature of this time scale, or by what other mechanism microscopic non-integrability may appear. In the present paper we discuss integrable QFT, which may be thought of as coming from integrable microscopic systems, hence there is true ballistic transport.

Remark 2.2. We may attempt to make the steady-state limit a bit more precise as follows. We require that the limit exists when each of the conditions $L \gg vt$ and $vt \gg \ell$ hold almost surely for all v, where v are propagation velocities of excitations, and ℓ is the observation length scale. Here we have in mind a distribution of propagation velocities associated with the available excited states, and the corresponding measure (discrete / continuous parts of the Hilbert space, etc); the phrase 'almost surely' means that the strong inequalities hold for all velocities except possibly for a set of velocities that is of measure zero. Then, the fact that the steady-state limit exists for any local observable can only be true if there is no stationary excitation with nonzero measure: the Hilbert space should not have a discrete part containing zero-velocity excitations.

2.2. Steady state in massive QFT

Assume now that the quantum chain has a parameter g (for instance, an external magnetic field) such that there is a quantum critical point at $g = g_c$ with unit dynamical exponent. Then, at $g = g_c$, the energy gap Δ is zero. At $g = g_c$ and low temperatures, the chain is described by a CFT. Let us now take the scaling limit where $g \to g_c$ and $T_{l,r} \propto \Delta$ (which tends to zero). This is the low-temperature, small-gap region near the quantum critical point. This limit is universal, and described by massive QFT, with the mass representing the infinitesimal gap Δ. The main result of [52, 68], which we take as our starting point, is a proposed exact description of the non-equilibrium density matrix ρ_{stat} in the scaling limit, that represents the steady-state limit (2),

$$\langle \mathcal{O} \rangle_{\text{stat}} = \text{Tr}\left(\mathfrak{n}[\rho_{\text{stat}}]\, \mathcal{O}\right). \tag{4}$$

It is expressed in terms of massive QFT data, and was derived using general QFT arguments.

The non-equilibrium steady-state density matrix $\rho_{\rm stat}$ is defined as follows. Let us consider a model of relativistic QFT with a spectrum of ℓ particle types, with masses $m_1, \dots, m_\ell$. The basis of asymptotic states (here we take them implicitly as asymptotic *in* states), which span the Hilbert space, is described by

$$|\mathrm{vac}\rangle, \qquad |\theta_1, \dots, \theta_n\rangle_{i_1,\dots,i_n} \ : \ \theta_1 > \cdots > \theta_n, \quad i_1, \dots, i_n \in \{1, 2, \dots, \ell\}, \quad n = 1, 2, \dots \tag{5}$$

where $|\mathrm{vac}\rangle$ is the vacuum, and θ_j are the rapidities of the asymptotic particles. The density matrix $\rho_{\rm stat}$ acts diagonally on the basis of asymptotic states. Its eigenvalues are simply given by $\rho_{\rm stat}|\mathrm{vac}\rangle = 1$ and

$$\rho_{\rm stat}|\theta_1, \dots, \theta_n\rangle_{i_1,\dots,i_n} = \mathrm{e}^{-\sum_k W_{i_k}(\theta_k)}|\theta_1, \dots, \theta_n\rangle_{i_1,\dots,i_n} \tag{6}$$

where

$$W_i(\theta) := m_i \cosh\theta \cdot \begin{cases} \beta_{\rm l} & (\theta > 0) \\ \beta_{\rm r} & (\theta < 0). \end{cases} \tag{7}$$

If we factorize the Hilbert space into a product of the space formed by positive-rapidity particles, and that formed by negative-rapidity particles, then (6) indicates that the steady-state density matrix factorizes accordingly. Specifically, on each factor, it is thermal with inverse temperature $\beta_{\rm l,r}$, respectively. Note that this density matrix is stationary and homogeneous (translation invariant).

The density matrix (6) agrees with the mathematical description of the energy-flow steady state in the XY model in [61, 62] and with that obtained in the Ising model from less rigorous arguments in [53]. Its natural counterpart in CFT, where right-movers and left-movers are thermalized at different temperatures, was proved in [52, 35].

Remark 2.3. The physical interpretation of the density matrix $\rho_{\rm stat}$ is rather simple. The steady-state density matrix is the long-time evolution $\rho_{\rm stat} = \lim_{t\to\infty} \mathrm{e}^{-\mathrm{i}Ht}\rho_0\mathrm{e}^{\mathrm{i}Ht}$ of the initial density matrix ρ_0. The initial density matrix represents the left- and right-hand sides of the system separately thermalized at inverse temperatures $\beta_{\rm l}$ and $\beta_{\rm r}$, respectively, and the time evolution is generated by the full Hamiltonian H where both halves are connected. In the scattering language, $\rho_{\rm stat} = \lim_{t\to\infty} \mathrm{e}^{-\mathrm{i}Ht}\mathrm{e}^{\mathrm{i}H_0t}\rho_0\mathrm{e}^{-\mathrm{i}H_0t}\mathrm{e}^{\mathrm{i}Ht} = S\rho_0S^{-1}$, where $S = \lim_{t\to\infty} \mathrm{e}^{-\mathrm{i}Ht}\mathrm{e}^{\mathrm{i}H_0t}$ is the scattering operator. Also, asymptotic states are, by definition, states on the line with the property that when evolved back in time, they become well-separated, well-defined wave packets behaving like free particles (the incoming asymptotic particles). In the scattering language, an asymptotic state has the form $|v\rangle = S|v\rangle_0$, where $|v\rangle_0$ is a free-particle state representing the asymptotically free particles. Hence, the action of $\rho_{\rm stat}$ on asymptotic states is isomorphic to the action of ρ_0 on the well-separated, well-defined wave packets: if $|v\rangle_0$ is an eigenvector of ρ_0, then $|v\rangle$ is an eigenvector of $\rho_{\rm stat}$ with the same eigenvalue. Since for positive rapidities these wave packets are far on the left, and for negative rapidities they are far on the right, the expression (7) follows. A more complete argument is presented in [68]. More precisely, this argument shows that for any local operator, the contributions of asymptotic states with finite numbers of particles to the steady-state average is given by (6) and (7).

doi:10.1088/1742-5468/2014/03/P03011

J. Stat. Mech. (2014) P03011

2.3. Current and fluctuations

In QFT, the energy current operator is simply the momentum density $\mathcal{J} = p(x)$ at the position $x = 0$, so that the average current is

$$J = \langle p(0) \rangle_{\text{stat}}.$$

Besides the current, its fluctuations are also of great interest in non-equilibrium steady states. In quantum mechanics, one has to define fluctuations of the current via appropriate measurement protocols: see for instance [28, 29] for discussions of an indirect measurement protocol, [30, 14, 77, 33, 52] for results within a two-time measurement protocol and connection with the former protocol, and the review [1]. In order to be specific, let us consider the two-time measurement protocol. We perform a first von Neumann measurement of the quantity

$$Q := \tfrac{1}{2}(H_{\text{r}} - H_{\text{l}}) \tag{8}$$

at time 0, returning the value q_0, and then another von Neumann measurement at time t, returning the value q_t. We are interested in the statistics of the difference $q := q_t - q_0$. By standard quantum mechanics, the probability distribution for q is

$$\Omega_t(q) = \text{Tr}\left(P_{Q=q_t} \mathrm{e}^{-\mathrm{i}Ht} P_{Q=q_0} \mathfrak{n}[\rho_0] P_{Q=q_0} \mathrm{e}^{\mathrm{i}Ht} P_{Q=q_t}\right) \tag{9}$$

where $P_{Q=a}$ is the projector onto the eigenspace of eigenvalue a of the operator Q. One may then evaluate the associated scaled cumulants

$$C_n := \lim_{t\to\infty} t^{-1} \langle q^n \rangle_{\Omega_t}^{\text{cumulant}}, \tag{10}$$

where $\langle q^n \rangle_{\Omega_t}^{\text{cumulant}}$ is the nth cumulant of q with respect to Ω_t. These may be gathered into a generating function as usual,

$$F(z) := \sum_{n=1}^{\infty} C_n z^n / n!, \qquad F(z) = \lim_{t\to\infty} t^{-1} \log\left(\langle \mathrm{e}^{qz} \rangle_{\Omega_t}\right) \tag{11}$$

(here z is a formal parameter). Note that the first cumulant $C_1 = J$ is the average current.

A result of the discussions cited above is that one expects $F(z)$ to have the following expression in terms of averages of quantum-mechanical operators:

$$F(z) = \lim_{t\to\infty} t^{-1} \log\left(\langle \mathrm{e}^{zQ(t)} \mathrm{e}^{-zQ} \rangle_{\text{stat}}\right). \tag{12}$$

In fact, we expect that in general, the scaled cumulants can also be expressed in terms of connected correlation functions[6] of time-evolved current operators,

$$C_n = \lim_{\epsilon\to 0^+} \int_{-\infty}^{\infty} \mathrm{d}u_1 \cdots \mathrm{d}u_{n-1} \, \langle \mathcal{J}(u_{n-1} + (n-1)\mathrm{i}\epsilon) \cdots \mathcal{J}(u_1 + \mathrm{i}\epsilon) \mathcal{J}(0) \rangle_{\text{stat}}^{\text{connected}} \tag{13}$$

where $\mathrm{i}\epsilon$ is an imaginary time shift that regularizes the correlators. This expression is derived, under certain assumptions that hold for integrable models, in appendix A.

[6] The term 'connected' has the same combinatoric meaning as 'cumulant', but is more common in the context of quantum field theory.

Note that an important symmetry relation satisfied by $F(z)$ is the fluctuation relation

$$F(\beta_\mathrm{l} - \beta_\mathrm{r} - z) = F(z). \tag{14}$$

This energy-flow–fluctuation relation was derived in various situations in [10]–[14] (but see [78] for limitations in the case of finite systems); [1, 2] present good reviews. It was derived recently in [15] within the present physical setup using a scattering formalism.

A recent result of Bernard and Doyon [15] is that in any system where the energy is purely transmitted (that is, $QS = -SQ$, where S is the system's scattering operator, see [15]), the scaled cumulant generating function $F(z)$ can be evaluated solely from the current at shifted inverse temperatures[7],

$$\frac{\mathrm{d}F(z)}{\mathrm{d}z} = J(\beta_\mathrm{l} - z, \beta_\mathrm{r} + z) \quad \Leftrightarrow \quad F(z) = \int_0^z \mathrm{d}z'\, J(\beta_\mathrm{l} - z', \beta_\mathrm{r} + z') \tag{15}$$

(recall that $F(0) = 0$). The upshot is that the scaled cumulants are simply given by derivatives of the current with respect to inverse temperatures,

$$C_{n+1} = \frac{\mathrm{d}^n}{\mathrm{d}z^n} J(\beta_\mathrm{l} - z, \beta_\mathrm{r} + z)\Big|_{z=0} \tag{16}$$

for $n = 0, 1, 2, \ldots$. Equation (15) was referred to as an *extended fluctuation relation* (EFR) in [15], as it actually implies the usual non-equilibrium fluctuation relations equation (14) if one assumes parity symmetry. As explained in [15], pure energy transmission, and therefore the EFR, is valid in any homogeneous integrable model and in CFT. Note that it implies a relationship between the non-equilibrium differential conductivity $G := \beta^2 \mathrm{d}J/\mathrm{d}\gamma$ (where $\beta = (\beta_\mathrm{r} + \beta_\mathrm{l})/2$ and $\gamma = \beta_\mathrm{r} - \beta_\mathrm{l}$) and the noise (second cumulant), which reads $\beta^2 C_2 = 2G$.

2.4. Previous exact results

Exact results for energy flow and fluctuations in the present physical setup are available in the XY and Ising models [61, 62, 53, 79], and in conformal field theory (critical models) [52, 35, 56]. To our knowledge, the first exact cumulant generating function for energy transfer in quantum systems was found in [51], within a slightly different physical construction of the non-equilibrium steady state using Caldeira–Leggett baths attached to a chain of harmonic oscillators. Here we just recall the CFT results, as these are most relevant for our purposes.

In general unitary CFT, the current was first calculated in [52] and found to be

$$J_\mathrm{CFT} = \frac{c\pi}{12}(T_\mathrm{l}^2 - T_\mathrm{r}^2). \tag{17}$$

This has a clear interpretation via the Stefan–Boltzmann law thanks to [80]. The scaled cumulant generating function $F_\mathrm{CFT}(z)$ was first evaluated exactly in [52], giving the

[7] Here the current describes the energy transfer from the left to the right, in contrast to the convention used in [15].

expression $F_{\rm CFT}(z) = (c\pi z/12)(\beta_{\rm l}^{-1}(\beta_{\rm l} - z)^{-1} - \beta_{\rm r}^{-1}(\beta_{\rm r} + z)^{-1})$, in agreement with (15). This means that the scaled cumulants are

$$C_{n\,\rm CFT} = \frac{c\pi n!}{12}(T_{\rm l}^{n+1} + (-1)^n T_{\rm r}^{n+1}). \tag{18}$$

The function $F_{\rm CFT}(z)$ was evaluated in [52] assuming the fluctuation relations (14); it was proved without this assumption in the CFT context using a local operator formalism in [35], and using the Virasoro algebra in [56] (where a more general star-graph configuration is considered). The expression (17) was verified numerically in the XXZ chain by Karrasch *et al* [72].

3. The non-equilibrium steady-state TBA equations

In the present paper, we obtain for the first time the exact energy current and scaled cumulant generating function in interacting (integrable) models.

In integrable models of relativistic QFTs, two crucial properties hold: the scattering of asymptotic particles is purely elastic (the set of momenta is preserved) and the scattering amplitudes always factorize into two-particle scattering processes. Hence, the only dynamical data necessary in order to fully define the model and its 'local structure' (its full scattering and its set of local observables) are the two-particle scattering amplitudes. In particular, two-particle scattering amplitudes are solutions of the Yang–Baxter equation, which is nontrivial whenever there are internal degrees of freedom and the two-particle scattering processes is not diagonal in the internal space. This is the essence of factorized scattering theory.

We now consider a general integrable model of relativistic QFT, under the simplifying assumption that the two-particle scattering matrix is diagonal in the internal space (there is no 'back-scattering': in a two-particle scattering process, only phases may occur).

3.1. The integral equations

According to (4), the average energy current J is obtained by evaluating the average momentum density $p(x)$ at an arbitrary point, say $x = 0$, using the density matrix (6):

$$J = \mathrm{Tr}\left(\mathfrak{n}[\rho_{\rm stat}]\, p(0)\right). \tag{19}$$

We have provided the exact density matrix (6) as an operator acting on asymptotic states with finitely many particles. In order to evaluate this trace, we further need the matrix elements of $p(0)$. But we need a bit more: we need to describe how to perform the trace operation. This implies understanding $\rho_{\rm stat}$ in states with nonzero densities of particles (i.e. infinitely many particles). In such finite-density states, the interaction between particles becomes important, and this affects the way the trace is defined. One could say that the information about the 'local structure' is encoded both into the matrix elements of $p(0)$ and into the way the trace is performed.

In order to add these two elements of information, we follow Zamolodchikov's TBA argument [25]. This is an argument that mixes the ideas of factorized scattering and of

the Bethe ansatz. For this purpose, we consider the model on a finite periodic space of circumference R. On the finite space, according to [25], the description of integrable models of QFT can be done similarly to that of Bethe ansatz integrable systems. Each state is characterized by its contents in quasi-particles, which possess momenta p_k and energies e_k whose sums give the total momentum and energy of the state, with a relativistic dispersion relation. Then, we construct a density matrix $\rho^R_{\rm stat}$ that approximates $\rho_{\rm stat}$. The natural choice for $\rho^R_{\rm stat}$ is defined by its action on every state $|v\rangle$ as follows:

$$\rho^R_{\rm stat}|v\rangle = \mathrm{e}^{-\sum_k W_k}|v\rangle, \qquad W_k = e_k \cdot \begin{cases} \beta_{\rm l} & (p_k > 0) \\ \beta_{\rm r} & (p_k < 0). \end{cases} \tag{20}$$

The finite-R approximation of the average current is the average of the local momentum density $p(0)$ with respect to $\rho^R_{\rm stat}$:

$$J_R = \frac{\mathrm{Tr}_R\left[\rho^R_{\rm stat} p(0)\right]}{\mathrm{Tr}_R[\rho^R_{\rm stat}]}, \qquad \lim_{R\to\infty} J_R = J. \tag{21}$$

Note that $\rho^R_{\rm stat}$ is translation invariant. By translation invariance, we may replace $p(0)$ by $R^{-1}\int_{-R/2}^{R/2}\mathrm{d}x\, p(x)$. We then have

$$J_R = R^{-1}\frac{\mathrm{Tr}_R\left[\rho^R_{\rm stat} P_R\right]}{\mathrm{Tr}_R[\rho^R_{\rm stat}]} \tag{22}$$

where $P_R := \int_{-R/2}^{R/2}\mathrm{d}x\, p(x)$ is the total momentum.

The current can then be calculated by conveniently introducing a generating parameter a associated with the momentum:

$$J = -\lim_{R\to\infty} R^{-1}\ \frac{\mathrm{d}}{\mathrm{d}a}\log \mathrm{Tr}_R\left(\rho^R_{\rm stat}\,\mathrm{e}^{-aP_R}\right)\Big|_{a=0}. \tag{23}$$

We may also define the 'free energy' f^a and write the current from it:

$$f^a := -\lim_{R\to\infty} R^{-1}\log \mathrm{Tr}_R\left(\rho^R_{\rm stat}\,\mathrm{e}^{-aP_R}\right), \qquad J = \frac{\mathrm{d}}{\mathrm{d}a} f^a\Big|_{a=0}. \tag{24}$$

The free energy f^a can be evaluated by extending the TBA arguments of Zamolodchikov presented in [25] (a similar extension of TBA arguments beyond Gibb's equilibrium was first done, to our knowledge, in the context of quantum quenches for the Lieb–Liniger model in [81]). This allows us to obtain the following expressions (see appendix B):

$$\begin{aligned} J(\beta_{\rm l},\beta_{\rm r}) &= \sum_{i=1}^{\ell}\int_{-\infty}^{\infty}\frac{\mathrm{d}\theta}{2\pi}\,\frac{m_i\cosh\theta\; x_i(\theta)}{1+\mathrm{e}^{\epsilon_i(\theta)}} \\ x_i(\theta) &= m_i\sinh\theta + \sum_{j=1}^{\ell}\int_{-\infty}^{\infty}\frac{\mathrm{d}\gamma}{2\pi}\,\frac{\varphi_{ij}(\theta-\gamma)\,x_j(\gamma)}{1+\mathrm{e}^{\epsilon_j(\gamma)}} \\ \epsilon_i(\theta) &= W_i(\theta) - \sum_{j=1}^{\ell}\int_{-\infty}^{\infty}\frac{\mathrm{d}\gamma}{2\pi}\;\varphi_{ij}(\theta-\gamma)\;\log(1+\mathrm{e}^{-\epsilon_j(\gamma)}) \end{aligned} \tag{25}$$

doi:10.1088/1742-5468/2014/03/P03011

J. Stat. Mech. (2014) P03011

where as usual $\varphi_{ij}(\theta) = -\mathrm{i}\partial_\theta S_{ij}(\theta)$ and $S_{ij}(\theta)$ is the two-particle scattering matrix, and where $W_i(\theta)$ is defined in (7). This is the exact non-equilibrium steady-state TBA (NESSTBA) expression for the energy current in general diagonal-scattering integrable relativistic QFT. It turns out that there are many equivalent expressions for the current. For instance (see appendix B),

$$\begin{aligned} J(\beta_{\mathrm{l}},\beta_{\mathrm{r}}) &= \sum_{i=1}^{\ell}\int_{-\infty}^{\infty}\frac{\mathrm{d}\theta}{2\pi}\,\frac{m_i\sinh\theta\;\mu_i(\theta)}{1+\mathrm{e}^{\epsilon_i(\theta)}} \\ \mu_i(\theta) &= m_i\cosh\theta + \sum_{j=1}^{\ell}\int_{-\infty}^{\infty}\mathrm{d}\gamma\,\frac{\varphi_{ij}(\theta-\gamma)\,\mu_j(\gamma)}{1+\mathrm{e}^{\epsilon_j(\gamma)}}. \end{aligned} \tag{26}$$

Note that it is customary to define the L-functions

$$L_i(\theta) = \log(1+\mathrm{e}^{-\epsilon_i(\theta)}), \tag{27}$$

as these functions possess interesting and perhaps clearer features than the pseudo-energies $\epsilon_i(\theta)$. Note also that the pseudo-energies, hence the L-functions, have jumps at $\theta = 0$, contrary to the equilibrium case

$$\epsilon_i(+\mathbf{0}) - \epsilon_i(-\mathbf{0}) = m(\beta_{\mathrm{l}} - \beta_{\mathrm{r}}). \tag{28}$$

We present various verifications of (25) in appendices C and D. We verify that the low-temperature expansion of (25) agrees with an explicit evaluation of the trace (22) in the large-L limit, using the finite-volume regularization methods of Pozsgay and Takács [82] (and assuming a single particle spectrum for simplicity). Using and generalizing the analysis performed by Zamolodchikov in [25], we also verify that the high-temperature expansion of (25) exactly reproduces the CFT prediction equation (17) of [52, 35], with the correct central charge.

As mentioned, in [15] it was shown that for integrable models of relativistic QFT, the energy-flow steady state satisfies the extended fluctuation relation (15). This relation immediately allows us to calculate the exact scaled cumulant generating function for such models using the NESSTBA expression above. That is, the generating function $F(z)$ defined in (11) for the scaled cumulants C_n defined in (10) to (13), is

$$\begin{aligned} F(z) &= \sum_{i=1}^{\ell}\int_{-\infty}^{\infty}\frac{\mathrm{d}\theta}{2\pi}\,m_i\cosh\theta\int_0^z\mathrm{d}z'\,\frac{x_i(\theta,z')}{1+\mathrm{e}^{\epsilon_i(\theta,z')}} \\ x_i(\theta,z) &= m_i\sinh\theta + \sum_{j=1}^{\ell}\int_{-\infty}^{\infty}\frac{\mathrm{d}\gamma}{2\pi}\,\frac{\varphi_{ij}(\theta-\gamma)\,x_j(\gamma,z)}{1+\mathrm{e}^{\epsilon_j(\gamma,z)}} \\ \epsilon_i(\theta,z) &= W_i(\theta) + z\,\mathrm{sgn}(\theta)\,m_i\cosh\theta - \sum_{j=1}^{\ell}\int_{-\infty}^{\infty}\frac{\mathrm{d}\gamma}{2\pi}\;\varphi_{ij}(\theta-\gamma)\;\log(1+\mathrm{e}^{-\epsilon_j(\gamma,z)}). \end{aligned} \tag{29}$$

Remark 3.1. Our verification that the low-temperature expansion of the trace itself agrees with the low-temperature expansion of (25) indicates that Zamolodchikov's TBA arguments indeed can be extended to the non-equilibrium steady-state density matrix (6) without additional subtleties. This is important, because the derivation presented in [68] of the form (6) of the density matrix is, to be correct, only applicable to states with finite numbers of particles, hence to the low-temperature expansion of the trace.

Remark 3.2. It is important to note that the ratio of traces on the right-hand side of (22) is not expected to be related in any way to the average total momentum in the physical non-equilibrium steady state. Indeed, the latter average does not exist because the total momentum is not a local operator (hence does not have a steady-state limit). Expression (22) is just a means to obtain a finite-R approximation of the actual steady-state current.

Remark 3.3. There are many subtleties involved in the derivation of (25) that we presented. Let us discuss some of them.

First, at equilibrium, the procedure for replacing the infinite-space density matrix by a finite-R approximation is clear, since even on finite periodic space, there is a clear notion of thermal states. Out of equilibrium, the procedure is less clear: the physical setup we use to construct the non-equilibrium steady state fundamentally requires the infinite-length limit to be taken. So, we must rely on a 'non-physical' density matrix $\rho^R_{\rm stat}$, with the requirement that its infinite-R limit reproduces $\rho_{\rm stat}$ in some 'topology' (for instance, for every individual matrix element). This is what we have done in (20) for integrable models using Zamolodchikov's ideas. Of course, the finite-R 'non-physical' density matrix (20) still describes some non-equilibrium steady state in the periodic system: it is a state where there is an imbalance between the populations of particles moving towards the right and of those moving towards the left. Importantly, however, it is a state whose infinite-R limit provides the correct population imbalance of asymptotic states for describing the physical non-equilibrium steady state.

Second, the validity of the statement $\lim_{R\to\infty} J_R = J$ in (21) relies on the fact that thanks to locality, in the infinite-R limit, the average of the local operator $p(0)$ does not depend on the actual boundary conditions taken (in particular, there are no topological effects that connect the energy density to boundary conditions). An argument can be made as follows. One can consider a different finite-R regularization, which by construction correctly gives the physical steady sate. One evolves the initial density matrix ρ_0 for a finite time t, and observes the system on a region of length $R = vt$ around the contact point, for $v = \tanh\theta_0$ the speed associated with some small rapidity $\theta_0 > 0$. The reduced density matrix $\tilde\rho^{R,\theta_0}$ on that region is an IR regularization, and its limit $R \to \infty$ gives by construction the correct steady state with respect to any local observable. But the point is that $\tilde\rho^{R,\theta_0}$ and $\rho^R_{\rm stat}$ differ from each other only because of two effects: the boundaries are different (in the former, it is the transient region; in the latter, it is a periodic boundary condition), and the presence of excitations at rapidities $|\theta| < \theta_0$. Therefore, by locality and assuming no topological effects, averages of operators supported in the bulk are equal with respect to both density matrices in the infinite-R limit, except possibly for differences of order $O(\theta_0)$. Since θ_0 can be made arbitrarily small for local operators a finite distance away from the contact point (because the boundary at distance vt is very far at large t for any $v > 0$), then the averages with respect with $\rho^R_{\rm stat}$ give the averages in the physical non-equilibrium steady state.

3.2. Physical interpretation

Formula (25) has a simple interpretation: the function $x_i(\theta)$ is the 'dressed' momentum at rapidity θ, the factor $L\,\mathrm{d}\theta\, m_i \cosh\theta/(2\pi) = Lm_i\,\mathrm{d}\sinh\theta/(2\pi)$ is the 'bare' (uninteracting)

number of levels around θ, and $1/(1+\mathrm{e}^{\epsilon_i(\theta)})$ is the filling fraction. Formula (26) has a similar and perhaps clearer interpretation: the quantity $L\,\mathrm{d}\theta\,\mu_i(\theta)/(2\pi)$ is the true, interacting number of levels around θ, and the factor $m_i \sinh(\theta)$ is the momentum at θ. Formula (25) encodes the steady-state density matrix into the driving term of the pseudo-energy, and the locality information of the QFT, including the state density and the momentum matrix elements, into the dressing operations based on the differential scattering phases $\varphi_{ij}(\theta)$.

The specialization of (25) to the Ising model, where there is only one particle type and the differential scattering phase is zero, gives a simple formula for the exact energy current,

$$J_{\mathrm{Ising}}(\beta_{\mathrm{l}},\beta_{\mathrm{r}}) = \frac{m^2}{4\pi}\int_{-\infty}^{\infty}\mathrm{d}\theta\,\frac{\sinh 2\theta}{1+\mathrm{e}^{W(\theta)}} = \frac{1}{2\pi}\int_{m}^{\infty}\mathrm{d}E\,E\left(\frac{1}{1+\mathrm{e}^{\beta_{\mathrm{l}}E}}-\frac{1}{1+\mathrm{e}^{\beta_{\mathrm{r}}E}}\right). \tag{30}$$

This can also be obtained in various other ways, and can be extracted for instance from the exact results in the XY and Ising chains in [61, 62, 53].

The second form of J_{Ising} in (30) has the structure of the Landauer formula: with $\mathrm{d}E\,E = \mathrm{d}p\,p$, where E is the energy and p is the momentum, we see that we have the number of available channels $\mathrm{d}p$, times the current through these channels p, weighted by the fermionic filling fractions for particles from the right (with temperature T_{l}) and from the left (with temperature T_{r}). Such a form was also observed in CFT in [52]: there the filling fraction at energy E can be taken as being proportional to the Boltzmann occupation $\mathrm{e}^{-\beta E}$. There is however no immediate Landauer form for the non-equilibrium energy current in the general interacting case, because there is no separation between the state densities and filling fractions of right-movers and left-movers: the presence of particles at some energy affect the state density at other energies.

In fact, the correct interpretation of both the Ising and the interacting energy flow should be obtained following what was done in the CFT context in [52]: one must analyze not only the current, but also the fluctuations, and one must look for a formulation where these appear via independent stochastic processes. It turns out that in CFT, the Boltzmann occupation $\mathrm{e}^{-\beta E}$ does provide the correct density for independent Poisson processes describing the current and all fluctuations [52]. But, as we will see in section 7, the fermionic or interacting filling fractions are not the correct densities; the correct one will be calculated there.

4. The integrable models considered

In the coming sections we will study the non-equilibrium steady-state current and cumulants for several models. We have chosen here three models as good representatives of increasingly complex families of IQFTs: the sinh-Gordon model, which may be regarded as the simplest interacting IQFT and therefore provides an ideal starting point for testing our approach; the roaming trajectories model, which is still a very simple theory from a particle content and S-matrix point of view, but where the dependence of the S-matrix on the free parameter θ_0 leads to a number of new interesting features of the current and its cumulants; finally, the sine-Gordon model at the simplest nontrivial reflectionless point, which gives us the opportunity to study a theory with a more complicated particle

J. Stat. Mech. (2014) P03011

content but still a diagonal S-matrix. It is also a theory which has a well-known discrete counterpart (e.g. the gapped XXZ chain) and therefore results for this model may prove useful when comparing to numerical simulations of the XXZ quantum spin chain.

4.1. The sinh-Gordon and roaming trajectories model

The sinh-Gordon model is one of the simplest interacting QFTs and as such it constitutes an ideal testing ground for the ideas above. It has a single-particle spectrum and no bound states. The two-particle S-matrix of the model is

$$S(\theta) = \frac{\tanh(1/2)\,(\theta - \mathrm{i}\pi B/2)}{\tanh(1/2)\,(\theta + \mathrm{i}\pi B/2)}. \tag{31}$$

The scattering matrix, hence the kernel, depend on the parameter $B \in [0, 2]$ known as the effective coupling constant. This parameter is related to the coupling constant β (not related to the inverse temperatures $\beta_\mathrm{l}, \beta_\mathrm{r}$!) in the sinh-Gordon Lagrangian [83, 84]

$$\mathcal{L} = \frac{1}{2}(\partial_\mu \phi)^2 - \frac{m^2}{\beta^2}\cosh(\beta\phi), \tag{32}$$

where m is a mass scale and ϕ is the sinh-Gordon field, as

$$B(\beta) = \frac{2\beta^2}{8\pi + \beta^2}, \tag{33}$$

under CFT normalization [20]. The S-matrix is obviously invariant under the transformation $B \to 2 - B$, a symmetry which is also referred to as weak–strong coupling duality, as it corresponds to $B(\beta) \to B(\beta^{-1})$ in (33). The point $B = 1$ is known as the self-dual point. In our numerics for simplicity we will concentrate on the $B = 1$ case, for which

$$\varphi(\theta) = 2\,\mathrm{sech}\,\theta. \tag{34}$$

The sinh-Gordon model is intimately related to the roaming trajectories model [85]: the latter can be understood as a 'deformation' of the sinh-Gordon model. Its S-matrix is obtained by setting $B = 1 + 2\mathrm{i}\theta_0/\pi$ in (31), where $\theta_0 \in \mathbb{R}^+$. The resulting S-matrix famously satisfies all the required properties (e.g. unitary and crossing symmetry), thus describing a new integrable model. The new kernel is then

$$\varphi(\theta) = \mathrm{sech}(\theta - \theta_0) + \mathrm{sech}(\theta + \theta_0). \tag{35}$$

The presence of the free parameter θ_0 turns out to have a profound effect on the features of all TBA quantities (e.g. pseudo-energies, L-functions, c-functions, etc). Indeed the roaming trajectories model's name refers to the special features of the effective central charge $c_\mathrm{eff}(r)$, which is a particular *c-function*, within the equilibrium TBA approach [25] as calculated in [85]. For massive QFTs it is expected that the function $c_\mathrm{eff}(r)$, whose definition we recall in section 6, 'flows' from the value zero in the infrared (large r) to a finite value in the ultraviolet (small r). For many theories, including the sinh-Gordon model, the constant value reached as $r \to 0$ is the effective central charge of the underlying

doi:10.1088/1742-5468/2014/03/P03011

conformal field theory associated with the model [86]–[88] (which equals the CFT central charge in unitary models). In this case, that theory is the free massless boson, a conformal field theory with central charge $c = 1$. Therefore, in the sinh-Gordon model, the function $c_{\text{eff}}(r)$ flows from the value zero to the value one as r decreases.

Crucially, when the same function $c_{\text{eff}}(r)$ is computed for the roaming trajectories model it shows a very different behavior. It still flows from the value zero to the value one, but it does so by 'visiting' infinitely many intermediate values of c, giving rise to a staircase (or roaming) pattern. The values of c that are visited correspond exactly to the central charges of the unitary minimal models $\mathcal{M}_p$ of conformal field theory,

$$1 - \frac{6}{p(p-1)}, \qquad \text{with } p = 3, 4, 5 \ldots \tag{36}$$

As we will discuss later, interesting staircase patterns for several non-equilibrium thermodynamic quantities can also be found for this model.

Another observation made in [85] is that the size of the intermediate plateaux that the function $c_{\text{eff}}(r)$ develops at the values (36) is determined by the value of θ_0. For $\theta_0 = 0$ there is a single plateau at $c = 1$, thus the usual sinh-Gordon behavior is recovered, whereas the plateaux at (36) become more prominent as θ_0 is increased. In the limit $\theta_0 \to \infty$ a single plateau at $c = \frac{1}{2}$ remains, which reflects the fact that the S-matrix (31) becomes -1 in this limit, hence the model reduces to the Ising field theory. This interesting limiting behavior was studied in [89] using the form factor approach.

Generalizations of the roaming trajectories model have been constructed based on more complex theories in which case the associated functions $c_{\text{eff}}(r)$ have staircase patterns which visit different families of CFTs [90]. Other families of theories exist where these staircase patterns also arise naturally, albeit involving a finite number of steps which are in one-to-one correspondence with the onset of unstable particles in the spectrum. These theories are the homogeneous sine-Gordon models, whose S-matrix was constructed in [91]. TBA analysis of these models has yielded a variety of staircase patterns [92]–[94] which we would also expect to see replicated in computations of the non-equilibrium normalized current and cumulants.

4.2. The sine-Gordon model at reflectionless points

We will now consider the sine-Gordon model. This is a more involved theory including several particle types and bound states. In general, the sine-Gordon model has a non-diagonal scattering matrix, which greatly complicates the TBA equations (in non-diagonal models, there is a different formulation that is more efficient [95]–[99]). These S-matrices depend, however, on a continuous parameter ν which for particular values leads to a diagonal theory. Those values correspond to so-called reflectionless points. At reflectionless points, the theory consists of two fundamental particles of mass m, usually called soliton (s) and antisoliton ($\bar{s}$), as well as a 'tower' of bound states of the former and of each other known as breathers. The number and masses of the breathers depend on the values of the coupling constant. The scattering matrices involving the soliton, antisoliton and first

J. Stat. Mech. (2014) P03011

breather (b) are [100]:

$$S_{ss}^{ss}(\theta) = S_{\bar{s}\bar{s}}^{\bar{s}\bar{s}}(\theta) = \exp\left(\int_0^\infty \frac{\mathrm{d}t}{t}\frac{\sinh((1-\nu)t/2)}{\sinh(\nu t/2)\cosh t}\sinh\frac{t\theta}{\mathrm{i}\pi}\right), \tag{37}$$

$$S_{s\bar{s}}^{s\bar{s}}(\theta) = S_{\bar{s}s}^{\bar{s}s}(\theta) = \frac{\sinh(\theta/\nu)}{\sinh((\mathrm{i}\pi-\theta)/\nu)}S_{ss}^{ss}(\theta), \tag{38}$$

$$S_{s\bar{s}}^{\bar{s}s}(\theta) = S_{\bar{s}s}^{s\bar{s}}(\theta) = \frac{\sinh(\mathrm{i}\pi/\nu)}{\sinh((\mathrm{i}\pi-\theta/\nu)}S_{ss}^{ss}(\theta), \tag{39}$$

$$S_{sb}^{sb}(\theta) = S_{\bar{s}b}^{\bar{s}b}(\theta) = \frac{\sinh\theta+\mathrm{i}\sin(\pi(1+\nu)/2)}{\sinh\theta-\mathrm{i}\sin(\pi(1+\nu)/2)}, \qquad S_{bb}^{bb}(\theta) = \frac{\sinh\theta+\mathrm{i}\sin\pi\nu}{\sinh\theta-\mathrm{i}\sin\pi\nu}. \tag{40}$$

As we can see, the S-matrix $S_{s\bar{s}}^{\bar{s}s}(\theta)$ vanishes whenever ν^{-1} takes integer values; these are the reflectionless points. In those cases the S-matrices in fact become those of a well-known diagonal theory, namely the $D_{\nu^{-1}+1}$-minimal Toda theory (see e.g. [101]).

Here we will be interested in the simplest reflectionless point, namely when $\nu = \frac{1}{2}$. In this case only the first breather exists and its mass is given by $m_\mathrm{b} = \sqrt{2}m$. The scattering amplitudes above simplify greatly and we obtain:

$$S_{ss}^{ss}(\theta) = S_{\bar{s}\bar{s}}^{\bar{s}\bar{s}}(\theta) = S_{s\bar{s}}^{s\bar{s}}(\theta) = S_{\bar{s}s}^{\bar{s}s}(\theta) = -\frac{\sinh(1/2)\,(\theta+\mathrm{i}\pi/2)}{\sinh(1/2)\,(\theta-\mathrm{i}\pi/2)}. \tag{41}$$

As anticipated earlier $S_{s\bar{s}}^{\bar{s}s}(\theta) = S_{\bar{s}s}^{s\bar{s}}(\theta) = 0$, and

$$S_{sb}^{sb}(\theta) = S_{\bar{s}b}^{\bar{s}b}(\theta) = \frac{\sinh\theta+\mathrm{i}/\sqrt{2}}{\sinh\theta-\mathrm{i}/\sqrt{2}}, \qquad S_{bb}^{bb}(\theta) = \frac{\sinh\theta+\mathrm{i}}{\sinh\theta-\mathrm{i}}. \tag{42}$$

The corresponding TBA kernels are

$$\varphi_{ss}(\theta) = \varphi_{\bar{s}\bar{s}}(\theta) = \varphi_{s\bar{s}}(\theta) = \varphi_{\bar{s}s}(\theta) = \tfrac{1}{2}\varphi_{bb}(\theta) = -\mathrm{sech}\theta, \tag{43}$$

and

$$\varphi_{sb}(\theta) = \varphi_{\bar{s}b}(\theta) = -2\sqrt{2}\cosh\theta\,\mathrm{sech}2\theta. \tag{44}$$

The sine-Gordon model describes the scaling limit of a well-known spin chain system, namely the XXZ quantum spin chain in the gapped regime. We hope therefore that some of our results for this model may be comparable to spin chain results.

5. L-functions and current in non-equilibrium TBA

In this section we present results for the L-functions and current of several models obtained numerically by solving equations (25). We will start with one of the simplest interacting integrable QFTs: the sinh-Gordon model. Results for this model will provide a benchmark for all the general features of the current and L-functions. In addition the subtle differences between the equilibrium and non-equilibrium quantities will become apparent when analyzing this model. Throughout this and later sections, we will use the variable

$$\sigma = \frac{\beta_\mathrm{r}}{\beta_\mathrm{l}} = \frac{T_\mathrm{l}}{T_\mathrm{r}}.$$

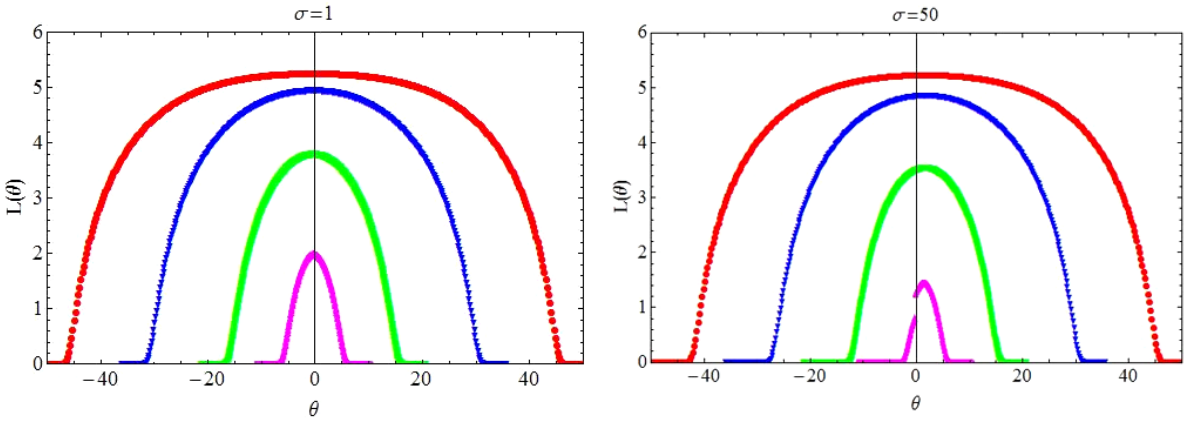

Figure 2. The function $L(\theta)$ for $m\beta_l = 6e^{-20}$ (red), $m\beta_l = 2e^{-13}$ (blue), $m\beta_l = 6e^{-7}$ (green) and $m\beta_l = 2e^{-5}$ (pink) and two values of $\sigma = \beta_r/\beta_l$.

5.1. The sinh-Gordon model

Since in this model we only have one particle type we will for now drop the particle indices in (25). Employing the kernel (34) in the equations (25) we can now solve for $\epsilon(\theta)$ and $L(\theta)$ by applying a numerical recursive algorithm starting with the free solution $\epsilon(\theta) = W(\theta)$. Figure 2 gives the L-functions for different values of $m\beta_l$ and $m\beta_r$, where m is the mass of the particle.

The first figure with $\sigma = 1$, that is $\beta_l = \beta_r$, gives the equilibrium quantities which are known from solving the standard TBA equations. It is a common observation from TBA studies that both the pseudo-energies and L-functions develop a plateau at high energies in the region $-\log(2/m\beta) \ll \theta \ll \log(2/m\beta)$ when $\beta = \beta_l = \beta_r$. For most integrable models the values of $L(\theta)$ and $\epsilon(\theta)$ at the plateau can be obtained exactly by solving so-called constant TBA equations, which are a high-energy limit of the original equations [25, 104].

From the figures above it appears that we start to see this plateau in the red curves. However, the sinh-Gordon model is rather an exception in this respect as in the limit $m\beta \to 0$ the value of $\epsilon(0)$ tends to minus infinity, hence $L(0)$ tends to infinity. This fact has been understood more generally in [102, 103], where it was noted that it is a feature of all affine Toda field theories (of which the sinh-Gordon model is but the simplest example). We will see later that for other models a clear and finite plateau is reached. Comparing the equilibrium case ($\sigma = 1$) to the case when $\sigma = 50$, thus $\beta_l \neq \beta_r$, we observe two main changes:

- The L-functions develop a discontinuity at $\theta = 0$. This is because of the discontinuity in the function $W(\theta)$ due to the different left and right temperatures. This discontinuity is present for all temperatures and the size of the jump is linear $\beta_l - \beta_r$ (see (28)). Thus when both temperatures are high no discontinuity can be seen. However, it is very apparent for relatively large values of $m\beta_l$, as can be seen in the pink curve of the second figure.

doi:10.1088/1742-5468/2014/03/P03011

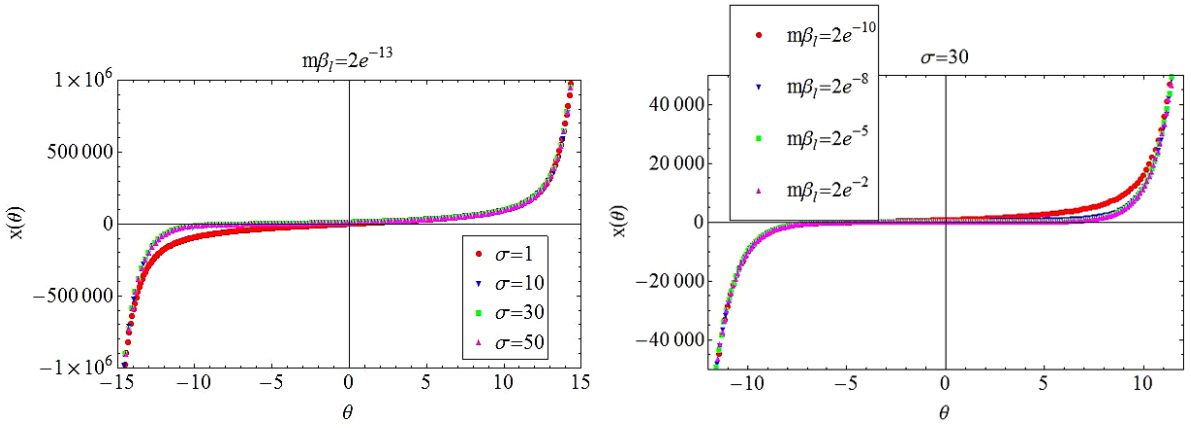

Figure 3. The function $x(\theta)$ for fixed $m\beta_{\rm l}$ and various values of σ (first figure) and for fixed σ and various values of $m\beta_{\rm l}$ (second figure).

- The L-functions cease to be even functions of θ. Again this can be best appreciated for low energies, where it is clear that the maximum of the L-functions is not located at the origin. Comparing to the equilibrium case, all functions have experienced a shift towards the right. For high energies we have again a plateau of the same height as in the equilibrium case which now extends in the region $-\log(2/m\beta_{\rm r}) \ll \theta \ll \log(2/m\beta_{\rm l})$.

In summary, for $\sigma > 1$ we observe a discontinuity at the origin and a shift towards the right of the L-functions. Due to the symmetry of the TBA equations a shift towards the left will occur for $\sigma < 1$.

Let us now turn our attention to the functions $x(\theta)$ and $\mu(\theta)$. Numerically solving (25) we obtain $x(\theta)$ as shown in figure 3.

As expected we see that the large-scale features of all functions are dominated by the $\sinh\theta$ function in the x-equation of (25). However, because $\epsilon(\theta) \neq \epsilon(-\theta)$ we find that in general $x(\theta) \neq -x(-\theta)$. The oddness of the function $x(\theta)$ is only restored in two limiting cases: (1) at equilibrium ($\sigma = 1$); (2) when both left and right temperatures tend to zero ($m\beta_{\rm l}, m\beta_{\rm r}$ large). For this reason all functions in the second figure (except the red-dotted one) are almost perfectly odd.

We have seen in the previous section that the sets of equations (25) and (26) are in fact equivalent to each other. Figure 4 provides several examples of the function $\mu(\theta)$ for the sinh-Gordon model.

The features of the level density $\mu(\theta)$ are analogous to those of $x(\theta)$ with the difference that the large-scale features are now dictated by the $\cosh\theta$ term in (26). As a consequence all figures look like deformed cosh-functions, where the evenness is broken for $\sigma \neq 1$ and large temperatures. Recalling that $\mu(\theta)$ is proportional to the density of energy levels, we see that more energy levels are available at positive rapidities if $\sigma > 1$, which agrees with the presence of a nonzero current from the left to the right (more right-moving energy levels available).

doi:10.1088/1742-5468/2014/03/P03011

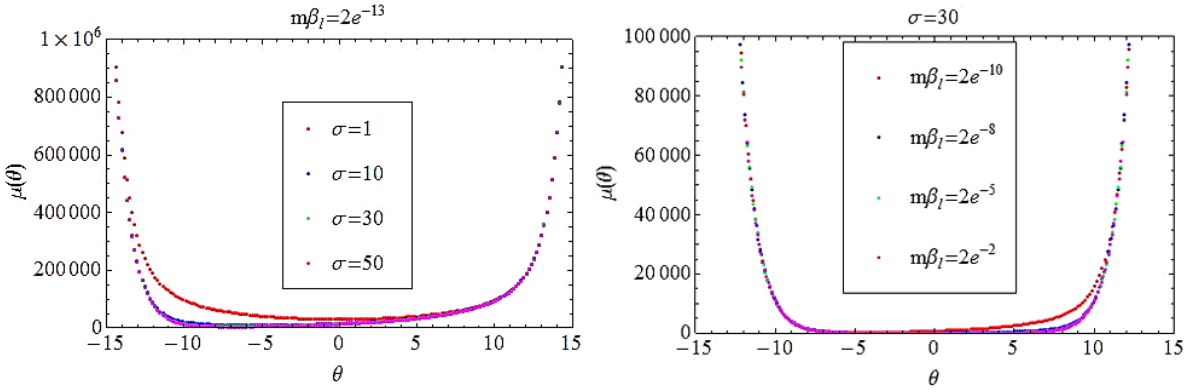

Figure 4. The function $\mu(\theta)$ for fixed $m\beta_1$ and various values of σ (first figure) and for fixed σ and various values of $m\beta_1$ (second figure).

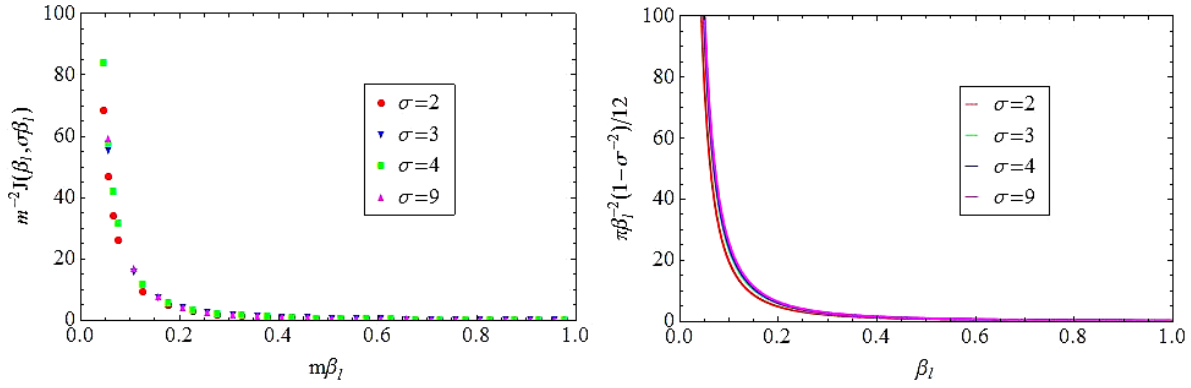

Figure 5. The current $J(\beta_1, \sigma\beta_1)$ for the sinh-Gordon model and its CFT counterpart for several values of σ.

Finally, we present the results for the current in figure 5. As expected the current in the massive model and its CFT counterpart expression agree very closely for high temperatures; both tend to zero for low temperatures and the disagreement also appears small in that region.

5.2. The roaming trajectories model

As indicated above, the roaming trajectories model is an interesting deformation of the sinh-Gordon model (from the S-matrix point of view) which displays many new interesting features for all the relevant thermodynamic quantities we study here. Figures 6 and 7 show the new structure displayed by L-functions and x-functions.

The asymmetry of the L-functions with respect to the origin is visible in most of the graphs in figure 6 as all curves appear shifted towards the right with respect to the equilibrium solutions presented in [85]. For lower temperatures the discontinuity at the

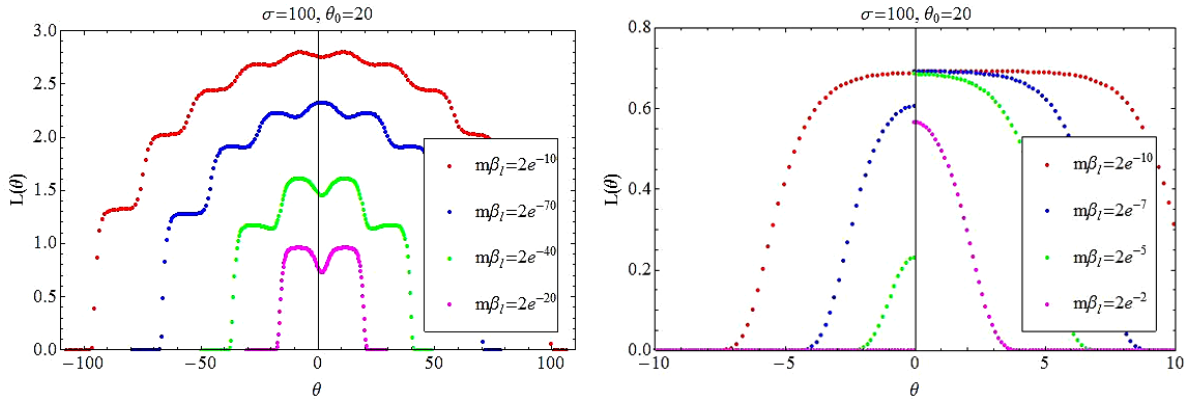

Figure 6. L-function for various temperatures in the roaming trajectories model with $\theta_0 = 20$ and $\sigma = 100$.

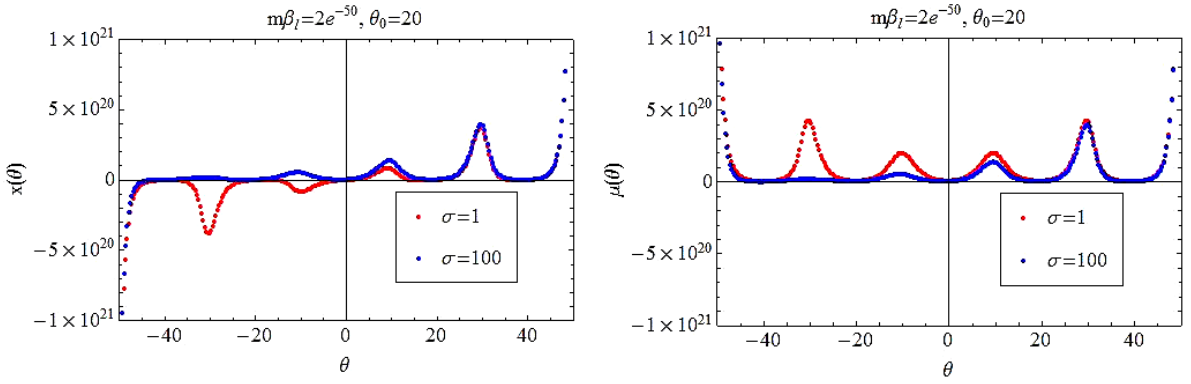

Figure 7. The functions $x(\theta)$ and $\mu(\theta)$ at and out of equilibrium for $\theta_0 = 20$ and $m\beta_1 = 100$.

origin becomes apparent once more. The presence of the θ_0 parameter leads to intricate staircase patterns reminiscent of the equilibrium results.

The function $x(\theta)$ displays a very interesting new structure with an alternation of maxima and zeros at values of θ which appear to be multiples of θ_0. This structure is surprising at first sight as it is rather what we would expect the function $\mathrm{d}\epsilon/\mathrm{d}\theta$ to look like in view of figure 6. However, $x(\theta)$ is a derivative w.r.t. the parameter a, not θ, as expressed in the paragraph after (B.4) in appendix B. This can be understood as follows. At equilibrium, when $\sigma = 1$ the function $x(\theta)$ as defined by the second equation in (25) can be identified with $\mathrm{d}\epsilon/\mathrm{d}\theta$. In other words, if we differentiate the last equation in (25) with respect to θ at $\sigma = 1$ we would exactly obtain the second equation in (25) up to the identification $x(\theta) := \mathrm{d}\epsilon/\mathrm{d}\theta$. This ceases to hold when $\sigma \neq 1$; however, the equilibrium features of $x(\theta)$ are still preserved to a large extent with certain deformations. In particular for $\theta < 0$ the sinh-function now dominates the behavior of $x(\theta)$, suppressing the negative

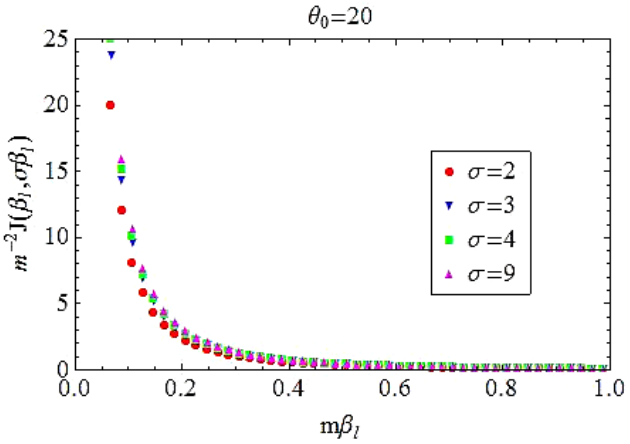

Figure 8. The current for several values of σ.

minima of its equilibrium version. A similar deformation occurs for the function $\mu(\theta)$, where again the out-of-equilibrium features for $\theta < 0$ are dominated by the cosh-function.

Finally, we take a look at the current in figure 8. Comparing to figure 5 we see that the functions seem hardly to have changed. There are however important differences which only become apparent when studying the normalized current (e.g. the current divided by $T_{\rm l}^2 - T_{\rm r}^2$) and associated cumulants. We will study these in section 5.3.

5.3. The sine-Gordon model at reflectionless points

As explained earlier we will consider here only a very special case of the sine-Gordon model, namely the situation when the whole spectrum consists of soliton, antisoliton and one breather and there is no back-scattering. Once more we will start by examining the general behavior of the L-functions for several values of the energy. These are presented in figure 9. In this case the L-functions clearly develop a plateau for high energies in the region $-\log(2/m\beta_{\rm r}) \ll \theta \ll \log(2/m\beta_{\rm l})$, which in the first figure corresponds approximately to $-16 \ll \theta \ll 21$. The exact height of the plateau is the same as in the equilibrium case which has been studied in [105] by solving the constant TBA equations. The plateaux are located at $L_{\rm b}(0) = 0.287\,682$ and $L_s(0) = 0.405\,465$, which correspond to the solutions $\mathrm{e}^{\epsilon_s(0)} = 2$ and $\mathrm{e}^{\epsilon_{\rm b}(0)} = 3$.

The functions $x_{s,b}(\theta)$ and $\mu_{s,b}(\theta)$ in figure 10 display the same main features already observed for other models. The same applies to the current, which for this reason we will not present here.

6. Non-equilibrium c-functions

A c-function is a function of the energy scale (some physical quantity such as the temperature or the distance in a correlation function), or of the position on a renormalization group (RG) trajectory, which represents well the effective number of degrees of freedom at this scale or at that point on the trajectory. In unitary models, it

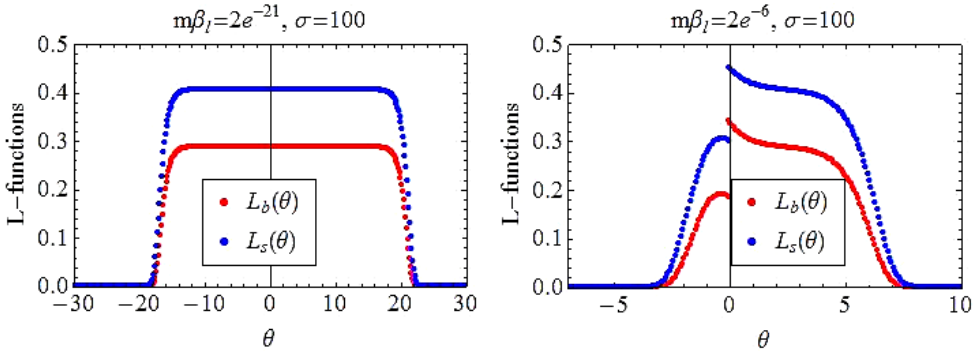

Figure 9. Soliton and breather L-functions at high and medium temperatures.

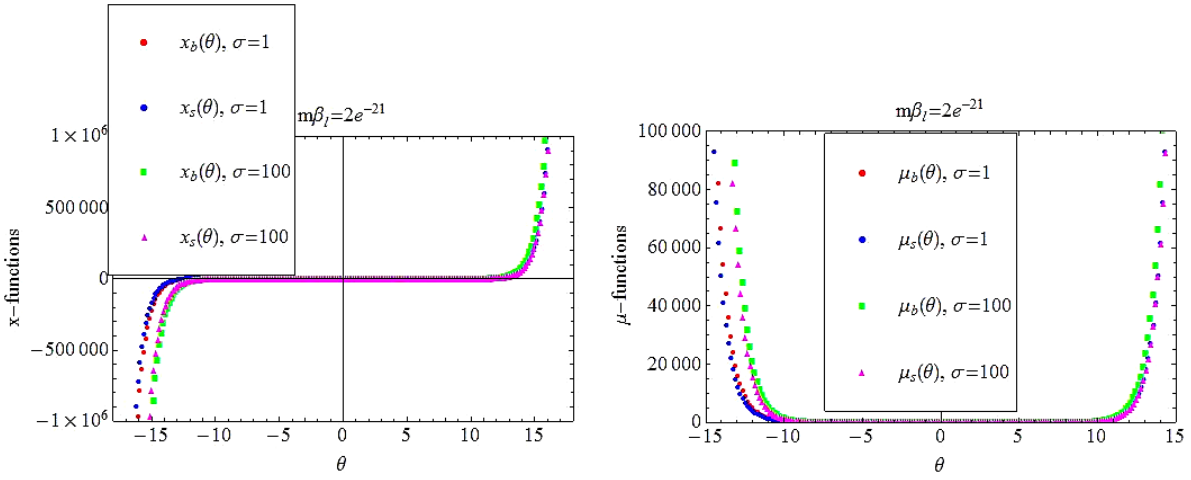

Figure 10. The functions $x_{s,b}(\theta)$ and $\mu_{s,b}(\theta)$ for high temperatures.

should satisfy two properties: it should be constant and equal to the CFT central charge at fixed points of the renormalization group (critical points), and it should monotonically increase with the energy scale. The original c-function was defined by Zamolodchikov in [106] in terms of two-point correlation functions of the stress-tensor, where he used it to prove the inequality $c_{\rm UV} > c_{\rm IR}$ between central charges at UV and IR fixed points of an RG trajectory. Zamolodchikov defined a new c-function based on (equilibrium) TBA [25], sometimes referred to as the effective central charge or scaling function,

$$c_{\rm eff}(r) := \frac{3r}{\pi^2}\int_{-\infty}^{\infty} {\rm d}\theta \cosh\theta \, \log(1+{\rm e}^{-\epsilon(\theta)}), \tag{45}$$

where r is the distance scale or inverse temperature scale entering the TBA equations.

Given the behavior of the current in CFT (17), we expect that the normalized current

$$c_1(T_{\rm l},T_{\rm r}) := \frac{12J(T_{\rm l}^{-1},T_{\rm r}^{-1})}{\pi(T_{\rm l}^2-T_{\rm r}^2)} = \frac{6}{\pi^2(T_{\rm l}^2-T_{\rm r}^2)}\sum_{i=1}^{\ell}\int_{-\infty}^{\infty}{\rm d}\theta\, m_i\cosh\theta\frac{x_i(\theta)}{1+{\rm e}^{\epsilon_i(\theta)}} \tag{46}$$

gives a function which approaches the value of the UV central charge at high temperatures or low masses, i.e. near quantum critical points. Further, at very low temperatures, the current decays exponentially fast, hence $c_1(T_\mathrm{l}, T_\mathrm{r})$ tends to zero. This means that $c_1(T_\mathrm{l}, T_\mathrm{r})$ satisfies the first property of a c-function. It is interesting to enquire if this function is actually a good c-function: that is, if it is also *monotonic with temperature scale*. Thanks to the CFT result (18) for the higher cumulants, one can similarly enquire if the functions

$$c_n(T_\mathrm{l}, T_\mathrm{r}) = \frac{12\, C_n(T_\mathrm{l}, T_\mathrm{r})}{\pi n!\,(T_\mathrm{l}^{n+1} + (-1)^n T_\mathrm{r}^{n+1})} \tag{47}$$

are good c-functions.

6.1. Numerical observations

Our numerics indeed confirm this: we observe that for every order n of the cumulant and every temperature ratio $\sigma = T_\mathrm{l}/T_\mathrm{r}$, the function (47) is a c-function. Note that these are non-equilibrium c-functions, defined intrinsically with respect to physical quantities characterizing a non-equilibrium steady state. It is particularly interesting to test this for the roaming trajectories model, where the functions above are expected to display a nontrivial plateau structure. A variety of such functions are presented and compared to each other in figure 11.

All insets in figure 11 confirm the assumption that we may regard the functions defined in (47) as c-functions. In fact, in the first figure of the second row we compare to (45), and we see that the new functions essentially carry the same information as the standard TBA scaling function. Each plateau is indeed located at a height corresponding to the central charge of a minimal model and there is a staircase pattern running from $c_n = 0$ (low temperatures) to $c_n = 1$ (high temperatures), as can be seen for $n = 1, 2$ and 3 in the figures. There are, however, also some subtle and interesting differences with respect to the equilibrium scaling function.

The size of the plateaux of the function (45) is exactly $\theta_0/2$, as can be seen in the original work [85]. This is due to the structure of the TBA equations, which for high energies can be conveniently mapped into 'massless' TBA equations, as explained in [107]. These equations naturally describe the c-function's flow between two different minimal models. In practice, these massless equations are obtained by performing the shifts $\theta \to \theta \pm \theta_0/2$ and these shifts give rise to a pair of equations which involve the new energy scales $mr\mathrm{e}^{\pm\theta_0/2}$, where $\theta_0/2$ now becomes a natural scale of the problem and r is the inverse temperature.

Observing the first figure in row one carefully, we can easily see that the size of the plateaux of $c_1(T_\mathrm{l}, T_\mathrm{r})$ depends on σ and in fact increases with σ. The reason for this is very similar to the massless TBA argument given above. At high energies (temperatures) we can once more map our TBA equation into a pair of 'massless' TBA equations. However, we have now two parameters in the problem, that is, θ_0 and σ. By performing the shifts $\theta \to \theta \pm (\theta_0 + \log\sigma)/2$ we obtain two massless equations involving the energy scales $m\beta_\mathrm{l}\mathrm{e}^{\pm(\theta_0+\log\sigma)/2}$ so that the quantity $\frac{1}{2}(\theta_0 + \log\sigma)$ becomes a new natural scale of the problem. For this reason the size of the plateaux of the new c-functions $c_n(T_\mathrm{l}, T_\mathrm{r})$ is

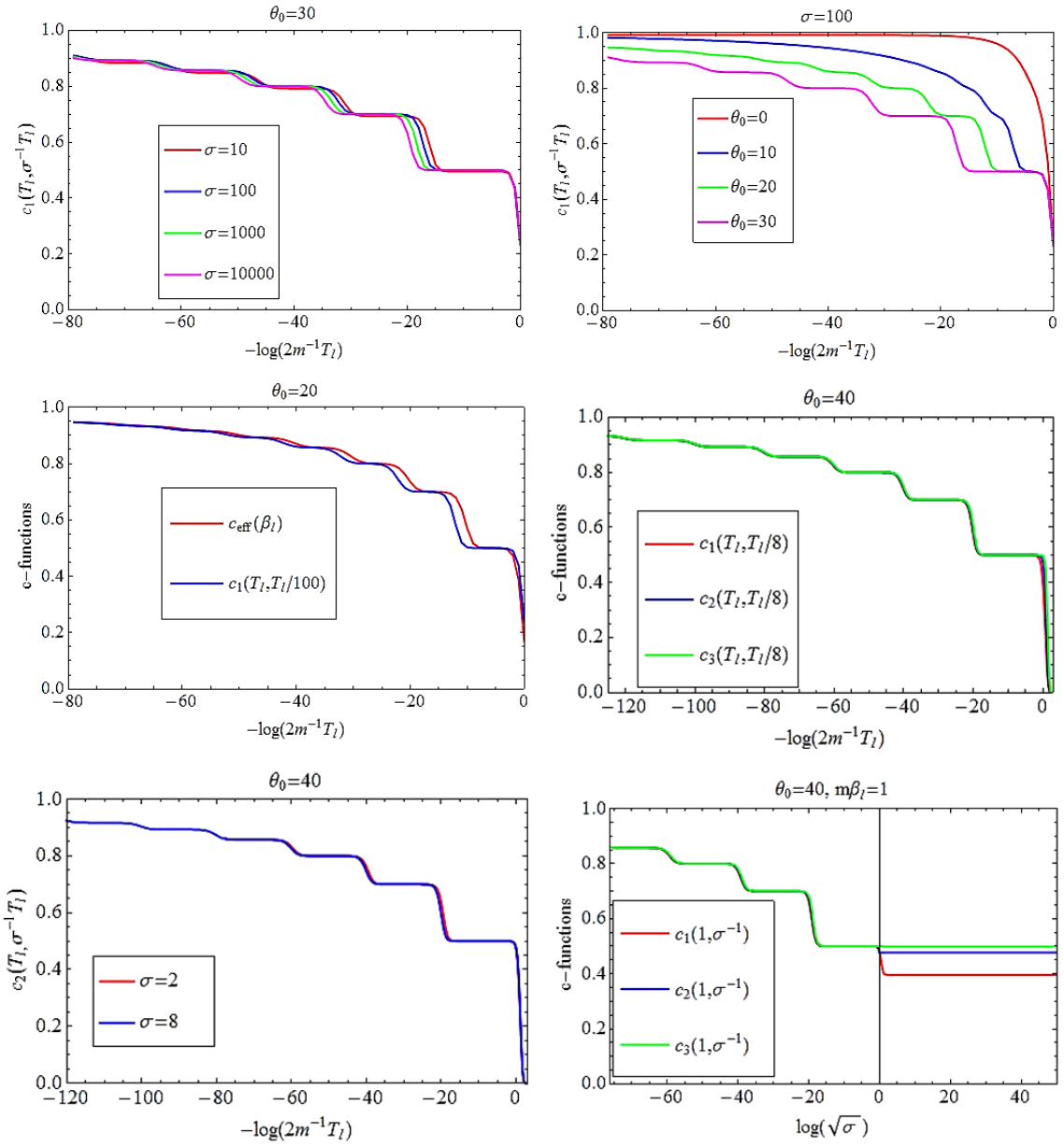

Figure 11. *c*-functions for the roaming trajectories model.

precisely given by $\frac{1}{2}(\theta_0 + \log\sigma)$. This is confirmed by the first figure, where the size of the plateaux is approximately 16, 17, 19 and 20 for $\sigma = 10, 100, 1000$ and 10 000, respectively, and the same holds for other figures. For instance, it is noticeable how the plateaux of $c_1(T_l, T_l/100)$ in the first figure of the second row are larger than those of $c_{\text{eff}}(T_l)$. This plateau size argument applies to all the new *c*-functions (47), so that plotting $c_n(T_l, \sigma^{-1}T_l)$ for various values of n with the same σ gives a set of extremely alike functions, as can be seen in the last figure of row two and the first figure of row three.

Finally, the last diagram of figure 11 deserves particular attention. At first sight it looks much as other diagrams in the same page. However, it is immediately striking that

it has an additional plateau which appears to extend indefinitely on the right-hand side, and that the variable in the horizontal axis is now $\frac{1}{2}\log\sigma$. Here we present the functions $c_n(T_\mathrm{l}, T_\mathrm{r})$ with $n = 1, 2, 3$ for a fixed value of $m\beta_\mathrm{l} = 1$. When $\log\sigma < 0$, that is $m\beta_\mathrm{r} < 1$, we observe the standard high-temperature behavior of the c-functions, namely plateaux for all values of c corresponding to the minimal models. This is quite natural as we are looking at a region where $m\beta_\mathrm{r} \ll 0$. This behavior changes at $\log\sigma = 0$, which corresponds to $m\beta_\mathrm{l} = m\beta_\mathrm{r} = 1$. For $\log\sigma > 0$ all c-functions reach a plateau (different for each) which cannot be matched with the central charge of any minimal model. For $\log\sigma > 0$ and $m\beta_\mathrm{l} = 1$ we are looking at a region where both temperatures are low, thus we do not expect to recover CFT results. In fact it is rather easy to predict, at least approximately, the position of the plateaux that we observe for $\log\sigma > 0$. Since we are looking at the low-temperature or large-$m\beta_{\mathrm{l,r}}$ regime this means that at first order the solutions to the TBA equations can be approximated by the free solutions $\epsilon(\theta) = W(\theta)$. Thus the current in this region should be well approximated by the Ising solution given in (30). In terms of this solution, the functions $c_{1,2,3}(T_\mathrm{l}, T_\mathrm{r})$ admit the following expressions:

$$
\begin{aligned}
c_1^{\mathrm{Ising}}(T_\mathrm{l}, T_\mathrm{r}) &= \frac{3}{\pi^2(T_\mathrm{l}^2 - T_\mathrm{r}^2)} \int_0^\infty \mathrm{d}\theta \sinh(2\theta) \left(\frac{1}{1 + \mathrm{e}^{m\beta_\mathrm{l}\cosh\theta}} - \frac{1}{1 + \mathrm{e}^{m\beta_\mathrm{r}\cosh\theta}} \right), \\
c_2^{\mathrm{Ising}}(T_\mathrm{l}, T_\mathrm{r}) &= \frac{3}{2\pi^2(T_\mathrm{l}^3 + T_\mathrm{r}^3)} \int_0^\infty \mathrm{d}\theta \cosh\theta \sinh(2\theta) \\
&\quad \times \left(\frac{\mathrm{e}^{m\beta_\mathrm{l}\cosh\theta}}{(1 + \mathrm{e}^{m\beta_\mathrm{l}\cosh\theta})^2} + \frac{\mathrm{e}^{m\beta_\mathrm{r}\cosh\theta}}{(1 + \mathrm{e}^{m\beta_\mathrm{r}\cosh\theta})^2} \right), \\
c_3^{\mathrm{Ising}}(T_\mathrm{l}, T_\mathrm{r}) &= \frac{1}{2\pi^2(T_\mathrm{l}^4 - T_\mathrm{r}^4)} \int_0^\infty \mathrm{d}\theta \cosh^2\theta \sinh(2\theta) \\
&\quad \times \left(\frac{\mathrm{e}^{m\beta_\mathrm{l}\cosh\theta}(-1 + \mathrm{e}^{m\beta_\mathrm{l}\cosh\theta})}{(1 + \mathrm{e}^{m\beta_\mathrm{l}\cosh\theta})^3} - \frac{\mathrm{e}^{m\beta_\mathrm{r}\cosh\theta}(-1 + \mathrm{e}^{m\beta_\mathrm{r}\cosh\theta})}{(1 + \mathrm{e}^{m\beta_\mathrm{r}\cosh\theta})^3} \right).
\end{aligned}
\tag{48}
$$

Evaluating these functions numerically for $T_\mathrm{l}/m = 1$ and $T_\mathrm{r}/m \to 0$ we obtain

$$
c_1^{\mathrm{Ising}}(1, 0) = 0.396\,314, \qquad c_2^{\mathrm{Ising}}(1, 0) = 0.478\,062 \qquad \text{and} \quad c_3^{\mathrm{Ising}}(1, 0) = 0.497\,983, \tag{49}
$$

which reproduce extremely well (there is agreement up to five decimal places) the height of the last plateau in the graph. It is even possible to get a very accurate value for the same functions at $\log\sigma = 0$ by taking the limit when $T_\mathrm{l}/m \to T_\mathrm{r}/m = 1$. This gives

$$
c_1^{\mathrm{Ising}}(1, 1) = 0.478\,062, \qquad c_2^{\mathrm{Ising}}(1, 1) = 0.478\,062 \qquad \text{and} \quad c_3^{\mathrm{Ising}}(1, 1) = 0.500\,284. \tag{50}
$$

The good agreement of (49) and (50) is remarkable as $m\beta_\mathrm{l} = 1$ does not really correspond to extremely high temperatures where the Ising approximation should hold best. It appears from this computation that this approximation is in fact extremely accurate already for temperatures around $T_{\mathrm{l,r}}/m = 1$.

It is also interesting to observe that the size of the plateaux for $\log\sigma < 0$ is constant and appears to equal $\theta_0/2$. This can be explained with a similar argument as that employed earlier in predicting the size of the plateaux of other functions. As discussed

J. Stat. Mech. (2014) P03011

earlier the quantities $m\beta_{\rm l}{\rm e}^{\pm(\theta_0+\log\sigma)/2}$ are natural energy scales of the problem (for high temperatures). We are now fixing $m\beta_{\rm l}$ and plotting against $\frac{1}{2}\log\sigma$ so that we recover the usual plateau size $\theta_0/2$ at high temperatures.

6.2. Physical interpretation

Since $c_n(T_{\rm l},T_{\rm r})$ are dimensionless, they are functions of the dimensionless variables $T_{\rm l}/m$ and $T_{\rm r}/m$ only, where m is the mass scale (say the mass of the lightest particle). Hence, the observation that the c-functions $c_n(T_{\rm l},T_{\rm r})$ expressed in (47) are non-decreasing with the temperature scale, implies that upon a *reduction of the mass scale*, all *cumulants are non-decreasing*:

$$\frac{\mathrm{d}}{\mathrm{d}m}C_n \le 0. \tag{51}$$

This means that as the mass scale is decreased, the average energy transferred increases, and the fluctuations are stronger, the probability distribution becoming overall 'flatter'. This has an immediate interpretation in terms of available energy carriers. By lowering the mass scale, i.e. the gap, while keeping the temperature scale the same, we make more energy carriers available as more quasi-particles can be created. This obviously implies that the energy current should indeed be higher, as the situation is similar to that of lowering the resistance while keeping the voltage the same in an electric circuit. But also, the availability of energy carriers at lower energies means that the energy carriers cover a wider energy spectrum, providing a wider scope for fluctuations of energy transfer. Naturally, as $m\to 0$, one should recover the CFT result (18). This means that we have *exact upper bounds* on the cumulants, given by the cumulants of the UV fixed point:

$$C_n \le \frac{c\pi n!}{12}(T_{\rm l}^{n+1}+(-1)^n T_{\rm r}^{n+1}). \tag{52}$$

We expect these results to hold in any integrable model with diagonal scattering, and possibly much more generally.

7. The probability distribution and its Poisson process interpretation

In this subsection, for simplicity let us restrict ourselves to a single-particle spectrum, with mass m.

As was shown in [52], in CFT, the large-time scaled energy transfer statistics may be described by Poisson processes. Specifically, the scaled cumulant generating function in CFT is that of a combination of independent Poisson processes at every energy E representing jumps in both directions, weighted by the Maxwell–Boltzmann factor ${\rm e}^{-\beta_{\rm l,r}E}$ (for jumps towards the right and left respectively):

$$F_{\rm CFT}(z)=\int \mathrm{d}q\,\omega_{\rm CFT}(q)\,({\rm e}^{zq}-1),\qquad \omega_{\rm CFT}=\frac{c\pi}{12}\cdot\begin{cases}{\rm e}^{-\beta_{\rm l}q} & (q>0)\\ {\rm e}^{\beta_{\rm r}q} & (q<0)\end{cases} \tag{53}$$

where ${\rm e}^{zq}-1$ is the cumulant generating function for a single Poisson process.

Is the scaled cumulant generating function for energy transfer in IQFT also described by Poisson processes? That is, is it true that

$$F(z) = \int \mathrm{d}q\, \omega(q)\, (\mathrm{e}^{zq} - 1) \tag{54}$$

for some nonnegative weights $\omega(q)$? In order to answer this question, we recall that our exact form for $F(z)$ comes from the exact current and the extended fluctuation relations (15), which relate $F(z)$ to the current at shifted temperatures. This means that if (54) holds, then the weights $\omega(q)$ are simply related to the Fourier transform of the current as a function of inverse temperature differences:

$$\omega(q) = \frac{1}{q} \int \frac{\mathrm{d}\lambda}{2\pi}\, J(\beta_\mathrm{l} - \mathrm{i}\lambda, \beta_\mathrm{r} + \mathrm{i}\lambda)\, \mathrm{e}^{-\mathrm{i}\lambda q}. \tag{55}$$

Note that this is real if $J(\beta_\mathrm{l}, \beta_\mathrm{r})$ is a real-analytic function. We may interpret the large-time scale energy transfer as being composed of Poisson processes if and only if this $\omega(q)$ is also nonnegative.

For the Ising model, using (30) in the form

$$J_\mathrm{Ising}(\beta_\mathrm{l}, \beta_\mathrm{r}) = \frac{1}{2\pi} \int_m^\infty \mathrm{d}E\, E \sum_{n=1}^\infty (-1)^{n-1} (\mathrm{e}^{-n\beta_\mathrm{l} E} - \mathrm{e}^{-n\beta_\mathrm{r} E})$$

we find

$$\omega_\mathrm{Ising}(q) = \sum_{n=1}^\infty \frac{(-1)^{n-1}}{2\pi n^2} \cdot \begin{cases} \mathrm{e}^{-\beta_\mathrm{l} q} & \text{for } q > nm \\ \mathrm{e}^{\beta_\mathrm{r} q} & \text{for } q < -nm \\ 0 & \text{otherwise} \end{cases} \tag{56}$$

For every finite q, this is a finite sum. Since $\sum_{n=1}^N ((-1)^{n-1}/2\pi n^2)$ is positive for every N, then indeed $\omega_\mathrm{Ising}(q)$ is a positive weight. Hence in the Ising model, there is a Poisson process for every transfer $|q| > m$ with finite positive weight proportional to the Maxwell–Boltzmann factor, and as an integer multiple of m is passed, the proportionality factor changes abruptly (increasing or decreasing). In the limit $m = 0$ the proportionality factor is constant with q, and equals $\sum_{n=1}^\infty ((-1)^{n-1}/2\pi n^2) = \pi/24$, as it should (CFT with central charge $c = 1/2$).

In the interacting case, the question is more complicated, because we cannot analytically Fourier transform the NESSTBA expression (25) for the current. However, we can analytically study the large-m limit (or low-temperature limit) using the second-order expansion (D.7), derived in appendix D. This is divided into two contributions, (D.8) and (D.9). The contributions (D.8) are exactly of the Ising form (to second order), so that they contribute terms of the form (56) to the weight $\omega(q)$. In fact, to every order there will be terms of that form, so that we can write $\omega(q) = \omega_\mathrm{Ising}(q) + \omega_\mathrm{inter}(q)$, where $\omega_\mathrm{inter}(q)$ incorporates all effects of the particle interactions. The contributions (D.9), with interaction terms, are purely of second order. This implies that for low enough energies, the scaled energy transfer statistics can indeed be described by a continuum of Poisson processes; more precisely, for all $|q| < 2m$, the weight is exactly the Ising weight $\omega_\mathrm{Ising}(q)$.

The contributions (D.9) give the exact $\omega_\mathrm{inter}(q)$ for all $0 < |q| < 3m$. In order to show that $\omega(q)$ is nonnegative, it is sufficient to show that $\omega_\mathrm{inter}(q)$ is nonnegative, since $\omega_\mathrm{Ising}(q)$

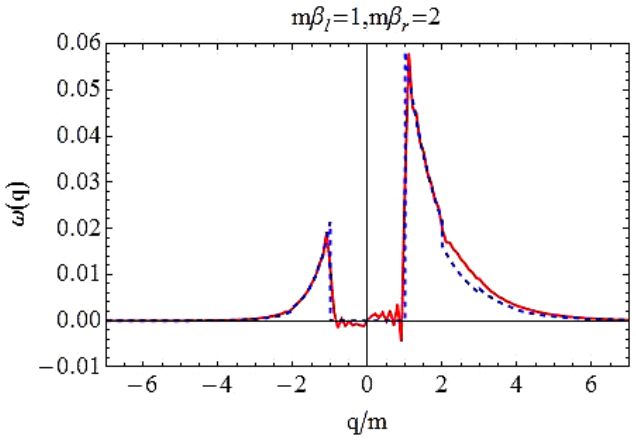

Figure 12. The function $\omega(q)$ for the sinh-Gordon (red, solid curve) and Ising (blue, dashed curve) models.

is. The contributions (D.9) may be analyzed using the result expressed in the last two lines in (D.13). Fourier transforming, we find

$$
\begin{aligned}
q\,\omega_{\mathrm{inter}}(q) \overset{0<|q|<3m}{=} \frac{m^2}{4\pi^2}\int_0^\infty \mathrm{d}\theta\,\mathrm{d}\gamma\,\Big(&\mathrm{e}^{-\beta_\mathrm{l}(m\cosh\theta+m\cosh\gamma)}\delta(m\cosh\theta+m\cosh\gamma-q)\\
&-\mathrm{e}^{-\beta_\mathrm{r}(m\cosh\theta+m\cosh\gamma)}\delta(m\cosh\theta+m\cosh\gamma+q)\Big)\\
&\times\cosh\theta\,\varphi(\theta-\gamma)\,(\sinh\theta+\sinh\gamma)\\
&+\frac{m^2}{8\pi^2}\int_0^\infty \mathrm{d}\theta\,\mathrm{d}\gamma\,\mathrm{e}^{-\beta_\mathrm{l}m\cosh\theta-\beta_\mathrm{r}m\cosh\gamma}\delta(m\cosh\theta-m\cosh\gamma-q)\\
&\times\varphi(\theta+\gamma)(\sinh(2\theta)-\sinh(2\gamma)+2\sinh(\theta-\gamma)).
\end{aligned}
\tag{57}
$$

As is apparent, the right-hand side is exactly zero for $0<|q|<2m$, and is positive for $q>2m$ and negative for $q<-2m$. This shows that $\omega_{\mathrm{inter}}(q)$ is a nonnegative function of q for all $0<|q|<3m$, hence that there is a Poisson process interpretation in this whole range of energy transfer.

A proof to all orders, however, is more difficult. Instead, we compute $\omega(q)$ by numerically evaluating the Fourier transform in (55). Figure 12 shows the result (solid curve) for the sinh-Gordon model. This is clearly a nonnegative function, up to oscillations that are stronger near sharp changes due to numerical imprecisions.

A comparison between the function $\omega(q)$ in the sinh-Gordon model and the function $\omega_{\mathrm{Ising}}(q)$ is also presented in figure 12. The two functions display very similar features. For values of $|q|<2m$ we should find complete agreement between both curves. This indeed appears to be the case up to the limited precision of our numerical procedure. For example, for $|q|<m$ the Fourier transform should be zero (as it is for Ising). Instead, we see oscillations about the value zero. As explained above, for $2m<|q|<3m$ the function $\omega(q)$ of the sinh-Gordon model should start differing from the Ising case, through the correction (57). Although we are not plotting the contribution from this correction here, it is apparent that the two curves start to disagree more for $2m<|q|$. The two curves

doi:10.1088/1742-5468/2014/03/P03011

become almost indistinguishable for large values of $|q|/m$ (CFT limit), where they both display exponential decay $\omega(q) \propto \mathrm{e}^{-\beta_{\mathrm{l,r}}|q|}$ according to (53). Although the coefficient of this exponential decay should be twice as large for the sinh-Gordon model (since $c = 1$) this is hard to observe explicitly by comparing the two functions, as the exponential decay is the dominating feature. We have also evaluated numerically $\omega(q)$ for the roaming trajectories model, confirming that it is nonnegative.

The form (54) of the scaled cumulant generating function means that the complete, large-time scaled statistics of the energy transfer is that of independent, classical packets of energies $|q|$ jumping towards the right ($q > 0$) or left ($q < 0$) in a Poissonian fashion with intensity $\mathrm{d}q\,\omega(q)$ for some positive weight $\omega(q)$. This Poisson process description may be seen as an improvement on the idea behind the Landauer formula for non-equilibrium currents. In the Landauer formula, one assumes that two baths at different temperatures/chemical potentials with independent equilibrium distributions are emitting excitations through available channels. A similar picture holds for all fluctuations in CFT, as the weight function $\omega_{\mathrm{CFT}}(q)$ is proportional to the Boltzmann distribution times the flat state density, as observed in [52]. However, this is not the case in general: the weight function is not just that determined by the Boltzmann distribution times the state density, but is a more complicated function, encoding nontrivially the full interaction.

8. (Non-)additivity of the current

As recalled above, in [52] it was shown that in CFT the current takes the form

$$J_{\mathrm{CFT}}(\beta_{\mathrm{l}}, \beta_{\mathrm{r}}) = f(\beta_{\mathrm{l}}) - f(\beta_{\mathrm{r}}) \tag{58}$$

for some function f. This form of the current is equivalent to the *additivity property*

$$J_{\mathrm{CFT}}(\beta_1, \beta_2) + J_{\mathrm{CFT}}(\beta_2, \beta_3) - J_{\mathrm{CFT}}(\beta_1, \beta_3) = 0. \tag{59}$$

As was observed in [72], additivity, or the existence of the function f as in (58), implies that the non-equilibrium current is completely determined by the linear (equilibrium) conductance

$$G^{\mathrm{eq}}_{\mathrm{CFT}}(T) = \frac{\partial}{\partial T_1} J_{\mathrm{CFT}}(T_1^{-1}, T_2^{-1})\Big|_{T_1=T_2=T}, \tag{60}$$

that is

$$J_{\mathrm{CFT}}(T_1^{-1}, T_2^{-1}) = \int_{T_2}^{T_1} G^{\mathrm{eq}}_{\mathrm{CFT}}(T)\,\mathrm{d}T. \tag{61}$$

Although this observation is not useful in CFT because the current can be evaluated exactly by other means, if the additivity property were to hold beyond CFT, equation (61) could have deep and important physical consequences. It was indeed suggested in [72], based on a numerical analysis, that additivity holds in the critical XXZ chain beyond the low-temperature limit, hence beyond the universal region that is expected to be described by CFT. In fact, it was also suggested in [68] that additivity could hold in massive quantum field theory.

We show that the additivity property *does not hold* in general: the non-equilibrium current is not determined by the equilibrium conductance. However, as we observe in the sine-Gordon model, the breaking of additivity may be very small. The breaking is due to a delicate imbalance that arises because, in strongly interacting models, level densities are affected by level occupations at different energies.

8.1. Proof and numerical observations

Let us define the additivity deficit

$$P(\beta,\sigma) := \frac{J(\beta,\sigma\beta)+J(\sigma\beta,\sigma^2\beta)-J(\beta,\sigma^2\beta)}{J(\beta,\sigma^2\beta)}. \tag{62}$$

We show in appendix E that

$$P(\beta,\sigma)\neq 0. \tag{63}$$

That is, we show, in the formulation (4), (7) of the non-equilibrium steady state and in general diagonal-scattering integrable QFT, that for any low enough temperature, $\beta m > \beta_0 m$ for some β_0, and any large enough temperature ratio, $\sigma > \sigma_0$ for some $\sigma_0 > 1$, the quantity $P(\beta,\sigma)$ is nonzero. For technical reasons, we will assume that the differential scattering phases $\varphi_{ij}(\theta)$ have a fixed sign (i.e. $\varphi_{ij}(\theta)$ is positive for every i,j and θ, or is negative for every i,j and θ); this condition is satisfied for all models studied in this paper. Our proof will also show that, for instance, $P(\beta,\sigma)$ for $\sigma > \sigma_0$ has a positive sign for the sinh-Gordon and roaming trajectories model, and a negative sign for the reflectionless sine-Gordon model studied above; hence in general, it does not have a fixed, model-independent sign.

Numerical evaluations of the additivity deficit in the sinh-Gordon, roaming trajectories and reflectionless sine-Gordon model also confirm that it is nonzero. The evaluations yield another important insight: the additivity deficit, although nonzero, is actually very small in most cases. The maximum value of the additivity deficit $P(\beta,\sigma)$ as function of β depends on the ratio of temperatures σ, but for ratios below ten the maximum does not go beyond about 4% in the sinh-Gordon model. It increases as σ is increased, but the region where $P(\beta,\sigma)$ is large becomes smaller. All these features can be observed in the first graph of figure 13, where the values depicted have been obtained by numerically solving the NESSTBA equations. The second graph represents the same quantity as obtained by approximating the current by its low-temperature expansion given in appendix D. We can see that both figures show a similar set of features, however they differ considerably in magnitude, especially for high energies.

A more involved structure is found when studying the function $P(\beta,\sigma)$ in the roaming trajectories model (see figure 14). We have used a logarithmic scale in this case to show more clearly the correspondence between regions where the additivity deficit is zero and plateaux in the corresponding c-functions. In order to make this correspondence even more explicit we present both the function c_1 and the (re-scaled) additivity deficit in the first figure. As we can see, maxima of the additivity deficit are situated at values of $\log(m\beta/2)$ which are exactly multiples of $(\theta_0+\log\sigma)/2$. These values correspond to the middle point of c-function steps which connect two consecutive plateaux. As expected,

doi:10.1088/1742-5468/2014/03/P03011

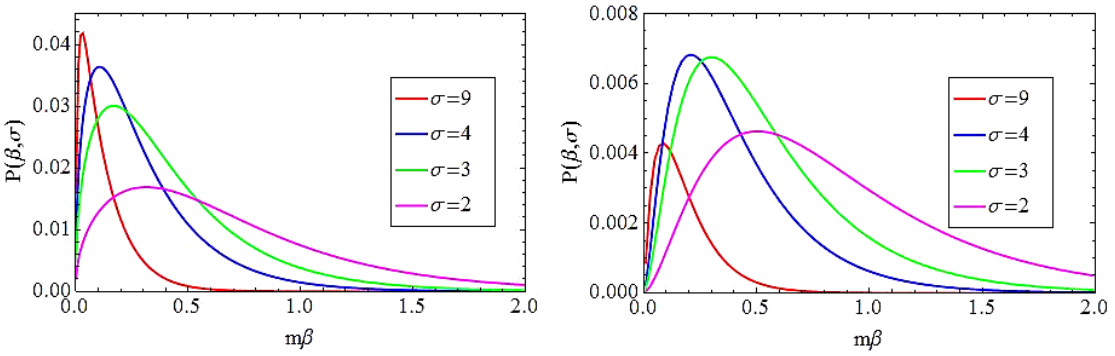

Figure 13. The function $P(\beta, \sigma)$ for various values of σ and θ_0 in the sinh-Gordon model.

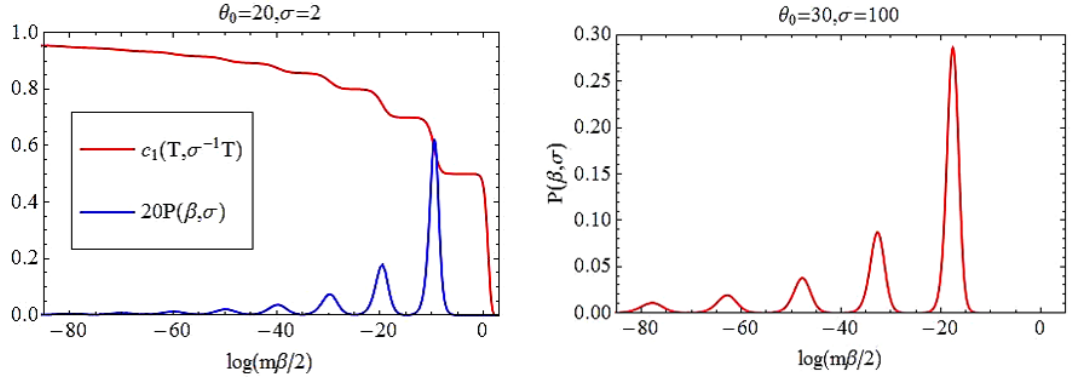

Figure 14. The function $P(\beta, \sigma)$ for two values of σ in the roaming trajectories model.

the additivity deficit vanishes between such maxima exactly in those regions where the c-function develops plateaux, where the system is essentially described by a CFT. From this description, it is interesting to note that there is an exception, namely the first step of the c-function (connecting the values $c_1 = 0$ and $c_1 = \frac{1}{2}$) does not have an associated maximum of the additivity deficit. In fact this first step and the subsequent plateau at $c_1 = \frac{1}{2}$ give us the c-function associated with the Ising model. As is easy to observe from (30), the Ising model (both massive and massless) enjoys the additivity property. Therefore the additivity deficit vanishes in this region. The same features are observed as well in the second figure.

It is also worth noting that the maximum value of the additivity deficit increases with σ, as for the sinh-Gordon model. However, for the roaming trajectories model it seems that the additivity deficit can be rather large for large σ. For example, in the second figure it sometimes reaches values near 30%. We observe that for the flow between the minimal models $\mathcal{M}_5$ and $\mathcal{M}_4$ (central charge 7/10 and 1/2 respectively), the additivity deficit is the largest.

In contrast, for the reflectionless sine-Gordon model, with σ in the range between 3 and 9 the maximum deviation does not go beyond 0.15%.

doi:10.1088/1742-5468/2014/03/P03011

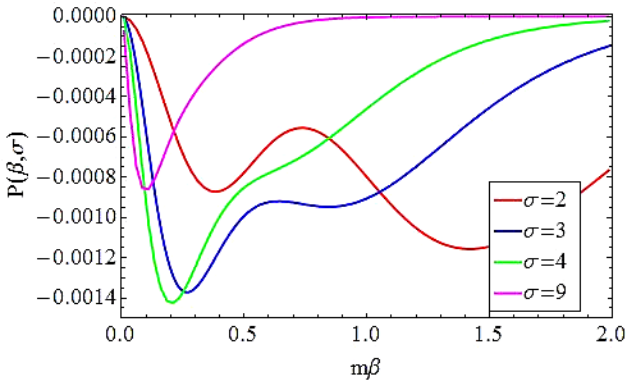

Figure 15. The function $P(\beta, \sigma)$ for various values of σ in the reflectionless sine-Gordon model.

This is important, because the numerical analysis of [72], from which it was concluded that additivity exactly held, is not expected to reach the accuracy necessary to detect such small effects. There is of course *a priori* no contradiction between our results and the conclusions of [72], because our results are in the context of near-critical, universal low-temperature systems, while the analysis of [72] is in the context of the non-universal, higher temperature regime of gapless chains. Yet, our remark that the additivity deficit may be lower than the precision achieved in [72] sheds doubt about the precise conclusions reached there. It is however rather interesting that the results of [72] and our present results indicate that additivity may be *approximately* satisfied in many cases.

8.2. Physical interpretation

The additivity property holds exactly in massive quantum field theory in three situations: (i) at high temperatures, where the CFT regime is recovered; (ii) in free-particle models; and (iii) at low temperatures.

In order to understand, at least in the context of integrable QFT, why in the three above-mentioned situations the additivity property should hold, and why it should break, although sometimes weakly, in other situations, let us recall and analyze in a bit more depth the argument for additivity presented in [68]. We start with the expression (22) for the finite-L counterpart of the non-equilibrium current (the latter being obtained by taking the limit $L \to \infty$). As we argued, this makes good sense in integrable QFT, thanks to the description of the finite-L Hilbert space in terms of Bethe ansatz quasi-particles. Labeling quasi-particles in a state $|v\rangle$ by k, they have well-defined energies e_k and momenta p_k. Clearly, for every state $|v\rangle$ with n quasi-particles, we have $P|v\rangle = (\sum_{k=1}^{n} p_k)\,|v\rangle$. Let us introduce the operators $P_\pm$ and $E_\pm$ that measure the momenta and energies of positive- and negative-momentum quasi-particles respectively:

$$P_\pm|v\rangle = \left(\sum_{k:\ p_k \gtrless 0} p_k\right)|v\rangle, \qquad E_\pm|v\rangle = \left(\sum_{k:\ p_k \gtrless 0} e_k\right)|v\rangle.$$

Clearly, we have $P = P_+ + P_-$, and also, on every state $|v\rangle$, the finite-L density matrix $\rho^L_{\rm stat}$ given by (20) factorizes, $\rho^L_{\rm stat}|v\rangle = {\rm e}^{-\beta_{\rm l}E_+ - \beta_{\rm r}E_-}|v\rangle$. Using the fact that $e_{k'} = e_k$ if $p_{k'} = -p_k$, and the fact that by parity invariance, the spectrum of momenta is symmetric under change of signs, it was then concluded in [68] that the average (22) should give, in the large-L limit, the form $f(\beta_{\rm l}) - f(\beta_{\rm r})$ for $J(\beta_{\rm l}, \beta_{\rm r})$, hence the additivity property.

There is, however, one missing argument: in order to reach this conclusion, we also need the trace itself to factorize, ${\rm Tr}_L = {\rm Tr}_{\{p_k<0\}}{\rm Tr}_{\{p_k>0\}}$. This, unfortunately, does not hold in general. Indeed, according to the Bethe ansatz equations, the density of quasi-particles around a certain momentum depends in a nontrivial and nonnegligible way on the density of quasi-particles at other momenta. This non-factorization is true at finite L, and in the large-L limit factorization *is not* recovered. This is of course what leads to coupled integral equations determining the pseudo-energy in the TBA formulation above. The fact that the relatively small effect of the breaking of the factorization of the trace is at the basis of the breaking of the additivity property may explain why additivity is broken only very slightly for the sinh-Gordon and sine-Gordon models studied here.

Factorization of the trace, hence additivity, does hold, however, in the three situations mentioned above. It is clear that it holds in the situation (ii), in the case of free particles: the defining property of free particles is that the density of states of the quasi-particles is unaffected by the presence or absence of other quasi-particles. In the situation (iii), at low temperatures, it is also clear that the trace factorizes: in this case, one may restrict the trace to excitations containing only one quasi-particle, so that the level density is not affected by the presence of any other quasi-particle. In the situation (i), at high temperatures, factorization of the trace occurs because of the large-energy *rapidity-space factorization*: the scattering matrix asymptotically tends to a constant, whence the differential scattering phases $\varphi_{ij}(\theta)$ tends to zero. This implies that the density of particles at momenta largely separated do not influence each other, so that the trace can be factorized into large-energy right-movers and left-movers.

9. Conclusion

In this paper we considered non-equilibrium steady states with energy flows in integrable QFT. The steady states are obtained from the setup where an initial state representing two independently thermalized halves of the system is allowed to evolve for an infinite time. In this setup, it is the asymptotic regions of the system itself that play the roles of reservoirs providing and absorbing energy (Hamiltonian reservoirs). The exact non-equilibrium density matrix describing averages of local observables in the steady state was proposed, and derived from QFT arguments, in [52, 68]. Using this density matrix, we obtained for the first time the exact energy current in any integrable model of relativistic QFT with diagonal-scattering matrix by generalizing the thermodynamic Bethe ansatz (TBA) method first developed by Zamolodchikov in [25]. Employing the extended fluctuation relation (15) derived by Bernard and Doyon [15], we further obtain the scaled cumulant generating function of the heat current.

We have verified that our formula for the current (25) agrees with known results and techniques in both the high- and low-temperature limits. For high temperatures, Bernard and Doyon's CFT result [52] is exactly recovered by generalizing the high-temperature

limit analysis of TBA equations in [25]. The low-temperature expansion of (25) also agrees with the result obtained by using the finite-volume regularization methods of Pozgay and Takacs in [82].

We have solved the equations (25) numerically for three models: the sinh-Gordon model, the roaming trajectories model and the sine-Gordon model at a particular reflectionless point. The numerical results for the currents in these three models agree well with the analytic results both for high and low temperatures. Also the numerics, in particular of the roaming trajectories model, suggest the existence of an infinite family of c-functions which are given in terms of the cumulants (these functions are verified to satisfy the required properties: positivity, monotonicity, constant limiting values corresponding to the CFT central charges at RG fixed points). They display a very similar behavior to that of the standard TBA scaling function, recovering for instance CFT central charges of minimal models in the roaming trajectories model. These allowed us to establish upper bounds for cumulants in any integrable model with diagonal scattering.

We verified that the scaled cumulant generating function can be seen as that of a family of independent Poisson processes, one for every value of the transferred energy. Hence, the complete, large-time scaled statistics of the energy transfer is that of independent, classical packets of energies jumping towards the right or left in a Poissonian fashion with weight $\omega(q)$. We have evaluated $\omega(q)$ numerically for the sinh-Gordon and roaming trajectories models, thus verifying that it is nonnegative. The Poisson process description may be seen as an improvement on the idea behind the Landauer formula.

Finally, we have proved that the additivity of the non-equilibrium current does not hold in a general diagonal theory both analytically and numerically, except at very large and very small temperatures. The additivity deficit has been found to be very small in the numerical analysis of the sinh-Gordon and sine-Gordon models considered here, although it can be rather large for large temperature ratios in the roaming trajectories model.

There are many directions to explore from our results. First, an independent verification of our results, perhaps from perturbation theory or from numerical calculations, would be very helpful for confirming both that our techniques work, and that the non-equilibrium density matrix derived in [68] is the correct one. In particular, DMRG numerics has been performed in [72] for the XXZ spin chain in the quench situation that we consider here. It would be possible to adapt this to gapped chains whose massive scaling limit is the reflectionless sine-Gordon model that we studied. It would also be very interesting to extend our analysis of the sine-Gordon model to the non-diagonal case or even to more complex reflectionless points and to check if we still have c-functions and a Poisson process interpretation, and if the deviation from additivity is small or not. In the non-diagonal case, TBA becomes much more complicated. The development of nonlinear integral equations for the current, paralleling the equilibrium case, could be helpful. Further, we have only evaluated the Poisson weight by numerically Fourier transforming the current. It would be interesting to have an exact expression in some form (such as an integral equation). Additionally, it is natural to think that the c-functions we proposed apply much more generally than in integrable QFT; it would be very interesting to have general arguments or a general proof that they are c-functions. Finally, an interesting question is to understand if the Poisson process interpretation still holds beyond integrability.

doi:10.1088/1742-5468/2014/03/P03011

Acknowledgments

OCA and BD thank Francesco Ravanini for comments on our non-equilibrium thermodynamic Bethe ansatz and on the non-diagonal generalization. BD thanks Denis Bernard for general comments on the manuscript and fruitful past (and future) collaborations, as well as Fabian Essler and Joel Moore for discussions and email communications.

Appendix A. Cumulants in terms of correlators

The expression (12) for the scaled cumulant generating function can be simplified to its 'naive' form in the case of pure-transmission systems (and in slightly more general cases as well), as was shown in [15]:

$$F(z) = \lim_{t\to\infty} t^{-1} \log\left(\langle \mathrm{e}^{z\Delta Q(t)}\rangle_{\mathrm{stat}}\right) \tag{A.1}$$

where we recall that $\Delta Q(t) = Q(t) - Q$. Hence, cumulants have the form

$$C_n = \lim_{t\to\infty} t^{-1} \langle (\Delta Q(t))^n\rangle_{\mathrm{stat}}^{\mathrm{connected}} \tag{A.2}$$

where the superscript 'connected' has the usual combinatoric meaning, e.g.

$$\langle A^2\rangle_{\mathrm{stat}}^{\mathrm{connected}} = \langle A^2\rangle_{\mathrm{stat}} - \left(\langle A\rangle_{\mathrm{stat}}\right)^2,$$

$$\langle A^3\rangle_{\mathrm{stat}}^{\mathrm{connected}} = \langle A^3\rangle_{\mathrm{stat}} - 3\langle A\rangle_{\mathrm{stat}}\langle A^2\rangle_{\mathrm{stat}} + 2\left(\langle A\rangle_{\mathrm{stat}}\right)^3.$$

We may now use, by definition of the current operator,

$$\Delta Q(t) = \int_0^t \mathrm{d}s\, \mathcal{J}(t)$$

so that

$$C_n = \lim_{t\to\infty} t^{-1} \lim_{\epsilon\to 0^+} \int_0^t \mathrm{d}s_0 \cdots \mathrm{d}s_{n-1} \langle \mathcal{J}(s_{n-1} + (n-1)\mathrm{i}\epsilon)\cdots\mathcal{J}(s_1+\mathrm{i}\epsilon)\mathcal{J}(s_0)\rangle_{\mathrm{stat}}^{\mathrm{connected}} \tag{A.3}$$

where we have included an imaginary time shift that agrees with the ordering of the operators in the product $(\Delta Q(t))^n$, and that regularizes the correlation functions. By stationarity of the steady state, we shift all time variables by a common value. Hence, changing variables to $u_j = s_j - s_0$ for $j = 1, \ldots, n-1$, we find

$$\begin{aligned} C_n &= \lim_{t\to\infty} t^{-1} \lim_{\epsilon\to 0^+} \int_0^t \mathrm{d}s_0 \int_{-t}^t \mathrm{d}u_1 \cdots \mathrm{d}u_{n-1} \\ &\quad \times \langle \mathcal{J}(u_{n-1} + (n-1)\mathrm{i}\epsilon)\cdots\mathcal{J}(u_1+\mathrm{i}\epsilon)\mathcal{J}(0)\rangle_{\mathrm{stat}}^{\mathrm{connected}} \\ &= \lim_{t\to\infty} t^{-1} \lim_{\epsilon\to 0^+} \int_{-t}^t \mathrm{d}u_1 \cdots \mathrm{d}u_{n-1} \\ &\quad \times \langle \mathcal{J}(u_{n-1} + (n-1)\mathrm{i}\epsilon)\cdots\mathcal{J}(u_1+\mathrm{i}\epsilon)\mathcal{J}(0)\rangle_{\mathrm{stat}}^{\mathrm{connected}} \\ &\quad \times \int_{\max(-u_1,\ldots,-u_{n-1},0)}^{\min(t-u_1,\ldots,t-u_n,t)} \mathrm{d}s_0. \end{aligned} \tag{A.4}$$

Since we expect that connected correlation functions decay exponentially at large time separations, whenever any u_j variable is large the integrand is exponentially suppressed. Hence the last factor can be approximated, for large t, by its value with $u_1 = \cdots = u_{n-1} = 0$, giving a factor of t. This shows (13).

Appendix B. Derivation of the NESSTBA equations

In this section we follow the arguments presented in [25] in order to obtain the TBA representation (25) of the exact non-equilibrium current. For simplicity, we restrict ourselves to models with a single-particle spectrum, but the derivation easily generalizes to many-particle types with diagonal scattering.

The idea of [25], in the present context, is to consider the trace representation (24) of the free energy f^a on a periodic space of finite length L, and to evaluate it in the limit $L \to \infty$ by analyzing the state that provides the leading contribution in this limit. At finite L, one assumes that the states are described by the Bethe ansatz associated with the QFT two-particle scattering matrix $S(\theta)$. In particular, there is a discrete set of states, and the distribution of Bethe roots is fixed from Bethe ansatz equations, the periodicity condition of the wavefunction on the circle of length L. One must also make a choice of density matrix ρ^L_{stat} which extrapolates to ρ_{stat} at $L \to \infty$, and as said in the text, here we choose (20).

One describes the Bethe ansatz states using densities of 'levels' or single-particle states $\rho(\theta)$, and of particles $\nu(\theta)$, as functions of the rapidity (so that $\rho(\theta)\,\mathrm{d}\theta$ and $\nu(\theta)\,\mathrm{d}\theta$ are the number of available levels and the number of particles, respectively, between rapidities θ and $\theta + \mathrm{d}\theta$). The Bethe ansatz equations relate these two as follows:

$$2\pi\rho(\theta) = L\frac{\mathrm{d}p(\theta)}{\mathrm{d}\theta} + \int \mathrm{d}\gamma\, \varphi(\theta-\gamma)\,\nu(\gamma) \tag{B.1}$$

where $p(\theta) := m\sinh\theta$ is the momentum at rapidity θ and $\varphi(\theta) = -\mathrm{i}\partial_\theta S(\theta)$. This equation simply means that the non-interacting level density $(1/2\pi)(\mathrm{d}p(\theta)/\mathrm{d}\theta)$ at rapidity θ is modified, thanks to the interaction, by the presence of particles at other rapidities. The densities giving rise to the leading contribution of the trace of the operator $\rho^L_{\mathrm{stat}}\mathrm{e}^{-aP}$ in (24) are evaluated by minimizing the free energy functional $\mathcal{F}^a[\rho,\nu] := W^a[\nu] - \mathcal{L}[\rho,\nu]$. The term $W^a[\nu]$ is the functional of the particle density $\nu(\theta)$ that corresponds to the negative of the logarithm of the operator $\rho^L_{\mathrm{stat}}\mathrm{e}^{-aP}$; this is, thanks to (20) and (7),

$$W^a[\nu] = \int \mathrm{d}\theta\,(W(\theta) + a\,p(\theta))\,\nu(\theta).$$

The term $\mathcal{L}[\rho,\nu]$ is the number of actual Bethe states (entropy) corresponding to ρ and ν in the 'fermionic case' (the one that applies in the models considered here), see [25],

$$\mathcal{L}[\rho,\nu] = \int \mathrm{d}\theta\,\big(\rho(\theta)\log\rho(\theta) - \nu(\theta)\log\nu(\theta) - (\rho(\theta)-\nu(\theta))\log(\rho(\theta)-\nu(\theta))\big).$$

The minimization of $\mathcal{F}^a[\rho,\nu]$ under the constraint (B.1) leads to the equation

$$\epsilon(\theta) = W(\theta) + a\,p(\theta) - \int \frac{\mathrm{d}\gamma}{2\pi}\,\varphi(\theta-\gamma)\log(1+\mathrm{e}^{-\epsilon(\gamma)}) \tag{B.2}$$

for the pseudo-energy

$$\epsilon(\theta) := \log\left(\frac{\rho(\theta)}{\nu(\theta)} - 1\right). \tag{B.3}$$

The value of the trace $\mathrm{Tr}_L\left(\rho_{\mathrm{stat}}^L \mathrm{e}^{-aP}\right)$ in (24) as $L \to \infty$ is hence dominated by the choice of the densities satisfying simultaneously (B.1) and (B.2). Let us denote these densities by $\rho^a(\theta)$ and $\nu^a(\theta)$, and let us similarly use $\epsilon^a(\theta)$ for the associated pseudo-energy. The value of the trace is then $\mathrm{e}^{-Lf^a+O(1)}$, where $Lf^a = \mathcal{F}^a[\rho^a, \nu^a]$. Using (B.1) and (B.2) it turns out [25] that this value can be expressed solely in terms of the pseudo-energy,

$$f^a = -\int \frac{\mathrm{d}\theta}{2\pi}\frac{\mathrm{d}p(\theta)}{\mathrm{d}\theta}\log(1+\mathrm{e}^{-\epsilon^a(\theta)}). \tag{B.4}$$

This is easily generalizable to a spectrum of more than one-particle type, as long as the scattering is diagonal; in this case we have many pseudo-energies $\epsilon_i^a(\theta)$ for $i = 1, \ldots, \ell$ particle types (as well as many level densities and particle densities). Along with the expression of J in (24), we then find (25), where we note that $x_i(\theta) = \mathrm{d}\epsilon_i^a(\theta)/\mathrm{d}a\big|_{a=0}$ and $\epsilon_i(\theta) = \epsilon_i^{a=0}(\theta)$.

In order to obtain (26), we observe that the current (25) can be written as

$$J(\beta_{\mathrm{l}}, \beta_{\mathrm{r}}) = (E, (1-\varphi)^{-1} \star p). \tag{B.5}$$

Here we define the inner product

$$(f, g) := \frac{1}{2\pi}\sum_i \int \frac{\mathrm{d}\theta}{1+\mathrm{e}^{\epsilon_i(\theta)}} f_i(\theta)\, g_i(\theta) \tag{B.6}$$

and the linear operation

$$(\mathcal{O} \star f)_i(\theta) := \frac{1}{2\pi}\sum_j \int \frac{\mathrm{d}\gamma}{1+\mathrm{e}^{\epsilon_j(\gamma)}} \mathcal{O}_{ij}(\theta-\gamma) f_j(\gamma), \tag{B.7}$$

and we use $E_i(\theta) := m_i \cosh(\theta)$ and $p_i(\theta) := m_i \sinh(\theta)$. Indeed (B.5) holds because, in this notation and according to (25), we have $J = (E, x)$, where x satisfies the equation $x = p + \varphi \star x$, whose solution is $x = (1-\varphi)^{-1} \star p = p + \varphi \star p + \varphi \star \varphi \star p + \ldots$.

We note that by unitarity, $S_{ij}(\theta)S_{ji}(-\theta) = 1$. Hence, $\varphi_{ij}(\theta) = \varphi_{ji}(-\theta)$. This implies that φ is a Hermitian operator under our inner product and linear operation:

$$(f, \varphi \star g) = (\varphi \star f, g). \tag{B.8}$$

Hence also $(1-\varphi)^{-1}$ is Hermitian, so that we have

$$J(\beta_{\mathrm{l}}, \beta_{\mathrm{r}}) = (p, (1-\varphi)^{-1} \star E). \tag{B.9}$$

This is (26). It is simple to see that $\mu_i(\theta) = ((1-\varphi)^{-1} \star E)_i(\theta)$ is in fact equal to $2\pi\rho_i(\theta)/L$, proportional to the level density for particle type i at rapidity θ, thanks to (B.1) and (B.3) (generalized to many-particle types).

doi:10.1088/1742-5468/2014/03/P03011

Taking linear combinations of (25) and (26), one may obtain various expressions for the current. For instance, going back to the case of a single-particle spectrum $\ell = 1$ for simplicity, we may define

$$\pm m\mathrm{e}^{y_\pm(\theta)} = x(\theta) \pm \mu(\theta) \tag{B.10}$$

and we find the expression

$$\begin{aligned} J(\beta_\mathrm{l}, \beta_\mathrm{r}) &= \frac{m^2}{8\pi} \int \mathrm{d}\theta \, \frac{\mathrm{e}^{\theta + y_+(\theta)} - \mathrm{e}^{-\theta + y_-(\theta)}}{1 + \mathrm{e}^{\epsilon(\theta)}} \\ \mathrm{e}^{y_\pm(\theta)} &= \mathrm{e}^{\pm\theta} + \int \frac{\mathrm{d}\theta}{2\pi} \, \frac{\varphi(\theta - \gamma)\, \mathrm{e}^{y_\pm(\gamma)}}{1 + \mathrm{e}^{\epsilon(\gamma)}}. \end{aligned} \tag{B.11}$$

The equality of (25) and (26) further gives

$$\int \mathrm{d}\theta \, \frac{\mathrm{e}^{\theta + y_-(\theta)}}{1 + \mathrm{e}^{\epsilon(\theta)}} = \int \mathrm{d}\theta \, \frac{\mathrm{e}^{-\theta + y_+(\theta)}}{1 + \mathrm{e}^{\epsilon(\theta)}}. \tag{B.12}$$

We note that in combination with the symmetry of $\epsilon(\theta)$ under the simultaneous exchange $\theta \leftrightarrow -\theta$ and $\beta_\mathrm{l} \leftrightarrow \beta_\mathrm{r}$, the above implies that both sides of (B.12) are actually invariant under $\beta_\mathrm{l} \leftrightarrow \beta_\mathrm{r}$.

Appendix C. High-temperature limit

In this appendix we will consider the expression for the current presented in (25) in terms of thermodynamic quantities and carry out its high-temperature limit. We will rigorously show how this limit leads to the known CFT expression (17). Our computation follows closely the work [25], where a similar analysis was carried out for the effective central charge $c_\mathrm{eff}(r)$.

Recall the relationship between the current and the free energy (24) which, in an ℓ-particle system, is given by

$$f^a = -\sum_{i=1}^{\ell} \int \frac{\mathrm{d}\theta}{2\pi} m_i \cosh\theta \log(1 + \mathrm{e}^{-\epsilon_i(\theta)}). \tag{C.1}$$

We can rewrite (C.1) as

$$f^a = -\sum_{i=1}^{\ell} \int_{-\infty}^{0} \frac{\mathrm{d}\theta}{2\pi} \frac{r_{ir}}{\beta_\mathrm{r}} \cosh\theta L_i(\theta) - \sum_{i=1}^{\ell} \int_{0}^{\infty} \frac{\mathrm{d}\theta}{2\pi} \frac{r_{il}}{\beta_\mathrm{l}} \cosh\theta L_i(\theta) := f^a_\mathrm{r} + f^a_\mathrm{l} \tag{C.2}$$

where $r_{ir} = m_i\beta_\mathrm{r}$ and $r_{il} = m_i\beta_\mathrm{l}$. We can obtain the steady-state current in CFT by taking the limits $r_{ir} \to 0$ and $r_{il} \to 0$. In this high-temperature limit, $\epsilon_i(\theta)$ and consequently $L_i(\theta)$ are constants with limiting values $\epsilon_i(0), L_i(0)$ in the central region $-\log(2/r_{ir}) \ll \theta \ll \log(2/r_{il})$ and it goes to infinity at the two edges. Therefore, $L_i(\theta)$ exhibits a typical plateau behavior in the central region and has a double exponential falloff outside this region (we have seen many graphical examples of this in previous sections). As r_{il} and

doi:10.1088/1742-5468/2014/03/P03011

r_{ir} go to zero, the plateaux become wider and the form of their two edges tends to some universal pattern. The limiting form of the left edge is determined by the 'kink' solution $L_{ik-}(\theta)$ which satisfies the equation

$$-\left(1-\frac{a}{\beta_r}\right)\mathrm{e}^{-\theta}+\epsilon_{ik-}(\theta)+\sum_{j=1}^{\ell}\int\frac{\mathrm{d}\theta'}{2\pi}\varphi_{ij}(\theta-\theta')L_{jk-}(\theta')=0 \tag{C.3}$$

where $\epsilon_{ik-}(\theta)\equiv\epsilon_i[\theta-\log(2/r_{ir})]$ and $L_{ik-}(\theta)\equiv L_i[\theta-\log(2/r_{ir})]$. Similarly, the limiting form of the right edge is determined by the function $L_{ak+}(\theta)$ which satisfies the equation

$$-\left(1+\frac{a}{\beta_l}\right)\mathrm{e}^{\theta}+\epsilon_{ik+}(\theta)+\sum_{j=1}^{\ell}\int\frac{\mathrm{d}\theta'}{2\pi}\varphi_{ij}(\theta-\theta')L_{jk+}(\theta')=0 \tag{C.4}$$

where $\epsilon_{ik+}(\theta)\equiv\epsilon_i[\theta+\log(2/r_{il})]$ and $L_{ik+}(\theta)\equiv L_i[\theta+\log(2/r_{il})]$. These equations follow from (29) by performing the indicated rapidity shifts. We can now rewrite the high-temperature limit of the 'free energies' $f^a_{\mathrm{r,l}}$ in terms of these new 'kink' functions as

$$f^a_{\mathrm{r}}=-\frac{1}{\beta_r}\sum_{i=1}^{\ell}\int\frac{\mathrm{d}\theta}{2\pi}\mathrm{e}^{-\theta}L_{ik-}(\theta),\qquad f^a_{\mathrm{l}}=-\frac{1}{\beta_l}\sum_{i=1}^{\ell}\int\frac{\mathrm{d}\theta}{2\pi}\mathrm{e}^{\theta}L_{ik+}(\theta). \tag{C.5}$$

Differentiating (C.3) and (C.4) with respect to θ we have

$$\left(1-\frac{a}{\beta_r}\right)\mathrm{e}^{-\theta}+\frac{\partial\epsilon_{ik-}(\theta)}{\partial\theta}+\sum_{j=1}^{\ell}\int\frac{\mathrm{d}L_{jk-}(\theta')}{2\pi}\varphi_{ij}(\theta-\theta')=0 \tag{C.6}$$

and

$$-\left(1+\frac{a}{\beta_l}\right)\mathrm{e}^{\theta}+\frac{\partial\epsilon_{ik+}(\theta)}{\partial\theta}+\sum_{j=1}^{\ell}\int\frac{\mathrm{d}L_{jk+}(\theta')}{2\pi}\varphi_{ij}(\theta-\theta')=0. \tag{C.7}$$

Solving these equations for $\mathrm{e}^{\pm\theta}$ and substituting $\mathrm{e}^{-\theta}$ in f^a_{r} and e^{θ} in f^a_{l} we obtain

$$f^a_{\mathrm{r}}=\frac{1}{\beta_r-a}\sum_{i=1}^{\ell}\int\frac{\mathrm{d}\theta}{2\pi}\left(\frac{\partial\epsilon_{ik-}(\theta)}{\partial\theta}+\sum_{j=1}^{\ell}\int\frac{\mathrm{d}L_{jk-}(\theta')}{2\pi}\varphi_{ij}(\theta-\theta')\right)L_{ik-}(\theta) \tag{C.8}$$

and

$$f^a_{\mathrm{l}}=-\frac{1}{\beta_l+a}\sum_{i=1}^{\ell}\int\frac{\mathrm{d}\theta}{2\pi}\left(\frac{\partial\epsilon_{ik+}(\theta)}{\partial\theta}+\sum_{j=1}^{\ell}\int\frac{\mathrm{d}L_{jk+}(\theta')}{2\pi}\varphi_{ij}(\theta-\theta')\right)L_{ik+}(\theta). \tag{C.9}$$

Let us consider f^a_{r} in more detail. When $r_{ir},r_{il}\to 0$ we can rewrite it as

$$f^a_{\mathrm{r}}=\frac{1}{\beta_r-a}\frac{1}{2\pi}\left[\sum_{i=1}^{\ell}\int_{\epsilon_i(0)}^{\infty}\mathrm{d}\epsilon\log(1+\mathrm{e}^{-\epsilon})-\sum_{i,j=1}^{\ell}\int_{\epsilon_i(0)}^{\infty}\frac{\mathrm{d}\epsilon_{ik-}}{1+\mathrm{e}^{\epsilon_{ik-}}}\varphi_{ij}*L_{jk-}(\theta)\right], \tag{C.10}$$

doi:10.1088/1742-5468/2014/03/P03011

where we assumed there is parity invariance $\varphi_{ij}(\theta) = \varphi_{ji}(\theta)$ and used $\mathrm{d}L = -\mathrm{d}\epsilon/(1+\mathrm{e}^{\epsilon})$. We can now substitute the convolution $\varphi_{ij} * L_{jk-}(\theta)$ by its expression from equation (C.3), which leads to

$$\int_{\epsilon_i(0)}^{\infty} \frac{\mathrm{d}\epsilon_{ik-}}{1+\mathrm{e}^{-\epsilon_{ik-}}} \varphi_{ij} * L_{jk-}(\theta) = -\int_{\epsilon_i(0)}^{\infty} \frac{\epsilon_{ik-}\mathrm{d}\epsilon_{ik-}}{1+\mathrm{e}^{\epsilon_{ik-}}} + \frac{\beta_{\mathrm{r}}-a}{\beta_{\mathrm{r}}} \int_{L_i(0)}^{\infty} \mathrm{e}^{-\theta}\mathrm{d}L_{ik-}$$

$$= -\int_{\epsilon_i(0)}^{\infty} \frac{\epsilon_{ik-}\mathrm{d}\epsilon_{ik-}}{1+\mathrm{e}^{\epsilon_{ik-}}} + \frac{\beta_{\mathrm{r}}-a}{\beta_{\mathrm{r}}} \int_{-\log(r_{ir}/2)}^{\infty} \mathrm{e}^{-\theta} L_{ik-}\mathrm{d}\theta. \qquad \text{(C.11)}$$

In the last line we have used integration by parts. We note that the last term is (up to constants and summing up in i) nothing but the original function f_{r}^a. We can therefore substitute in (C.10) and solve for f_{r}^a. An identical calculation can be performed for f_{l}^a, leading to:

$$f^a = \frac{1}{4\pi}\left(\frac{1}{\beta_{\mathrm{r}}-a} - \frac{1}{\beta_{\mathrm{l}}+a}\right) \sum_{i=1}^{\ell} \int_{\epsilon_i(0)}^{\infty} \mathrm{d}\epsilon \left(\log(1+\mathrm{e}^{-\epsilon}) + \frac{\epsilon}{1+\mathrm{e}^{\epsilon}}\right). \qquad \text{(C.12)}$$

Differentiating (C.12) with respect to a and setting $a = 0$, finally we have

$$J(\beta_{\mathrm{l}}, \beta_{\mathrm{r}}) = \frac{1}{4\pi}\left[\frac{1}{\beta_l^2} - \frac{1}{\beta_r^2}\right] \sum_{i}^{\ell} \int_{\epsilon_i(0)}^{\infty} \mathrm{d}\epsilon \left(\log(1+\mathrm{e}^{-\epsilon}) + \frac{\epsilon}{1+\mathrm{e}^{\epsilon}}\right) = \frac{\pi c}{12}(T_{\mathrm{l}}^2 - T_{\mathrm{r}}^2). \qquad \text{(C.13)}$$

The last equality follows from the identification of the central charge with the integral above (up to the constant $\pi^2/3$). This integral provides a representation of Roger's dilogarithm function. The connection of this function with the central charge has been discussed in detail in the classic literature on the subject [25, 104]. The values $\epsilon_i(0)$ can be obtained by solving the constant TBA equations which were introduced in [104]. These can be obtained from the original (both at and out of equilibrium) TBA equations by exploiting the additional fact that the TBA kernel is usually picked about $\theta = 0$. This implies that in the high-energy (temperature) limit the kernels $\varphi_{ij} * L_j(\theta)$ may be approximated by assuming that $L_j(\theta)$ is constant for θ near zero

$$\varphi_{ij} * L_j(\theta) \approx N_{ij} \log(1+\mathrm{e}^{-\epsilon_i(0)}), \qquad \text{(C.14)}$$

with $N_{ij} = -(1/2\pi)\int \varphi_{ij}(\theta)\mathrm{d}\theta$ so that the TBA equations become

$$\epsilon_i(0) = \sum_{j=1}^{\ell} N_{ij} \log(1+\mathrm{e}^{-\epsilon_j(0)}). \qquad \text{(C.15)}$$

This is a set of coupled algebraic equations which have been solved for many families of models and which exhibit very interesting structures (see e.g. [108] for a recent review).

Another interesting physical situation corresponds to the case when one temperature is kept constant and low while the other temperature becomes very large. Thus we have $r_{il} = \text{const.}$ and $r_{ir} \to 0$. In order to study the current in this case we may follow identical steps as above, starting with the separation of the ground state energy into the two contributions (C.2). In this situation the functions $\epsilon_i(\theta)$ are no longer continuous at $\theta = 0$

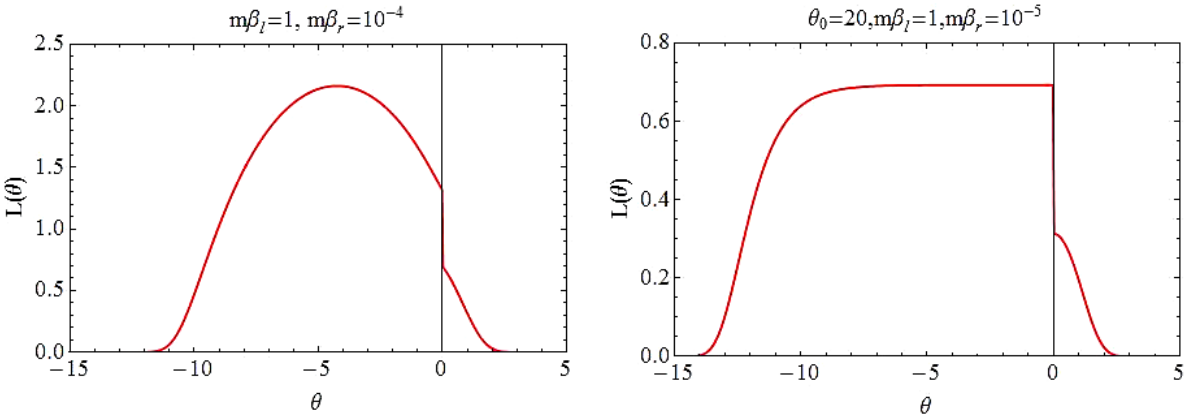

Figure C.1. L-functions for large values of $m\beta_\mathrm{l}$ and small values of $m\beta_\mathrm{r}$ in the sinh-Gordon and roaming trajectories model.

due to the presence of $W(\theta)$ in the TBA equations. Thus, they have two different limiting values at $\theta = 0$ with the relation:

$$\epsilon_{i+}(0) = \epsilon_{i-}(0) - r_{il}, \tag{C.16}$$

where we use the notation $\epsilon_{i+}(\theta)$ and $\epsilon_{i-}(\theta)$ to represent $\epsilon(\theta)$ in the regions $\theta > 0$ and $\theta < 0$, respectively. Also we have to note that the left–right asymmetry of the L-function has been broken. The left part of the L-function remains the same: it has a plateau at $\log(1 + \mathrm{e}^{-\epsilon_{i-}(0)})$ in the region $-\log(2/r_{ir}) \ll \theta < 0$. But the right part has only a quick exponential falloff, since $\epsilon_{i+}(\theta) \approx r_{il} \cosh\theta$ for $\theta > 0$ and $r_{il} \geq 1$. Therefore it does not show any plateau behavior. These features are particularly clear in the second plot of figure C.1, which gives the L-function of the roaming trajectories model. A clear discontinuity is also observed in the first figure, albeit the L-function does not display a plateau on the left-hand side due to the particular features of the sinh-Gordon model already discussed in section 5.

Thus f_l^a is simply defined by the second term in (C.2) and cannot be further simplified. f_r^a can be computed exactly as before, leading to the same result, that is the first term in (C.12). By differentiating with respect to a and setting $a = 0$ the following result is obtained:

$$\begin{aligned} J(\beta_\mathrm{l}, \beta_\mathrm{r}) &= \sum_{i=1}^{\ell} \left[\int_0^\infty \frac{\mathrm{d}\theta}{2\pi} m_i \cosh\theta \frac{x_{i+}(\theta)}{1 + \mathrm{e}^{\varepsilon_{i+}(\theta)}} + \frac{1}{4\pi\beta_\mathrm{r}^2} \int_{\epsilon_{i-}(0)}^\infty \mathrm{d}\epsilon \left(\log(1 + \mathrm{e}^{-\epsilon}) + \frac{\epsilon}{1 + \mathrm{e}^{\epsilon}} \right) \right] \\ &= \sum_{i=1}^{\ell} \int_0^\infty \frac{\mathrm{d}\theta}{2\pi} m_i \cosh\theta \frac{x_{i+}(\theta)}{1 + \mathrm{e}^{\varepsilon_{i+}(\theta)}} + \frac{\pi c}{12\beta_\mathrm{r}^2}, \end{aligned} \tag{C.17}$$

where $x_{i+}(\theta)$ can be obtained from (B.2) as $x_{i+}(\theta) = \mathrm{d}\epsilon_{i+}(\theta)/\mathrm{d}a|_{a=0}$.

An interesting conclusion to be drawn from this is that a configuration where one temperature is high and the other is low will still give rise to c-functions $c_n(T_\mathrm{l}, T_\mathrm{r})$ such

as the ones shown in figure 11. This is because when dividing the cumulants by $T_{\rm l}^{n+1} + (-1)^n T_{\rm r}^{n+1}$ the coefficient of the singularities of the cumulants is extracted and this is the same as when both right and left temperatures are high. This is the reason why in the last graph of figure 11 we can still see the usual plateau structure, even though $m\beta_{\rm l} = 1$ is rather large.

Appendix D. Low-temperature expansion

Although the TBA equations generally need to be solved numerically, at low temperatures a perturbative expansion may be used, leading to analytic results. In particular these analytic results will allow us to establish rigorously the result $P(\beta, \sigma\beta) \neq 0$ as discussed in appendix E. In order to do this, we will consider once more the original TBA equations (25). For simplicity, let us consider a theory with a single-particle spectrum (such as the sinh-Gordon model). We will start by rewriting the TBA equation as follows:

$$y(\theta) = \eta(\theta) \exp\left((\varphi * L)(\theta)\right), \tag{D.1}$$

where $y(\theta) := \mathrm{e}^{-\epsilon(\theta)}$ and $\eta(\theta) := \mathrm{e}^{-W(\theta)}$. For low temperatures, the function $W(\theta)$ takes large values, thus $y(\theta)$ is generally very small. We can therefore expand the exponential on the right-hand side of (D.1) up to and including the second order in $\eta(\theta)$ as

$$y(\theta) = \eta(\theta)\left(1 + (\varphi * L)(\theta) + \tfrac{1}{2}(\varphi * L)^2(\theta) + \cdots\right), \tag{D.2}$$

and approximate the L-function as

$$L(\theta) = \log(1 + y(\theta)) \approx y(\theta) - \frac{y(\theta)^2}{2} + \frac{y(\theta)^3}{3!} + \cdots. \tag{D.3}$$

Combining these two expansions and keeping only up to order $\eta(\theta)^2$ terms we find

$$y(\theta) \approx \eta(\theta)\left(1 + (\varphi * \eta)(\theta)\right). \tag{D.4}$$

We now want to use this result to study the non-additivity of the current $J(\beta_{\rm l}, \beta_{\rm r})$. As seen earlier, the current is of the form

$$J(\beta_{\rm l}, \beta_{\rm r}) = \frac{m}{2\pi}\int_{-\infty}^{\infty} \mathrm{d}\theta \cosh\theta \frac{x(\theta)y(\theta)}{1 + y(\theta)} \approx \frac{m}{2\pi}\int_{-\infty}^{\infty} \mathrm{d}\theta \cosh\theta x(\theta)y(\theta)(1 - y(\theta)), \tag{D.5}$$

The product $x(\theta)y(\theta)$ can be approximated as

$$-x(\theta)y(\theta) = y'(\theta) = \eta'(\theta)\left(1 + (\varphi * \eta)(\theta)\right) + \eta(\theta)(\varphi * \eta')(\theta), \tag{D.6}$$

where $y'(\theta) = \mathrm{d}y(\theta)/\mathrm{d}a|_{a=0}$ and $y(\theta, z)$ is the function $\mathrm{e}^{\epsilon(\theta)}$ as defined by the equation (B.2) and similarly for $\eta'(\theta)$. Thus, at order η^2 the current is

$$J(\beta_{\rm l}, \beta_{\rm r}) \approx \frac{m^2}{2\pi}\int_{-\infty}^{\infty} \mathrm{d}\theta \cosh\theta\eta(\theta)\left(\sinh\theta\left(1 - \eta(\theta) + (\varphi * \eta)(\theta)\right) - (\varphi * \eta')(\theta)\right), \tag{D.7}$$

doi:10.1088/1742-5468/2014/03/P03011

where we used the fact that $\eta'(\theta) = -m\sinh\theta\,\eta(\theta)$. Due to the structure of $W(\theta)$ it is clear that the terms

$$e(\beta_{\rm l},\beta_{\rm r}) := \frac{m^2}{4\pi}\int_{-\infty}^{\infty}{\rm d}\theta\sinh 2\theta\,\eta(\theta)\,(1-\eta(\theta))\,, \tag{D.8}$$

provide an additive contribution in the sense that they have the structure $f(\beta_{\rm l}) - f(\beta_{\rm r})$. We will now show that this is not the case for the other two terms. We will call this contribution to the current $r(\beta_{\rm l},\beta_{\rm r})$ and it is given by

$$r(\beta_{\rm l},\beta_{\rm r}) := \frac{m^2}{2\pi}\int_{-\infty}^{\infty}{\rm d}\theta\cosh\theta\,\eta(\theta)\,(\sinh\theta(\varphi*\eta)(\theta) - (\varphi*\eta')(\theta))\,. \tag{D.9}$$

Let us write the function explicitly:

$$\begin{aligned} r(\beta_{\rm l},\beta_{\rm r}) \;=\; & m^2\int_{-\infty}^{\infty}\int_{-\infty}^{\infty}\frac{{\rm d}\theta\,{\rm d}\gamma}{2(2\pi)^2}\sinh 2\theta\,{\rm e}^{W(\theta)}\varphi(\theta-\gamma){\rm e}^{W(\gamma)} \\ & + m^2\int_{-\infty}^{\infty}\int_{-\infty}^{\infty}\frac{{\rm d}\theta\,{\rm d}\gamma}{2\pi}\cosh\theta\sinh\beta\,{\rm e}^{W(\theta)}\varphi(\theta-\gamma){\rm e}^{W(\gamma)}. \end{aligned} \tag{D.10}$$

Employing the definition of $W(\theta)$, the integrals above split into four regions, depending on the sign of θ and γ:

$$\begin{aligned} r(\beta_{\rm l},\beta_{\rm r}) = {} & m^2\int_0^{\infty}\int_0^{\infty}\frac{{\rm d}\theta\,{\rm d}\gamma}{2(2\pi)^2}\sinh(2\theta){\rm e}^{-\beta_{\rm l}m\cosh\theta}\varphi(\theta-\gamma){\rm e}^{-\beta_{\rm l}m\cosh\gamma} \\ & + m^2\int_0^{\infty}\int_{-\infty}^{0}\frac{{\rm d}\theta\,{\rm d}\gamma}{2(2\pi)^2}\sinh(2\theta){\rm e}^{-\beta_{\rm l}m\cosh\theta}\varphi(\theta-\gamma){\rm e}^{-\beta_{\rm r}m\cosh\gamma} \\ & + m^2\int_{-\infty}^{0}\int_{-\infty}^{0}\frac{{\rm d}\theta\,{\rm d}\gamma}{2(2\pi)^2}\sinh(2\theta){\rm e}^{-\beta_{\rm r}m\cosh\theta}\varphi(\theta-\gamma){\rm e}^{-\beta_{\rm r}m\cosh\gamma} \\ & + m^2\int_{-\infty}^{0}\int_{0}^{\infty}\frac{{\rm d}\theta\,{\rm d}\gamma}{2(2\pi)^2}\sinh(2\theta){\rm e}^{-\beta_{\rm r}m\cosh\theta}\varphi(\theta-\gamma){\rm e}^{-\beta_{\rm l}m\cosh\gamma} \\ & + m^2\int_0^{\infty}\int_0^{\infty}\frac{{\rm d}\theta\,{\rm d}\gamma}{2\pi}\cosh\theta\sinh\gamma{\rm e}^{-\beta_{\rm l}m\cosh\theta}\varphi(\theta-\gamma){\rm e}^{-\beta_{\rm l}m\cosh\gamma} \\ & + m^2\int_0^{\infty}\int_{-\infty}^{0}\frac{{\rm d}\theta\,{\rm d}\gamma}{2\pi}\cosh\theta\sinh\gamma{\rm e}^{-\beta_{\rm l}m\cosh\theta}\varphi(\theta-\gamma){\rm e}^{-\beta_{\rm r}m\cosh\gamma} \\ & + m^2\int_{-\infty}^{0}\int_{-\infty}^{0}\frac{{\rm d}\theta\,{\rm d}\gamma}{2\pi}\cosh\theta\sinh\gamma{\rm e}^{-\beta_{\rm r}m\cosh\theta}\varphi(\theta-\gamma){\rm e}^{-\beta_{\rm r}m\cosh\gamma} \\ & + m^2\int_{-\infty}^{0}\int_{0}^{\infty}\frac{{\rm d}\theta\,{\rm d}\gamma}{2\pi}\cosh\theta\sinh\gamma{\rm e}^{-\beta_{\rm r}m\cosh\theta}\varphi(\theta-\gamma){\rm e}^{-\beta_{\rm l}m^2\cosh\gamma}. \end{aligned} \tag{D.11}$$

It is now a tedious though simple computation to group these integrals together by changing variables $\theta\to-\theta$ and $\gamma\to-\gamma$ where appropriate. When doing this we will

use the fact that the kernel $\varphi(\theta)$ is, by definition, an even function. Grouping terms together we finally obtain

$$r(\beta_{\rm l},\beta_{\rm r}) = m^2\int_0^\infty\int_0^\infty \frac{{\rm d}\theta\,{\rm d}\gamma}{2(2\pi)^2}\left({\rm e}^{-\beta_{\rm l}m(\cosh\theta+\cosh\gamma)}-{\rm e}^{-\beta_{\rm r}m(\cosh\theta+\cosh\gamma)}\right)\sinh(2\theta)\varphi(\theta-\gamma)$$
$$+m^2\int_0^\infty\int_0^\infty \frac{{\rm d}\theta\,{\rm d}\gamma}{2\pi}\left({\rm e}^{-\beta_{\rm l}m(\cosh\theta+\cosh\gamma)}-{\rm e}^{-\beta_{\rm r}m(\cosh\theta+\cosh\gamma)}\right)\varphi(\theta-\gamma)\cosh\theta\sinh\gamma$$
$$+m^2\int_0^\infty\int_0^\infty \frac{{\rm d}\theta\,{\rm d}\gamma}{2(2\pi)^2}{\rm e}^{-\beta_{\rm l}m\cosh\theta}{\rm e}^{-\beta_{\rm r}m\cosh\gamma}\varphi(\theta+\gamma)\left(\sinh(2\theta)-\sinh(2\gamma)+2\sinh(\theta-\gamma)\right). \tag{D.12}$$

Examining the function $r(\beta_{\rm l},\beta_{\rm r})$ we see that the first two lines above again provide additive contributions, that is, they have the structure $f(\beta_{\rm l})-f(\beta_{\rm r})$. However, the last contribution, on the last line, is not additive as it is possible to show both analytically and numerically that it is nonzero. An analytical proof is provided in appendix E, whereas numerical evidence has been provided in section 8 for the sinh-Gordon and sine-Gordon models. Generalizing to an ℓ-particle spectrum and using the short-hand notation $l_\theta^i := \exp(-\beta_{\rm l}m_i\cosh\theta)$ and $r_\theta^i := \exp(-\beta_{\rm r}m_i\cosh\theta)$, we find the following low-temperature approximation

$$J(\beta_{\rm l},\beta_{\rm r}) \approx \sum_{i=1}^{\ell} m_i^2\int_0^\infty\frac{{\rm d}\theta}{2(2\pi)}\left(l_\theta^i-r_\theta^i-(l_\theta^i)^2+(r_\theta^i)^2\right)\sinh(2\theta)$$
$$+\sum_{i,j=1}^{\ell} m_i^2\int_0^\infty\int_0^\infty\frac{{\rm d}\theta\,{\rm d}\gamma}{(2\pi)^2}\left(l_\theta^i l_\gamma^j-r_\theta^i r_\gamma^j\right)\cosh(\theta)\varphi_{ij}(\theta-\gamma)(\sinh\theta+\sinh\gamma)$$
$$+\sum_{i,j=1}^{\ell} m_i^2\int_0^\infty\int_0^\infty\frac{{\rm d}\theta\,{\rm d}\gamma}{2(2\pi)^2}l_\theta^i r_\gamma^j\varphi_{ij}(\theta+\gamma)\left(\sinh(2\theta)\right.$$
$$\left.-\sinh(2\gamma)+2\sinh(\theta-\gamma)\right). \tag{D.13}$$

This low-temperature expansion can be compared with an expansion obtained directly from the trace expression (4)–(7) (we again assume a single-particle spectrum for simplicity). For convention, the finite-volume multi-particle states can be denoted as

$$|\theta_1,\ldots,\theta_n\rangle_L.$$

The corresponding energy levels are determined by the well-known Bethe ansatz equations

$$Q_k(\theta_1,\ldots,\theta_n) = mL\sinh\theta_k+\sum_{l\neq k}\delta(\theta_k-\theta_{\rm l}) = 2\pi I_k,\qquad k=1,\ldots,n \tag{D.14}$$

where I_k are momentum quantum numbers and $\delta(\theta) = -{\rm i}\log S(\theta)$ is the two-particle scattering phase-shift. The density of multi-particle states can be obtained by

$$\rho(\theta_1,\ldots,\theta_n) = \det\mathcal{J}^{(n)},\qquad \mathcal{J}^{(n)}_{kl} = \frac{\partial Q_k(\theta_1,\ldots,\theta_n)}{\partial\theta_{\rm l}},\quad k,l=1,\ldots,n. \tag{D.15}$$

doi:10.1088/1742-5468/2014/03/P03011

J. Stat. Mech. (2014) P03011

Let us expand the traces in (22):

$$\mathrm{Tr}_L(\rho^L_{\mathrm{stat}}P) = \sum_{\theta^{(1)}} \mathrm{e}^{-W(\theta^{(1)})} m\sinh\theta^{(1)} + \tfrac{1}{2}\sum{}'_{\theta^{(2)}_1\theta^{(2)}_2} \mathrm{e}^{-\sum_{i=1}^2 W(\theta^{(2)}_i)} \sum_{i=1}^{2} m\sinh\theta^{(2)}_i$$
$$+ \tfrac{1}{6}\sum{}'_{\theta^{(3)}_1\theta^{(3)}_2\theta^{(3)}_3} \mathrm{e}^{-\sum_{i=1}^3 W(\theta^{(3)}_i)} \sum_{i=1}^{3} m\sinh\theta^{(3)}_i + O(\mathrm{e}^{-4W}) \tag{D.16}$$

and

$$\mathrm{Tr}_L(\rho^L_{\mathrm{stat}}) = 1 + \sum_{\theta^{(1)}} \mathrm{e}^{-W(\theta^{(1)})} + \tfrac{1}{2}\sum{}'_{\theta^{(2)}_1\theta^{(2)}_2} \mathrm{e}^{-\sum_{i=1}^2 W(\theta^{(2)}_i)}$$
$$+ \tfrac{1}{6}\sum{}'_{\theta^{(3)}_1\theta^{(3)}_2\theta^{(3)}_3} \mathrm{e}^{-\sum_{i=1}^3 W(\theta^{(3)}_i)} + O(\mathrm{e}^{-4W}) \tag{D.17}$$

At low temperature, we have the expansion

$$\frac{1}{\mathrm{Tr}_L(\rho^L_{\mathrm{stat}})} = 1 - \sum_{\theta^{(1)}} \mathrm{e}^{-W(\theta^{(1)})} + \left(\sum_{\theta^{(1)}} \mathrm{e}^{-W(\theta^{(1)})}\right)^2 - \frac{1}{2}\sum{}'_{\theta^{(2)}_1\theta^{(2)}_2} \mathrm{e}^{-\sum_{i=1}^2 W(\theta^{(2)}_i)}$$
$$- \left(\sum_{\theta^{(1)}} \mathrm{e}^{-W(\theta^{(1)})}\right)^3 + \left(\sum_{\theta^{(1)}} \mathrm{e}^{-W(\theta^{(1)})}\right)\sum{}'_{\theta^{(2)}_1\theta^{(2)}_2} \mathrm{e}^{-\sum_{i=1}^2 W(\theta^{(2)}_i)}$$
$$- \tfrac{1}{6}\sum{}'_{\theta^{(3)}_1\theta^{(3)}_2\theta^{(3)}_3} \mathrm{e}^{-\sum_{i=1}^3 W(\theta^{(3)}_i)} + O(\mathrm{e}^{-4W}). \tag{D.18}$$

The prefactors $1/n!$ for every multi-particle sum take into account overcounted states with different ordering of the same set of rapidities. The prime in the multi-particle sum indicates all quantum numbers (rapidities) for the state are different. The upper indices of the rapidities and W represent the number of particles in the state.

With (D.16) and (D.18), we can now compute the current up to exponential corrections at finite volume L. In the limit $L \to \infty$, the low-temperature expansion of the current performed in the first part of this appendix should be recovered. Here, we present the calculation of the current up to the first three orders. Let us discuss the first-order contribution J_1 in detail. At first order we have the contribution

$$J^L_1 = \frac{1}{L}\sum_{\theta^{(1)}} \mathrm{e}^{-W(\theta^{(1)})} m\sinh\theta^{(1)}. \tag{D.19}$$

In order to compare with the low-temperature expansion we must consider infinite volume. This amounts to taking the limit $L \to \infty$ by replacing the sum over rapidities by an integral over the states in the rapidity space, that is $\sum_{\theta^{(1)}} \to \int(\mathrm{d}\theta/2\pi)\rho_1(\theta)$. The density of one-particle states $\rho_1(\theta)$ is obtained by

$$\rho_1(\theta) = L\frac{\mathrm{d}\,p(\theta)}{\mathrm{d}\theta} = \frac{\mathrm{d}\,m\sinh\theta}{\mathrm{d}\theta} = mL\cosh\theta. \tag{D.20}$$

doi:10.1088/1742-5468/2014/03/P03011

Therefore, the first-order term of the current is

$$J_1 = \lim_{L\to\infty} J_1^L = m^2 \int \frac{\mathrm{d}\theta}{2\pi} \mathrm{e}^{-W(\theta)} \sinh\theta \cosh\theta. \tag{D.21}$$

It can be easily seen that this agrees perfectly with the first contribution (e.g. order η) in equation (D.8). A similar computation can be performed for second-order terms. We define

$$\begin{aligned} J_2^L = \frac{1}{L}\Bigg[& -\sum_{\theta^{(1)}} \mathrm{e}^{-W(\theta^{(1)})} m\sinh\theta^{(1)} \sum_{\theta^{(1)}} \mathrm{e}^{-W(\theta^{(1)})} + \frac{1}{2}{\sum}' _{\theta_1^{(2)}\theta_2^{(2)}} \mathrm{e}^{-\sum_{i=1}^2 W(\theta_i^{(2)})} \sum_{i=1}^2 m\sinh\theta_i^{(2)} \Bigg] \\ = \frac{1}{L}\Bigg[& -\sum_{\theta^{(1)}} \mathrm{e}^{-W(\theta^{(1)})} m\sinh\theta^{(1)} \sum_{\theta^{(1)}} \mathrm{e}^{-W(\theta^{(1)})} \\ & + \tfrac{1}{2} \sum_{\theta_1^{(2)}\theta_2^{(2)}} \mathrm{e}^{-\sum_{i=1}^2 W(\theta_i^{(2)})} \sum_{i=1}^2 m\sinh\theta_i^{(2)} \\ & - \tfrac{1}{2} \sum_{\theta_1^{(2)}=\theta_2^{(2)}} \mathrm{e}^{-2W(\theta_1^{(2)})} 2m\sinh\theta_1^{(2)} \Bigg]. \end{aligned}$$

The last term has $\theta_1^{(2)} = \theta_2^{(2)}$ and corresponds to a two-particle state with equal quantum numbers of the two particles. In this case, the two-particle Bethe ansatz equations degenerate to a one-particle equation, which means that density of this two-particle state is again ρ_1. In the large-L limit, we may replace the sums with integrals as $\sum_{\theta^{(1)}} \to \int(\mathrm{d}\theta/2\pi)\rho_1(\theta)$, $\sum_{\theta_1^{(2)}=\theta_2^{(2)}} \to \int(\mathrm{d}\theta/2\pi)\rho_1(\theta)$ and $\sum_{\theta_1^{(2)}\theta_2^{(2)}} \to \int(\mathrm{d}\theta_1/2\pi)(\mathrm{d}\theta_2/2\pi)\rho_2(\theta_1,\theta_2)$. The Bethe ansatz equations for a two-particle state are

$$\begin{aligned} mL\sinh\theta_1 + \delta(\theta_1-\theta_2) &= Q_1(\theta_1\theta_2) \\ mL\sinh\theta_2 + \delta(\theta_2-\theta_1) &= Q_2(\theta_1\theta_2), \end{aligned} \tag{D.22}$$

so that the relevant density of two-particle states is given by

$$\rho_2(\theta_1,\theta_2) = \det \begin{pmatrix} mL\cosh\theta_1 + \varphi(\theta_1-\theta_2) & -\varphi(\theta_1-\theta_2) \\ -\varphi(\theta_1-\theta_2) & mL\sinh\theta_2 + \varphi(\theta_1-\theta_2) \end{pmatrix}.$$

Exploiting the fact that $\varphi(\theta) = \varphi(-\theta)$, relabeling integration variables and exchanging the order of integration, we obtain

$$\begin{aligned} J_2 \;=\; & m^2 \int \frac{\mathrm{d}\theta_1\,\mathrm{d}\theta_2}{(2\pi)^2} \cosh\theta_1(\sinh\theta_1 + \sinh\theta_2)\varphi(\theta_1-\theta_2)\mathrm{e}^{-W(\theta_1)-W(\theta_2)} \\ & - m^2 \int \frac{\mathrm{d}\theta}{2\pi} \cosh\theta\sinh\theta \mathrm{e}^{-2W(\theta)}. \end{aligned} \tag{D.23}$$

Once more this is in full agreement with (D.10) plus the second contribution in (D.8). Finally, we look at third-order contributions

$$J_3^L = \frac{1}{L}\Bigg[\sum_{\theta^{(1)}} \mathrm{e}^{-W(\theta^{(1)})} m\sinh\theta^{(1)} \Bigg(\sum_{\theta^{(1)}} \mathrm{e}^{-W(\theta^{(1)})}\Bigg)^2 - \frac{1}{2}\sum_{\theta^{(1)}} m\sinh\theta^{(1)} {\sum}'_{\theta_1^{(2)}\theta_2^{(2)}} \mathrm{e}^{-\sum_{i=1}^2 W(\theta_i^{(2)})}$$

$$- \tfrac{1}{2}{\sum}'_{\theta_1^{(2)}\theta_2^{(2)}} \mathrm{e}^{-\sum_{i=1}^2 W(\theta_i^{(2)})} \sum_{i=1}^{2} m\sinh\theta_i^{(2)} \sum_{\theta^{(1)}} \mathrm{e}^{-W(\theta^{(1)})}$$

$$+ \tfrac{1}{6}{\sum}'_{\theta_1^{(3)}\theta_2^{(3)}\theta_3^{(3)}} \mathrm{e}^{-\sum_{i=1}^3 W(\theta_i^{(3)})} \sum_{i=1}^{3} m\sinh\theta_i^{(3)}\Bigg]. \tag{D.24}$$

By using the relations

$${\sum}'_{\theta_1^{(2)}\theta_2^{(2)}} = \sum_{\theta_1^{(2)}\theta_2^{(2)}} - \sum_{\theta_1^{(2)}=\theta_2^{(2)}}$$

$${\sum}'_{\theta_1^{(3)}\theta_2^{(3)}\theta_3^{(3)}} = \sum_{\theta_1^{(3)}\theta_2^{(3)}\theta_3^{(3)}} - 3\sum_{\theta_1^{(3)},\theta_2^{(3)}=\theta_3^{(3)}} + 2\sum_{\theta_1^{(3)}=\theta_2^{(3)}=\theta_3^{(3)}}$$

we can rewrite

$$J_3^L = \frac{1}{L}\Bigg[\sum_{\theta^{(1)}} \mathrm{e}^{-W(\theta^{(1)})} m\sinh\theta^{(1)} \Bigg(\sum_{\theta^{(1)}} \mathrm{e}^{-W(\theta^{(1)})}\Bigg)^2 - \frac{1}{2}\sum_{\theta^{(1)}} m\sinh\theta^{(1)} \sum_{\theta_1^{(2)}\theta_2^{(2)}} \mathrm{e}^{-\sum_{i=1}^2 W(\theta_i^{(2)})}$$

$$+ \tfrac{1}{2}\sum_{\theta^{(1)}} m\sinh\theta^{(1)} \sum_{\theta_1^{(2)}=\theta_2^{(2)}} \mathrm{e}^{-2W(\theta_1^{(2)})}$$

$$- \tfrac{1}{2}\sum_{\theta_1^{(2)}\theta_2^{(2)}} \mathrm{e}^{-\sum_{i=1}^2 W(\theta_i^{(2)})} \sum_{i=1}^{2} m\sinh\theta_i^{(2)} \sum_{\theta^{(1)}} \mathrm{e}^{-W(\theta^{(1)})}$$

$$+ \tfrac{1}{2}\sum_{\theta_1^{(2)}=\theta_2^{(2)}} \mathrm{e}^{-2W(\theta_1^{(2)})} 2m\sinh\theta_1^{(2)} \sum_{\theta^{(1)}} \mathrm{e}^{-W(\theta^{(1)})}$$

$$+ \tfrac{1}{6}\sum_{\theta_1^{(3)}\theta_2^{(3)}\theta_3^{(3)}} \mathrm{e}^{-\sum_{i=1}^3 W(\theta_i^{(3)})} \sum_{i=1}^{3} m\sinh\theta_i^{(3)}$$

$$- \tfrac{1}{2}\sum_{\theta_1^{(3)},\theta_2^{(3)}=\theta_3^{(3)}} \mathrm{e}^{-W(\theta_1^{(3)})-2W(\theta_2^{(3)})} (m\sinh\theta_1^{(3)} + 2m\sinh\theta_2^{(3)})$$

$$+ \tfrac{1}{3}\sum_{\theta_1^{(3)}=\theta_2^{(3)}=\theta_3^{(3)}} \mathrm{e}^{-3W(\theta_1^{(3)})} 3m\sinh\theta_1^{(3)}\Bigg]. \tag{D.25}$$

In the large-L limit, we replace the sums with integrals as in previous cases with the addition of $\sum_{\theta_1^{(2)}\theta_2^{(2)}\theta_1^{(3)}} \to \int(\mathrm{d}\theta_1/2\pi)(\mathrm{d}\theta_2/2\pi)(\mathrm{d}\theta_3/2\pi)\rho_3(\theta_1,\theta_2,\theta_3)$, $\sum_{\theta_1^{(2)},\theta_2^{(2)}=\theta_1^{(3)}} \to$

$\int(\mathrm{d}\theta_1/2\pi)(\mathrm{d}\theta_2/2\pi)\rho_3(\theta_1,\theta_2=\theta_3)$ and $\sum_{\theta_1^{(2)}=\theta_2^{(2)}=\theta_1^{(3)}} \to \int(\mathrm{d}\theta/2\pi)\rho_1(\theta)$. The density $\rho_3(\theta_1, \theta_2=\theta_3)$ can be obtained from the Bethe ansatz equations for a three-particle state with two equal quantum numbers

$$\begin{aligned} mL\sinh\theta_1 + 2\delta(\theta_1-\theta_2) &= Q_1(\theta_1,\theta_2) \\ mL\sinh\theta_2 + \delta(\theta_2-\theta_1) &= Q_2(\theta_1,\theta_2). \end{aligned} \tag{D.26}$$

The relevant density is given by

$$\rho_3(\theta_1,\theta_2=\theta_3) = \det\begin{pmatrix} mL\cosh\theta_1 + 2\varphi(\theta_1-\theta_2) & -2\varphi(\theta_1-\theta_2) \\ -\varphi(\theta_1-\theta_2) & mL\sinh\theta_2+\varphi(\theta_1-\theta_2) \end{pmatrix}$$

Similarly, we can obtain $\rho_3(\theta_1,\theta_2,\theta_3)$ from the equations

$$\begin{aligned} mL\sinh\theta_1 + \delta(\theta_1-\theta_2)+\delta(\theta_1-\theta_3) &= Q_1(\theta_1,\theta_2,\theta_3) \\ mL\sinh\theta_2 + \delta(\theta_2-\theta_1)+\delta(\theta_2-\theta_3) &= Q_2(\theta_1,\theta_2,\theta_3) \\ mL\sinh\theta_3 + \delta(\theta_3-\theta_1)+\delta(\theta_3-\theta_2) &= Q_3(\theta_1,\theta_2,\theta_3), \end{aligned} \tag{D.27}$$

as

$$\det\begin{pmatrix} E_1L+\varphi(\theta_{12})+\varphi_(\theta_{13}) & -\varphi(\theta_{12}) & -\varphi(\theta_{13}) \\ -\varphi(\theta_{12}) & E_2L+\varphi(\theta_{12})+\varphi(\theta_{23}) & -\varphi(\theta_{23}) \\ -\varphi(\theta_{13}) & -\varphi(\theta_{23}) & E_3L+\varphi(\theta_{13})+\varphi(\theta_{23}) \end{pmatrix}, \tag{D.28}$$

where for convenience we used the notation $E_i \equiv m\cosh\theta_i$ and $\varphi(\theta_{ij}) \equiv \varphi(\theta_i-\theta_j)$. Therefore, by doing a similar but more tedious computation, we can obtain the third-order term of the current

$$\begin{aligned} J_3 = &-\frac{1}{2}m^2\int\frac{\mathrm{d}\theta_1\,\mathrm{d}\theta_2}{(2\pi)^2}\cosh\theta_1(\sinh\theta_1+2\sinh\theta_2)\varphi(\theta_1-\theta_2)\mathrm{e}^{-W(\theta_1)-2W(\theta_2)} \\ &+m^2\int\frac{\mathrm{d}\theta_1\,\mathrm{d}\theta_2\,\mathrm{d}\theta_3}{(2\pi)^3}\cosh\theta_1\sum_{i=1}^{3}(\sinh\theta_i)\varphi(\theta_1-\theta_2)\varphi(\theta_2-\theta_3)\mathrm{e}^{-\sum_{i=1}^3 W(\theta_i)} \\ &+\frac{1}{2}m^2\int\frac{\mathrm{d}\theta_1\mathrm{d}\theta_2\mathrm{d}\theta_3}{(2\pi)^3}\cosh\theta_1\sum_{i=1}^{3}(\sinh\theta_i)\varphi(\theta_1-\theta_2)\varphi(\theta_1-\theta_3)\mathrm{e}^{-\sum_{i=1}^3 W(\theta_i)} \\ &-m^2\int\frac{\mathrm{d}\theta_1\,\mathrm{d}\theta_2}{(2\pi)^2}\cosh\theta_1(2\sinh\theta_1+\sinh\theta_2)\varphi(\theta_1-\theta_2)\mathrm{e}^{-2W(\theta_1)-W(\theta_2)} \\ &+m^2\int\frac{\mathrm{d}\theta}{2\pi}\cosh\theta\sinh\theta\mathrm{e}^{-3W(\theta)}. \end{aligned} \tag{D.29}$$

Appendix E. Proof of non-additivity of the current

We consider a diagonal-scattering integrable QFT, assuming that all kernels $\varphi_{ij}(\theta)$ have a fixed sign (i.e. $\varphi_{ij}(\theta)$ is positive for every i,j and θ, or is negative for every i,j and θ).

This assumption is valid both for the sinh-Gordon model and the reflectionless sine-Gordon model studied above whose kernels only involve cosh functions. We analyze the second leading order in the low-temperature expansion of the additivity deficit (62), and show that it is nonzero for large enough βm and large enough σ. This is sufficient to prove that additivity does not hold in general. The derivation below is mathematically rigorous.

To second leading order in the low-temperature expansion, the current in a general diagonal-scattering model is

$$J(\beta_{\rm l},\beta_{\rm r})=\sum_{i=1}^{\ell}\frac{m_i^2}{2\pi}\int \mathrm{d}\theta\,\cosh\theta\,\eta_i(\theta)\Big(\sinh\theta\,(1-\eta_i(\theta))+(\varphi_{ij}*\eta_j)(\theta)-(\varphi_{ij}*\eta_j')(\theta)\Big), \tag{E.1}$$

which generalizes (D.7) to a multi-particle theory. As seen in appendix D the only non-additive contribution to (E.1) takes the form $\sum_{i,j} r_{ij}$ with

$$r_{ij}=\frac{m_i^2}{2(2\pi)^2}\int_0^\infty \mathrm{d}\theta\int_0^\infty \mathrm{d}\gamma\,\mathrm{e}^{-\beta_{\rm l}m_i\cosh\theta}\mathrm{e}^{-\beta_{\rm r}m_j\cosh\gamma}\,\varphi_{ij}(\theta+\gamma)$$
$$\times\Big(\sinh 2\theta-\sinh 2\gamma+2\sinh(\theta-\gamma)\Big) \tag{E.2}$$

that is, the last term in (D.13). Note that the function

$$U(\theta,\gamma):=\varphi_{ij}(\theta+\gamma)\Big(\sinh 2\theta-\sinh 2\gamma+2\sinh(\theta-\gamma)\Big), \tag{E.3}$$

is anti-symmetric under exchange of the rapidities, has a fixed sign for all $\theta>\gamma$. Let us denote $m_i:=am$ and $m_j:=bm$ for some mass scale m and positive numbers a,b (one may always take either $a=1$ or $b=1$ by an appropriate choice of scale m). Further, let us use the notation

$$e_\theta:=\mathrm{e}^{-\beta m\cosh\theta}. \tag{E.4}$$

Then the contribution of r_{ij} to the 'normalized' additivity deficit $\tilde P(\beta,\sigma)=\sum_{i,j=1}^{\ell}\tilde P_{ij}(\beta,\sigma)$ (62) is

$$\tilde P_{ij}(\beta,\sigma)=\frac{m_i^2}{2(2\pi)^2}\int_0^\infty \mathrm{d}\theta\int_0^\infty \mathrm{d}\gamma\,U(\theta,\gamma)\,\Big(e_\theta^a e_\gamma^{b\sigma}+e_\theta^{a\sigma}e_\gamma^{b\sigma^2}-e_\theta^a e_\gamma^{b\sigma^2}\Big), \tag{E.5}$$

where $\tilde P(\beta,\sigma)=J(\beta,\sigma^2\beta)\sum_{i,j=1}^{\ell}P_{ij}(\beta,\sigma)$. Symmetrizing under $\theta\leftrightarrow\gamma$ we find

$$\tilde P_{ij}(\beta,\sigma)=\frac{m_i^2}{2(2\pi)^2}\int_0^\infty \mathrm{d}\theta\int_0^\theta \mathrm{d}\gamma\,U(\theta,\gamma)\,\Big(e_\theta^a e_\gamma^{b\sigma}-e_\gamma^a e_\theta^{b\sigma}+e_\theta^{a\sigma}e_\gamma^{b\sigma^2}$$
$$-\,e_\gamma^{a\sigma}e_\theta^{b\sigma^2}-e_\theta^a e_\gamma^{b\sigma^2}+e_\gamma^a e_\theta^{b\sigma^2}\Big). \tag{E.6}$$

We now show that for every $\sigma>\max(a/b,1)$, every βm large enough, and every $\theta>\gamma$, the sum of the terms in the parenthesis on the right-hand side is positive. This then implies that the integrand has a fixed sign, and since it is obviously nonzero, it shows that the additivity deficit is nonzero.

First we have, for the middle two terms,

$$e_\theta^{a\sigma} e_\gamma^{b\sigma^2} - e_\gamma^{a\sigma} e_\theta^{b\sigma^2} = e_\theta^{a\sigma} e_\gamma^{a\sigma} \left(e_\gamma^{b\sigma^2 - a\sigma} - e_\theta^{b\sigma^2 - a\sigma} \right). \tag{E.7}$$

If $\sigma > a/b$, then thanks to $\theta > \gamma$ the factor in the parenthesis on the right-hand side is positive. The first factor is also obviously positive, hence the left-hand side is positive.

Second, for the remaining four terms, we find

$$e_\theta^a e_\gamma^{b\sigma} - e_\gamma^a e_\theta^{b\sigma} - e_\theta^a e_\gamma^{b\sigma^2} + e_\gamma^a e_\theta^{b\sigma^2} = e_\theta^a e_\gamma^a \left(e_\gamma^{b\sigma - a}(1 - e_\gamma^{b\sigma(\sigma-1)}) - e_\theta^{b\sigma - a}(1 - e_\theta^{b\sigma(\sigma-1)}) \right). \tag{E.8}$$

Let us consider the two terms in the outermost parenthesis on the right-hand side

$$K := e_\gamma^{b\sigma - a}(1 - e_\gamma^{b\sigma(\sigma-1)}) - e_\theta^{b\sigma - a}(1 - e_\theta^{b\sigma(\sigma-1)}). \tag{E.9}$$

The ratio of these two terms is

$$\left(\frac{e_\gamma}{e_\theta}\right)^{b\sigma - a} \frac{1 - e_\gamma^{b\sigma(\sigma-1)}}{1 - e_\theta^{b\sigma(\sigma-1)}} > \left(\frac{e_\gamma}{e_\theta}\right)^{b\sigma - a} \left(1 - e_\gamma^{b\sigma(\sigma-1)}\right) > \left(\frac{e_\gamma}{e_\theta}\right)^{b\sigma - a} \left(1 - \mathrm{e}^{-b\sigma(\sigma-1)\beta m}\right) \tag{E.10}$$

where the two inequalities hold if $\sigma > 1$. Then if $\sigma > a/b$ and if $\cosh\theta - \cosh\gamma$ is greater than

$$\frac{\log\left(1 - \mathrm{e}^{-b\sigma(\sigma-1)\beta m}\right)}{(b\sigma - a)\beta m},$$

which can be made as small as desired by taking βm large enough, the right-hand side of the last inequality above is greater than one, whence K is positive. Further, it is clear that K is zero at $\gamma = \theta$ and continuous and differentiable for $\gamma \in [0, \theta]$. We now show that it has no minimum in that range. Denoting $x = e_\gamma$ and $y = e_\theta$, we look for a minimum in x in the range $x \in [y, 1]$, for $y > 0$. Differentiating with respect to x, a minimum may occur if

$$(b\sigma - a)x^{b\sigma - a - 1} - (b\sigma^2 - a)x^{b\sigma^2 - a - 1} = 0 \quad \Rightarrow \quad x = \frac{1}{b\sigma(\sigma - 1)} \log\left(\frac{b\sigma - a}{b\sigma^2 - a}\right).$$

The right-hand side is smaller than zero if $\sigma > 1$, which puts the minimum outside of the range for any $y > 0$.

References

[1] Esposito M, Harbola U and Mukamel S, *Nonequilibrium fluctuations, fluctuation theorems and counting statistics in quantum systems*, 2009 *Rev. Mod. Phys.* **81** 16651702

[2] Campisi M, Hänggi P and Talkner P, *Colloquium: quantum fluctuation relations: foundations and applications*, 2011 *Rev. Mod. Phys.* **83** 771

[3] Utsumi Y, Golubev D, Marthaler M, Saito K, Fujisawa T and Schön G, *Bidirectional single-electron counting and the fluctuation theorem*, 2010 *Phys. Rev.* B **81** 125331

[4] Nakamura S, Yamauchi Y, Hashisaka M, Chida K, Kobayashi K, Ono T, Leturcq R, Ensslin K, Saito K, Utsumi Y and Gossard A C, *Nonequilibrium fluctuation relations in a quantum coherent conductor*, 2010 *Phys. Rev. Lett.* **104** 080602

[5] Nakamura S, Yamauchi Y, Hashisaka M, Chida K, Kobayashi K, Ono T, Leturcq R, Ensslin K, Saito K, Utsumi Y and Gossard A C, *Fluctuation theorem and microreversibility in a quantum coherent conductor*, 2011 *Phys. Rev.* B **83** 155431

[6] Sánchez R and Büttiker M, *Detection of single-electron heat transfer statistics*, 2012 *Europhys. Lett.* **100** 47008
[7] Saira O-P, Yoon Y, Tanttu T, Möttönen M, Averin D and Pekola J, *Test of the Jarzynski and Crooks fluctuation relations in an electronic system*, 2012 *Phys. Rev. Lett.* **109** 180601
[8] Battista F, Moskalets M, Albert M and Samuelsson P, *Quantum heat fluctuations of single-particle sources*, 2013 *Phys. Rev. Lett.* **110** 126602
[9] Nyquist H, *Thermal agitation of electric charge in conductors*, 1928 *Phys. Rev.* **32** 110
[10] Kurchan J, *A quantum fluctuation theorem* 2000 arXiv:cond-mat/0007360
[11] Yukawa S, *A quantum analogue of the Jarzynski equality*, 2000 *J. Phys. Soc. Japan* **69** 2367
[12] De Roeck W and Maes C, *Quantum version of free-energy–irreversible-work relations*, 2004 *Phys. Rev.* E **69** 026115
[13] Mukamel S, *Quantum extension of the Jarzynski relation: analogy with stochastic dephasing*, 2003 *Phys. Rev. Lett.* **90** 170604
[14] Jarzynski C and Wójcik D, *Classical and quantum fluctuation theorems for heat exchange*, 2004 *Phys. Rev. Lett.* **92** 230602
[15] Bernard D and Doyon B, *Time-reversal symmetry and fluctuation relations in non-equilibrium quantum steady states*, 2013 *J. Phys. A: Math. Theor.* **46** 372001
[16] Das A, 1989 *Integrable Models (World Scientific Lecture Notes in Physics)* **30** (Singapore: World Scientific)
[17] Rajaraman R, 1982 *Solitons and Instantons* (Amsterdam: North-Holland)
[18] Faddeev L D, How Algebraic Bethe Ansatz works for integrable models, Les Houches lectures arXiv:hep-th/9605187
[19] Karowski M, *Exact S matrices and form-factors in* $(1+1)$*-dimensional field theoretic models with soliton behaviour*, 1979 *Phys. Rep.* **49** 229
[20] Zamolodchikov A and Zamolodchikov A, *Factorized S-matrices in two-dimensions as the exact solutions of certain relativistic quantum field models*, 1979 *Ann. Phys.* **120** 253
[21] Abdalla E, Abdalla M C B and Rothe K D, 1991 *Non-perturbative Methods in Two-dimensional Quantum Field Theory* (Singapore: World Scientific)
[22] Mussardo G, *Off critical statistical models: factorized scattering theories and bootstrap program*, 1992 *Phys. Rep.* **218** 215
[23] Dorey P, *Exact S matrices* 1998; arXiv:hep-th/9810026
[24] Mussardo G, 2010 *Statistical Field Theory: An Introduction to Exactly Solved Model in Statistical Physics* (Oxford: Oxford University Press)
[25] Zamolodchikov A, *Thermodynamic Bethe ansatz in relativistic models. Scaling three state Potts and Lee-Yang models*, 1990 *Nucl. Phys.* B **342** 695
[26] Belavin A A, Polyakov A M and Zamolodchikov A B, *Infinite conformal symmetry in two-dimensional quantum field theory*, 1984 *Nucl. Phys.* B **241** 333
[27] Di Francesco P, Mathieu P and Senechal D, 1997 *Conformal Field Theory* (Berlin: Springer)
[28] Levitov L S and Lesovik G B, *Charge distribution in quantum shot noise*, 1993 *JETP Lett.* **58** 230
[29] Levitov L S and Lesovik G B, *Quantum measurement in electric circuit*, 1994 cond-mat/9401004
[30] Klich I, *An elementary derivation of Levitov's formula*, 2003 *Quantum Noise in Mesoscopic Physics (Nato Science Series, vol 97)* ed Y V Nazarov Kluwer Academic Publisher pp 397–402
[31] Schoenhammer K, *Full counting statistics for noninteracting fermions: exact results and the Levitov–Lesovik formula*, 2007 *Phys. Rev.* B **75** 205329
[32] Avron J, Bachmann S, Graf G and Klich I, *Fredholm determinants and the statistics of charge transport*, 2008 *Commun. Math. Phys.* **280** 807
[33] Bernard D and Doyon B, *Full counting statistics in the resonant-level model*, 2012 *J. Math. Phys.* **53** 122302
[34] Gutman D, Gefen Y and Mirlin A, *Full counting statistics of a Luttinger liquid conductor*, 2010 *Phys. Rev. Lett.* **105** 256802
[35] Bernard D and Doyon B, *Non-equilibrium steady-states in conformal field theory* 2013 arXiv:1302.3125
[36] Saleur H and Weiss U, *Point-contact tunneling in the fractional quantum Hall effect: an exact determination of the statistical fluctuations*, 2001 *Phys. Rev.* B **63** 201302
[37] Komnik A and Saleur H, *Quantum fluctuation theorem in an interacting setup: point contacts in fractional quantum Hall edge state devices*, 2011 *Phys. Rev. Lett.* **107** 100601
[38] Fendley P, Ludwig A W W and Saleur H, *Exact nonequilibrium transport through point contacts in quantum wires and fractional quantum Hall devices*, 1995 *Phys. Rev.* B **52** 8934
[39] Fendley P, Ludwig A W W and Saleur H, *Exact conductance through point contacts in the* $\nu = 1/3$ *fractional quantum Hall effect*, 1995 *Phys. Rev. Lett.* **74** 3005

J. Stat. Mech. (2014) P03011

[40] Fendley P, Ludwig A and Saleur H, *Exact nonequilibrium dc shot noise in Luttinger liquids and fractional quantum Hall devices*, 1995 *Phys. Rev. Lett.* **75** 2196

[41] Fendley P, Lesage F and Saleur H, *A unified framework for the Kondo problem and for an impurity in a Luttinger liquid*, 1996 *J. Stat. Phys.* **85** 211

[42] Konik R, Saleur H and Ludwig A, *Transport through quantum dots: analytic results from integrability*, 2001 *Phys. Rev. Lett.* **87** 236801

[43] Konik R M, Saleur H and Ludwig A, *Transport in quantum dots from the integrability of the Anderson model*, 2002 *Phys. Rev.* B **66** 125304

[44] Castro-Alvaredo O and Fring A, *Unstable particles versus resonances in impurity systems, conductance in quantum wires*, 2002 *J. Phys.: Condens. Matter* **14** L721

[45] Castro-Alvaredo O and Fring A, *From integrability to conductance, impurity systems*, 2003 *Nucl. Phys.* B **649** 449

[46] Castro-Alvaredo O and Fring A, *Rational sequences for the conductance in quantum sires from affine Toda field theories*, 2003 *J. Phys. A: Math. Theor.* **36** L425

[47] Mehta P and Andrei N, *Nonequilibrium transport in quantum impurity models: the Bethe ansatz for open systems*, 2006 *Phys. Rev. Lett.* **96** 216802

[48] Mehta P, Chao S P and Andrei N, *Erratum: nonequilibrium transport in quantum impurity models (Bethe-Ansatz for open systems)*, 2006 *Phys. Rev. Lett.* **96** 216802

[49] Boulat E and Saleur H, *Exact low-temperature results for transport properties of the interacting resonant level model*, 2008 *Phys. Rev.* B **77** 033409

[50] Boulat E, Saleur H and Schmitteckert P, *Twofold advance in the theoretical understanding of far-from-equilibrium properties of interacting nanostructures*, 2008 *Phys. Rev. Lett.* **101** 140601

[51] Saito K and Dhar A, *Fluctuation theorem in quantum heat conduction*, 2007 *Phys. Rev. Lett.* **99** 180601

[52] Bernard D and Doyon B, *Energy flow in non-equilibrium conformal field theory*, 2012 *J. Phys. A: Math. Gen.* **45** 362001

[53] De Luca A, Viti J, Bernard D and Doyon B, *Non-equilibrium thermal transport in the quantum Ising chain* 2013 arXiv:1305.4984

[54] Mintchev M, *Non-equilibrium steady states of quantum systems on star graphs*, 2011 *J. Phys. A: Math. Theor.* **44** 5201

[55] Mintchev M and Sorba P, *Luttinger liquid in a non-equilibrium steady state*, 2013 *J. Phys. A: Math. Gen.* **46** 095006

[56] Doyon B, Hoogeveen M and Bernard D, *Energy flow and fluctuations in non-equilibrium conformal field theory on star graphs* 2013 arXiv:1306.3192

[57] Bonetto F, Lebowitz J and Rey-Bellet L, *Fouriers law: a challenge to theorists*, 2000 *Mathematical Physics 2000* ed A Fokas, A Grigoryan, A Kibble and B Zegarlinski (London: World Scientific, Imperial College Press) p 128

[58] Keldysh L V, *Diagram technique for nonequilibrium processes*, 1965 *Sov. Phys. JETP* **20** 1018

[59] Caroli C, Combescot R, Nozieres P and Saint-James D, *Direct calculation of the tunneling current*, 1971 *J. Phys. C: Solid State Phys.* **4** 916

[60] Spohn H and Lebowitz J, *Stationary non-equilibrium states of infinite harmonic systems*, 1977 *Commun. Math. Phys.* **54** 97

[61] Ho T G and Araki H, *Asymptotic time evolution of a partitioned infinite two-sided Isotropic XY-chain*, 2000 *Problems of the Modern Mathematical Physics, Collection of Papers Dedicated to the 90th Anniversary of Academician Nikolai Nikolaevich Bogolyubov (Tr. Mat. Inst. Steklova)* vol 228 (Moscow: Nauka) p 203

[62] Aschbacher W H and Pillet C-A, *Non-equilibrium steady states of the XY chain*, 2003 *J. Stat. Phys.* **12** 1153

[63] Ruelle D, *Natural nonequilibrium states in quantum statistical mechanics*, 2000 *J. Stat. Phys.* **98** 57

[64] Jakšić V and Pillet C-A, *Mathematical theory of non-equilibrium quantum statistical mechanics*, 2002 *J. Stat. Phys.* **108** 787

[65] Hershfield S, *Reformulation of steady state nonequilibrium quantum statistical mechanics*, 1993 *Phys. Rev. Lett.* **70** 2134

[66] Aschbacher W, Jaksic V, Pautrat Y and Pillet C-A, *Topics in non-equilibrium quantum statistical mechanics*, 2006 *Open Quantum Systems III (Lecture Notes in Mathematics vol 1882)* ed S Attal, A Joye and C-A Pillet (Berlin: Springer) p 66

[67] Doyon B and Andrei N, *Universal aspects of nonequilibrium currents in a quantum dot*, 2006 *Phys. Rev.* B **73** 245326

[68] Doyon B, *Nonequilibrium density matrix for thermal transport in quantum field theory Les Houches lectures* 2012 arXiv:1212.1077

J. Stat. Mech. (2014) P03011

[69] Araki H and Barouch E, *On the dynamics and ergodic properties of the XY model*, 1983 *J. Stat. Phys.* **31** 327

[70] Araki H, *On the XY-model on two-sided infinite chain*, 1984 *Publ. RIMS Kyoto Univ.* **20** 277

[71] Ogata Y, *Nonequilibrium properties in the transverse XX chain*, 2002 *Phys. Rev.* E **66** 016135

[72] Karrasch C, Ilan R and Moore J E, *Nonequilibrium thermal transport and its relation to linear response* 2012 arXiv:1211.2236

[73] Doyon B, *The density matrix for quantum impurities out of equilibrium*, 2009 *Lecture Notes for the Fifth Capri Spring School on Transport in Nanostructure*

[74] Castella H, Zotos X and Prelovšek P, *Integrability and ideal conductance at finite temperatures*, 1995 *Phys. Rev. Lett.* **74** 972

[75] Giamarchi T and Millis A J, *Conductivity of a Luttinger liquid*, 1992 *Phys. Rev.* B **46** 9325

[76] Sirker J, Pereira R G and Affleck I, *Diffusion and ballistic transport in one-dimensional quantum systems*, 2009 *Phys. Rev. Lett.* **103** 216602

[77] Schonhammer K, *Full counting statistics for non-interacting fermions: exact results and the Levitov–Lesovik formula*, 2007 *Phys. Rev.* B **75** 205329

[78] Akagawa S and Hatano N, *The exchange fluctuation theorem in quantum mechanics*, 2009 *Prog. Theor. Phys.* **121** 1157

[79] Aschbacher W, *From the microscopic to the van Hove regime in the XY chain out of equilibrium*, 2013 *Rev. Math. Phys.* **25** 1330008

[80] Cardy J, *The ubiquitous 'c': from the Stefan–Boltzmann law to quantum information*, 2010 *J. Stat. Mech.* P10004

[81] Mossel J and Caux J-S, *Generalized TBA and generalized Gibbs*, 2012 *J. Phys. A: Math. Theor.* **45** 255001

[82] Pozsgay B and Takacs G, *Form factor expansion for thermal correlators*, 2010 *J. Stat. Mech.* P11012

[83] Arinshtein A, Fateev V and Zamolodchikov A, *Quantum S-matrix of the (1 + 1)-dimensional Toda chain*, 1979 *Phys. Lett.* B **87** 389

[84] Mikhailov A, Olshanetsky M and Perelomov A, *Two-dimensional generalized Toda lattice*, 1981 *Commun. Math. Phys.* **79** 473

[85] Zamolodchikov A, *Resonance factorized scattering and roaming trajectories*, 2006 *J. Phys. A: Math. Gen.* **39** 12847

[86] Blöte H, Cardy J and Nightingale M, *Conformal invariance, the central charge, and universal finite-size amplitudes at criticality*, 1986 *Phys. Rev. Lett.* **56** 742

[87] Affleck I, *Universal term in the free energy at a critical point and the conformal anomaly*, 1986 *Phys. Rev. Lett.* **56** 746

[88] Itzykson C, Saleur H and Zuber J-B, *Conformal invariance of nonunitary 2d-models*, 1986 *Europhys. Lett.* **2** 91

[89] Ahn C, Delfino G and Mussardo G, *Mapping between the sinh-Gordon and Ising models*, 1993 *Phys. Lett.* B **317** 573

[90] Dorey P and Ravanini F, *Generalizing the staircase models*, 1993 *Nucl. Phys.* B **406** 708

[91] Miramontes J L and Fernandez-Pousa C R, *Integrable quantum field theories with unstable particles*, 2000 *Phys. Lett.* B **472** 392

[92] Castro-Alvaredo O A, Fring A, Korff C and Miramontes J L, *Thermodynamic Bethe ansatz of the homogeneous sine-Gordon models*, 2000 *Nucl. Phys.* B **575** 535

[93] Castro-Alvaredo O, Dreißig J and Fring A, *Integrable scattering theories with unstable particles*, 2004 *Eur. Phys. J.* C **35** 393

[94] Dorey P and Miramontes J, *Mass scales and crossover phenomena in the homogeneous sine-Gordon models*, 2004 *Nucl. Phys.* B **697** 405

[95] Destri C and de Vega H, *Light cone lattice approach to fermionic theories in 2-D: the massive Thirring model*, 1987 *Nucl. Phys.* B **290** 363

[96] Destri C and de Vega H, *New thermodynamic Bethe ansatz equations without strings*, 1992 *Phys. Rev. Lett.* **69** 2313

[97] Destri C and De Vega H, *Unified approach to thermodynamic Bethe Ansatz and finite size corrections for lattice models and field theories*, 1995 *Nucl. Phys.* B **438** 413

[98] Pearce P and Klümper A, *Finite size corrections and scaling dimensions of solvable lattice models: an analytic method*, 1991 *Phys. Rev. Lett.* **66** 974

[99] Klümper A, Batchelor M and Pearce P, *Central charges of the 6- and 19-vertex models with twisted boundary conditions*, 1991 *J. Phys. A: Math. Gen.* **24** 3111

[100] Zamolodchikov A B, *Exact S-matrix of quantum solitons of the sine-Gordon model*, 1977 *JETP Lett.* **25** 468

[101] Braden H, Corrigan E, Dorey P and Sasaki R, *Affine Toda field theory and exact S-matrices*, 1990 *Nucl. Phys.* B **338** 689
[102] Fring A, Korff C and Schulz B J, *The ultraviolet behaviour of integrable quantum field theories, affine Toda field theory*, 1999 *Nucl. Phys.* B **549** 579
[103] Fring A and Korff C, *Large and small density approximations to the thermodynamic Bethe ansatz*, 2000 *Nucl. Phys.* B **579** 617
[104] Klassen T R and Melzer E, *The thermodynamics of purely elastic scattering theories and conformal perturbation theory*, 1991 *Nucl. Phys.* B **350** 635
[105] Klassen T and Melzer E, *Purely elastic scattering theories and their ultraviolet limits*, 1990 *Nucl. Phys.* B **338** 485
[106] Zamolodchikov A B, *Irreversibility of the flux of the renormalization group in a 2-D field theory*, 1986 *JETP Lett.* **43** 730
[107] Zamolodchikov A, *From tricritical Ising to critical Ising by thermodynamic Bethe ansatz*, 1991 *Nucl. Phys.* B **358** 524
[108] Kuniba A, Nakanishi T and Suzuki J, *T-systems and Y-systems in integrable systems*, 2011 *J. Phys. A: Math. Theor.* **44** 103001

Chapter 5

Discussion and outlook

"I don't see much sense in that", said Rabbit. "No," said Pooh humbly, "there isn't. But there was going to be when I began it. It's just that something happened to it along the way."

- A.A. Milne, *Winnie-the-Pooh*

In this thesis we have studied the thermal cut-and-glue quench in one-dimensional integrable systems that are at, or close to a quantum critical point. Continuing the work of Bernard and Doyon [1] in which two critical, independently thermalized semi-infinite systems were connected and allowed to evolve unitarily until a steady state was reached, we investigated the state after the quench further by studying the evolution of entanglement, both in the steady state and in the time leading up to it. We confirm the behaviour first found numerically in [111] for CFTs with trivial pairing, which is an initial growth logarithmic in t, which is independent of the temperatures of the left and right system, followed by a "prethermal" plateau which is reached after a sufficiently long time (but with $t < \ell$, where ℓ is the length of the intervals for which we are computing the entanglement), and an instantaneous decrease of entanglement to its NESS value as soon as $t = \ell$. A possible explanation comes from the quasiparticle picture: very shortly after the quench, the pairs of particles contributing to the growth of entanglement are those created very close to the junction. These particles have not traveled enough to become mixed, so one may expect them not to have information on the temperature. After such a short time, the pair hasn't had to survive for a long time, and one may expect many

to still be entangled. After a longer time, however, the additional contributions that one gets as the system evolves with time are those from the pairs that survive for a longer time, and that have traveled a lot, so the temperature has an effect on (reduce) their survival. The longer the state is left to evolve, the more pronounced the effect on the temperature becomes, until the pre-thermal plateau is reached (assuming we still have $t < \ell$). As soon as the quasiparticles reach the end of the intervals, the system reaches the thermal state (NESS), as any entangled pairs coming from the quench will have left the intervals, and buildup of entanglement between the relevant systems stops. In a CFT, this happens instantaneously at $t = \ell$. Furthermore, we have found that the difference between the plateaus (pre-thermal and thermal) is universal. We also found a universal difference between the pre-thermal plateau and the behaviour just after the quench ($t \ll 1$), whose form seems to indicate that the negativity of an interval with respect to the rest of the system at finite temperatures has, when the interval is sufficiently large, two independent contributions coming from the boundary points, due to the finite effective correlation length generated by the nonzero temperature.

Besides further studying the thermal cut-and-glue quench for two critical one-dimensional quantum systems by computing the entanglement dynamics, we have generalized the setup of [1] in two ways: one is to include effects of a (small) energy gap, which would be present for a system which is close to a quantum critical point, but not exactly critical. Here, we considered the off-critical case in which the system can be described by any integrable model of relativistic QFT (IQFT) with diagonal scattering matrix. The other generalization is to consider the thermal cut-and-glue quench between not two, but N critical one-dimensional systems arranged in a star graph with temperature imbalances amongst the legs of the graph, and a simple connection condition at the vertex. For these setups, we have studied the energy current and its fluctuations in the NESS. In both cases, we found exact expressions[1] for the energy current and the scaled cumulant generating function. In both cases, the energy current does not obey Fourier's law, as the steady-state limit effectively pushes the reservoirs to infinity, and the temperature gradient approaches zero. The fact that in both cases the steady-state energy current is nonzero implies that the current has a ballistic component[2]. For both generalizations, we then verified that the scaled cumulant generating function can be seen as that of a

[1] a closed form expression for the case of the critical systems in the star graph, and an expression in terms of integral equations for the case of the IQFT

[2] in fact, in the critical case it is purely ballistic

family of independent Poisson processes, one for every value of the transferred energy:

$$F(z) = \int dq\, \omega(q)\, (e^{zq} - 1)\,. \tag{5.1}$$

Hence, the complete, large-time scaled statistics of the energy transfer is that of independent, classical packets of energies jumping towards the right or left in a Poissonian fashion with a weight $\omega(q)$, whose form depends on the model in question (with a particularly simple form for the critical case). Another result of [1] was that the energy current depends on the temperatures of the left and right reservoirs as:

$$J(T_l, T_r) = f(T_l) - f(T_r), \tag{5.2}$$

with $f(T) = \frac{\pi c}{12} T^2$. We found that a generalization of (5.2) still holds for the case of N critical systems in a star graph. However, for systems away from criticality, we have proved both analytically and numerically that the additivity of the non-equilibrium current does not hold in a general diagonal theory, except at very large and very small temperatures. We have solved the integral equations for the energy current numerically for three models: the sinh-Gordon model, the roaming trajectories model and the sine-Gordon model at a particular reflectionless point. The additivity deficit has been found to be very small in the numerical analyses of the sinh-Gordon and sine-Gordon models, although it can be rather large for large temperature ratios in the roaming trajectories model. The numerics, in particular of the roaming trajectories model, also suggest the existence of an infinite family of c-functions which are given in terms of the cumulants (these functions are verified to satisfy the required properties: positivity, monotonicity, constant limiting values corresponding to the CFT central charges at RG fixed points). They display a very similar behavior to that of the standard TBA scaling function, recovering for instance CFT central charges of minimal models in the roaming trajectories model. These allowed us to establish upper bounds for cumulants in any integrable model with diagonal scattering.

5.1 Open problems

In order to obtain the entanglement evolution in Chapter 3 we have assumed that the pairing between holomorphic and anti-holomorphic modules of the CFT is trivially factorized. This is not the case in general, and therefore the relations we have found between the logarithmic negativity after a quench and the logarithmic negativity in equilibrium do not hold in general. However, as explained, in certain time regimes the results are expected to become independent of pairing data. Further, it is possible that the above physically compelling particle-pair-creation picture could have more general validity. A next step would be to learn more about the way in which pairing affects our computations. In particular, we would like to find limits in which the results are independent of pairing, and determine the corrections that our general relations would get for CFT models with nontrivial pairing data. Furthermore, in Chapter 3 we used a different (simpler) argument than the one used in [93, 94] of why the partial transpose used in the computation of the (logarithmic) negativity can be computed by reversing the order of the twist fields and the anti-twist fields on the transposed intervals. It would be useful to gain a better understanding in terms of the field theory. This can be done using the methods in [98, 99]. It would be interesting to see if one can generalize the results for entanglement evolution to integrable QFTs, and to cases with nontrivial impurities after the connection (that situation has been studied in the recent work [123]). Another avenue would be to apply the ideas developed in this and related work to other observables.

Finally, it would be extremely interesting to understand the evolution of entanglement in higher-dimensional CFT in the cut-and-glue setup, possibly using methods of gauge-gravity duality. Gauge-gravity duality (also called "holography") has proved to be a useful tool in understanding certain processes in condensed matter systems by finding a holographic realisation in terms of some gravitational process in a higher-dimensional theory [124]. For the energy current in the NESS in the setup of the thermal cut-and-glue quench, results have been obtained in a series of papers [61, 125, 126]. If we want to understand the entanglement in a higher-dimensional setup, however, we encounter problems for mixed states: while the entanglement entropy has a clear holographic interpretation in the form of minimal surfaces [127], computing the entanglement in the thermal cut-and-glue setup involves mixed states, which means that we need to find the

holographic realisation of the negativity. Exploratory work has been done [128–132], but it is still an open question whether we can find a convenient way to compute the negativity in the thermal cut-and-glue setup.

Another important open question is the proof that the non-equilibrium density matrix derived in [74] is the correct one to describe the NESS for integrable QFT. It would also be very interesting to extend our analysis of the sine-Gordon model to the non-diagonal case or even to more complex reflectionless points and to check if we still have c-functions and a Poisson process interpretation, and if the deviation from additivity is small or not. Additionally, it is natural to think that the c-functions we proposed apply much more generally than in integrable QFT; it would be very interesting to have general arguments or a general proof that they are c-functions. Finally, an interesting question is to understand if the Poisson process interpretation still holds beyond integrability.

In reality, diffusion is expected to become more important after the quench for a system at finite temperature. It would be interesting to consider a perturbation of the CFT system and investigate these effects when the system is not exactly integrable. In this case, one might be able to test Fourier's law (see Chapter 1).

Bibliography

[1] D. Bernard and B. Doyon. Energy flow in non-equilibrium conformal field theory. *J. Phys. A*, 45(36):362001, 2012. URL http://stacks.iop.org/1751-8121/45/i=36/a=362001.

[2] B. Doyon, M. Hoogeveen, and D. Bernard. Energy flow and fluctuations in non-equilibrium conformal field theory on star graphs. *J. Stat. Mech.*, 2014(3):P03002, 2014.

[3] O. Castro-Alvaredo, Y. Chen, B. Doyon, and M. Hoogeveen. Thermodynamic bethe ansatz for non-equilibrium steady states: exact energy current and fluctuations in integrable qft. *J. Stat. Mech.*, 2014(3):P03011, 2014.

[4] M. Hoogeveen and B. Doyon. Entanglement negativity and entropy in non-equilibrium conformal field theory. *Nucl. Phys. B*, 898:78 – 112, 2015. ISSN 0550-3213. doi: http://dx.doi.org/10.1016/j.nuclphysb.2015.06.021. URL http://www.sciencedirect.com/science/article/pii/S0550321315002242.

[5] H. Nyquist. Thermal agitation of electric charge in conductors. *Physical review*, 32(1):110–113, 1928.

[6] H. Callen and T. Welton. Irreversibility and generalized noise. *Physical Review*, 83(1):34–40, 1951.

[7] M. Green. Markoff random processes and the statistical mechanics of time-dependent phenomena. *The Journal of Chemical Physics*, 20:1281, 1952.

[8] M. Green. Markoff random processes and the statistical mechanics of time-dependent phenomena. ii. irreversible processes in fluids. *The Journal of Chemical Physics*, 22:398, 1954.

[9] R. Kubo. Statistical-mechanical theory of irreversible processes. i. general theory and simple applications to magnetic and conduction problems. *Journal of the Physical Society of Japan*, 12(6):570–586, 1957.

[10] I. Bloch, J. Dalibard, and W. Zwerger. Many-body physics with ultracold gases. *Rev. Mod. Phys.*, 80:885–964, July 2008. doi: 10.1103/RevModPhys.80.885. URL http://link.aps.org/doi/10.1103/RevModPhys.80.885.

[11] T. Kinoshita, T. Wenger, and D.S. Weiss. A quantum newton's cradle. *Nature*, 440 (7086):900–903, April 2006. URL http://dx.doi.org/10.1038/nature04693.

[12] S. Sachdev. Quantum criticality: Competing ground states in low dimensions. *Science*, 288:475–480, 2000.

[13] F. Bonetto, J. L. Lebowitz, and L. Rey-Bellet. Fourier's Law: a Challenge for Theorists. *ArXiv Mathematical Physics e-prints*, February 2000.

[14] S. Lepri, R. Livi, and A. Politi. Heat conduction in chains of nonlinear oscillators. *Phys. Rev. Lett.*, 78:1896–1899, March 1997. doi: 10.1103/PhysRevLett.78.1896. URL http://link.aps.org/doi/10.1103/PhysRevLett.78.1896.

[15] A. Dhar. Heat transport in low-dimensional systems. *Adv. Phys.*, 57(5):457–537, 2008. doi: 10.1080/00018730802538522. URL http://www.tandfonline.com/doi/abs/10.1080/00018730802538522.

[16] P. Mazur. Non-ergodicity of phase functions in certain systems. *Physica*, 43(4):533 – 545, 1969. ISSN 0031-8914. doi: http://dx.doi.org/10.1016/0031-8914(69)90185-2. URL http://www.sciencedirect.com/science/article/pii/0031891469901852.

[17] X. Zotos, F. Naef, and P. Prelovsek. Transport and conservation laws. *Phys. Rev. B*, 55:11029–11032, May 1997. doi: 10.1103/PhysRevB.55.11029. URL http://link.aps.org/doi/10.1103/PhysRevB.55.11029.

[18] B. Doyon. Lower bounds for ballistic current and noise in non-equilibrium quantum steady states. *Nucl. Phys. B*, 892(0):190 – 210, March 2015. ISSN 0550-3213. doi: http://dx.doi.org/10.1016/j.nuclphysb.2015.01.007. URL http://www.sciencedirect.com/science/article/pii/S0550321315000103.

[19] D. Evans and D. Searles. Equilibrium microstates which generate second law violating steady states. *Phys. Rev. E*, 50:1645–1648, Aug 1994. doi: 10.1103/PhysRevE.50.1645. URL http://link.aps.org/doi/10.1103/PhysRevE.50.1645.

[20] M. Esposito, U. Harbola, and S. Mukamel. Nonequilibrium fluctuations, fluctuation theorems, and counting statistics in quantum systems. *Rev. Mod. Phys.*, 81 (4):1665, 2009. doi: 10.1103/RevModPhys.81.1665. URL http://link.aps.org/doi/10.1103/RevModPhys.81.1665.

[21] Denis J. Evans and Debra J. Searles. The fluctuation theorem. *Adv. Phys.*, 51(7): 1529–1585, 2002. doi: 10.1080/00018730210155133. URL http://dx.doi.org/10.1080/00018730210155133.

[22] GN Bochkov and Iu E Kuzovlev. Contribution to the general theory of thermal fluctuations in nonlinear systems. *Zhurnal Eksperimental noi i Teoreticheskoi Fiziki*, 72:238–247, 1977.

[23] C. Jarzynski. Equilibrium free-energy differences from nonequilibrium measurements: A master-equation approach. *Phys. Rev. E*, 56(5), 1997.

[24] D. Evans, E. G. D. Cohen, and G. P. Morriss. Probability of second law violations in shearing steady states. *Phys. Rev. Lett.*, 71:2401–2404, Oct 1993. doi: 10.1103/PhysRevLett.71.2401. URL http://link.aps.org/doi/10.1103/PhysRevLett.71.2401.

[25] G. Gallavotti and E. Cohen. Dynamical ensembles in nonequilibrium statistical mechanics. *Phys. Rev. Lett.*, 74(14):2694–2697, 1995. doi: 10.1103/PhysRevLett.74.2694. URL http://link.aps.org/doi/10.1103/PhysRevLett.74.2694.

[26] G. Crooks. Nonequilibrium measurements of free energy differences for microscopically reversible markovian systems. *J. Stat. Phys.*, 90(5-6):1481–1487, 1998.

[27] G. Crooks. Entropy production fluctuation theorem and the nonequilibrium work relation for free energy differences. *Phys. Rev. E*, 60(3):2721, 1999.

[28] G. Crooks. Path-ensemble averages in systems driven far from equilibrium. *Phys. Rev. E*, 61(3):2361, 2000.

[29] J. Kurchan. Fluctuation theorem for stochastic dynamics. *J. Phys. A*, 31(16): 3719, 1998.

[30] J. Lebowitz and H. Spohn. A gallavotti–cohen-type symmetry in the large deviation functional for stochastic dynamics. *J. Stat. Phys.*, 95(1-2):333–365, 1999.

[31] L.S. Levitov and G.B. Lesovik. Charge distribution in quantum shot noise. *JETP letters*, 58:230–230, 1993.

[32] C. Jarzynski and D. Wójcik. Classical and quantum fluctuation theorems for heat exchange. *Physical review letters*, 92(23):230602, 2004.

[33] M. Nielsen and I. Chuang. *Quantum computation and quantum information*. Cambridge university press, 2010.

[34] F. Verstraete, M. Popp, and J. I. Cirac. Entanglement versus correlations in spin systems. *Phys. Rev. Lett.*, 92:027901, Jan 2004. doi: 10.1103/PhysRevLett.92.027901. URL http://link.aps.org/doi/10.1103/PhysRevLett.92.027901.

[35] R. Horodecki, P. Horodecki, M. Horodecki, and K. Horodecki. Quantum entanglement. *Rev. Mod. Phys.*, 81:865–942, June 2009. doi: 10.1103/RevModPhys.81.865. URL http://link.aps.org/doi/10.1103/RevModPhys.81.865.

[36] A. Einstein, B. Podolsky, and N. Rosen. Can quantum-mechanical description of physical reality be considered complete? *Phys. Rev.*, 47:777–780, May 1935. doi: 10.1103/PhysRev.47.777. URL http://link.aps.org/doi/10.1103/PhysRev.47.777.

[37] E. Schrödinger. Discussion of probability relations between separated systems. *Math. Proc. Cambridge*, 31:555–563, 10 1935. ISSN 1469-8064. doi: 10.1017/S0305004100013554. URL http://journals.cambridge.org/article_S0305004100013554.

[38] J. Bell. On the einstein-podolsky-rosen paradox. *Physics*, 1(3):195–200, 1964.

[39] D. Boschi, S. Branca, F. De Martini, L. Hardy, and S. Popescu. Experimental realization of teleporting an unknown pure quantum state via dual classical and einstein-podolsky-rosen channels. *Phys. Rev. Lett.*, 80:1121–1125, Feb 1998. doi: 10.1103/PhysRevLett.80.1121. URL http://link.aps.org/doi/10.1103/PhysRevLett.80.1121.

[40] B. Hensen, H. Bernien, A. E. Dreau, A. Reiserer, N. Kalb, M. S. Blok, J. Ruitenberg, R. F. L. Vermeulen, R. N. Schouten, C. Abellan, W. Amaya, V. Pruneri, M. W. Mitchell, M. Markham, D. J. Twitchen, D. Elkouss, S. Wehner, T. H. Taminiau, and R. Hanson. Loophole-free bell inequality violation using electron spins separated by 1.3 kilometres. *Nature*, 526:682 – 686, October 2015. ISSN 0028-0836. doi: 10.1038/nature15759. URL http://dx.doi.org/10.1038/nature15759.

[41] N. Gisin. Bell's inequality holds for all non-product states. *Phys. Lett. A*, 154(5):201 – 202, 1991. ISSN 0375-9601. doi: http://dx.doi.org/10.1016/0375-9601(91)90805-I. URL http://www.sciencedirect.com/science/article/pii/037596019190805I.

[42] S. Yu, Q. Chen, C. Zhang, C. H. Lai, and C. H. Oh. All entangled pure states violate a single bell's inequality. *Phys. Rev. Lett.*, 109:120402, September 2012. doi: 10.1103/PhysRevLett.109.120402. URL http://link.aps.org/doi/10.1103/PhysRevLett.109.120402.

[43] R. Werner. Quantum states with einstein-podolsky-rosen correlations admitting a hidden-variable model. *Phys. Rev. A*, 40:4277–4281, October 1989. doi: 10.1103/PhysRevA.40.4277. URL http://link.aps.org/doi/10.1103/PhysRevA.40.4277.

[44] N. J. Cerf, N. Gisin, S. Massar, and S. Popescu. Simulating maximal quantum entanglement without communication. *Phys. Rev. Lett.*, 94:220403, Jun 2005. doi: 10.1103/PhysRevLett.94.220403. URL http://link.aps.org/doi/10.1103/PhysRevLett.94.220403.

[45] S. Popescu and D. Rohrlich. Thermodynamics and the measure of entanglement. *Phys. Rev. A*, 56:R3319–R3321, Nov 1997. doi: 10.1103/PhysRevA.56.R3319. URL http://link.aps.org/doi/10.1103/PhysRevA.56.R3319.

[46] G. Vidal. Entanglement monotones. *J. Mod. Optic.*, 47(2-3):355–376, 2000.

[47] M. Plenio and S. Virmani. An introduction to entanglement measures. *arXiv preprint quant-ph/0504163*, 2005.

[48] C. Bennett, D. DiVincenzo, J. Smolin, and W. Wootters. Mixed-state entanglement and quantum error correction. *Phys. Rev. A*, 54:3824–3851, November

1996. doi: 10.1103/PhysRevA.54.3824. URL http://link.aps.org/doi/10.1103/PhysRevA.54.3824.

[49] S. Popescu. Bell's inequalities and density matrices: Revealing "hidden" nonlocality. *Phys. Rev. Lett.*, 74:2619–2622, Apr 1995. doi: 10.1103/PhysRevLett.74.2619. URL http://link.aps.org/doi/10.1103/PhysRevLett.74.2619.

[50] A. Peres. Separability criterion for density matrices. *Phys. Rev. Lett.*, 77:1413–1415, August 1996. doi: 10.1103/PhysRevLett.77.1413. URL http://link.aps.org/doi/10.1103/PhysRevLett.77.1413.

[51] M. Horodecki, P. Horodecki, and R. Horodecki. Separability of mixed states: necessary and sufficient conditions. *Phys. Lett. A*, 223(12):1 – 8, 1996. ISSN 0375-9601. doi: http://dx.doi.org/10.1016/S0375-9601(96)00706-2. URL http://www.sciencedirect.com/science/article/pii/S0375960196007062.

[52] G. Vidal and R. Werner. Computable measure of entanglement. *Phys. Rev. A*, 65 (3):032314, February 2002. ISSN 1050-2947. doi: 10.1103/PhysRevA.65.032314. URL http://link.aps.org/doi/10.1103/PhysRevA.65.032314.

[53] M. Plenio. Logarithmic negativity: A full entanglement monotone that is not convex. *Phys. Rev. Lett.*, 95:090503, Aug 2005. doi: 10.1103/PhysRevLett.95.090503. URL http://link.aps.org/doi/10.1103/PhysRevLett.95.090503.

[54] E. Barouch, B. McCoy, and M. Dresden. Statistical mechanics of the XY model. i. *Phys. Rev. A*, 2:1075–1092, Sep 1970. doi: 10.1103/PhysRevA.2.1075. URL http://link.aps.org/doi/10.1103/PhysRevA.2.1075.

[55] E. Barouch and B. McCoy. Statistical mechanics of the xy model. ii. spin-correlation functions. *Phys. Rev. A*, 3:786–804, Feb 1971. doi: 10.1103/PhysRevA.3.786. URL http://link.aps.org/doi/10.1103/PhysRevA.3.786.

[56] E. Barouch and B. McCoy. Statistical mechanics of the XY model. iii. *Phys. Rev. A*, 3:2137–2140, Jun 1971. doi: 10.1103/PhysRevA.3.2137. URL http://link.aps.org/doi/10.1103/PhysRevA.3.2137.

[57] B. McCoy, E. Barouch, and D. Abraham. Statistical mechanics of the XY model. iv. time-dependent spin-correlation functions. *Phys. Rev. A*, 4:2331–2341, Dec

1971. doi: 10.1103/PhysRevA.4.2331. URL http://link.aps.org/doi/10.1103/PhysRevA.4.2331.

[58] P. Calabrese and J. Cardy. Evolution of Entanglement Entropy in One-Dimensional Systems. *J. Stat. Mech.*, 2005(04):26, March 2005. ISSN 1742-5468. doi: 10.1088/1742-5468/2005/04/P04010. URL http://stacks.iop.org/1742-5468/2005/i=04/a=P04010?key=crossref.7e427f5b65ccbfcf3b82757d806c7b35http://arxiv.org/abs/cond-mat/0503393.

[59] P. Calabrese and J. Cardy. Time dependence of correlation functions following a quantum quench. *Phys. Rev. Lett.*, 96:136801, Apr 2006. doi: 10.1103/PhysRevLett.96.136801. URL http://link.aps.org/doi/10.1103/PhysRevLett.96.136801.

[60] P. Calabrese and J. Cardy. Quantum quenches in extended systems. *J. Stat. Mech.*, 2007(06):P06008, 2007. URL http://stacks.iop.org/1742-5468/2007/i=06/a=P06008.

[61] B. Doyon, A. Lucas, K. Schalm, and M. J. Bhaseen. Non-equilibrium steady states in the klein-gordon theory. *J. Phys. A*, 48(9):095002, 2015. URL http://stacks.iop.org/1751-8121/48/i=9/a=095002.

[62] B. Doyon and N. Andrei. Universal aspects of nonequilibrium currents in a quantum dot. *Phys. Rev. B*, 73:245326, Jun 2006. doi: 10.1103/PhysRevB.73.245326. URL http://link.aps.org/doi/10.1103/PhysRevB.73.245326.

[63] B. Doyon. The density matrix for quantum impurities out of equilibrium. *lecture notes for the Fifth Capri Spring School on Transport in Nanostructure*, 2009. URL http://tfp1.physik.uni-freiburg.de/Capri09/lectures/Doyon_QuantumImpurities.pdf.

[64] D. Bernard and B. Doyon. Full counting statistics in the resonant-level model. *Journal of Mathematical Physics*, 53(12):122302, 2012. ISSN 00222488. doi: 10.1063/1.4763471. URL http://link.aip.org/link/JMAPAQ/v53/i12/p122302/s1&Agg=doi.

[65] H. Spohn and J.L. Lebowitz. Stationary non-equilibrium states of infinite harmonic systems. *Commun. Math. Phys.*, 54(2):97–120, 1977. ISSN 0010-3616. doi: 10.1007/BF01614132. URL http://dx.doi.org/10.1007/BF01614132.

[66] T. Ho and H. Araki. Asymptotic time evolution of a partitioned infinite two-sided isotropic xy-chain. *Proc. Steklov Inst. Math.*, 228:203–216, 2000.

[67] W. Aschbacher and C.-A. Pillet. Non-equilibrium steady states of the xy chain. *J. Stat. Phys.*, 112(5-6):1153–1175, 2003. ISSN 0022-4715. doi: 10.1023/A:1024619726273. URL http://dx.doi.org/10.1023/A%3A1024619726273.

[68] D. Ruelle. Natural nonequilibrium states in quantum statistical mechanics. *J. Stat. Phys.*, 98(1-2):57–75, 2000. ISSN 0022-4715. doi: 10.1023/A:1018618704438. URL http://dx.doi.org/10.1023/A%3A1018618704438.

[69] D. Bernard and B. Doyon. Time-reversal symmetry and fluctuation relations in non-equilibrium quantum steady states. *J. Phys. A*, 46(37):372001, 2013. URL http://stacks.iop.org/1751-8121/46/i=37/a=372001.

[70] T. Giamarchi and A. J. Millis. Conductivity of a luttinger liquid. *Phys. Rev. B*, 46:9325–9331, Oct 1992. doi: 10.1103/PhysRevB.46.9325. URL http://link.aps.org/doi/10.1103/PhysRevB.46.9325.

[71] H. Castella, X. Zotos, and P. Prelovšek. Integrability and ideal conductance at finite temperatures. *Phys. Rev. Lett.*, 74:972–975, Feb 1995. doi: 10.1103/PhysRevLett.74.972. URL http://link.aps.org/doi/10.1103/PhysRevLett.74.972.

[72] J. Sirker, R. G. Pereira, and I. Affleck. Diffusion and ballistic transport in one-dimensional quantum systems. *Phys. Rev. Lett.*, 103:216602, Nov 2009. doi: 10.1103/PhysRevLett.103.216602. URL http://link.aps.org/doi/10.1103/PhysRevLett.103.216602.

[73] D. Bernard and B. Doyon. Non-equilibrium steady states in conformal field theory. *Annales Henri Poincaré*, 16(1):113–161, 2015. ISSN 1424-0637. doi: 10.1007/s00023-014-0314-8. URL http://dx.doi.org/10.1007/s00023-014-0314-8.

[74] B. Doyon. Nonequilibrium density matrix for thermal transport in quantum field theory. *arXiv preprint arXiv:1212.1077*, 2012.

[75] A. M. Polyakov. Conformal Symmetry of Critical Fluctuations (Originally published in Russian Volume 12, Number 11). *Soviet Journal of Experimental and Theoretical Physics Letters*, 12:381, 1970.

[76] V. Riva and J. Cardy. Scale and conformal invariance in field theory: a physical counterexample. *Phys. Lett. B*, 622(34):339 – 342, 2005. ISSN 0370-2693. doi: http://dx.doi.org/10.1016/j.physletb.2005.07.010. URL http://www.sciencedirect.com/science/article/pii/S0370269305009615.

[77] AB Zamolodchikov. Irreversibility of the flux of the renormalization group in a 2d field theory. *JETP Lett.*, 43(12):730–732, 1986.

[78] J. Cardy. Central charge and universal combinations of amplitudes in two-dimensional theories away from criticality. *Phys. Rev. Lett.*, 60:2709–2711, Jun 1988. doi: 10.1103/PhysRevLett.60.2709. URL http://link.aps.org/doi/10.1103/PhysRevLett.60.2709.

[79] V. Bazhanov, S. Lukyanov, and AlexanderB. Zamolodchikov. Integrable structure of conformal field theory, quantum kdv theory and thermodynamic bethe ansatz. *Commun. Math. Phys.*, 177(2):381–398, 1996. ISSN 0010-3616. doi: 10.1007/BF02101898. URL http://dx.doi.org/10.1007/BF02101898.

[80] J-S Caux and J. Mossel. Remarks on the notion of quantum integrability. *J. Stat. Mech.*, 2011(02):P02023, 2011. URL http://stacks.iop.org/1742-5468/2011/i=02/a=P02023.

[81] A.B. Zamolodchikov. Integrable field theory from conformal field theory. *Adv. Stud. Pure Math*, 19:641, 1989.

[82] A. B. Zamolodchikov and Al. B. Zamolodchikov. Factorized s-matrices in two dimensions as the exact solutions of certain relativistic quantum field theory models. *Annals of Physics*, 120(2):253 – 291, 1979. ISSN 0003-4916. doi: http://dx.doi.org/10.1016/0003-4916(79)90391-9. URL http://www.sciencedirect.com/science/article/pii/0003491679903919.

[83] R. Shankar and E. Witten. s matrix of the supersymmetric nonlinear σ model. *Phys. Rev. D*, 17:2134–2143, Apr 1978. doi: 10.1103/PhysRevD.17.2134. URL http://link.aps.org/doi/10.1103/PhysRevD.17.2134.

[84] S. Coleman and J. Mandula. All possible symmetries of the s matrix. *Phys. Rev.*, 159:1251–1256, Jul 1967. doi: 10.1103/PhysRev.159.1251. URL http://link.aps.org/doi/10.1103/PhysRev.159.1251.

[85] C. N. Yang and C. P. Yang. Thermodynamics of a onedimensional system of bosons with repulsive deltafunction interaction. *J. Math. Phys.*, 10(7):1115–1122, 1969. doi: http://dx.doi.org/10.1063/1.1664947. URL http://scitation.aip.org/content/aip/journal/jmp/10/7/10.1063/1.1664947.

[86] E. Lieb and W. Liniger. Exact analysis of an interacting bose gas. i. the general solution and the ground state. *Phys. Rev.*, 130:1605–1616, May 1963. doi: 10.1103/PhysRev.130.1605. URL http://link.aps.org/doi/10.1103/PhysRev.130.1605.

[87] T.C. Dorlas, J.T. Lewis, and J.V. Pulé. The yang-yang thermodynamic formalism and large deviations. *Commun. Math. Phys.*, 124(3):365–402, 1989. ISSN 0010-3616. doi: 10.1007/BF01219656. URL http://dx.doi.org/10.1007/BF01219656.

[88] Al.B. Zamolodchikov. Thermodynamic bethe ansatz in relativistic models: Scaling 3-state potts and lee-yang models. *Nucl. Phys. B*, 342(3):695 – 720, 1990. ISSN 0550-3213. doi: http://dx.doi.org/10.1016/0550-3213(90)90333-9. URL http://www.sciencedirect.com/science/article/pii/0550321390903339.

[89] C. Callan and F. Wilczek. On geometric entropy. *Phys. Lett. B*, 333(12):55 – 61, 1994. ISSN 0370-2693. doi: http://dx.doi.org/10.1016/0370-2693(94)91007-3. URL http://www.sciencedirect.com/science/article/pii/0370269394910073.

[90] C. Holzhey, F. Larsen, and F. Wilczek. Geometric and renormalized entropy in conformal field theory. *Nucl. Phys. B*, 424(3):443–467, August 1994. ISSN 05503213. doi: 10.1016/0550-3213(94)90402-2. URL http://linkinghub.elsevier.com/retrieve/pii/0550321394904022.

[91] P. Calabrese and J. Cardy. Entanglement entropy and quantum field theory. *J. Stat. Mech.*, 2004(06):P06002, June 2004. doi: 10.1088/1742-5468/2004/06/P06002. URL http://stacks.iop.org/1742-5468/2004/i=06/a=P06002?key=crossref.2fead8410474dca993bc18682138a41f.

[92] G. Parisi. On the replica approach to glasses. *arXiv preprint cond-mat/9701068*, 1997.

[93] P. Calabrese, J. Cardy, and E. Tonni. Entanglement Negativity in Quantum Field Theory. *Phys. Rev. Lett.*, 109(13):130502, September 2012. ISSN 0031-9007. doi: 10.1103/PhysRevLett.109.130502. URL http://link.aps.org/doi/10.1103/PhysRevLett.109.130502.

[94] P. Calabrese, J. Cardy, and E. Tonni. Entanglement negativity in extended systems: a field theoretical approach. *J. Stat. Mech.*, 2013(02): P02008, February 2013. ISSN 1742-5468. doi: 10.1088/1742-5468/2013/02/P02008. URL http://stacks.iop.org/1742-5468/2013/i=02/a=P02008?key=crossref.71ac916bad2977e20b75eeaa43ce672d.

[95] V. Knizhnik. Analytic fields on Riemann surfaces. II. *Commun. Math. Phys.*, 112(4):567–590, December 1987. ISSN 0010-3616. doi: 10.1007/BF01225373. URL http://link.springer.com/10.1007/BF01225373http://link.springer.com/article/10.1007/BF01225373.

[96] J. Cardy, O. Castro-Alvaredo, and B. Doyon. Form Factors of Branch-Point Twist Fields in Quantum Integrable Models and Entanglement Entropy. *J. Stat. Phys.*, 130(1):129–168, October 2007. ISSN 0022-4715. doi: 10.1007/s10955-007-9422-x. URL http://link.springer.com/10.1007/s10955-007-9422-x.

[97] L. Dixon, D. Friedan, E. Martinec, and S. Shenker. The conformal field theory of orbifolds. *Nucl. Phys. B*, 282(0):13 – 73, 1987. ISSN 0550-3213. doi: http://dx.doi.org/10.1016/0550-3213(87)90676-6. URL http://www.sciencedirect.com/science/article/pii/0550321387906766.

[98] O. Castro-Alvaredo and B. Doyon. Permutation operators, entanglement entropy, and the xxz spin chain in the limit $\Delta \to -1^+$. *J. Stat. Mech.*, 2011(02):P02001, 2011. URL http://stacks.iop.org/1742-5468/2011/i=02/a=P02001.

[99] O. Castro-Alvaredo and B. Doyon. Entanglement entropy of highly degenerate states and fractal dimensions. *Phys. Rev. Lett.*, 108:120401, Mar 2012. doi: 10.1103/PhysRevLett.108.120401. URL http://link.aps.org/doi/10.1103/PhysRevLett.108.120401.

[100] G. Vidal, J. I. Latorre, E. Rico, and A. Kitaev. Entanglement in quantum critical phenomena. *Phys. Rev. Lett.*, 90:227902, June 2003. doi: 10.1103/PhysRevLett.90.227902. URL http://link.aps.org/doi/10.1103/PhysRevLett.90.227902.

[101] B.-Q. Jin and V.E. Korepin. Quantum spin chain, toeplitz determinants and the fisherhartwig conjecture. *J. Stat. Phys.*, 116(1-4):79–95, 2004. ISSN 0022-4715. doi: 10.1023/B:JOSS.0000037230.37166.42. URL http://dx.doi.org/10.1023/B%3AJOSS.0000037230.37166.42.

[102] A. Its, B-Q Jin, and V. Korepin. Entanglement in the xy spin chain. *J. Phys. A*, 38(13):2975, 2005. URL http://stacks.iop.org/0305-4470/38/i=13/a=011.

[103] F. Franchini, A. R. Its, and V. E. Korepin. Renyi entropy of the xy spin chain. *J. Phys. A*, 41(2):025302, 2008. URL http://stacks.iop.org/1751-8121/41/i=2/a=025302.

[104] F. Iglói and R. Juhász. Exact relationship between the entanglement entropies of xy and quantum ising chains. *Europhys. Lett.*, 81(5):57003, 2008. URL http://stacks.iop.org/0295-5075/81/i=5/a=57003.

[105] V. Korepin. Universality of Entropy Scaling in One Dimensional Gapless Models. *Phys. Rev. Lett.*, 92(9):096402, March 2004. ISSN 0031-9007. doi: 10.1103/PhysRevLett.92.096402. URL http://link.aps.org/doi/10.1103/PhysRevLett.92.096402.

[106] P. Calabrese, J. Cardy, and E. Tonni. Finite temperature entanglement negativity in conformal field theory. *J. Phys. A*, 48(1):015006, 2015. URL http://stacks.iop.org/1751-8121/48/i=1/a=015006.

[107] H.-Q. Zhou, T. Barthel, J. Fjærestad, and U. Schollwöck. Entanglement and boundary critical phenomena. *Phys. Rev. A*, 74(5):050305, November 2006.

[108] N. Laflorencie, E. Sørensen, M.-S. Chang, and I. Affleck. Boundary effects in the critical scaling of entanglement entropy in 1d systems. *Phys. Rev. Lett.*, 96:100603, March 2006. doi: 10.1103/PhysRevLett.96.100603. URL http://link.aps.org/doi/10.1103/PhysRevLett.96.100603.

[109] I. Affleck and A.W.W. Ludwig. Universal noninteger "ground-state degeneracy" in critical quantum systems. *Phys. Rev. Lett.*, 67(2):161–164, July 1991. ISSN

0031-9007. doi: 10.1103/PhysRevLett.67.161. URL http://link.aps.org/doi/10.1103/PhysRevLett.67.161.

[110] P. Calabrese and J. Cardy. Entanglement and correlation functions following a local quench: a conformal field theory approach. *J. Stat. Mech.*, 2007(10): P10004, October 2007. ISSN 1742-5468. doi: 10.1088/1742-5468/2007/10/P10004. URL http://stacks.iop.org/1742-5468/2007/i=10/a=P10004?key=crossref.a2195b7400eb98fcf530610305bc246e.

[111] V. Eisler and Z. Zimboras. Entanglement negativity in the harmonic chain out of equilibrium. *New J. Phys.*, 16(12):123020, 2014. URL http://stacks.iop.org/1367-2630/16/i=12/a=123020.

[112] K. Saito and Y. Utsumi. Symmetry in full counting statistics, fluctuation theorem, and relations among nonlinear transport coefficients in the presence of a magnetic field. *Phys. Rev. B*, 78:115429, Sep 2008. doi: 10.1103/PhysRevB.78.115429. URL http://link.aps.org/doi/10.1103/PhysRevB.78.115429.

[113] D. Andrieux, P. Gaspard, T. Monnai, and S. Tasaki. The fluctuation theorem for currents in open quantum systems. *New J. Phys.*, 11(4):043014, 2009. URL http://stacks.iop.org/1367-2630/11/i=4/a=043014.

[114] M. Campisi, P. Talkner, and P. Hänggi. Fluctuation theorems for continuously monitored quantum fluxes. *Phys. Rev. Lett.*, 105:140601, Sep 2010. doi: 10.1103/PhysRevLett.105.140601. URL http://link.aps.org/doi/10.1103/PhysRevLett.105.140601.

[115] K. Saito and A. Dhar. Fluctuation theorem in quantum heat conduction. *Phys. Rev. Lett.*, 99(18):180601, 2007. doi: 10.1103/PhysRevLett.99.180601. URL http://link.aps.org/doi/10.1103/PhysRevLett.99.180601.

[116] L. Mandel and E. Wolf. *Optical coherence and quantum optics*. Cambridge university press, 1995.

[117] L. Levitov and G. Lesovik. Charge distribution in quantum shot noise. *JETP Lett.*, 58:230–230, 1993.

[118] Ya.M. Blanter and M. Büttiker. Shot noise in mesoscopic conductors. *Physics Reports*, 336(12):1 – 166, 2000. ISSN 0370-1573. doi: http://dx.doi.org/10.

1016/S0370-1573(99)00123-4. URL http://www.sciencedirect.com/science/article/pii/S0370157399001234.

[119] Y. Nazarov. *Quantum Noise in Mesoscopic Physics*. Springer Science & Business Media, 2003.

[120] D. Bernard and B. Doyon. Full counting statistics in the resonant-level model. *J. Math. Phys.*, 53(12):122302, 2012. doi: http://dx.doi.org/10.1063/1.4763471. URL http://scitation.aip.org/content/aip/journal/jmp/53/12/10.1063/1.4763471.

[121] C. Karrasch, R. Ilan, and J. E. Moore. Nonequilibrium thermal transport and its relation to linear response. *Phys. Rev. B*, 88:195129, Nov 2013. doi: 10.1103/PhysRevB.88.195129. URL http://link.aps.org/doi/10.1103/PhysRevB.88.195129.

[122] Al B Zamolodchikov. Thermodynamic bethe ansatz in relativistic models: scaling 3-state potts and lee-yang models. *Nucl. Phys. B*, 342(3):695–720, 1990.

[123] D. Bernard, B. Doyon, and J. Viti. Non-equilibrium conformal field theories with impurities. *J. Phys. A*, 48(5):05FT01, 2015. URL http://stacks.iop.org/1751-8121/48/i=5/a=05FT01.

[124] S.A. Hartnoll. Lectures on holographic methods for condensed matter physics. *Classical Quant. Grav.*, 26(22):224002, 2009. URL http://stacks.iop.org/0264-9381/26/i=22/a=224002.

[125] M.J. Bhaseen, B. Doyon, A. Lucas, and K. Schalm. Energy flow in quantum critical systems far from equilibrium. *Nat. Phys.*, pages 1745–2481, May 2015. doi: 10.1038/nphys3220. URL http://dx.doi.org/10.1038/nphys3220.

[126] A. Lucas, K. Schalm, B. Doyon, and M.J. Bhaseen. Shock waves, rarefaction waves and non-equilibrium steady states in quantum critical systems. *arXiv preprint arXiv:1512.09037*, 2015.

[127] T. Takayanagi. Entanglement entropy from a holographic viewpoint. *Classical Quant. Grav.*, 29(15):153001, 2012. URL http://stacks.iop.org/0264-9381/29/i=15/a=153001.

[128] M. Rangamani and M. Rota. Comments on entanglement negativity in holographic field theories. *J. High Energy Phys.*, 2014(10):60, 2014. doi: 10.1007/JHEP10(2014)060. URL http://dx.doi.org/10.1007/JHEP10%282014%29060.

[129] M. Rangamani and M. Rota. Entanglement structures in qubit systems. *arXiv preprint arXiv:1505.03696*, 2015.

[130] E. Perlmutter, M. Rangamani, and M. Rota. Central charges and the sign of entanglement in 4d conformal field theories. *Phys. Rev. Lett.*, 115:171601, Oct 2015. doi: 10.1103/PhysRevLett.115.171601. URL http://link.aps.org/doi/10.1103/PhysRevLett.115.171601.

[131] S. Kanno, J. Shock, and J. Soda. Entanglement negativity in the multiverse. *J. Cosmol. Astropart. P.*, 2015(03):015, 2015. URL http://stacks.iop.org/1475-7516/2015/i=03/a=015.

[132] V. Eisler and Z. Zimborás. Entanglement negativity in two-dimensional free lattice models. *Phys. Rev. B*, 93:115148, Mar 2016. doi: 10.1103/PhysRevB.93.115148. URL https://link.aps.org/doi/10.1103/PhysRevB.93.115148.